



INSTITUTO DE
TECNOLOGÍA
QUÍMICA



CSIC
CONSEJO SUPERIOR DE INVESTIGACIONES CIENTÍFICAS



UNIVERSITAT
POLITÈCNICA
DE VALÈNCIA

INTENSIFICATION OF THE METHANE DEHYDROAROMATIZATION PROCESS ON CATALYTIC REACTORS

Thesis submitted by

Raquel Zanón González

To apply for the Degree of Doctor

Supervisor

Prof. José Manuel Serra Alfaro

Valencia, March 2017

A mi madre

A David

“Si hortum in bibliotheca habes, deerit nihil”:

Si cerca de la biblioteca tienes un jardín, nada te faltará

Marco Tulio Cicerón (106 a.C. – 43 a.C.)

Table of Contents

1. Thesis outline and Objectives	17
1.1. Thesis outline	17
1.2. Objectives of the thesis	18
2. Introduction	23
2.1. Energy context	23
2.2. Utilization of natural gas	26
2.3. Aromatic hydrocarbons production	30
2.4. Zeolites as catalysts	34
2.5. Methane dehydroaromatization over Mo/zeolite catalysts	37
2.5.1. State and location of molybdenum in Mo/zeolite catalysts	42
2.5.2. The nature of carbonaceous deposits	45
2.5.3. Addition of different co-reactants on methane dehydroaromatization reaction	48
2.6. H ₂ pumping through proton-conducting ceramic membranes	52
2.7. Methane dehydroaromatization over Mo/HZSM-5 catalyst with continuous H ₂ removal or O ₂ injection	56
2.8. References	59
3. Methodology	69
3.1. Reactants	69
3.2. Zeolite preparation	69
3.2.1. ZSM-5 zeolite	69

3.2.2. MCM-22 zeolite _____	71
3.2.3. IM-5 zeolite _____	72
3.2.4. ITQ-13 zeolite _____	73
3.2.5. TNU-9 zeolite _____	74
3.2.6. Chabazite zeolite _____	75
3.2.7. ZSM-22 zeolite _____	76
3.2.8. NU-87 zeolite _____	77
3.2.9. NU-85 zeolite _____	78
3.2.10. Mazzite zeolite _____	78
3.2.11. Beta zeolite _____	79
3.2.12. Mordenite zeolite _____	80
3.3. Catalyst manufacturing process _____	81
3.3.1. Granulated catalysts _____	81
3.3.1.1. Mo incorporation to the zeolite _____	81
3.3.1.2. Shaped of the catalyst _____	82
3.3.2. Extrudated catalysts _____	82
3.3.2.1. Extrudated I catalyst _____	82
3.3.2.2. Extrudated II catalyst _____	83
3.4. BaZr_{0.7}Ce_{0.2}Y_{0.1}O₃₋₆ dense ceramic membranes manufacture _____	83
3.4.1. Electrode preparation _____	84
3.4.1.1. Mo ₂ C/Cu/BZCY72 anode _____	85
3.4.1.2. Copper anode _____	85
3.5. Characterization techniques _____	86
3.5.1. Nitrogen sorption analysis _____	86
3.5.2. Ammonia temperature programmed desorption (NH ₃ -TPD) _____	86
3.5.3. Thermogravimetric and derivative thermogravimetric analyses (TGA/DTA) _____	87

3.5.4. Temperature programmed oxidation (TPO)	87
3.5.5. X-Ray Diffraction (XRD)	88
3.5.6. ²⁷ Al MAS NMR (Magic-Angle Spinning Nuclear Magnetic Resonance)	88
3.5.7. X-Ray Photoelectron Spectroscopy (XPS)	89
3.5.8. X-Ray Absorption Near Edge Structure (XANES)	90
3.5.9. Scanning Electron Microscopy (SEM)	92
3.5.10. Elemental Analysis	93
3.5.11. Fourier Transform Infrared Spectroscopy (FTIR)	93
3.5.12. Inductively Coupled Plasma Optical Emission Spectroscopy (ICP-OES)	94
3.5.13. Gas Chromatography and Mass Spectrometry (GC-MS)	94
3.6. Catalytic evaluation of methane dehydroaromatization	95
3.6.1. Fixed Bed Reactor	95
3.6.1.1. Experimental procedure	98
3.6.1.2. Different operating conditions	109
3.6.1.2.1. Use of different co-feeding gas in the MDA reaction with the FBR	109
3.6.1.2.1.1. Co-feeding of 6% of H ₂	109
3.6.1.2.1.2. Co-feeding of H ₂ O	110
3.6.1.2.1.3. Co-feeding of 2% of CO ₂	111
3.6.1.2.2. Use of different catalyst activation on MDA reaction with the FBR	112
3.6.1.2.2.1. Pre-coking of the 6% (wt.) Mo/HZSM-5 catalyst	112
3.6.1.2.2.2. Catalyst activation with a gas mixture of CH ₄ :H ₂ , 1:4 (vol. ratio)	113
3.6.1.2.3. Catalyst regeneration with H ₂ using the FBR	113

3.6.1.2.4. Use of different space velocity and change the catalyst amount and the feed gas flow using the same space velocity (1500 mL·h ⁻¹ ·g _{cat} ⁻¹) with the FBR _____	114
3.6.1.2.4.1. Use of different space velocity with the 6% (wt.) Mo/MCM-22 catalyst _____	114
3.6.1.2.4.2. Change the catalyst amount and the feed gas flow using the same space velocity with the 6% (wt.) Mo/HZSM-5 catalyst _____	115
3.6.2. Catalytic Membrane Reactor _____	115
3.6.2.1. Catalytic Membrane Reactor with continuous H ₂ removal through BaZr _{0.7} Ce _{0.2} Y _{0.1} O _{3-δ} tubular membranes _____	116
3.6.2.1.1. Experimental procedure _____	121
3.6.2.1.2. Operating conditions of each experiment with CMR-TM _____	125
3.6.2.2. Catalytic Membrane Reactor with Quartz Tube (CMR-QT) _____	128
3.6.2.2.1. Experimental procedure _____	129
3.6.2.2.2. Different operating conditions _____	130
3.6.2.2.2.1. Use of different space velocities with the CMR-QT _____	130
3.6.2.2.2.2. Co-feeding of H ₂ using the CMR-QT _____	131
3.7. References _____	132
<i>4. Effect of the zeolite on MDA reaction _____</i>	<i>137</i>
4.1. Different HZSM-5 zeolites with 3% (wt.) of Mo _____	137
4.1.1. Effect of the Si/Al ratio _____	142
4.1.2. Effect of the crystal size _____	143
4.2. Effect of the Mo content on the best HZSM-5 _____	144

4.3. Different zeolites versus the best HZSM-5 with 3% (wt.) Mo	148
4.4. MCM-22 versus the best HZSM-5 with 6% (wt.) Mo	153
4.5. Conclusions	163
4.6. References	165
5. Effect of the catalyst activation on MDA reaction	169
5.1. 6% (wt.) Mo/HZSM-5 catalyst	169
5.2. 6% (wt.) Mo/MCM-22 catalyst	173
5.3. Conclusions	177
5.4. References	178
6. Effect of the space velocity on MDA reaction	183
6.1. Effect of the 6% (wt.) Mo/HZSM-5 catalyst amount and the feed gas flow using a space velocity of $1500 \text{ mL}\cdot\text{h}^{-1}\cdot\text{g}_{\text{cat}}^{-1}$	183
6.2. Effect of the space velocity on MDA reaction using the 6% (wt.) Mo/MCM-22 catalyst	186
6.2.1. Effect of the space velocity using the standard activation	186
6.2.2. Effect of the space velocity using the new activation	189
6.3. Conclusions	195
6.4. References	196
7. Effect of the co-feeding gas on MDA reaction	199
7.1. Effect of co-feeding H ₂ O	199
7.1.1. Thermodynamic study of co-feeding H ₂ O	199

7.1.2. Effect of co-feeding H ₂ O over 6% (wt.) Mo/HZSM-5 catalyst on MDA reaction_____	202
7.1.3. Effect of co-feeding H ₂ O over 6% (wt.) Mo/MCM-22 catalyst on MDA reaction_____	206
7.1.3.1. Effect of co-feeding 1.08% of H ₂ O after different times on stream in dry conditions for the 6% (wt.) Mo/MCM-22 catalyst _____	206
7.1.3.2. Effect of co-feeding 1.08% and 0.86% of H ₂ O over 6% (wt.) Mo/MCM-22 catalyst_____	212
7.2. Effect of co-feeding H₂ _____	225
7.2.1. Thermodynamic study of co-feeding H ₂ _____	225
7.2.1.1. Thermodynamic study of co-feeding H ₂ without and with the addition of H ₂ O _____	227
7.2.2. Effect of co-feeding 6% of H ₂ with the standard activation of the catalyst _____	230
7.2.3. Effect of co-feeding H ₂ over the 6%Mo/MCM-22 catalyst with the new activation _____	235
7.2.3.1. Effect of co-feeding different concentrations of H ₂ without and with H ₂ O addition _____	240
7.3. Effect of co-feeding CO₂ _____	246
7.3.1. Thermodynamic study of co-feeding CO ₂ _____	247
7.3.2. Effect of co-feeding 2% of CO ₂ over 6% (wt.) Mo/zeolite catalysts on MDA reaction _____	248
7.4. Conclusions_____	255
7.5. References _____	259

8. Effect of catalyst regeneration with H₂ on MDA reaction

	263
8.1. Effect of the 6%Mo/HZSM-5 catalyst regeneration with H₂	263
8.1.1. Effect of the 6%Mo/HZSM-5 catalyst regeneration with H ₂ in dry conditions	263
8.1.2. Effect of the 6%Mo/HZSM-5 catalyst regeneration with H ₂ in wet conditions	266
8.2. Effect of the 6%Mo/MCM-22 catalyst regeneration with H₂ in dry conditions	269
8.3. Conclusions	272
8.4. References	272

9. Effect of the catalyst manufacturing process on MDA reaction

9.1. Granulated catalysts obtained by different procedures: 6%Mo/HZSM-5 and 6%Mo/MCM-22	275
9.2. Extrudated catalyst obtained by a new procedure: 6%Mo/MCM-22	283
9.3. Conclusions	290
9.4. References	291

10. Effect of H₂ removal through BaZr_{0.7}Ce_{0.2}Y_{0.1}O_{3-δ} tubular membranes on MDA reaction

10.1. Effect of H₂ removal through BaZr_{0.7}Ce_{0.2}Y_{0.1}O_{3-δ} tubular membrane on MDA reaction	296
--	------------

10.2. Effect of the anode type on the BZCY72 tubular membrane on MDA reaction with H₂ removal	311
10.3. Effect of the temperature on MDA reaction with H₂ removal	317
10.4. Effect of co-feeding 10% of H₂ on MDA reaction with H₂ removal	325
10.5. Effect of the current density applied on the electrochemical cell on MDA reaction with H₂ removal	331
10.6. Conclusions	337
10.7. References	340
11. Conclusions	345
List I Figures	353
List II Tables	367
List III Abbreviations	375
Resumen/Resum/Summary	379
Scientific Contribution	387
Agradecimientos/Acknowledgements	389

Chapter 1.

THESIS OUTLINE AND OBJECTIVES

1. Thesis outline and Objectives

1.1. Thesis outline

This thesis consists of 10 chapters, of which 7 (Chapter 4 - 10) are dedicated for showing the methane dehydroaromatization (MDA) reaction and characterization results obtained. Moreover, the conclusions of these 7 chapters are summarized in Chapter 11.

Chapter 2 aims to provide an overview of different contexts concerning the energy, the utilization of natural gas, the aromatic hydrocarbons production and the zeolites as catalysts. Furthermore, this includes a literature review based on the MDA reaction under non-oxidative conditions. In particular, the Mo sites and the carbonaceous deposits in/on the catalyst, the addition of different co-reactants to the feed and the continuous H₂ removal or O₂ injection are studied. A brief review of the H₂ pumping through proton-conducting ceramic membranes is also included.

Chapter 3 is focused on the experimental work performed in this thesis, describing the different procedures employed to: synthesize the MCM-22 zeolite, prepare the different catalysts and perform the fixed bed reactor (FBR) and catalytic membrane reactor (CMR) experiments. In this chapter the characterization techniques and the zeolites used are briefly exposed. Moreover, the calculations employed in the catalytic evaluation are detailed.

In Chapter 4 a preliminary investigation about the effect of the zeolite is shown, by comparing different HZSM-5 zeolites, with different crystal sizes and Si/Al ratios. Further, the Mo content and the effect of the topology and the channel dimensions of different zeolites are also studied.

Chapters 5, 6 and 7 are focused on changing some operating conditions over the 6%Mo/HZSM-5 and 6%Mo/MCM-22 catalysts aiming to improve the stability and the MDA performance, in particular: the catalyst activation, the space velocity and the addition of H₂O, H₂ and CO₂, respectively. Additionally, Chapter 7 includes a thermodynamic study for each co-reactant added to the methane feed. The catalyst regeneration using pure H₂ is exhibited in Chapter 8 on the 6%Mo/HZSM-5 and 6%Mo/MCM-22 catalysts. Moreover, Chapter 9 shows the MDA results obtained for two Extrudated catalysts.

Chapter 10 includes the MDA results achieved using the CMR with the 6%MoMCM-22 catalyst and the electrochemical co-ionic proton and oxide ion conducting BaZr_{0.7}Ce_{0.2}Y_{0.1}O_{3-δ} (BZCY72) tubular membranes, by means of which the shift of the thermodynamic equilibrium and the suppression of part of the coke deposited are achieved.

1.2. Objectives of the thesis

Methane dehydroaromatization reaction is a promising alternative route to produce benzene under non-oxidative conditions instead of the traditional production from petroleum. However, MDA reaction presents several constraints that prevent its industrial application, i.e., the methane conversion is thermodynamically limited (~ 12%) and the catalyst rapidly deactivates through the formation of carbonaceous deposits. Taking into account these limitations, the objectives of the present thesis are focused on the improvement of the activity and the stability on MDA reaction. The specific objectives are:

- The study of different Mo/zeolite catalysts (HZSM-5 with different Si/Al ratios and crystal sizes, zeolites with different topologies and pore sizes, including the MCM-22 zeolite) and Mo contents (3 - 6%). Besides the production and use of two extrudated (6%Mo/HZSM-5 and 6%Mo/MCM-22) catalysts.

- The optimization of some operating conditions, such as: the catalyst activation, the space velocity, the addition of H₂O, H₂ and CO₂ to the methane feed and the catalyst regeneration aiming to extend the catalyst lifetime.
- The development and implementation of a catalytic membrane reactor for intensification of the MDA reaction, via the 6%Mo/MCM-22 catalyst and the electrochemical co-ionic proton and oxide ion conducting BZCY72 tubular membrane.

Chapter 2.

INTRODUCTION

2. Introduction

2.1. Energy context

Today the abundant and uninterrupted energy supply is fundamental for industrial and domestic purposes [1]. The world's total human population is over 7.2 billion nowadays and its growth is quicker than previously estimated. Recent estimates anticipate that the world population will reach 9.6 billion by 2050. Population and consumption trends will unavoidably increase the pressure on limited available natural resources, ecosystems, societies and economies, [2] being economically, environmentally and socially unsustainable. The carbon dioxide emissions related to energy will double by 2050 and the rising fossil energy demand will increase the concerns about the energy supplies. For all this, it is necessary to develop and apply energy efficiency techniques, renewable energy, carbon capture and storage (CCS), nuclear power and new transport technologies [3].

The instability of oil prices have promoted an improvement in the energy efficiency, an effort in the oil dependence reduction, as well as the development of the resources difficult or costly to utilize. Regarding the natural gas, in spite of its unstoppable worldwide expansion nowadays there is no global reference price, unlike for oil. There are three major regional markets: North America, Asia-Pacific and Europe; in each one of them the natural gas prices are set by different mechanisms. Therefore always there have been differences in price among these three major markets, owing to the different demand and supply balances and pricing systems, being those for North America market the lowest prices. Likewise the global coal market is divided in several regional markets that can be distinguished by the geography, the coal quality or the infrastructure limitations. The coal prices directly depend on the

harshness of climate policy measures and its competition with the natural gas in power generation. Despite the progress in the development and utilization of clean energy technologies and the energy efficiency improvement, this seems insufficient to reach the announced political objectives [4].

The carbon capture storage (CCS) is a promising technology to achieve the internationally agreed target of limiting average global temperature increase to 2 °C. The use of CCS technologies and the retrofit of fossil fuel plants can help to improve the economic feasibility of reaching the climate goal, especially in regions where the CO₂ storage is easier due to its geological formations. Nevertheless, though some progress has been made to develop regulatory frameworks, its deployment is being deficient and, moreover without a signal price, the technological development is too difficult. A progressive carbon reduction needs a shift to low-carbon fuels in the transport sector, although only this improvement will not be sufficient [4].

In 2013 the consumption and the production of all fuels was increased, except for nuclear power. The global consumption of the fossil fuels rose faster than the production, suggesting that the global CO₂ emissions from energy use were higher, although they were lower than the average. Global primary energy consumption increased by 2.3% in 2013, being an increase higher than in 2012 (+1.8%). This growth was due to oil, coal and nuclear power, though it was lower than the 10-years average of 2.5% (except in North America). Despite during 2013 oil was the world's dominant fuel, with 32.9% of global energy consumption, this was the fourteenth consecutive year losing market share. Emerging economies accounted for 80% of the global increase in energy consumption. While the US growth (+ 2.9%) represented all of the net increase in the OECD, the consumption in EU and Japan decreased 0.3% and 0.6%, respectively. Specifically Spain had the greater volumetric decline in energy consumption (- 5%) [5].

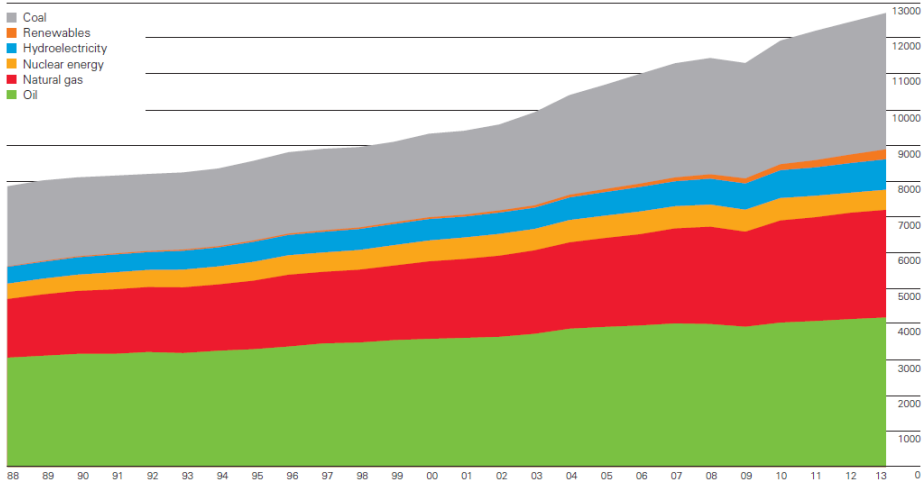


Figure 1. World primary energy consumption (Million tones oil equivalent: Mtoe) since 1988 until 2013 [5].

The non-OECD countries accounted for the 51% of global oil consumption, representing again all of the net growth. The OECD countries had an oil consumption reduction of 0.4%, being the seventh consecutive year that decreased. For the first time since 1999, in 2013 the US growth in global oil consumption surpassed the Chinese growth. Globally, natural gas accounted for 23.7% of primary energy consumption. Further, world natural gas consumption rose by 1.4%, in the OECD countries the consumption increase was higher than the average (+ 1.8%), whereas in the non-OECD countries was lower (+ 1.1%). Regarding coal, the coal's share of global primary energy consumption reached 30.1%, the highest since 1970. Nevertheless nuclear generation represented 4.4% of global energy consumption, the smallest since 1984 [5]. However ten new facilities started to be constructed during 2013, up from seven in 2012 [6]. Additionally, hydroelectric output accounted for 6.7% of global energy consumption. Finally, in 2013 the renewable energy sources, both in power generation and transport, achieved a record 2.7% of global energy consumption, up from 0.8% a decade ago. It should be noted that, worldwide, the wind energy and the solar power generation are leading this consumption

growth [5]. Nevertheless, it is necessary to keep in mind that the expected renewables growth is subject to strong regional differences, and moreover depends on policy uncertainty [6].

The chemical and petrochemical sector was by far the largest industrial energy consumer, representing about 10% of total worldwide final energy demand and 7% of global greenhouse gases (GHG) emissions. But chemical products and technologies also contribute in some way in the saving of energy. The chemical industry has a strategic role in the generation, usage and storage of energy. In addition the catalytic process advances can be used to reduce both energy consumption and GHG emissions in chemical industry. Catalysis is essential to obtain efficient production in many industrial sectors. Roughly the 90% of chemical processes use catalysts, as almost all petroleum refining processes. Furthermore the catalysts are used in daily life in different applications such as catalytic converters in cars, self-cleaning surfaces, indoor air control and laundry detergents. However, some catalysis applications affect indirectly to the energy saving or the reduction of GHG emissions [3].

2.2. Utilization of natural gas

The natural gas is a power source that competes with other fossil fuels such oil and coal. Its purity, its physical state, the simplicity of the combustion process control and its ease of transport allow to describe it as a clean and economical fuel, regarding the achieved energy yields [7]. These qualities drive the direct utilization of natural gas in homes and businesses, in centralized power generation and in some countries also in the transport sector. Additionally, the combustion of natural gas generates at least 25 - 30% less CO₂ than oil and 40 - 50% less than coal. If the natural gas is used in high efficiency applications, like gas turbine based electricity generation, the CO₂ emissions are lower [1].

The natural gas is formed by different paraffinic hydrocarbons (mainly methane and, in a lesser extent, other hydrocarbons from the ethane to the heptane) and some non-hydrocarbonated compounds (nitrogen, H₂, carbon dioxide, hydrogen sulphide, H₂O vapor and noble gases) in varying ratios. The natural gas composition varies according to its place of origin, though usually has methane content greater than 70%. Depending on the composition, the natural gas can be classified into four main groups [7]:

- *Dry natural gas*: the one with liquids content lower than 13.40 m³ per 106 m³ of natural gas.
- *Producer natural gas*: when the liquid content is between 13.40 and 40.10 m³ per 106 m³ of natural gas.
- *Wet natural gas*: if the liquid content is greater than 40.10 m³ per 106 m³ of natural gas.
- *Sour natural gas*: when the hydrogen sulphide content is significant.

Worldwide use of natural gas is highly diversified, owing to both many applications and a wide variety of technologies for each application. Among these applications, the following should be noted:

- Electric power generation, often as co-generation of electricity and heat (CHP; combined heat and power) [1]. The power generation sector will remain the main driver of gas demand in most regions, but the price of the fuel will determine the range of its use. With the New Policies Scenario the combined-cycle gas turbines (CCGTs) will be the preferential option for new power stations in many cases. Thus combining operational, economic and environmental aspects, due to the CCGTs have high thermal efficiency, relatively low cost and fast construction, are flexible to operate and its CO₂ emissions are lower than other fossil fuels-based technologies [8].

- Industrial applications such as drying, heating and mechanical drives (turbines, gas motors) as well as industrially integrated CHP.
 - Residential and commercial (heating, cooking, cooling).
 - As fuel for buses, trucks, cars, trains or ships in the form of compressed natural gas (CNG), LPG or LNG.
 - H₂ production for energy purposes (e.g. refineries).
 - Material (non-energy use, chemical industry, plastics, fertilizer, etc.)
- [1].

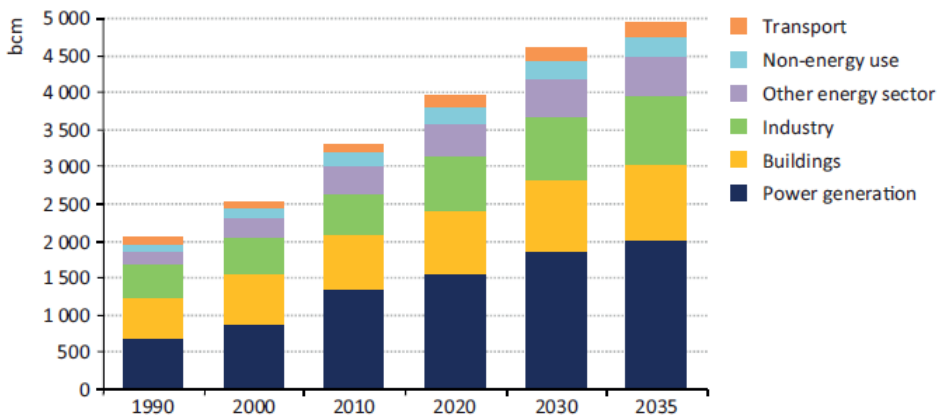


Figure 2. World natural gas demand by sector in the New Policies Scenario (“bcm” stands billion cubic meters) [8].

Nowadays methane is considered as an alternative source to synthesize products with high added value currently obtained from petroleum. Many applications of methane are hampered by its high thermal and chemical stability [9]. The greater use of natural gas is performed by making synthesis gas (syngas) containing principally H₂ and CO (carbon monoxide). Furthermore it can contain nitrogen and/or CO₂ (carbon dioxide), depending on the end use. The synthesis gas is used to synthesize organic or inorganic compounds, produce liquid fuels, reduce iron ore, generate necessary reducing atmospheres in the manufacture processes of glass and steel, etc [10]. Moreover, one of new pathways is methane dehydroaromatization over Mo/zeolite catalysts, in which

benzene and H_2 are directly obtained under non-oxidative conditions from methane (Equation 1) [9]. Besides the HZSM-5 zeolite, different zeolites were tested to improve the aromatics selectivity, HMCM-22 and HMCM-49 show similar MDA activity, higher benzene selectivity and a better tolerance to carbonaceous deposits [11].



There are two major methods for methane processing: direct conversion to products and indirect conversion, most frequently, via synthesis gas (Figure 3):

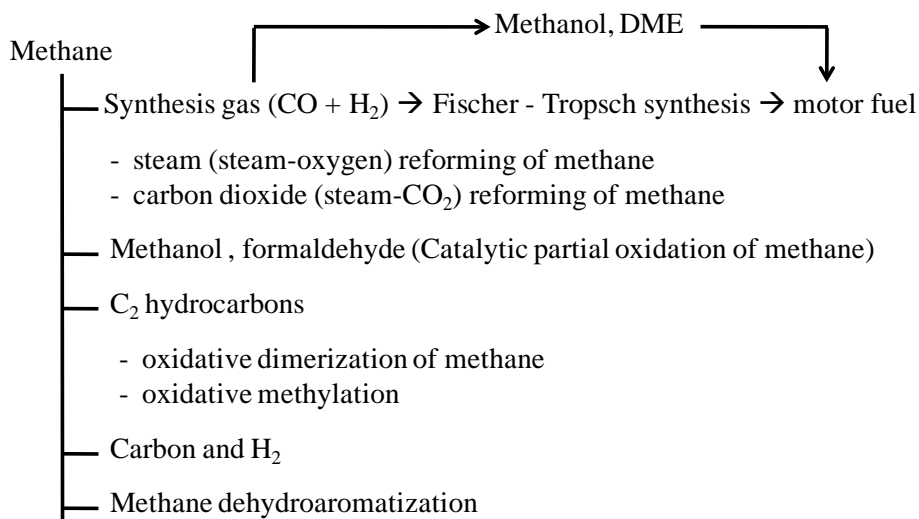


Figure 3. Main methods used for methane processing [9].

Today, the synthesis gas is the main product of methane processing and it is used in the catalytic synthesis of methanol, synthetic gasoline, diesel and DME (dimethyl ether). For example, the industrial synthesis of methanol is carried out using syngas with a ratio $CO:H_2$, 1:2, with a pressure of 200 bar and a temperature between 200 and 300 °C on alumina catalysts doped with Cu-Zn. Producing DME from synthesis gas is considered to be a promising process due to their main characteristics (productivity and conversion of synthesis gas in one

stage) are higher than those observed during the synthesis of methanol. Furthermore, a significant part of the synthesis gas is dedicated to the production of ammonia, from which many products are obtained, such as nitric acid and chemical fertilizers [9].

Among the processes of direct conversion of methane to products, (i) partial oxidation of methane to form methanol and formaldehyde, and (ii) oxidative dimerization of methane to yield ethane and ethylene are being studied intensively (Figure 3). However, so far it is not demonstrated economic benefits of none of them. The methane dehydroaromatization can be performed in both oxidative and non-oxidative conditions, but using oxidative conditions the benzene selectivity is very low ($\sim 3\%$ at $600\text{ }^{\circ}\text{C}$) due to formation of large quantities of CO and CO₂. Another example of methane catalytic conversion in one stage is its decomposition under oxygen-free conditions to H₂ and carbon filaments without impurities of CO and CO₂. This carbon can be used as catalysts support, while H₂ can be applied in fuel cells at low temperature. The process is carried out in a temperature range between 600 and 1000 °C in the presence of iron catalysts [9].

2.3. Aromatic hydrocarbons production

The aromatic hydrocarbons are present in petroleum and, as increases petroleum molecular weight the aromatic hydrocarbons proportion rises. Nevertheless, aromatic hydrocarbons without naphthene rings or alkyl-substituted derivatives are in significant quantities only in lower weight fractions of petroleum. Benzene, toluene and xylene are present in the gasoline fractions but the benzene content is lower than for the other two aromatics. Moreover in the higher weight fractions normally the rings are condensed together. The compounds with two aromatic rings are assumed that are naphthalene derivatives and those with three aromatic rings phenanthrene

derivatives, it is due to the natural origin of petroleum products. Therefore all the hydrocarbons with aromatic rings and alkyl chains and naphthenic rings within the same molecule are denominated aromatic hydrocarbons. The heavy (higher molecular weight) constituents of petroleum are formed mainly by naphthenoaromatic and naphthenic hydrocarbons [12].

Reforming is an oil refining operation that produces reformate, a high-octane gasoline blending component. Reformate contains important quantities of benzene, toluene and xylene, which makes it an important source of feedstock for the petrochemical industry. One of the byproducts of reforming is H_2 , which can itself be used in other refining processes or sold for other industrial applications. In the reforming process, heavy naphtha is used, which is the second lightest liquid stream from an atmospheric distillation column to produce reformate. In the reforming complex, a feed pre-treater removes sulfur from the reformer feed using H_2 and a desulfurization catalyst. Then the pre-treated feed is sent to the reformer reactor where a catalyst and heat are used to reform low octane naphtha into higher octane hydrocarbon molecules that are valuable gasoline blending components. The process turns straight-chain hydrocarbons into cyclic compounds while removing H_2 . The cyclic compounds have a much higher octane rating than the straight-chain feedstock and enable economic production of high-octane lead-free gasoline [12].

Thus petrochemicals are obtained mainly from petroleum but also from coal and biomass. The final products obtained from petrochemicals are part of the daily life, such as additives, solvents, fertilizers, household cleaning products, beauty products, refrigerant fluids, pesticides, anti-microbial agents, synthetic fibres, paints and inks, etc. However, around 90% of petrochemical final products come from seven petrochemicals, also known as petrochemical building blocks: ethylene, propylene and butadiene (as olefins), benzene, toluene and para-xylene (as aromatics) and methanol [13].

Among these petrochemicals ethylene is the most demanded, propylene is next due to the polypropylene production [13], and benzene is the main of the aromatics produced. These seven products are the feedstock for the production of thousands of chemical products. The worldwide benzene demand is governed by two intermediates products, ethylbenzene and cumene, roughly 70-75%. In addition ethylbenzene was the chemical product most demanded in 2014, nearly 50% of global demand, to produce mainly styrene monomer [14].

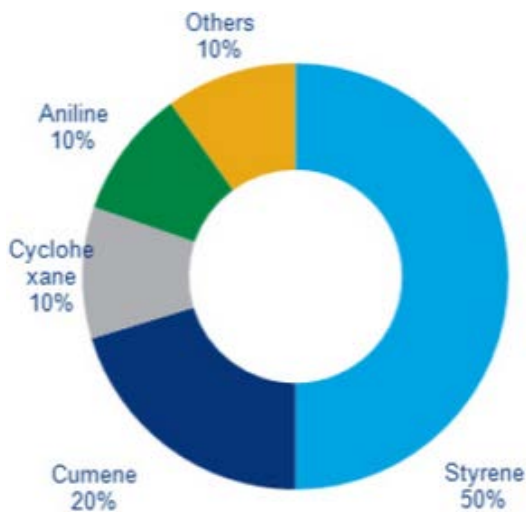


Figure 4. Global benzene demand by segment in 2014 [15].

In particular among the aromatic hydrocarbons, benzene, toluene and xylenes (BTXs) are used to produce different intermediate products as Table 1 details [16]:

Table 1. Main uses of aromatic products in 2011 [16].

Aromatics	Chemical Product	Intermediate Product	Final Product	
Xylenes	o-xylene	Phthalic anhydride, polyester polyol	Plasticizers; resins used auto parts, coatings, furniture; urethanes used in foams and insulation	
	p-xylene	Isophthalic acid	Polyamide resins used in adhesives	
	m-xylene	Terephthalic acid	Polyester fibers used in apparel; polyethylene terephthalate (PET) used in bottles, film and other products	
Benzene	Ethylbenzene	Styrene	Polystyrene (cups, insulation); styrene acrylonitrile resins (instrument lenses, houseware); styrene butadiene rubber (tires, footwear, sealants); styrene butadiene latex (carpet backing, paper coatings)	
	Cumene	Phenol	Bisphenol A, used to make polycarbonate resins (eyeglasses, containers, computers) and epoxy resins (coatings, adhesives); phenolic resins, used in plywood and other applications	
	Cyclohexane	Caprolactam	Nylon fibers and resins	
	Aniline	Isocyanates; rubber chemicals; pesticides; dyes		
	Chlorobenzenes		Pesticides, dyes	
		Benzene + xylenes		
	Toluene	Toluene diisocyanate		Urethane foams used in bedding, insulation; urethane elastomers used in footwear; urethane coatings used in varnishes, adhesives, sealants
Solvents				

In the following figure the world consumption of benzene is shown in a pie chart, it can be observed that China, USA and Western Europe present the largest benzene consumption [14]:

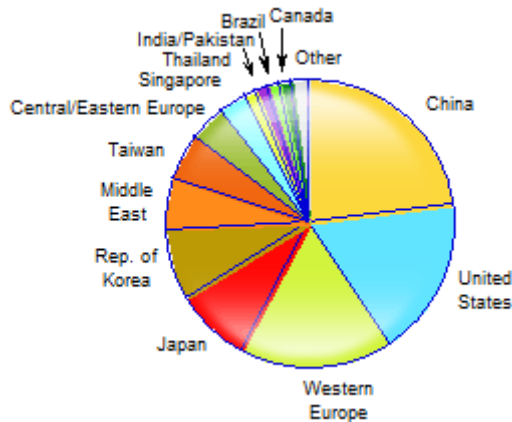


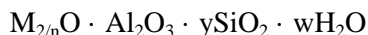
Figure 5. World consumption of benzene in 2014 [14].

2.4. Zeolites as catalysts

Zeolites were first described in 1756 by Cronstedt, a Swedish mineralogist, when he discovered a mineral (stilbite) that leaked H_2O when it was heated. He called this material *zeolite*, from Greek *zeo* (to boil) and *lithos* (stone) [17]. Nevertheless, until appearance of synthetic zeolites in the period 1948-1955, mainly due to the work performed by Barrer and Milton, these porous materials had no great relevance in catalysis. In 1962 synthetic faujasites (zeolites X and Y) were first used on an industrial scale FCC (fluid catalytic cracking) process of heavy petroleum distillates, one of the most important chemical processes worldwide [18].

Zeolites are crystalline silicates and aluminosilicates, its structure is based on a three-dimensional framework composed of tetrahedra of SiO_4 and AlO_4 which are linked together sharing their oxygen atoms [18, 19]. The connection through one oxygen between two aluminum is precluded by the

Löwensteing's rule [20]. Each AlO_4 tetrahedron in the framework bears one negative charge. The framework structure contains intracrystalline channels, channel intersections and/or cages with dimensions from 0.2 to 1 nm. Inside these channels or interconnected voids are small cations or protons and H_2O molecules which compensate the negative charge [18, 21]. Zeolites are represented by the empirical formula:



Where "M" represents the exchangeable cation, usually from the group I or II ions, though other metal, non-metal and organic cations can be utilized to balance the framework charge, 'n' is the cation valence, 'y' is ≥ 2 as Al^{3+} does not occupy adjacent tetrahedral sites and 'w' represents the H_2O contained in the voids of the zeolite [21, 22]. The cations (frequently Na^+ ions) are mobile and generally undergo ion exchange. Moreover, the H_2O can be desorbed upon heating without damage the crystalline structure. The intracrystalline channels can be one-, two- or three-dimensional. The diameter of the channels is determined by the number of tetrahedra that form it, which are denominated number of member rings (MR). The channel diameter will determine the ability of the material as a molecular sieve [18, 21]. Zeolites are usually classified according to the number of member rings of their channels/pores [21]:

- *Small pore zeolites*: 8 MR, with pore diameters of 3 to 4.5 Å (A, ferrierite, chabazite).
- *Medium pore zeolites*: 10 MR, with pore diameters of 4.5 to 6 Å (ZSM-5, MCM-22).
- *Large pore zeolites*: 12 MR, with pore diameters of 6 to 8 Å (Beta, Mordenite, Y).
- *Extra-large pore zeolites*: 14 MR, with pore diameters up to 10 Å (UTD-1, CIT-5).

The zeolites are tridimensional networks of well-defined micropores, which can act as reaction channels. The activity and selectivity of these channels will increase with the introduction of active sites. Within the pores of the zeolite there are strong electric fields and controllable adsorption properties producing a unique type of catalyst. Zeolites are useful catalysts in a wide range of reactions, from acid to base and redox catalysis, and they have the following properties [19]:

- High surface area.
- Pores or channels with molecular dimensions.
- High adsorption capacity.
- Separation of reactant/products.
- The electronic properties of the active sites can be modified.
- The molecules can be pre-activated when they are inside the pores by strong electric fields and molecular confinement.

One of the most significant properties of the zeolites is their surface acidity that is directly related to the Brønsted acid sites and the Lewis acid sites. The former are bridging hydroxyl groups that consist of a proton and a framework oxygen in an AlO_4 tetrahedron, and the latter are formed from the Brønsted acid sites dehydroxylation after heat treatment (≥ 500 °C) with water splitting. Thus, the Brønsted acidity is strongly related to the framework aluminum (tetrahedral). Moreover three types of shape selectivity of the zeolites can be defined [18]:

- *Reactant shape selectivity*: the penetration of reactant molecules inside the channels is facilitated or prevented.
- *Product shape selectivity*: the diffusion of the least large products is facilitated, whereas the diffusivity of bulky products is greatly reduced.
- *Restricted transition state shape selectivity*: in this case, the cavity of the zeolite allows a specific geometrical arrangement of the reactants in

their closeness, allowing the selective formation of a specific intermediate transient product, which leads to the formation of a particular final product.

2.5. Methane dehydroaromatization over Mo/zeolite catalysts

The direct conversion of methane to fuels and high-value petrochemical products still remains one of the major challenges in the field of heterogeneous catalysis. Since 1993 when Prof. Wang and its group [23] published for the first time the formation of benzene over Mo/HZSM-5 catalysts, the methane dehydroaromatization (MDA) under non-oxidative conditions has focused many researches. In addition to aromatics, H₂ is obtained in the MDA process, which can be use for fuel cells or other industrial uses.

Nevertheless, it is known that the MDA process has different constraints that complicate its commercialization. One of them is the limitation by thermodynamics, as the equilibrium methane conversion is about 12% to an almost equimolar mixture of benzene and naphthalene in typical conditions for MDA (700 °C and atmospheric pressure) [24]. The other great limitation is the deactivation of the catalyst with the time on stream due to the formation of heavy carbonaceous deposits on the catalyst surface. These deposits are formed by consecutive reactions of primary aromatics on both molybdenum carbide species and Brønsted acid sites of the zeolite [25, 26]. This has led to research intensively the acid sites of the zeolite and the molybdenum species.

Over the past two decades many Mo-zeolite catalysts had been tested in this reaction, Zhang et al. [27] studied different catalysts prepared using HZSM-5, HZSM-8, HZSM-11, HBETA, HMCM-41, HSAPO-34, HMOR, HX, HY, HSAPO-5, HSAPO-11, with 3% (wt.) of molybdenum (Mo) and Si/Al = 25. Catalysts made with HMCM-41 and HSAPO-34 shown low activity in MDA

reaction, whereas those prepared with HMOR, HX and HY had low methane conversion and the products obtained were C₂ hydrocarbons and CO. No hydrocarbon products were observed over Mo/HSAPO-5 and Mo/HSAPO-11 catalysts. The best results in MDA performance were obtained with the catalysts prepared using HZSM-5, HZSM-8 and HZSM-11 zeolites. Moreover, different Mo-supported catalysts were studied on MDA reaction using as the base materials FSM-16, SiO₂, Al₂O₃ [28], HMCM-22 [29], HMCM-49 [30], HMCM-36 [31], ITQ-2 [32], ITQ-13 [33], HMCM-56 [34], IM-5 [35] and TNU-9 [36].

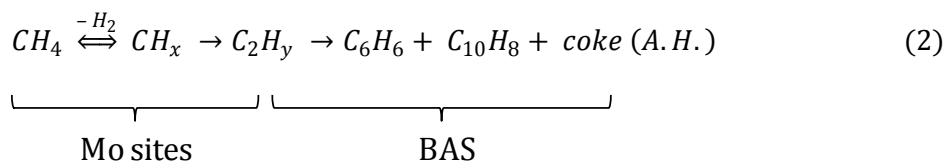
The HZSM-5 and HMCM-22 zeolites have a pore aperture of 10 member rings (10 MR) and, therefore, are close to the kinetic diameter of benzene molecule, around 5 Å [37]. The HZSM-5 zeolite has a three-dimensional channels system that consists of two types of intersecting straight (5.3 x 5.6 Å) and zig-zag (5.1 x 5.5 Å) channels without large cavities. While the HMCM-22 zeolite has a unique pore structure with two independent pore systems: a smaller 2D (two-dimensional), with an aperture of 10 member rings (10 MR), sinusoidal pore system (4.1 x 5.1 Å), and a larger 3D (three-dimensional), with an aperture of 12 member rings (12 MR), super cage system interconnected by 10 MR windows (4.0 x 5.5 Å) [38]. This pore structure and the super cages presence are the responsible for the high coke accumulation capacity of HMCM-22, besides its shape selectivity. Therefore, the selectivity to benzene and the catalyst stability improve with this zeolite.

Lunsford et al. [39] studied different transition metal ions (TMI): Mo, W, Fe, V and Cr, varying the TMI content between 2-4% (wt) over HZSM-5 zeolite. They confirmed that Mo is the best for the performance of MDA reaction among these TMI. Ichikawa and co-workers [40] showed that 5% (wt.) Re/HZSM-5 catalyst is also a good catalyst for MDA and introduced 0.5% (wt.) of Co to 5% (wt.) Re/HZSM-5 catalyst. Bao and co-workers [29] investigated

different Mo contents 2, 4, 6, 8 and 10% (wt) over HMCM-22 zeolite, obtaining the highest benzene yield with 6% (wt.) Mo/HMCM-22 catalyst. Moreover Mn [41] and Co-Ga [42] were tested over HZSM-5 zeolite, as well as 6% (wt.) Mo over HZSM-5 [43, 44] and over HMCM-22 and 10% (wt.) Re [44] over both zeolites HZSM-5 and HMCM-22. In order to improve the Mo/HZSM-5 and Mo/HMCM-22 catalysts different TMI had been added as promoters, among them are: Fe [45, 46], Co [45, 46], Pt [47], Rh [47], Pd [46, 48], Ir [48], Cu [46, 49], Zn [46, 49], Cr [46], Mn [46] and Ru [46, 50]. Briefly, the benzene formation rate and the methane conversion were slightly increased on the 1% (wt.) Fe or 1% (wt.) Co-modified 3% (wt.) Mo/HZSM-5 [45]; the coke selectivity was lower over Pt-Mo/HZSM-5 catalyst than over Rh-Mo/HZSM-5, therefore Pt is more effective than Rh for hydrogenation of carbonaceous species [47]; and 0.5% (wt.) Pd and 0.5% (wt.) Ir-modified 6% (wt.) Mo/HZSM-5 catalysts enhanced the ethylene selectivity [48].

Furthermore, Chen et al. [51] tested different contents of Li and P on 2% (wt.) Mo/HZSM-5 catalyst and both were detrimental for the MDA performance since the catalyst activity was reduced, specially for Li.

It is widely accepted that the Mo/zeolite catalyst is bifunctional in methane dehydroaromatization with the participation of both Mo sites and Brønsted acid sites [24, 28, 52-54]. Methane is activated in Mo sites, which are responsible for methane dehydrogenation and formation of CH_x species. Then, the products of their dimerization C_2H_y oligomerize on the Brønsted acid sites (BAS) of the zeolite to form benzene and naphthalene mainly. The mechanism of methane dehydroaromatization proposed by Ohnishi et al. [45] is as follows:



The ethylene is considered by most authors [53, 54] as an intermediate of the MDA reaction. The major hydrocarbons produced are benzene (the main aromatic product), naphthalene and toluene as aromatics and C₂ hydrocarbons such as ethylene and ethane. The other carbon containing products, such as CO, methyl-naphthalene, phenanthrene, fluorene and indene are only produced in trace amounts. The following simplified reactions occur in MDA:



Many researchers have observed that the Mo introduction in the HZSM-5 and HMCM-22 zeolites followed by the calcination reduces both the surface area and the pore volume. This effect is stronger when the Mo loading is increased, since the large molybdenum oxide crystals block the zeolite channels [29, 51].

It is well known that the Si/Al ratio is directly related to the concentration and strength of Brønsted acid sites of zeolites and it can be varied in a wide range depending on the zeolite type. For instance, Liu et al. [28] tested eight HZSM-5 zeolites with different SiO₂/Al₂O₃ ratios from 24 to 1900 in the 3% (wt.) Mo/HZSM-5 catalyst. The best MDA performance was achieved by the catalyst with SiO₂/Al₂O₃ ratio of 39.5 (Si/Al ~ 20), in coincidence with the maximum Brønsted acidity for the HZSM-5 zeolite with the same Si/Al ratio. Thus, it was demonstrated the great dependence between the catalytic MDA performance and the Brønsted acidity. Furthermore, the same dependence was observed for the HMCM-22 zeolite [55] in a study carried out over the 6% (wt.) Mo/HMCM-22 catalyst with five different SiO₂/Al₂O₃ ratios. In this case, the

best MDA results were obtained for the catalyst with SiO₂/Al₂O₃ ratio of 25 (Si/Al ~ 12.5), being this Si/Al ratio with which the maximum Brønsted acidity was reached for the HMCM-22 zeolite. Thus, merely framework aluminum contributes to Brønsted acid sites.

Additionally, the influence of the zeolite crystal size on the MDA performance was studied by Zhang et al. [56] over Mo/HZSM-5 catalysts. They obtained that both methane conversion and benzene selectivity were higher on the HZSM-5 with 1000 nm than on the HZSM-5 with 70 nm. In accordance with the multinuclear solid-state NMR data, the formation of aluminum molybdate (Al₂(MoO₄)₃) happened easily on the catalyst prepared with the zeolite with 70 nm, which caused the aluminum extraction of the framework. Moreover, on this zeolite the Mo was located predominantly on the external surface, reducing thereby the shape selectivity.

Regarding the space velocity used during the experiments, Shu et al. [29] concluded that the maximum benzene yield was obtained with a weight hourly space velocity (WHSV) of 1500 mL·h⁻¹·g_{cat}⁻¹ over the 6% (wt.) Mo/MCM-22 catalyst at 700 °C. Since the methane dehydroaromatization was extremely slowed by its products, as these were strongly adsorbed being their diffusion very slow. Probably this is because of the methane was struggling with the other hydrocarbons for the active sites. Furthermore, Ma et al. [57] found that on the 6% (wt.) Mo/HZSM-5 catalyst at 750 °C using high space velocities, it was deactivated quickly and the total benzene and H₂ formation amounts were increased until 5400 mL·h⁻¹·g_{cat}⁻¹. However, over 4.5% (wt.) Mo/HZSM-5 catalyst at 725 °C [58] a higher and more stable benzene yield was obtained with a space velocity of 1000 mL·h⁻¹·g_{cat}⁻¹. Further, the temperature at which the experiments were performed affects the results significantly, as at 800 °C the catalyst was rapidly deactivated and at 700 °C the benzene yield was the most stable throughout the time on stream (TOS).

2.5.1. State and location of molybdenum in Mo/zeolite catalysts

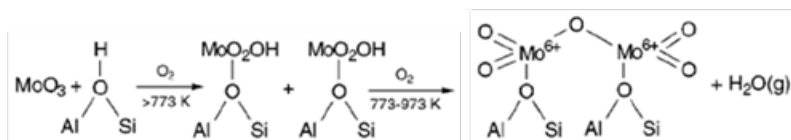
The state and location of Mo in the zeolite have been investigated intensively. The incipient wetness impregnation method has been widely used to prepare the Mo/zeolite catalysts, using ammonium heptamolybdate, $(\text{NH}_4)_6\text{Mo}_7\text{O}_{24}\cdot 4\text{H}_2\text{O}$, as the source of Mo. Xu et al. [59] applied FT-IR spectroscopy to characterize the Mo species after the zeolite impregnation with ammonium heptamolybdate (AHM) solution. They showed that Mo remained in the form of AHM on the zeolite surface after drying in air at 120 °C. Furthermore, when the catalyst was calcined at 300 °C the AHM crystallites were decomposed to MoO_3 , and after calcining at 500 °C part of the MoO_3 migrated into the zeolite channels. In the catalysts with high Mo content (10% (wt.)) at higher calcination temperature (700°C), aluminum molybdate ($\text{Al}_2(\text{MoO}_4)_3$) was formed in addition to MoO_3 . Therefore, the extraction of framework aluminum rose with increasing Mo loading and calcination temperature. They also done NH_3 -TPD measurements of Mo/HZSM-5 catalysts and observed that Mo species interacted with the Brønsted acid sites because these acted as powerful traps. Ma et al. [60] reinforced these results with ^{27}Al MAS, ^{29}Si MAS and ^1H MAS NMR experiments on fresh and used Mo/HMCM-22 catalysts. The ^{27}Al MAS and ^{29}Si MAS experiments demonstrated that Mo inside the zeolite channels reacted preferably with bridging hydroxyls groups and it was anchored to the framework aluminum via bridging oxygen atoms. Nevertheless, as the Mo content increases this interaction became stronger causing the removal of aluminum from the zeolite lattice and the formation of octahedral extra-framework aluminum and $\text{Al}_2(\text{MoO}_4)_3$ crystallites. In addition, both the ^{27}Al MAS and the ^1H MAS spectra indicated that Mo was better distributed into the channels of MCM-22 zeolite than in the HZSM-5, since it reacted mainly with Brønsted acid sites

(framework aluminum). Whereas, in the ZSM-5 zeolite the Mo interacted preferentially with silanol groups located on the external surface.

Iglesia and co-workers [61-63] used different technologies to characterize the structure of Mo species over Mo/HZSM-5 catalyst prepared mixing MoO₃ and HZSM-5 physically, including XANES, ²⁷Al MAS NMR, Raman spectroscopy, TPO and TPR. Their results revealed that below 350 °C MoO₃ and HZSM-5 crystallites were not affected; but between 350 °C and 500 °C, the MoO_x species spread over external zeolite surface forming a MoO₃ monolayer, and these species also migrated into the zeolite channels. If Mo loading was higher than that necessary to form a MoO₃ monolayer (~4% (wt.)), the MoO_x species could sublime as (MoO₃)_n or react with Al present in the zeolite framework to form Al₂(MoO₄)₃. Moreover, between 500 and 700 °C, the MoO_x species migrated into the zeolite channels via gas-phase and surface transport and within the channels reacted with the Brønsted acid sites. They suggested that after exchange each Mo ion replaced one H⁺ in the zeolite. However, Tessonier et al. [64] through the titration of the Brønsted acid sites via H₂O/D₂O isotope exchange found that the density of acid sites in the zeolite is directly related to the bonding mode of the Mo species inside its channels. Thus obtaining that each Mo ion substituted two H⁺ in a HZSM-5 zeolite with a Si/Al ratio of 15. While for a HZSM-5 zeolite having a Si/Al = 40, only one H⁺ is replaced by each Mo ion. These results were confirmed by Gao et al. [65] by *in situ* Raman spectroscopy.

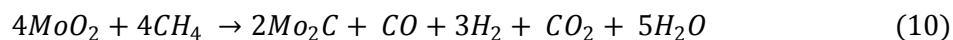
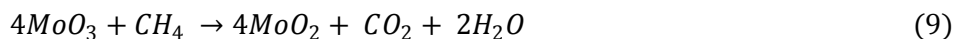
Iglesia and co-workers [61] proposed that the Mo species had a ditetrahedral structure based on (Mo₂O₅)²⁺ interacting with two zeolite exchange sites (Equation 8). The stoichiometry of these intermediate Mo species (Mo(=O)₂(OH)⁺) was verified and identified as the Mo species formed when the Mo oxide interacted with a single Al framework. While when the Mo oxide

species were connected with acid sites with two Al atoms, the Mo species formed were $\text{Mo}(=\text{O})_2^{2+}$ [65].



(8) [61]

The $(\text{Mo}_2\text{O}_5)^{2+}$ species are reduced and carburized to MoC_x during the initial stages of CH_4 conversion to hydrocarbons under non oxidative conditions, being the active sites for the activation of C-H bond [61]. According to previous studies [24, 52] there is an induction period (about 1 h) in the first stages of the MDA over Mo/zeolite catalyst during which the MoO_3 (Mo^{6+}) is reduced by methane to Mo_2C , forming CO, H_2 , CO_2 , H_2O and carbonaceous deposits. The reduction of MoO_3 occurs in two stages agree with the results obtained by TPSR [66], firstly MoO_3 is reduced to MoO_2 and then the latter is carburized to Mo_2C as follows:



Moreover, the shift of MoO_3 to Mo_2C is easier on H_2 -pre-reduced catalysts, but this pre-reduction process will not prevent the induction period [66]. Ma et al. [67] determined by EPR that three different types of Mo species exist in/on Mo/HZSM-5 catalyst. The Mo species located on the external surface are both octahedral-coordinated MoO_3 crystallites and square-pyramidal coordinated MoO_x . The other Mo species are located within the zeolite channels and they are combined with the Al in the zeolite lattice, in two different locations. The authors suggested that Mo_2C is found on external surface, whereas inside the zeolite channels the Mo species associated with Al (Brønsted acid sites) are partial reduced. Liu et al. [68] verified these results and concluded that the Mo species combined with the Brønsted acid sites are key in

the MDA reaction, as they are more stable and active than the other Mo species. These conclusions were reinforced through the use of Ultrahigh Field ^{95}Mo NMR spectroscopy [69, 70], with which was demonstrated that the carburized Mo species associated with the Brønsted acid sites are the active centers for the MDA reaction. Furthermore, Liu et al. [71, 72] revealed that the Mo species partially reduced into the zeolite channels, likely were MoO_xC_y species in a hexagonally close packed (hcp) structure. Nevertheless, when the Mo/HZSM-5 catalyst is undergone a pre-reduction with H_2 the hcp turns into a fcc (face centered cubic) structure, being the latter species more stable and active than those with hcp structure. This topotactic transformation experimented by MoC_x species was firstly described by Lee et al. [73] using 20% of CH_4 in H_2 . Furthermore, some researchers carried out a pre-reduction treatment of the Mo/zeolite catalyst with H_2 [71, 72] and CO [24, 26], and pre-carburization by a $\text{CH}_4:\text{H}_2$ (1:4) gas mixture [53, 57] aiming to improve the subsequent MDA performance. Weckhuysen et al. [26] showed that the pre-reduction with CO at 700 °C did not affect the results obtained. While the pre-treatment with H_2 [71, 72] and $\text{CH}_4:\text{H}_2$ (1:4) gas mixture [57] was positive for the MDA performance due to the topotactic transformation abovementioned that suffer the MoC_x species.

2.5.2. The nature of carbonaceous deposits

The carbonaceous deposition on the Mo/zeolite catalysts during the MDA reaction is inevitable and, moreover, it is increased with the reaction temperature [51]. It may be said that three types of coke can be differentiated on the Mo/HZSM-5 catalyst after MDA reaction, according to the XPS [26, 53], TPO [72, 74] and ^{13}C CPMAS NMR [75] data: carbide-like carbon, pre-graphitic-like carbon and graphitic-like carbon. The same applies to the Mo/HMCM-22 catalyst after MDA reaction as showed by Bao and co-workers [76, 77].

Briefly, the XPS spectra in C 1S region [26] of 2% (wt.) Mo/HZSM-5 catalyst underwent MDA at 700 °C for 13 h revealed that the species characterized by a BE of 284.6 eV are attributed to graphitic-like carbon and are mainly located inside the zeolite channels; the species with a BE of 282.7 eV are due to carbide-like carbon and are mostly present on the external zeolite surface; and the species with BE of 283.2 eV are due to H₂-poor sp-type pre-graphitic-type carbon principally located on the external surface. The authors proposed that the sp-type carbon is responsible for the catalyst deactivation during MDA. Regarding the TPO profiles [72] of 6% (wt.) Mo/HZSM-5 catalyst underwent MDA at 700 °C for 1 h, it is observed that three peaks appear at 459, 511 and 558 °C, respectively. The carbonaceous deposits which burn at high temperatures (in this case above 527 °C) are associated with the Brønsted acid sites of the zeolite, while those that burn at lower temperatures are located on the Mo sites. The carbonaceous species which burn at 459 °C are associated with the Mo carbide species at the external surface and those that burn at 511 °C are located inside the channels of the zeolite with the Mo species. However, Ding et al. [74] showed that for 4% (wt.) Mo/HZSM-5 catalyst underwent MDA at 677 °C for different times on stream in the TPO profiles can be observed three different peaks. A peak at 257 °C, which after 1 h of reaction disappears, is related to the carbide-like carbon associated with MoC_x; a peak at 472 °C, that appears in all the reaction times tested, is due to carbonaceous deposits inside the zeolite channels close to the Mo species; and a peak at 547 °C, which appears after 0.3 h of reaction, is due to carbonaceous species far off the previous Mo species. Moreover, the ¹³C CPMAS NMR spectra [75] of Mo/HZSM-5 catalyst underwent MDA at 700 °C for 6 h showed that two bands appear: one of them between 10 and 40 ppm due to the carbonaceous deposits associated with the Brønsted acid sites of the zeolite and the other band at 130 ppm is related to the Mo sites.

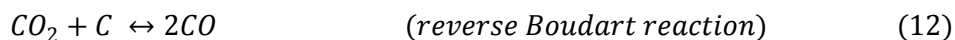
In addition, Ma et al. [76] found that for 6% (wt.) Mo/HMCM-22 catalyst underwent MDA at 700 °C for different times on stream in the TPO profiles it can be observed at least three different kinds of carbonaceous deposits. Only in the TPO of the catalyst after 10 min of MDA reaction a peak near 277 °C appears due to the carbide-like carbon in molybdenum carbide. At higher times on stream there are only two peaks: a peak at 421 °C and a peak at higher temperature than 527 °C. The former is due to the carbon related to Mo species and the latter is associated with the Brønsted acid sites. They concluded that after longer reaction times the Mo-associated coke will cover the molybdenum carbide species. Therefore, in TPO profiles of catalysts which have been used in MDA reaction for more than 10 min only one peak below 527 °C can be detected. Thereby the peak corresponding to the carbide-like carbon from molybdenum carbide species is buried in the peak corresponding to the Mo-associated coke [76]. However, in spite of the successive and uninterrupted deposition of carbon species on the Mo₂C species, the methane keeps on being activated on them. Therefore, the catalyst deactivation is mainly due to the aromatic-type coke on the zeolite acid sites [66].

Furthermore, Ma et al. [76] carried out several TP hydrogenation and subsequent TPO experiments over the 6% (wt.) Mo/HMCM-22 catalyst after 6 h of MDA reaction. They observed that the Mo-associated coke decreases about 60% and the aromatic-type coke related to Brønsted acid sites near 90%, transformed mainly into methane and lesser extent into ethylene, and a trace amount into benzene. After the TPH the activity of the catalyst is almost totally regenerated, thus the aromatic-type coke is likely the main responsible of catalyst deactivation.

2.5.3. Addition of different co-reactants on methane dehydroaromatization reaction

Different co-reactants have been added to methane feed aiming to improve the stability of Mo/zeolite catalyst in MDA reaction such as CO [45, 58, 78, 79], CO₂ [45, 58, 78-82], H₂O [58, 83, 84], H₂ [79, 84, 85], C₂H₄ [58] and C₂H₆ [58, 86-88]. The results obtained adding CO to methane feed are contradictory. On one hand, Iglesia and co-workers [79] suggested that 1% CO is inert in the MDA reaction at 677 °C on 4% (wt.) Mo/HZSM-5 catalyst. Nevertheless, Ichikawa and co-workers [45, 78] concluded that the addition of 1.8, 4 and 12% (v/v) of CO to methane feed at 700 °C on 3% (wt.) Mo/HZSM-5 enhances the formation rate of aromatic hydrocarbons and reduces the formation rate of C₂ hydrocarbons. Moreover Skutil et al. [58] showed that adding 8.5 % of CO to the feed on 4.5% (wt.) Mo/HZSM-5 at 725 °C the catalyst stability was increased.

The effect of CO₂ addition to the methane feed is assumed that is helpful to enhance the catalyst stability. Ohnishi et al. [45] observed that the addition of 1.6 % of CO₂ in MDA reaction at 700 °C and 1 bar on 3% (wt.) Mo/HZSM-5 catalyst increased the methane conversion and the formation rate of the aromatic hydrocarbons, while the formation rate of C₂ hydrocarbons was reduced. In this case no CO₂ was detected at the outlet of the reaction, but CO was observed. This is probably because CO₂ reacts with CH₄ or C to form CO and H₂ by the methane reforming reaction (Equation 11) or reverse Boudart reaction (Equation 12). Moreover, they showed that with higher CO₂ concentrations (> 4%) the aromatics hydrocarbons are greatly inhibited and CO and H₂ are increased.

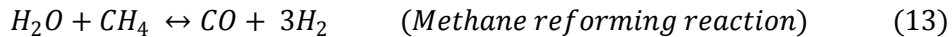


The stabilizing effect of CO₂ on the 6% (wt.) Mo/HZSM-5 catalyst in MDA reaction depends on different operation conditions: pressure, temperature, CO₂ concentration in the methane feed and space velocity [80]. First of all, the effect of the pressure on MDA reaction with and without CO₂ is significant. At 700 °C and 1350 mL·h⁻¹·g_{cat}⁻¹ without CO₂ in the methane feed, the benzene formation rate is high at lower pressures (between 0.28 and 1 bar) and lower reaction time but with time on stream it is attenuated. At 5 bar the benzene formation rate is reduced, while at 2 and 3 bar the benzene formation rate from the 3rd h of reaction is higher and more stable with time. However, when 5% of CO₂ is added to the methane feed at 800 °C and 2700 mL·h⁻¹·g_{cat}⁻¹, the optimum pressure is 3 bar. Secondly, without the CO₂ addition to the methane feed at temperatures higher than 700 °C, the catalyst is quickly deactivated. Nevertheless, by co-feeding 3% of CO₂ at 3 bar and 2700 mL·h⁻¹·g_{cat}⁻¹, the benzene formation rate is clearly enhanced when the temperature is increased from 700 °C until 775 °C, but at 800 °C and from the 3rd h on stream the benzene formation rate declined. Moreover, when the CO₂ concentration in the methane feed is increased to 5%, the benzene formation rate was more stable. At higher space velocities than 1350 mL·h⁻¹·g_{cat}⁻¹ the benzene formation rate increased during the first 3 h on stream, but then is faster decreased with time on stream. Finally, as seen from the TPO results, the CO₂ addition to the methane feed reduced the coke formation and moreover increased the H₂ content in the coke, thus preventing coke from becoming inactive graphitic-like carbon since it reacts previously with CO₂ [80].

Furthermore, Liu et al. [79] pointed out that the depletion of catalytic activity is reached during MDA reaction on 4% (wt.) Mo/HZSM-5 catalyst at 677 °C and 1 bar using a CO₂ concentration higher than 6%, because the active MoC_x species became inactive MoO_x species. The CO₂ concentration required to stop the catalytic activity depends on the temperature and the methane concentration in the feed. The detrimental CO₂ concentration is higher as the

applied temperature increases, and the harmful CO₂ concentration is lower as the CH₄ concentration decreases.

Regarding the addition of H₂O to the methane feed in MDA reaction, the benzene formation rate at 725 °C and 3 bar on 6% (wt.) Mo/HZSM-5 catalyst only was improved with the addition of 1.7% of H₂O. For 2.2% of H₂O the result obtained was very similar to that achieved without H₂O and with the addition of 2.6% of H₂O was decreased significantly. While the benzene formation rate at 800 °C with these three H₂O vapor concentrations decreased sharply. At 750 °C and 1.7 and 2.2% of H₂O the benzene formation rate was higher and more stable than with 0 and 2.6% of H₂O and with the other two temperatures used. Moreover, with the addition of H₂O to the methane feed both CO and H₂ increase their presence in the reaction products due to the methane reforming reaction (Equation 13) and other reactions that take place [83, 84]:



The TPO results showed that the coke on the 6% (wt.) Mo/HZSM-5 is reduced effectively with the addition of H₂O to the methane feed. ²⁷Al MAS NMR data indicated that for catalysts tested at 750 °C, after 22 h of MDA reaction, the aluminum remains in framework locations up to 2.2% of H₂O. However, at higher H₂O vapor concentrations the aluminum migrates to extra-framework locations, being this the reason for the abrupt decay of the activity using 2.6% of H₂O. Moreover, the Mo K-edge XAFS (X-ray Absorption Fine Structure) data obtained on the catalyst undergone MDA with 2.6% of H₂O at 750 °C and 3 bar and different times on stream revealed that for longer TOS part of the Mo-Mo bonds (present in Mo₂C) are transformed in Mo-O bonds [83].

The addition of H₂ to the methane feed was tested by Ma et al. over 6% (wt.) Mo/HZSM-5 catalyst at 750 °C, 3 bar and 2520 mL·h⁻¹·g_{cat}⁻¹, they used 3.6, 6 and 9% of H₂. The benzene formation rate was higher and more stable with the addition of 3.6 and 6% of H₂ after 5 h of reaction. This decrease in the product yield for the first 5 h of reaction is due to thermodynamic shortcomings. Even so, they concluded that the addition of H₂ in low concentrations to the methane feed is helpful to reduce the coke formation on the catalyst, mainly the coke associated with the Brønsted acid sites of the zeolite [85]. Nevertheless, the addition of high concentrations of H₂ virtually eliminates the methane conversion due to the equilibrium shift [84].

The co-addition of 5.4 % of H₂ and 1.8% of H₂O to the methane feed on 6% (wt.) Mo/HZSM-5 catalyst at 750 °C, 3 bar and 3000 mL·h⁻¹·g_{cat}⁻¹ [84] improved the removing of coke when compared with single H₂ or H₂O addition, and therefore the stability of the catalyst was higher. Moreover the coke related to the Brønsted acid sites of the zeolite was suppressed more successfully by the addition of 5.4% of H₂ than by the addition of 1.8% of H₂O, pointing out that the way of coke elimination is different among H₂ and H₂O. In spite of use of a high H₂O vapor concentration (2.6%), the simultaneous addition of 6% of H₂ reduced slightly the negative effect abovementioned of excess H₂O on catalyst activity. Liu et al. [83] through equilibrium calculations concluded that C and Mo₂C are unstable in the same extent in the presence of H₂O and CO₂, but C is much less stable (~1000 times) than Mo₂C in the presence of H₂.

Several authors added C₂H₄ [58] or/and C₂H₆ [58, 86-88] into the methane feed in MDA reaction over Mo/HZSM-5 catalyst to try increase the benzene formation rate. Skutil et al. [58] reported an increase in the benzene yield with the addition of 1% of C₂H₆, or 2% of C₂H₄, and with the two co-reactants in the same experiment, over 4.5% (wt.) Mo/HZSM-5 catalyst at 725 °C and 1500 mL·h⁻¹·g_{cat}⁻¹. Chu et al. [86] also obtained higher benzene

formation rate over 6% (wt.) Mo/HZSM-5 catalyst at 725 °C, 3 bar and 2700 mL·h⁻¹·g_{cat}⁻¹ by adding C₂H₆ to the methane feed, from 2.8 up to 6.3%. For higher C₂H₆ concentrations the catalytic activity declined sharply. They suggested that among methane and C₂H₆ exist a synergy that favors the MDA performance, as the C₂H₆ is activated easier than the CH₄ and, therefore, this facilitates the subsequent reaction between these activated C₂H₆ species and CH₄.

2.6. H₂ pumping through proton-conducting ceramic membranes

Some oxides, typically with perovskite-type structure with a general formula ABO₃, show protonic conduction at high temperatures. A-site can be either M⁺ (Na, K, etc.), M²⁺ (Ca, Sr, Ba, etc.), or M³⁺ (La, Fe, etc.) and the B-site can be occupied by M⁵⁺ (Nb, W, etc.), M⁴⁺ (Ce, Zr, Ti, etc.), or M³⁺ (Mn, Fe, etc.).

These proton-conducting oxides are devised to have oxide ion vacancies through the partial replacement of the B-site tetravalent cations for trivalent ones. For instance, a common proton-conducting oxide is SrCe_{0.95}Yb_{0.05}O_{3-δ} that is a solid solution based on the perovskite-type oxide SrCeO₃, in which 5% of Ce is replaced by Yb. The general formula is AB_{1-x}M_xO_{3-δ}, where M is a lower-valent cation and δ is the oxygen deficiency per unit formula [89]. The perovskite-type oxides possess the highest proton conductivities, in particular yttrium-doped barium cerate and zirconate exhibit the highest bulk proton conductivities, in the range of 0.01 S·cm⁻¹ at 600 °C in wet atmospheres [90].

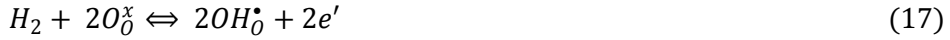
The cerates-based ceramics show higher proton conductivity than zirconates, but the latter have greater chemical and mechanical strength, besides barely react with acid solution and they are stable versus CO₂ [91]. One way to resolve these disadvantages is the synthesis of a solid proton conductor

combining both the higher chemical stability of the zirconates and the higher conductivity of the cerates [92]. Thus, the solid solutions of barium zirconate and barium cerate possess both a proper protonic conductivity and enough chemical and thermal stability. For instance, $\text{BaCe}_{0.9-x}\text{Zr}_x\text{Nd}_{0.1}\text{O}_{2.95}$ for $0.1 \leq x \leq 0.6$ [93], $\text{BaCe}_{0.9-x}\text{Zr}_x\text{Gd}_{0.1}\text{O}_{2.95}$ for $0 \leq x \leq 0.4$ [93] and $\text{BaCe}_{0.9-x}\text{Zr}_x\text{Y}_{0.1}\text{O}_{2.95}$ for $0 \leq x \leq 0.9$ [94], in which Nd, Gd and Y are used as trivalent dopants respectively, creating oxygen vacancies ($v_{\text{O}}^{\bullet\bullet}$) by charge compensation. Further, Iwahara and co-workers [95] confirmed that $\text{BaCe}_{0.9-x}\text{Zr}_x\text{Y}_{0.1}\text{O}_{3-\delta}$ (BCZY) had almost pure protonic conductivity under atmospheres with H_2 at high temperatures regardless of the Zr content. Nevertheless, these oxides exhibited protonic, oxide-ionic and electronic-mixed conductivity under atmospheres with high oxygen partial pressure. Moreover, as Zr content increases the chemical stability against CO_2 increases and the protonic conductivity decreases.

High temperature proton conducting oxides exhibit different charge carriers, such as, protons, oxygen vacancies, electrons and electron holes [96, 97]. The predominant charge carriers for these materials depend on the experimental conditions, that is to say, gas environments and temperature [98]. H_2 is a donor in oxides and is ionized to protons, which have a positive effective charge and contribute to the conductivity. Protons have the smallest ionic radius and they are placed in the electron cloud of an oxide ion, being the resulting species a hydroxide ion on the site of an oxide ion, which according to the Kröger-Vink notation is written as $\text{OH}_{\text{O}}^{\bullet}$ (where the subscript O indicates the oxygen site and the superscript \bullet indicates a positive effective charge). Also to simplify or to denote that the protons move as lone protons jumping between oxide ions (Grotthuss mechanism) they can be written as H^{\bullet} [96].

In wet atmospheres, the high temperature proton conducting oxides, such as BCZY, take protons from H_2O vapor present in the atmosphere due to

equilibrium with defects in the oxide lattice [91, 99, 100], thus the protons reside in the lattice as OH species (OH_O^\bullet):



where $v_O^{\bullet\bullet}$, O_O^x and OH_O^\bullet indicate oxide ion vacancy, oxide ion at the regular site and proton, respectively in the Kröger-Vink notation. The Equation 16 reveals that the humidification of the oxide by incorporating H_2O molecules into the oxide ion vacancies is important to produce mobile protons in the oxide. The hydration reaction is exothermic (Equation 16), i.e. the temperature increment causes that this equilibrium is displaced from the right to the left side, thus the oxide ionic conduction also increases through oxide ion vacancies. Therefore, cerates and zirconates are pure proton conductors at low temperatures and wet reducing atmospheres. While these compounds display p-type electronic (hole) conductivity in oxidizing atmospheres [100-102], as the electron hole concentration enlarges with $p(O_2)$ via the dissolution of oxygen (18):



where h^\bullet indicates electron hole in the Kröger-Vink notation. Moreover, at low partial pressure of oxygen the oxide ion vacancies are formed through the Equation 19 [100]:



Moreover, there are two methods to separate H_2 using proton-conducting perovskite-type oxides: electrochemical H_2 pumping with proton-conducting electrolytes and H_2 extraction via protonic-electronic mixed conductors [102]. The former method of H_2 pumping is schematized in Figure 6:

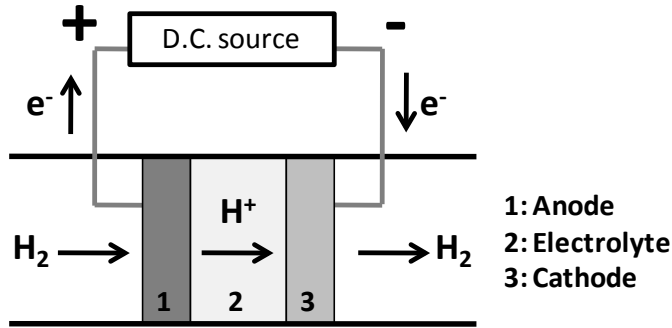
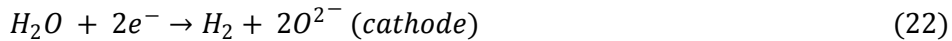


Figure 6. Scheme of a H_2 pump working principle.

Electrochemical H_2 pumps using a proton-conducting electrolyte based on perovskite-type oxides can pump electrochemically H_2 from the anode to the cathode when a direct current is imposed externally to the cell. H_2 is dissociated and ionized to form protons and they are transported through the electrolyte to the porous cathode, where they are discharged to form the H_2 gas, by the following electrode reactions [103] (Equations 20 and 21):



It is known that the H_2 evolution rate (H_2 flux) in this kind of devices shows a deviation from that calculated using Faraday's law at 700-900 °C when a too high current is applied, since a partial electronic conduction emerges in the electrolyte [103]. Thus, in a H_2 pump is detrimental that the electrolyte presents electronic conductivity, as it decreases its faradaic efficiency [100]. The maximum current density avoiding the faradaic efficiency reduction may be enhanced pointedly with the increase of the H_2O vapor quantity in the cathode carrier gas. Hence, the H_2O vapor may help to diminish the electronic conduction in the electrolyte. Further, it can be observed with a partial oxide-ionic conduction in the electrolyte that the H_2O is consumed, by the following electrode reactions [103] (Equations 22 and 23):



The H_2 pump may be used to separate, remove or supply H_2 . Furthermore, the H_2 pump can be modified to use it in a steam electrolyzer to produce H_2 , in a steam pump to dehumidify and in a membrane reactor to hydrogenate or dehydrogenate organic compounds in gas phase [104].

Specifically, for the co-ionic proton and oxide ion conducting $BaCe_{0.2}Zr_{0.7}Y_{0.1}O_{3-\delta}$ material (BCZY27) used as H_2 pump, Babiniec et al. [105] concluded that the faradaic efficiency is reduced as the applied current to the cell increases, especially when H_2 is transported against the H_2 concentration gradient. This is ascribed to the promotion of electronic conduction in the BCZY27 electrolyte when a very high voltage is reached, upon imposing different currents for the H_2 pumping. This effect is observed regardless of the gas composition. The authors assumed that electrochemical cerium reduction at the cathode might be the mechanism for electronic defect migration, thus prevailing the n-type electronic conductivity over the co-ionic proton and oxide ion conduction [105]. Moreover, for the $BaZr_{0.7}Ce_{0.2}Y_{0.1}O_{3-\delta}$ material (BZCY72) at temperatures higher than 600 °C the p-type conductivity rises at the expense of the protonic conductivity [94, 106].

2.7. Methane dehydroaromatization over Mo/HZSM-5 catalyst with continuous H_2 removal or O_2 injection

As abovementioned the methane dehydroaromatization process has two important shortcomings: (i) it is limited by thermodynamics achieving an equilibrium conversion of around 12% and (ii) the catalyst activity drops rapidly with the time on stream due to the accumulation of carbonaceous deposits on both Mo carbide species and Brønsted acid sites of the zeolite. The

catalytic sites alone cannot overcome these constraints, but a shift of thermodynamic equilibrium using selective membranes to remove H_2 [107-109] or supply oxygen [110] can help to surpass them. Nonetheless, H_2 extraction alone accelerates coking and catalyst deactivation; while oxygen injection alone leads to high carbon monoxide selectivity.

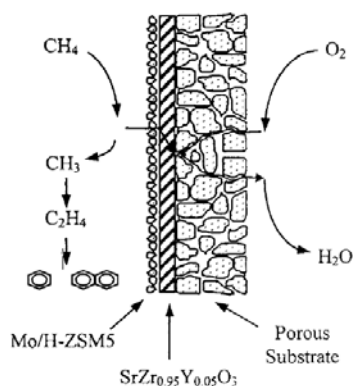


Figure 7. MDA with H_2 removal through $SrZr_{0.95}Yb_{0.05}O_{3-\delta}$ membrane [111].

Regarding the H_2 extraction Liu et al. [107] used a dense membrane of $SrCe_{0.95}Yb_{0.05}O_{3-\delta}$ (consisted of SCY dense film of 2 μm on a porous SCY substrate) to abstract the H_2 formed in the methane dehydroaromatization over 4% (wt.) Mo/HZSM-5 catalyst (Si/Al=15) at 677°C, removing very low fractions of H_2 (scheme similar to that shown in Figure 7). This slight extraction of H_2 favored the faster catalyst deactivation due to the decrease of C_2 - C_{12} hydrocarbons selectivities and the increase of heavy hydrocarbons selectivities. These negative effects were slightly reduced adding small amounts of CO_2 in the feed.

Moreover, Caro and co-workers [109] recently employed a U-shape H_2 permeable hollow fiber membrane composed by $La_{5.5}W_{0.6}Mo_{0.4}O_{11.25-\delta}$ (LWM0.4) to remove the H_2 from the MDA reaction side, on 6% (wt.) Mo/HZSM-5 catalyst at 700 °C and 840 $mL \cdot h^{-1} \cdot g_{cat}^{-1}$. They used argon or CO_2 as sweep gas, obtaining the highest H_2 extraction using argon. Owing to the

extraction of 40-60% of H₂ produced, they obtained a higher aromatics yield than without H₂ extraction during the first 5 h on stream. While after 10 h on stream by removing H₂, the aromatics yield obtained was lower than without H₂ removal from MDA reaction side. This is ascribed to the continuous coke deposition over both the catalyst and the membrane. Moreover, the MDA performance obtained after the oxidative regeneration of the coked membrane and catalyst was very similar to that achieved in the first run.

Kinage et al. [108] utilized a Pd membrane sheet (20 μm thickness) for H₂ extraction from the products of MDA reaction on 3% (wt.) Mo/HZSM-5 catalyst for 100 h at 610 °C. They achieved an extraction of H₂ between 50-60% through the membrane and enhanced the methane conversion two times above the equilibrium conversion. However the H₂ permeability was hampered by the coke deposition, since it was lower than that obtained without MDA reaction conditions.

Concerning the oxygen supply Cao et al. [110] used an asymmetric oxygen conducting Ba_{0.5}Sr_{0.5}Co_{0.8}Fe_{0.2}O_{3-δ} (BSCF) perovskite-type membrane (formed by BSCF dense layer of 20 μm on a porous BSCF support) to provide oxygen from the air side to the hydrocarbons side, in which it was depleted in MDA reaction over 6% (wt.) Mo/HZSM-5 catalyst (Si/Al=27) at 750 °C. The oxygen was fed 1 h after methane supply was started. The H₂ produced from MDA reaction was oxidized forming H₂O vapor that reduced the coke deposits and therefore enhanced the catalyst stability. They found that the methane conversion was higher than without the oxygen supply. Moreover, a partial methane oxidation to CO_x took place, which caused a decrease of aromatic hydrocarbons selectivities.

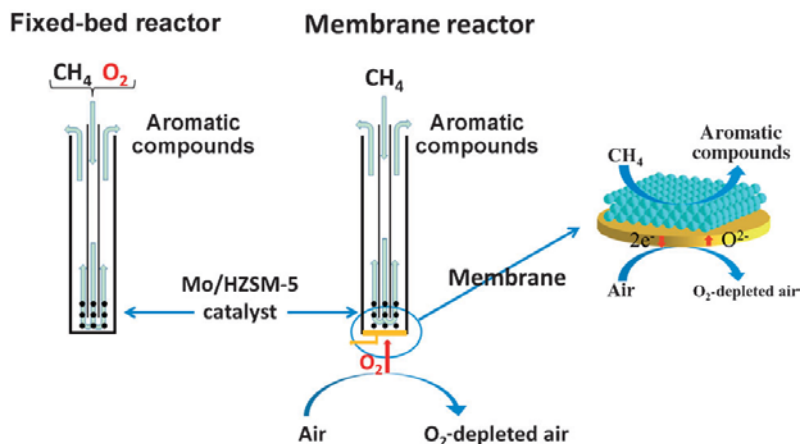


Figure 8. Methane dehydroaromatization in a Fixed-bed reactor and in a Membrane reactor with oxygen supply through BSCF membrane [110].

2.8. References

- [1] The contribution of the natural gas industry to climate change mitigation – Natural gas unlocking the low carbon future, International Gas Union (IGU). 24th World Gas Conference in Buenos Aires, October 2009.
- [2] Living Planet Report 2014, Species and Spaces, People and Places WWF (World Wildlife Fund.),
- [3] Technology Roadmap Energy and GHG Reductions in the Chemical Industry via Catalytic Processes, International Energy Agency, 2013.
- [4] World Energy Outlook 2013, International Energy Agency,
- [5] BP Statistical Review of World Energy, 2014.
- [6] Tracking Clean Energy Progress International Energy Agency (www.iea.org/etp/tracking), 2014.
- [7] J.R. Gonzalez, Información Tecnológica, 5 (1994) 11-17.
- [8] World Energy Outlook 2012 (IEA).
- [9] Z.R. Ismagilov, E.V. Matus, L.T. Tsikoza, Energy Environ. Sci., 1 (2008) 526-541.
- [10] J.R. González, Información Tecnológica, 5 (1994) 19-27.
- [11] S.Q. Ma, X.G. Guo, L.X. Zhao, S. Scott, X.H. Bao, J. Energy Chem., 22 (2013) 1-20.

- [12] J.G. Speight, *The Chemistry and Technology of Petroleum*, CRC Press/Taylor & Francis Group ed., 2014.
- [13] *World Oil Outlook 2014*, Organization of the Petroleum Exporting Countries,
- [14] *Chemical Economics Handbook 2014: Benzene*, IHS,
- [15] <http://www.woodmac.com/public/views/global-benzene-market>.
- [16] *Global chemicals Outlook, Towards Sound Management of Chemicals*, United Nations Environment Programme., 2012.
- [17] C. Colella, A.F. Gualtieri, *Microporous and Mesoporous Materials*, 105 (2007) 213-221.
- [18] J. Weitkamp, *Solid State Ionics*, 131 (2000) 175-188.
- [19] A. Corma, *Journal of Catalysis*, 216 (2003) 298-312.
- [20] W. Loewenstein, *American Mineralogist*, 39 (1954) 92-96.
- [21] S. Kulprathipanja, *Zeolites in Industrial Separation and Catalysis (C. 1 - 2)* Wiley-WCH, 2010.
- [22] R. Szostak, *Molecular Sieves: Principles of Synthesis and Identification (C. 1)*, Thomson Science, 1998.
- [23] L.S. Wang, L.X. Tao, M.S. Xie, G.F. Xu, J.S. Huang, Y.D. Xu, *Catalysis Letters*, 21 (1993) 35-41.
- [24] D.J. Wang, J.H. Lunsford, M.P. Rosynek, *Topics in Catalysis*, 3 (1996) 289-297.
- [25] Y.D. Xu, X.H. Bao, L.W. Lin, *Journal of Catalysis*, 216 (2003) 386-395.
- [26] B.M. Weckhuysen, M.P. Rosynek, J.H. Lunsford, *Catalysis Letters*, 52 (1998) 31-36.
- [27] C.L. Zhang, S.A. Li, Y. Yuan, W.X. Zhang, T.H. Wu, L.W. Lin, *Catalysis Letters*, 56 (1998) 207-213.
- [28] S.T. Liu, L. Wang, R. Ohnishi, M. Ichikawa, *Journal of Catalysis*, 181 (1999) 175-188.
- [29] Y.Y. Shu, D. Ma, L.Y. Xu, Y.D. Xu, X.H. Bao, *Catalysis Letters*, 70 (2000) 67-73.
- [30] D. Wang, Q.B. Kan, N. Xu, P. Wu, T.H. Wu, *Catal. Today*, 93-5 (2004) 75-80.
- [31] P. Wu, Q.B. Kan, D.Y. Wang, H.J. Xing, M.J. Jia, T.H. Wu, *Catalysis Communications*, 6 (2005) 449-454.

- [32] A. Martinez, E. Peris, G. Sastre, *Catal. Today*, 107-08 (2005) 676-684.
- [33] C. Xu, J. Guan, S. Wu, M. Jia, T. Wu, Q. Kan, *Reaction Kinetics Mechanisms and Catalysis*, 99 (2010) 193-199.
- [34] H. Xing, Y. Zhang, M. Jia, S. Wu, H. Wang, J. Guan, L. Xu, T. Wu, Q. Kan, *Catalysis Communications*, 9 (2008) 234-238.
- [35] H. Liu, S. Wu, Y. Guo, F. Shang, X. Yu, Y. Ma, C. Xu, J. Guan, Q. Kan, *Fuel*, 90 (2011) 1515-1521.
- [36] H. Liu, S. Yang, S. Wu, F. Shang, X. Yu, C. Xu, J. Guan, Q. Kan, *Energy*, 36 (2011) 1582-1589.
- [37] E. Bartsch, H. Bertagnolli, G. Schulz, P. Chieux, *Berichte Der Bunsen-Gesellschaft-Physical Chemistry Chemical Physics*, 89 (1985) 147-156.
- [38] <http://www.iza-structure.org/databases/>.
- [39] B.M. Weckhuysen, D.J. Wang, M.P. Rosynek, J.H. Lunsford, *Journal of Catalysis*, 175 (1998) 338-346.
- [40] L.S. Wang, R. Ohnishi, M. Ichikawa, *Catalysis Letters*, 62 (1999) 29-33.
- [41] P.L. Tan, C.T. Au, S.Y. Lai, *Catalysis Letters*, 112 (2006) 239-245.
- [42] J.-F. Liu, L. Jin, Y. Liu, Y.-S. Qi, *Catalysis Letters*, 125 (2008) 352-358.
- [43] L.L. Su, L. Liu, J.Q. Zhuang, H.X. Wang, Y.G. Li, W.J. Shen, Y.D. Xu, X.H. Bao, *Catalysis Letters*, 91 (2003) 155-167.
- [44] Y. Shu, R. Ohnishi, M. Ichikawa, *Appl. Catal. A-Gen.*, 252 (2003) 315-329.
- [45] R. Ohnishi, S.T. Liu, Q. Dong, L. Wang, M. Ichikawa, *Journal of Catalysis*, 182 (1999) 92-103.
- [46] Y. Xu, J. Wang, Y. Suzuki, Z.-G. Zhang, *Appl. Catal. A-Gen.*, 409 (2011) 181-193.
- [47] R. Kojima, S. Kikuchi, H. Ma, J. Bai, M. Ichikawa, *Catalysis Letters*, 110 (2006) 15-21.
- [48] A.K. Aboul-Gheit, A.E. Awadallah, S.M. El-Kossy, A.-L.H. Mahmoud, *Journal of Natural Gas Chemistry*, 17 (2008) 337-343.
- [49] A.K. Aboul-Gheit, A.E. Awadallah, A.A. Aboul-Enein, A.-L.H. Mahmoud, *Fuel*, 90 (2011) 3040-3046.
- [50] A. Hassan, A. Sayari, *Appl. Catal. A-Gen.*, 297 (2006) 159-164.
- [51] L.Y. Chen, L.W. Lin, Z.S. Xu, X.S. Li, T. Zhang, *Journal of Catalysis*, 157 (1995) 190-200.

- [52] F. Solymosi, A. Erdohelyi, A. Szoke, *Catalysis Letters*, 32 (1995) 43-53.
- [53] D.J. Wang, J.H. Lunsford, M.P. Rosynek, *Journal of Catalysis*, 169 (1997) 347-358.
- [54] F. Solymosi, J. Cserenyi, A. Szoke, T. Bansagi, A. Oszko, *Journal of Catalysis*, 165 (1997) 150-161.
- [55] L. Liu, D. Ma, H.Y. Chen, H. Zheng, M.J. Cheng, Y.D. Xu, X.H. Bao, *Catalysis Letters*, 108 (2006) 25-30.
- [56] W.P. Zhang, D. Ma, X.W. Han, X.M. Liu, X.H. Bao, X.W. Guo, X.S. Wang, *Journal of Catalysis*, 188 (1999) 393-402.
- [57] H. Ma, Kojima, R., Kikuchi, S., Ichikawa, M., *Journal of Natural Gas Chemistry*, 14 (2005) 129-139.
- [58] K. Skutil, M. Taniewski, *Fuel Processing Technology*, 87 (2006) 511-521.
- [59] Y.D. Xu, Y.Y. Shu, S.T. Liu, J.S. Huang, X.X. Guo, *Catalysis Letters*, 35 (1995) 233-243.
- [60] D. Ma, Y.Y. Shu, X.W. Han, X.M. Liu, Y.D. Xu, X.H. Bao, *Journal of Physical Chemistry B*, 105 (2001) 1786-1793.
- [61] R.W. Borry, Y.H. Kim, A. Huffsmith, J.A. Reimer, E. Iglesia, *Journal of Physical Chemistry B*, 103 (1999) 5787-5796.
- [62] W. Li, G.D. Meitzner, R.W. Borry, E. Iglesia, *Journal of Catalysis*, 191 (2000) 373-383.
- [63] Y.H. Kim, R.W. Borry, E. Iglesia, *Microporous and Mesoporous Materials*, 35-6 (2000) 495-509.
- [64] J.P. Tessonier, B. Louis, S. Walspurger, J. Sommer, M.J. Ledoux, C. Pham-Huu, *Journal of Physical Chemistry B*, 110 (2006) 10390-10395.
- [65] J. Gao, Y. Zheng, J.-M. Jehng, Y. Tang, I.E. Wachs, S.G. Podkolzin, *Science*, 348 (2015) 686-690.
- [66] D. Ma, Y.Y. Shu, M.J. Cheng, Y.D. Xu, X.H. Bao, *Journal of Catalysis*, 194 (2000) 105-114.
- [67] D. Ma, Y.Y. Shu, X.H. Bao, Y.D. Xu, *Journal of Catalysis*, 189 (2000) 314-325.
- [68] H.M. Liu, W.J. Shen, X.H. Bao, Y.D. Xu, *Appl. Catal. A-Gen.*, 295 (2005) 79-88.
- [69] H. Zheng, D. Ma, X. Bao, J.Z. Hu, J.H. Kwak, Y. Wang, C.H.F. Peden, *Journal of the American Chemical Society*, 130 (2008) 3722-+.

- [70] J.Z. Hu, J.H. Kwak, Y. Wang, C.H.F. Peden, H. Zheng, D. Ma, X. Bao, *Journal of Physical Chemistry C*, 113 (2009) 2936-2942.
- [71] H.M. Liu, W.J. Shen, X.H. Bao, Y.D. Xu, *Journal of Molecular Catalysis a-Chemical*, 244 (2006) 229-236.
- [72] H.M. Liu, X.H. Bao, Y.D. Xu, *Journal of Catalysis*, 239 (2006) 441-450.
- [73] J.S. Lee, L. Volpe, F.H. Ribeiro, M. Boudart, *Journal of Catalysis*, 112 (1988) 44-53.
- [74] W.P. Ding, S.Z. Li, G.D. Meitzner, E. Iglesia, *Journal of Physical Chemistry B*, 105 (2001) 506-513.
- [75] H. Jiang, L.S. Wang, W. Cui, Y.D. Xu, *Catalysis Letters*, 57 (1999) 95-102.
- [76] D. Ma, D.Z. Wang, L.L. Su, Y.Y. Shu, Y. Xu, X.H. Bao, *Journal of Catalysis*, 208 (2002) 260-269.
- [77] H.M. Liu, L.L. Su, H.X. Wang, W.J. Shen, X.H. Bao, Y.D. Xu, *Appl. Catal. A-Gen.*, 236 (2002) 263-280.
- [78] S. Liu, L. Wang, R. Ohnishi, M. Ichikawa, *Kinetics and Catalysis*, 41 (2000) 132-144.
- [79] Z. Liu, M.A. Nutt, E. Iglesia, *Catalysis Letters*, 81 (2002) 271-279.
- [80] Y.Y. Shu, R. Ohnishi, M. Ichikawa, *Journal of Catalysis*, 206 (2002) 134-142.
- [81] H.S. Lacheen, E. Iglesia, *Journal of Catalysis*, 230 (2005) 173-185.
- [82] J. Bai, S.L. Liu, S.J. Xie, L.Y. Xu, L.W. Lin, *Catalysis Letters*, 90 (2003) 123-130.
- [83] S.L. Liu, R. Ohnishi, M. Ichikawa, *Journal of Catalysis*, 220 (2003) 57-65.
- [84] H.T. Ma, R. Kojima, S. Kikuchi, M. Ichikawa, *Catalysis Letters*, 104 (2005) 63-66.
- [85] H.T. Ma, R. Ohnishi, M. Ichikawa, *Catalysis Letters*, 89 (2003) 143-146.
- [86] W. Chu, F.L. Qiu, *Topics in Catalysis*, 22 (2003) 131-134.
- [87] C.Y. Sun, S.D. Yao, W.J. Shen, L.W. Lin, *Chinese Journal of Catalysis*, 31 (2010) 78-83.
- [88] W. Chu, X.Y. Dai, X.D. Li, W.W. Jiang, *Chinese Chemical Letters*, 15 (2004) 591-593.
- [89] H. Iwahara, Y. Asakura, K. Katahira, M. Tanaka, *Solid State Ionics*, 168 (2004) 299-310.

- [90] K.D. Kreuer, *Annual Review of Materials Research*, 33 (2003) 333-359.
- [91] H. Iwahara, *Solid State Ionics*, 86-8 (1996) 9-15.
- [92] S. Wienstroer, H.D. Wiemhofer, *Solid State Ionics*, 101 (1997) 1113-1117.
- [93] K.H. Ryu, S.M. Haile, *Solid State Ionics*, 125 (1999) 355-367.
- [94] S. Ricote, N. Bonanos, M.C.M. de Lucas, G. Caboche, *Journal of Power Sources*, 193 (2009) 189-193.
- [95] K. Katahira, Y. Kohchi, T. Shimura, H. Iwahara, *Solid State Ionics*, 138 (2000) 91-98.
- [96] T. Norby, Y. Larring, *Current Opinion in Solid State & Materials Science*, 2 (1997) 593-599.
- [97] N. Bonanos, F.W. Poulsen, *Journal of Materials Chemistry*, 9 (1999) 431-434.
- [98] S. Ricote, N. Bonanos, G. Caboche, *Solid State Ionics*, 180 (2009) 990-997.
- [99] A.S. Nowick, Y. Du, *Solid State Ionics*, 77 (1995) 137-146.
- [100] N. Bonanos, *Solid State Ionics*, 145 (2001) 265-274.
- [101] H. Uchida, H. Yoshikawa, H. Iwahara, *Solid State Ionics*, 34 (1989) 103-110.
- [102] H. Matsumoto, T. Shimura, H. Iwahara, T. Higuchi, K. Yashiro, A. Kaimai, T. Kawada, J. Mizusaki, *Journal of Alloys and Compounds*, 408 (2006) 456-462.
- [103] H. Matsumoto, S. Hamajima, H. Iwahara, *Solid State Ionics*, 145 (2001) 25-29.
- [104] H. Iwahara, *Solid State Ionics*, 125 (1999) 271-278.
- [105] S.M. Babiniec, S. Ricote, N.P. Sullivan, *International Journal of Hydrogen Energy*, 40 (2015) 9278-9286.
- [106] S. Ricote, N. Bonanos, H.J. Wang, R. Haugsrud, *Solid State Ionics*, 185 (2011) 11-17.
- [107] Z. Liu, L. Li, E. Iglesia, *Catalysis Letters*, 82 (2002) 175-180.
- [108] A.K. Kinage, R. Ohnishi, M. Ichikawa, *Catalysis Letters*, 88 (2003) 199-202.
- [109] J. Xue, Y. Chen, Y. Wei, A. Feldhoff, H. Wang, J. Caro, *ACS Catalysis*, 6 (2016) 2448-2451.

[110] Z. Cao, H. Jiang, H. Luo, S. Baumann, W.A. Meulenber, J. Assmann, L. Mleczko, Y. Liu, J. Caro, *Angewandte Chemie-International Edition*, 52 (2013) 13794-13797.

[111] R.W. Borry, E.C. Lu, Y.H. Kim, E. Iglesia, Non-oxidative catalytic conversion of methane with continuous hydrogen removal, in: *Natural Gas Conversion V*, 1998, pp. 403-410.

Chapter 3.

METHODOLOGY

3. Methodology

3.1. Reactants

All commercial reagents used in the experimental procedures along the present thesis have been used as received, that is, without applying further treatments.

3.2. Zeolite preparation

3.2.1. ZSM-5 zeolite

The ZSM-5 zeolite is a synthetic zeolite of medium pore which code is MFI and its unit cell has the following chemical formula:

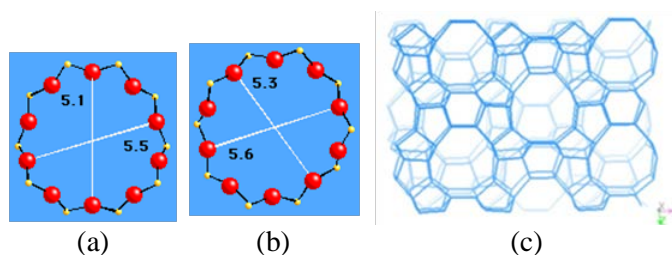


Figure 9. Projection of the rings of the ZSM-5 zeolite channels (a) 10 MR viewed along $[100]$; (b) 10 MR viewed along $[010]$; and projection of the structure (c) viewed along $[100]$ [1].

Moreover, the ZSM-5 zeolite has orthorhombic symmetry and its cell parameters are as follows: $a=20.07 \text{ \AA}$, $b=19.92 \text{ \AA}$, $c=13.42 \text{ \AA}$; $\alpha=\beta=\gamma=90^\circ$ [1]. This zeolite has a tridirectional channels system with an aperture of 10 member rings (10 MR): $[100] \text{ 10 } 5.1 \times 5.6 \text{ \AA} \leftrightarrow [010] \text{ 10 } 5.3 \times 5.6 \text{ \AA}$, and it has not large cavities. One of the channel systems is almost circular and parallel to the

crystallographic axis b, the other channel is elliptical and it is in zigzag along the axis a.

Preparation: For the preparation of the different catalysts used in the methane dehydroaromatization reaction, different ZSM-5 zeolites have been employed and their characteristics are shown in Table 2. The zeolites CBV3020, CBV8020, CBV5020 and CBV3024E were purchased from Zeolyst Int. (CBV3024E replaces CBV3020), and the zeolites TZP322 and TZP302H were purchased from Tricat, all of them are available in the ITQ as they are commercial. All the ammonium zeolites were calcined in air previously at 500 °C for 3 h to remove the ammonium ions and to obtain its acid form, because it is necessary to its use in the MDA reaction.

Table 2. ZSM-5 zeolites used in the preparation of the catalysts.

Zeolite	Form	Morphology	Pore size (Å)	Crystal size (µm)
CBV3020	Acid	Polycrystalline aggregates	5.3 x 5.6	~0.1
CBV8020	Acid	Spheres		~0.5-1
CBV5020	Ammonium	Spheres	5.1 x 5.5	~0.1
TZP322	Ammonium	Spheres		~0.1
TZP302H	Ammonium	Parallelepiped		~1-2
CBV3024E	Ammonium	-		~0.1-0.25

Table 2-Continued. ZSM-5 zeolites used in the preparation of the catalysts.

Zeolite	Micropore volumen (cm ³ /g)	S _{BET} (m ² /g)	Si/Al	Acidity (µmol pyridine/g)			
				Brønsted (°C)		Lewis (°C)	
				250	350	250	350
CBV3020	0.16	396	15	145	83	60	51
CBV8020	0.17	400	40	173	86	39	39
CBV5020	0.16	404	25	220	173	31	24
TZP322	0.17	391	10	530	403	17	15
TZP302H	0.17	391	10	490	350	6	4
CBV3024E	0.16	370	15	60	70	49	81

3.2.2. MCM-22 zeolite

The MCM-22 zeolite is a synthetic zeolite of medium pore which code is MWW, it has hexagonal symmetry and its cell parameters are as follows: $a=b=14.208 \text{ \AA}$, $c=24.945 \text{ \AA}$; $\alpha=\beta=90^\circ$, $\gamma=120^\circ$ [1]. The MCM-22 zeolite has a unique pore structure with two independent pore system: a smaller 2D (two-dimensional), with an aperture of 10 member rings (10 MR), sinusoidal pore system ($4.1 \times 5.1 \text{ \AA}$), and a larger 3D (three-dimensional), with an aperture of 12 member rings (12 MR), super cage system interconnected by 10 MR windows ($4.0 \times 5.5 \text{ \AA}$) [2].

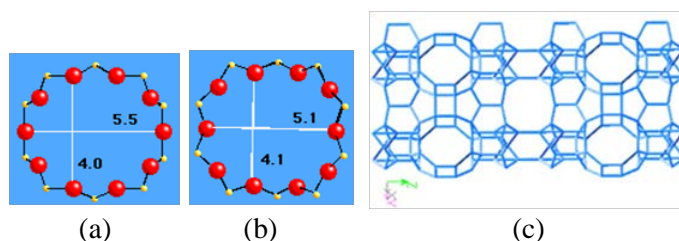
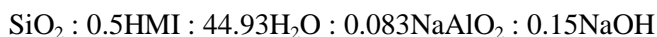


Figure 10. Projection of the rings of the MCM-22 zeolite channels (a) 10 MR viewed normal to $[001]$ between layers; (b) 10 MR viewed normal to $[010]$ within layers; and projection of the structure (c) viewed along $[100]$ [1].

Preparation: MCM-22 zeolite (Si/Al ratio ~ 15) was prepared using hexamethyleneimine as structure-directing agent (Aldrich, 99% purity), silica (Aerosil 200, Evonik), sodium aluminate (Carlo Erba, pure), sodium hydroxide (Scharlau, synthesis grade) and deionized H_2O . The molar chemical composition of the starting gel can be expressed as [3]:



The synthesis gel was transferred into teflon-lined stainless steel autoclaves of 60 mL and kept at $150 \text{ }^\circ\text{C}$ for 7 days. The resulting solid was filtered and washed with deionized H_2O , then this was dried at $120 \text{ }^\circ\text{C}$ and calcined in air at $580 \text{ }^\circ\text{C}$ for 3 h. However, in order to increase the zeolite

quantity obtained in one-step, the scaled up of both the synthesis gel and the teflon-lined stainless steel autoclave was carried out. Furthermore, a little bit of “seeding” was added to the gel to accelerate the process and the synthesis was performed at 150 °C for 4 days under stirring. Following the same steps abovementioned with the solid resulting, that is, filtering and washing with deionized H₂O, drying at 120 °C and calcining in air at 580 °C for 3 h. The “seeding” used is the MCM-22 zeolite synthesized in teflon-lined stainless steel autoclaves of 60 mL at 150 °C for 7 days. The Si/Al ratio of the as-synthesized MCM-22 zeolites was confirmed and determined by ICP-OES (section 3.5.12.).

Table 3. BET surface area, micropore volume and acidity of the synthesized MCM-22 (Si/Al ~ 15).

Zeolite	S _{BET} (m ² /g)	Micropore volumen (cm ³ /g)	Acidity (μmol pyridine/g)					
			Brønsted (°C)			Lewis (°C)		
			150	250	350	150	250	350
MCM-22	485	0.196	74	47	31	30	19	16

Additionally, MCM-22 zeolite with a Si/Al ratio = 25 was prepared in the ITQ using own methods.

3.2.3. IM-5 zeolite

The IM-5 zeolite has a tridirectional channels system with an aperture of 10 member rings (10 MR): [001] **10** 5.5 x 5.6 Å <-> [100] **10** 5.3 x 5.4 Å, <-> [010] **10** 5.3 x 5.9 Å, <-> [001] **10** 4.8 x 5.4 Å <-> [100] **10** 5.1 x 5.3 Å. However, the connectivity in the third dimension is interrupted every 2.5 nm, therefore diffusion is somewhat limited. Moreover, the IM-5 zeolite has orthorhombic symmetry and its cell parameters are as follows: a=14.296 Å, b=56.788 Å, c=20.29 Å; α=β=γ=90° [1]. This zeolite is of medium pore which code is IMF and its unit cell has the following chemical formula: [Si₂₈₈O₅₇₆]

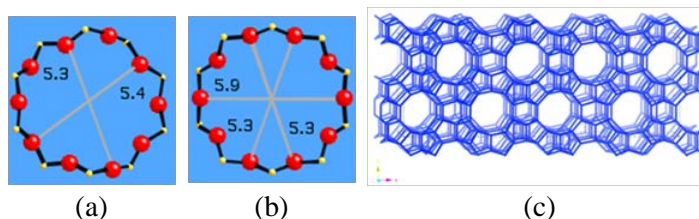
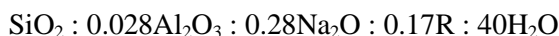


Figure 11. Projection of the rings of the IM-5 zeolite channels: (a) 10 MR viewed along [100]; (b) 10 MR viewed along [010]; and projection of the structure (c) viewed along [100] [1].

Preparation: IM-5 zeolite (Si/Al ratio = 12) was prepared in the ITQ using 1.5-bis(methylpyrrolidinium)pentane dibromide (R) as structure-directing agent, silica (Aerosil 200, Evonik), sodium aluminate (Carlo Erba, pure), sodium hydroxide (Scharlau, synthesis grade) and deionized H₂O [4]. The molar chemical composition of the starting gel can be expressed as:



The synthesis gel was transferred into teflon-lined stainless steel autoclaves of 60 mL and kept at 175 °C for 14 days. The resulting solid was filtered and washed with deionized H₂O, dried at 120 °C and calcined in air at 580 °C for 3 h. Then the solid was undergone to ionic exchange with NH₄Cl at 80 °C for 6 h. It was filtered and washed with deionized H₂O to remove the chloride ions, dried at 120 °C and calcined in air at 500 °C for 3 h to remove the ammonium ions. The IM-5 zeolite obtained has a BET surface area of 350 m²·g⁻¹ and a micropore volume of 0.16 cm³ g⁻¹.

3.2.4. ITQ-13 zeolite

The ITQ-13 zeolite has a tridirectional channels system with an aperture of 10 x 9 member rings (10 MR), which has three intercrossed medium pore channels: a 9 MR channel with a pore aperture of 4.0 x 4.8 Å, that is parallel to the crystallographic axis a; a 10 MR channel system (4.8 x 5.3 Å) that is parallel

to the crystallographic axis c , and other 10 MR channel system ($4.7 \times 5.1 \text{ \AA}$) that is parallel to the crystallographic axis b [5]. Furthermore, the ITQ-13 zeolite has orthorhombic symmetry and its cell parameters are as follows: $a=12.5655 \text{ \AA}$, $b=11.6615 \text{ \AA}$, $c=21.9303 \text{ \AA}$; $\alpha=\beta=\gamma=90^\circ$ [1]. This zeolite is of medium pore which code is ITH and its unit cell has the following chemical formula: $[(\text{CH}_3)_3\text{N}(\text{CH}_2)_6\text{N}(\text{CH}_3)_3]^{2+}\text{F}_2)_2[\text{Si}_{56}\text{O}_{112}]$

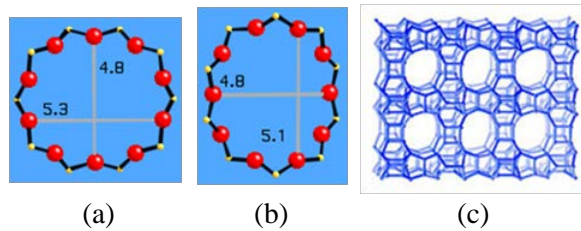


Figure 12. Projection of the rings of the ITQ-13 zeolite channels: (a) 10 MR viewed along $[001]$; (b) 10 MR viewed along $[010]$; and projection of the structure (c) viewed along $[010]$ [1].

Preparation: ITQ-13 zeolite (Si/Ge ratio = 13; (Si + Ge)/Al = 39) was prepared in the ITQ using the method described in the patent [6]. The ITQ-13 zeolite obtained has a BET surface area of $360 \text{ m}^2 \cdot \text{g}^{-1}$ and a micropore volume of $0.16 \text{ cm}^3 \cdot \text{g}^{-1}$.

3.2.5. TNU-9 zeolite

The TNU-9 zeolite has a tridirectional channels system with an aperture of 10 member rings (10 MR): $[010] \text{ } 10 \text{ } 5.6 \times 5.5 \text{ \AA} \leftrightarrow [10-1] \text{ } 10 \text{ } 5.4 \times 5.5 \text{ \AA}$, there are two different channels along $[010]$, the smaller are $5.1 \times 5.5 \text{ \AA}$. Moreover, the TNU-9 zeolite has monoclinic symmetry and its cell parameters are as follows: $a=27.8449 \text{ \AA}$, $b=20.0150 \text{ \AA}$, $c=19.5965 \text{ \AA}$; $\alpha=\gamma=90^\circ$, $\beta=93.2^\circ$. This zeolite is of medium pore which code is TUN and its unit cell has the following chemical formula [1]: $[\text{H}^+_{9.3}][\text{Al}_{9.3}\text{Si}_{182.7}\text{O}_{384}]$

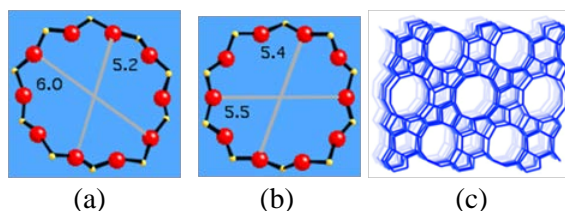
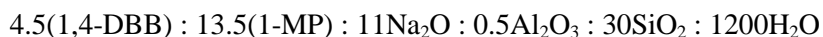


Figure 13. Projection of the rings of the TNU-9 zeolite channels: (a) 10 MR viewed along $[010]$; (b) 10 MR viewed along $[10-1]$; and projection of the structure (c) viewed along $[010]$ [1].

Preparation: TNU-9 zeolite (Si/Al ratio = 14) was prepared in the ITQ according to the procedure described in [7] using 1,4-dibromobutane (1,4-DBB) and 1-methylpyrrolidine (1-MP) as structure-directing agents, silica (Aerosil 200, Evonik), $\text{Al}(\text{NO}_3)_3 \cdot 9\text{H}_2\text{O}$ (Aldrich), NaOH (Scharlau, synthesis grade) and deionized H_2O [7]. The molar chemical composition of the starting gel can be expressed as:



The synthesis gel was transferred into teflon-lined stainless steel autoclaves of 60 mL and kept at 160 °C for 8 days. The resulting solid was filtered and washed with deionized H_2O , dried at 100 °C overnight and calcined in air at 580 °C for 3 h. Then the solid was undergone to ionic exchange with NH_4Cl at 80 °C for 6 h, it was filtered and washed with deionized H_2O to remove the chloride ions, dried at 120 °C and calcined in air at 500 °C for 3 h to remove the ammonium ions. The TNU-9 zeolite obtained has a BET surface area of $400 \text{ m}^2 \cdot \text{g}^{-1}$ and a micropore volume of $0.18 \text{ cm}^3 \cdot \text{g}^{-1}$.

3.2.6. Chabazite zeolite

The Chabazite zeolite is a natural zeolite that possesses the composition $\text{Ca}_6\text{Al}_{12}\text{-Si}_{24}\text{O}_{72}$ with a tridirectional channels system with an aperture of 8 member rings (8 MR): $[001]$ $\mathbf{8}$ $3.8 \times 3.8 \text{ \AA}$ and large ellipsoidal cavities of

8.35 Å. Furthermore, the Chabazite zeolite has rhombohedral symmetry and its cell parameters are as follows: $a=b=13.675$ Å, $c=14.767$ Å; $\alpha=\beta=90^\circ$; $\gamma=120^\circ$. Chabazite zeolite (Si/Al ratio = 10) was prepared in the ITQ using own methods. This zeolite is of small pore which code is CHA and its unit cell has the following chemical formula [1]: $[\text{Ca}^{2+}_6 (\text{H}_2\text{O})_{40}] [\text{Al}_{12}\text{Si}_{24} \text{O}_{72}]$

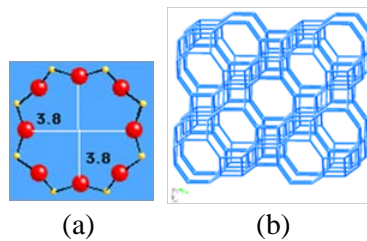


Figure 14. Projection of the rings of the Chabazite zeolite channels: (a) 8 MR viewed normal to [001]; and projection of the structure (b) viewed along [010] [1].

The Chabazite zeolite obtained has a BET surface area of $550 \text{ m}^2 \cdot \text{g}^{-1}$ and a micropore volume of $0.28 \text{ cm}^3 \cdot \text{g}^{-1}$.

3.2.7. ZSM-22 zeolite

The ZSM-22 zeolite has a unidirectional channels system with an aperture of 10 member rings (10 MR): [001] **10** 4.6×5.7 Å. Moreover, the HZSM-22 zeolite has orthorhombic symmetry and its cell parameters are as follows: $a=14.105$ Å, $b=17.842$ Å, $c=5.256$ Å; $\alpha=\beta=\gamma=90^\circ$. This zeolite is of medium pore which code is TON and its unit cell has the following chemical formula [1]:



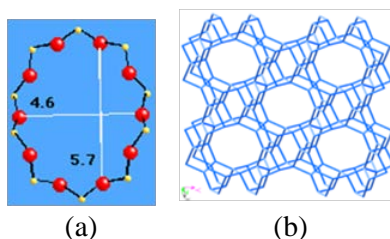


Figure 15. Projection of the rings of the ZSM-22 zeolite channels: (a) 10 MR viewed along [001]; and projection of the structure (b) viewed along [001] [1].

ZSM-22 zeolite (Si/Al ratio = 37.08) was prepared in the ITQ using own methods, then the zeolite was calcined in air previously at 500 °C for 3 h to remove the ammonium ions and to obtain its acid form, because it is necessary to its use.

3.2.8. NU-87 zeolite

This zeolite has a single structure formed by channels of 10 member rings, connected by short channels of 12 member rings (12 MR), creating a bidirectional structure. The access inside the 12 MR channels only is possible through the 10 MR channels. The dimensions of the 10 MR channels perpendicular to the direction [201] are alternatively 4.6 x 6.2 Å along each channel and the channel that connects between both channels has the dimensions 5.3 x 6.8 Å.

The NU-87 zeolite has a bidirectional channels system with an aperture of 10 member rings (10 MR): [100] **10** 4.8 x 5.7 Å. Furthermore, the NU-87 zeolite has monoclinic symmetry and its cell parameters are as follows: a=26.06 Å, b=13.88 Å, c=22.864 Å; $\alpha=\beta=\gamma= 90^\circ$. This zeolite is of medium pore which code is NES and its unit cell has the following chemical formula [1]:



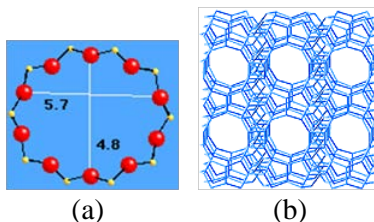


Figure 16. Projection of the rings of the NU-87 zeolite channels: (a) 10 MR viewed along [100]; and projection of the structure (b) viewed along [010] [1].

NU-87 zeolite (Si/Al ratio = 15.6) was prepared in the ITQ using own methods, then the zeolite was calcined in air previously at 500 °C for 3 h to remove the ammonium ions and to obtain its acid form, because it is necessary to its use. The NU-87 zeolite obtained has a BET surface area of 479 m²·g⁻¹.

3.2.9. NU-85 zeolite

The NU-85 zeolite is an intergrowth of zeolites EU-1 and NU-87, but have a multidimensional channel system. This zeolite is a useful catalyst in a wide variety of hydrocarbon conversion reactions including isomerization and alkylation. NU-85 zeolite was prepared in the ITQ using the method described in the patent [8]. Then the solid was undergone to ionic exchange with NH₄NO₃ at 80 °C for 2 h, it was filtered and washed with deionized H₂O to remove the nitrate ions, dried at 120 °C and calcined in air at 500 °C for 3 h to remove the ammonium ions. The NU-85 zeolite obtained has a BET surface area of 466 m²·g⁻¹.

3.2.10. Mazzite zeolite

The Mazzite zeolite has a unidirectional channels system with an aperture of 12 member rings (12 MR): [001] **12** 7.4 x 7.4 Å <-> [001] **8** 3.1 x 3.1 Å. Moreover, the Mazzite zeolite has hexagonal symmetry and its cell parameters are as follows: a=b=18.39 Å, c=7.64 Å; α=β= 90° y γ=120°. Mazzite

zeolite (Si/Al ratio = 13.7) was prepared in the ITQ using own methods and it has a BET surface area of $566 \text{ m}^2 \cdot \text{g}^{-1}$. This synthetic zeolite is of large pore which code is MAZ and its unit cell has the following chemical formula [1]:

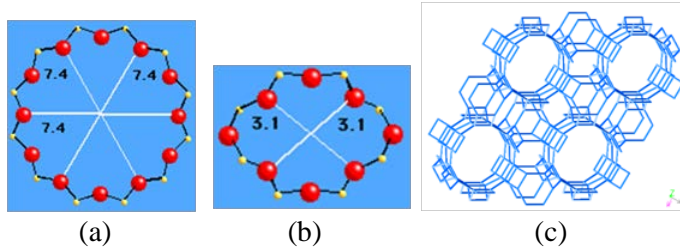
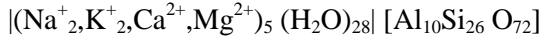
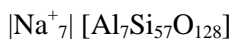


Figure 17. Projection of the rings of the Mazzite zeolite channels: (a) 12 MR viewed along [001]; (b) 8 MR viewed along [001]; and projection of the structure (c) viewed along [001] [1].

3.2.11. Beta zeolite

The Beta zeolite has a quite complex structure because of it is formed by two polymorphs A and B, both have a tridirectional channels system with an aperture of 12 member rings (12 MR): [100] $12 \text{ } 7.6 \times 6.4 \text{ \AA}$ \leftrightarrow [001] $12 \text{ } 5.6 \times 5.6 \text{ \AA}$; with elliptical section and perpendicular between them, coinciding with the three crystallographic axes. At the intersection of these three channels are cavities which dimensions vary between 0.9 and 1 nm. The two parallel channels to the axes a and b are straight and have a medium diameter of $7.6 \times 6.4 \text{ \AA}$, while the parallel channels to the axis c are tortuous and have a diameter of $5.6 \times 5.6 \text{ \AA}$. Moreover, the Beta zeolite has tetragonal symmetry and its cell parameters are as follows: $a=12.661 \text{ \AA}$, $b=12.661 \text{ \AA}$, $c=26.406 \text{ \AA}$; $\alpha=\beta=\gamma=90^\circ$. This synthetic zeolite is of large pore which code is BEA and its unit cell has the following chemical formula [1]:



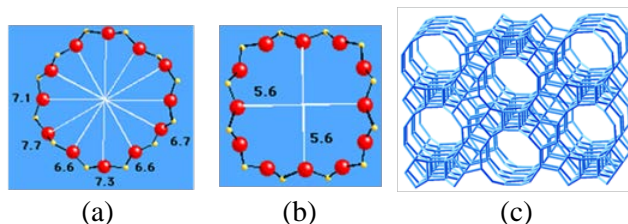
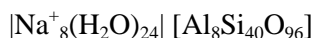


Figure 18. Projection of the rings of the Beta zeolite channels: (a) 12 MR viewed along [100]; (b) 12 MR viewed along [001]; and projection of the structure (c) viewed along [100] [1].

For the preparation of the different catalysts used in the methane dehydroaromatization reaction the zeolite CP811 (Si/Al=12.5) was purchased from Zeolyst Int. and it was available in the ITQ as it is commercial. The Beta zeolite has a BET surface area of $730 \text{ m}^2 \cdot \text{g}^{-1}$, a micropore volume of $0.17 \text{ cm}^3 \cdot \text{g}^{-1}$ and a crystal size between $0.1\text{-}0.2 \text{ }\mu\text{m}$.

3.2.12. Mordenite zeolite

The Mordenite zeolite has a channels system with an aperture of 12 member rings (12 MR), along the axis c , with a diameter of $6.5 \times 7 \text{ \AA}$. This zeolite is considered unidirectional, although it has some perpendicular channels to axis c formed by elliptical rings of 8 members of $2.6 \times 5.7 \text{ \AA}$ that intersect the main channels. The 8 member rings intersection creates an effective widening of these latter producing a lobed effect. Furthermore, the Mordenite zeolite has orthorhombic symmetry and its cell parameters are as follows: $a=18.1 \text{ \AA}$, $b=20.5 \text{ \AA}$, $c=7.5 \text{ \AA}$; $\alpha=\beta=\gamma=90^\circ$. This synthetic zeolite has an isomorphic structure with the natural zeolite Mordenite, is a zeolite of large pore which code is MOR and its unit cell has the following chemical formula [1]:



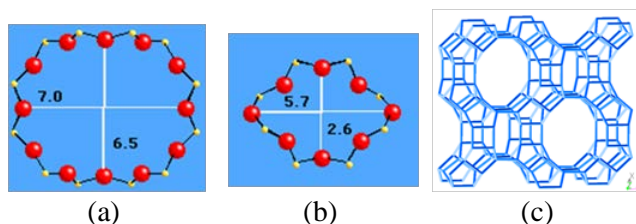


Figure 19. Projection of the rings of the Mordenite zeolite channels: (a) 12 MR viewed along [001]; (b) 8 MR viewed along [001]; and projection of the structure (c) viewed along [001] [1].

For the preparation of the different catalysts used in the methane dehydroaromatization reaction the zeolite CBV20A (Si/Al=10) was purchased from Zeolyst Int. and it was available in the ITQ as it is commercial. The Mordenite zeolite has a BET surface area of $423 \text{ m}^2 \cdot \text{g}^{-1}$, a micropore volume of $0.17 \text{ cm}^3 \cdot \text{g}^{-1}$ and a crystal size between $0.05\text{-}0.3 \text{ }\mu\text{m}$.

3.3. Catalyst manufacturing process

3.3.1. Granulated catalysts

3.3.1.1. Mo incorporation to the zeolite

The Mo incorporation to the different zeolites was done by the incipient wetness impregnation, with an aqueous solution that contained the required amount of the ammonium heptamolybdate tetrahydrate (AHM), (Fluka, 99%). The catalysts were dried at $120 \text{ }^\circ\text{C}$ overnight and when they were at room temperature were homogenized in a mortar, and finally the catalysts were calcined in the presence of air at $500 \text{ }^\circ\text{C}$ for 6 h.

3.3.1.2. *Shaped of the catalyst*

The catalyst was obtained like fine powder after the calcination, therefore, it was necessary to shape it in granules of 0.25 – 0.42 mm for catalytic evaluation. The procedure used in the shaped of the catalyst particles consisted of the formation of a disk in a die applying a pressure of $4 \text{ Tn}\cdot\text{m}^{-2}$ (39.24 MPa) for 1 minute with a hydraulic press. Then, the disk was crushed in a mortar and the granules obtained were sieved, this step was repeated as many times as necessary.

3.3.2. Extrudated catalysts

3.3.2.1. *Extrudated I catalyst*

The procedure described in the U.S. patent [9] was used to produce the Extrudated I catalysts, without the use of the pre-treatment with ammonium nitrate due to the observed worsening of the MDA performance. The zeolite, HZSM-5 or MCM-22 (Si/Al=15), was mixed in powder with a 10% of a plasticizer agent like the sodium carboxymethyl cellulose (Sigma Aldrich, average mol wt. 90000) in a mortar, and then a 30% of a Si-containing binder (Silres MSE 100 from Wacker Silicones) was added and kneaded by adding H_2O until a suitable viscosity of this mixture. The material thus obtained was extruded through a die with round cross section (diameter 2 mm) and the extrudates were dried at 120 °C overnight and calcined in air at 500 °C for 5 h.

Then, the extrudates were crushed in a mortar and the granules obtained were sieved between 0.25 – 0.42 mm, this step was repeated as many times as necessary. The Mo incorporation to the different zeolites was done by impregnation, with an aqueous solution that contained the required amount of the AHM to impregnate the zeolite with 6% (wt.) of Mo. The catalysts were

dried at 120 °C overnight and, finally, the catalysts were calcined in the presence of air at 500 °C for 4 h.

3.3.2.2. Extrudated II catalyst

Moreover, a bench scale catalyst was developed and produced by extrusion in this work, based on the procedure described in the U.S. patent [9]. This catalyst was optimized in order to facilitate the scaling of both the catalyst manufacture and the catalytic test to pilot scale.

The zeolite MCM-22 was mixed in powder with a 10% of a plasticizer agent like the sodium carboxymethyl cellulose in a mortar and a 30% of a Si-containing binder (Silres). Then, this mixture was kneaded until a suitable viscosity by adding an aqueous solution that contains the required amount of the AHM to impregnate this zeolite with 6% (wt.) of Mo. The material thus obtained was mixed with an emulsifier and this mixture was extruded through a die with round cross section (diameter 2 mm). The extrudates were dried at 120 °C overnight and calcined in air at 500 °C for 5 h. After calcining, the extrudates were slightly crushed achieving a wide range of sizes lower than or equal to 1 cm.

3.4. $BaZr_{0.7}Ce_{0.2}Y_{0.1}O_{3-\delta}$ dense ceramic membranes manufacture

In this work, $BaZr_{0.7}Ce_{0.2}Y_{0.1}O_{3-\delta}$ (BZCY72) tubular membranes close-one-end were used, these membranes were manufactured and provided by CoorsTek Membrane Sciences (Golden, CO, U.S.). Details on the fabrication of the BZCY72 ceramic membranes have been reported previously [10]. Briefly, a slip casting slurry was prepared using stoichiometric amounts of $BaSO_4$ (Solvay, grade Blanc Fixe N), CeO_2 (Neo Performance Materials, 99.5%), Y_2O_3

(HJD Intl, 99.99%), ZrO_2 (Neo Performance Materials, 99.5%) and NiO (Novamet, Black Nickel Oxide Grade F, 99.9%). After casting, the tubes were dried for 24 h and spray coated using a slurry with the same precursors as for the slip, but without NiO. The tubular green supports with electrolyte were mounted for hang firing and sintered in air at 1585 °C for 6 h, obtaining a dense 25-30 μm thick BZCY72 electrolyte film on a BZCY72-NiO support. The dimensions of the tubular membrane are 1 cm of outer diameter and ~25 cm of length.

The NiO was reduced to metallic nickel after being treated in reducing atmosphere at high temperature (at 1000 °C for 24 h in a flow of 4% H_2 balanced with Ar), forming a porous cermet cathode with sufficient catalytic activity for the H_2 evolution and reduction of steam. The 1% (wt.) NiO was not enclosed in the stoichiometry because nickel ions were placed in the grain boundaries and not in the perovskite structure after sintering [10, 11].



Figure 20. Picture of the reduced tubular membrane (length ~ 25 cm).

3.4.1. Electrode preparation

For integration of the BZCY72 tubular membranes into the Catalytic Membrane Reactor (CMR) a functional electrode (anode) is needed. A suitable electrode for the MDA reaction should have the following properties:

- Percolating electronic conductivity.
- Chemically stable to methane and other hydrocarbons.
- Coke resistant.
- Catalytically active for H_2 dissociation.
- Sufficient microstructure for gas diffusion or high H_2 flux.

3.4.1.1. $\text{Mo}_2\text{C}/\text{Cu}/\text{BZCY72}$ anode

With the cermet pathway a mixture of 40% (vol.) of Mo_2C , 30% (vol.) of Cu and 30% (vol.) of BZCY72 (with 1% (wt.) of NiO) was milled for 30 min in isopropanol to achieve a homogeneous mixture and then, it was dried at 120 °C to evaporate the alcohol. The ink was prepared mixing 58% (wt.) of the pre-mixed electrode powder with 42% (wt.) of polyvinylpyrrolidone (Sigma Aldrich, average mol wt. 10000) polymer in a mortar and then it was slurried with 50% (vol.) ethylene glycol in isopropanol to the desired viscosity. The $\text{Mo}_2\text{C}/\text{Cu}/\text{BZCY72}$ anode preparation procedure was based on a previous investigation [12] with different adjustments.

Subsequently two layers of the abovementioned ink and one layer of gold paste were deposited (4 cm along) at the sufficient distance to be in the isothermal zone in the reactor, firing at 1000 °C for 1 h between each layer under humidified 5% H_2 balanced with Ar, using the following firing profile: RT (room temperature), 2 °C·min⁻¹ → 1000 °C, 1 h dwell → 3 °C·min⁻¹, RT

3.4.1.2. Copper anode

On the electrolyte film a Cu-based anode was applied facing the catalyst, which promotes the electrochemical activation and removes H_2 without the activation of hydrocarbons to form coke, since the copper exhibits a high coking resistance [13]. In particular, the anode paste of metallic Cu (Heraeus C7440) was mixed with terpineol to facilitate its deposition on the reduced tubes, at the sufficient distance to be in the isothermal zone in the reactor, firing at 1000 °C for 1 h in 5% H_2 balanced with Ar, using the following firing profile: RT, 2 °C·min⁻¹ → 1000 °C, 1 h dwell → 3 °C·min⁻¹, RT

3.5. Characterization techniques

3.5.1. Nitrogen sorption analysis

The gas sorption technique is based on the study of gas-solid adsorption and desorption phenomena to obtain information about the textural properties of the adsorbent. The study of the textural properties is of great importance in heterogeneous catalysis because it allows quantify the microporosity, mesoporosity and external surface area of the solid.

N₂ adsorption isotherms were determined at -196 °C on Micromeritics ASAP 2420 equipment. Before measurements the solids were pre-treated at 400 °C and vacuum overnight. The specific surface areas were obtained using the BET model [14] and micropore volume by applying the *t*-plot approach to the adsorption branch of the isotherms.

3.5.2. Ammonia temperature programmed desorption (NH₃-TPD)

Characterization by ammonia temperature programmed desorption is often used to quantify the density and the strength distribution of the acid sites that a material possesses. The NH₃-TPD experiments consist of the saturation of the sample with pulses of ammonia. Subsequently, the ammonia is desorbed by increasing the temperature of the sample gradually, achieving a characteristic desorption profile. It is generally accepted that the ammonia molecules are desorbed from the acid sites in ascending order of strength with the increase of the desorption temperature.

Ammonia temperature programmed desorption (NH₃-TPD) experiments were carried out on an AutoChem 2920 apparatus from Micromeritics. Before adsorption of ammonia the catalyst was pre-treated at 300 °C in He for 1 h. The

ammonia was adsorbed at 175 °C until saturation of the sample. The acid strength distribution was measured by desorption of ammonia from 175 to 700 °C in He, at a heating rate of 10 °C·min⁻¹. The signals $m/z = 16$ and 17 recorded by the GC-MS were used to obtain the corresponding NH₃ desorption profiles.

3.5.3. Thermogravimetric and derivative thermogravimetric analyses (TGA/DTA)

Chemical and thermal stability of materials can be studied by TG technique, which is commonly used to investigate decomposition, dehydration, etc. The TG device registers the mass changes undergone by the sample as a function of temperature, time and atmosphere. The TG is combined with DTA, which records exothermic or endothermic processes that enclose transformations in the material when compared with an inert reference material.

Thermogravimetric and derivative thermogravimetric (TGA-DTA) analyses were done on a TGA/SDTA851e (Metler Toledo) instrument coupled to a thermobalance. The temperature was increased from room temperature up to 1000 °C in air at a heating rate of 10 °C·min⁻¹. In this study, the TG technique was used to quantify the coke amount over the catalysts used in the MDA reaction.

3.5.4. Temperature programmed oxidation (TPO)

Temperature programmed oxidation of the catalysts used in the MDA reaction allows determine the nature and location of carbonaceous species (coke) therein.

The TPO experiments were carried out on an AutoChem 2920 apparatus from Micromeritics. For TPO analysis the spent catalyst was pre-

treated at 300 °C in He. After cooling to 100 °C, a gas mixture comprising O₂ and He in a volumetric ratio of 0.5:9.5 was introduced increasing up to 900 °C at a heating rate of 5 °C·min⁻¹. Combustion profiles were monitored using the signals $m/z = 44$ (CO₂), 28 (CO), 18 (H₂O) derived from the mass spectrometer coupled.

3.5.5. X-Ray Diffraction (XRD)

X-ray diffraction (XRD) is a non-destructive technique that allows the identification of the crystalline phases and orientation of crystalline materials, their lattice parameters, crystallite size and thermal expansion. In a crystalline material the atoms are arranged in a regular pattern. The unit cell is the smallest volume element that by repetition in three dimensions describes the crystal. Three axes describe the dimensions of the unit cell: a, b, c and so the angles between them α , β , γ . Different combinations of these parameters release fourteen kinds of cells covering all possible point lattices or all crystals, which were classified by August Bravais [15].

X-Ray Diffraction was used to determine and confirm the crystalline structure of a solid sample. Powder X-ray diffraction (XRD) patterns were collected in a PANalytical CUBIX diffractometer equipped with a graphite monochromator, operating at 40 kV and 45 mA and employing nickel-filtered Cu K α radiation ($\lambda = 0.1542$ nm). XRD patterns were recorded in the 2θ range from 2° to 40° and analyzed using X'Pert Highscore Plus software.

3.5.6. ²⁷Al MAS NMR (Magic-Angle Spinning Nuclear Magnetic Resonance)

Nuclear Magnetic Resonance spectroscopy is a powerful and theoretically complex analytical tool, which is based on the splitting of energy

levels of a nucleus with spin different from zero by interaction of nuclear magnetic moments with an external magnetic field very intense which must be constant and uniform. This technique allows identify the chemical environment of the atoms within the solid by the variation of resonance frequency of the nucleus (known as chemical shift), due to the shielding by surrounding electrons is characteristic of the chemical environment of the nucleus. In this work this technique is used to study the environment and coordination of the aluminum atoms in zeolites by studying the ^{27}Al atom.

^{27}Al MAS NMR (Magic-Angle Spinning Nuclear Magnetic Resonance) spectra were recorded at room temperature in a Bruker AV400 spectrometer working at 104.26 MHz, using a 4 mm Bruker BL4 probe. The catalysts were placed into zirconia rotors and spun at 10 kHz and pulses of 0.5 μs . The ^{27}Al spectra was referred to a 0 ppm solution of $\text{Al}(\text{NO}_3)_3$.

3.5.7. X-Ray Photoelectron Spectroscopy (XPS)

The X-ray photoelectron spectroscopy (XPS) technique analyzes the surface chemistry of a material. This technique is based on the analysis of the kinetic energies of the electrons emitted from the sample when its surface is bombarded with X-ray radiation. The photon is absorbed by an atom in a molecule or solid, which leads to ionization and emission of a core (inner-shell) electron. The energy of electrons emitted by the material can be measured by using an appropriate electron energy analyzer and thus, a photoelectron spectrum can be recorded, given by: $E_K = h\nu + BE + E_W$ (24)

Being E_K the kinetic energy of the electrons emitted, $h\nu$ the energy of the incident photons, BE is the binding energy characteristic of each element and E_W is the work function of the spectrometer. The spectrum obtained shows a series of photoelectron peaks whose peak areas determine the composition of the materials surface. The shape of each peak and the binding energy can be

slightly altered by the chemical state of the emitting atom. Thus, these abnormalities can be used to extract chemical bonding information.

Photoelectron spectra (XPS) were recorded on a SPECS spectrometer by using Al K α radiation (Al K α =1486.6 eV), an analyzer pass energy of 30 V, an X-ray power of 100 W and under an operating pressure of 10⁻⁹ mbar. The binding energy (BE) scale was regulated by setting the C 1s transition at 284.6 eV. The accuracy of the BE was ± 0.1 eV. Spectra analysis has been performed using the CASA software.

3.5.8. X-Ray Absorption Near Edge Structure (XANES)

X-ray absorption fine structure (XAFS) concerns how X-rays are absorbed by an atom at energies near and greater than the core-level binding energies of that atom. XAFS spectra are particularly sensitive to the oxidation state, coordination chemistry, and the distances, coordination number and species of the atoms immediately surrounding the selected element. Thus, XAFS is useful to determine the chemical state and local atomic structure for a selected atomic species. The X-ray absorption spectrum can be divided in two parts: X-ray absorption near-edge spectroscopy (XANES) and extended X-ray absorption fine-structure spectroscopy (EXAFS). XANES is very sensitive to formal oxidation state and coordination chemistry (e.g., tetrahedral coordination) of the absorbing atom, while the EXAFS is utilized to determine the distances, coordination number and species of the neighbors of the absorbing atom.

The energy of the X-ray is in the range from ~ 500 eV up to 500 keV (or wavelengths from ~ 25 Å to 0.25 Å). Due to the photoelectric effect this light is absorbed by all matter. In this process an X-ray photon is absorbed by an electron in a firmly bound quantum core level (such as the 1s or 2p level) of

an atom. The BE of the core level must be lower than the energy of the incident X-ray to allow participate this core level in the absorption, causing the ejection of the electron from its quantum level. In this case, the X-ray is absorbed and the excess energy is given to a photo-electron that is ejected from the atom (Figure 21) [16].

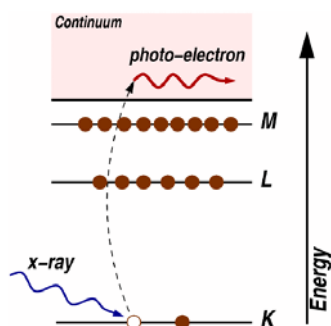


Figure 21. Photoelectric effect: an X-ray is absorbed and a core level electron is ejected from the atom [16].

When the incident X-ray has the same energy that the binding energy of a core level electron, the absorption undergoes a sharp rise (absorption edge), that corresponds to the promotion of this core level to the continuum. The absorption edge energies vary with atomic number and are well-known in the literature [16].

X-Ray Absorption spectra at the Mo K-edge (20000 eV) were collected at ALBA beamline CLÆSS (Barcelona, Spain). A double crystal Si (3 1 1) monochromator without detuning was used to select the X-ray radiation energy. The samples were measured in transmission mode using ionization chambers to record the incident (I_0) and transmitted (I_1) X-ray beam. Mo foil was measured in parallel for energy calibration and some reference Mo compounds: Mo₂C and MoO₃ were measured during the experiment to characterize different oxidation states of the Mo (+2 and +6 respectively). The self-supported pellets of the samples ($\varnothing = 13$ mm) were mounted in a sample holder and three measurements

were carried out at room temperature in air on each sample. The complete experiment (all included) took 5 h and 15 min of time.

3.5.9. Scanning Electron Microscopy (SEM)

Scanning electron microscopy (SEM) allows for high-resolution imaging of surfaces by using high-energy electrons (1.5-20 keV) generated by a heated tungsten filament. Briefly, an incident beam of monochromatic electrons causes a secondary emission across the sample surface, which is collected to form an image of the surface. It is possible to obtain diverse contrast images, i.e., backscattered electrons (BSE), Auger electrons (AES) and energy dispersive x-ray spectroscopy (EDS). BSE causes different contrast subjected to the atomic number, Z , of the elements, so changes in composition can be distinguished; and EDS is a qualitative and quantitative chemical microanalysis technique to characterize the elemental composition of the volume analyzed. EDS is performed in conjunction with a SEM, but uses the X-rays that are emitted from the sample due to the electron beam. The combination of SEM with EDS allows the analysis of the sample morphology and the composition of the different phases that are present.

Conducting materials do not need any handling of the sample but the poor conductors or insulators need a conducting layer that does not modify the topography and allows the transport of the incident beam electrons. This is achieved by coating the sample in vacuum with Au (or graphite for EDS) using a sputter coater.

The SEM micrographs were recorded in a microscope Jeol JSM 6300 with an acceleration voltage of 20 kV. The EDS microanalyses were carried out with a detector from Oxford Instruments. The Software INCAEnergy/Wave was used for the interpretation of the X-ray patterns obtained. Moreover, a ZEISS Ultra55 field emission SEM (FE-SEM) has been also used.

3.5.10. Elemental Analysis

The Elemental Analysis of the different catalysts was performed in EuroEA Elemental Analyzer (Eurovector) to determine the carbon content, using as reference sulphanilamide.

3.5.11. Fourier Transform Infrared Spectroscopy (FTIR)

Infrared spectroscopy technique provides information about the structure, the surface and the acid/basic properties of solid materials through absorption of IR radiation ($\lambda = 750 - 10^5$ nm) due to energy transitions in certain vibrational levels of the chemical bonds. A FTIR spectrum shows specific bands, characteristic vibrations of tension or flexion, for each group of atoms, that are characterized by the intensity and frequency range in which are produced. FTIR technique combined with the use of probe molecules provides information about e.g. the acidity, the basicity and the nature of chemical elements present in the catalyst surface. In particular, in this work this technique was combined with the adsorption/desorption of a basic probe molecule like the pyridine, that allows obtain an estimation of the number and the strength distribution of the Brønsted and Lewis acid sites of a solid sample, from the bands at 1545 cm^{-1} and 1450 cm^{-1} , respectively. The amount of adsorbed pyridine on each type of acid site is determined from the integration of the corresponding bands considering the pellet diameter (13 mm), the weight and the extinction coefficients determined by Emeis [17]:

- Pyridine adsorbed on Brønsted acid sites ($\mu\text{mol Pyr}\cdot\text{g}^{-1}$): $302 \times$ [band intensity at 1545 cm^{-1}]
- Pyridine adsorbed on Lewis acid sites ($\mu\text{mol Pyr}\cdot\text{g}^{-1}$): $153 \times$ [band intensity at 1450 cm^{-1}]

Measurements were performed on Nicolet 710 FT-IR equipment using self-consistent pellets of $10 \text{ mg}\cdot\text{cm}^{-2}$ previously dehydrated for 12 h at $400 \text{ }^\circ\text{C}$ and dynamic vacuum of 10^{-2} Pa . After the dehydration treatment, the sample was cooled up to room temperature and $1.8\cdot 10^3 \text{ Pa}$ of pyridine were introduced into the cell until reach the equilibrium. Then the excess of base was removed by vacuum, the sample was undergone to desorption treatments at different temperatures ($150, 250$ and $350 \text{ }^\circ\text{C}$), and the spectrum was recorded at room temperature after each desorption stage, with the removing of the base line. Measurements were made in a special cell of CaF_2 and the deformation vibration region of adsorbed organic molecules was recorded (1300 cm^{-1} to 2500 cm^{-1}).

3.5.12. Inductively Coupled Plasma Optical Emission Spectroscopy (ICP-OES)

The Si/Al ratio of the synthesized zeolites and the metal content on the catalysts were confirmed and determined by ICP-OES on a Varian 715-ES. The solid samples in powder (30 mg) were dispersed in a volumetric mixture of $\text{HNO}_3:\text{HF}:\text{HCl}$, 1:1:3 (vol. ratio). In all cases, the calibration curve was adjusted to the expected analyte concentration and was determined using standard solutions (Aldrich).

3.5.13. Gas Chromatography and Mass Spectrometry (GC-MS)

The combination of gas chromatography with mass spectrometry (GC-MS) is a technique used to identify the different substances of a compound. In general, the technique consists of a gas chromatograph which separates the different products, while the corresponding molecules are ionized and fragmented by the mass spectrometer in order to allow their identification.

The GC-MS technique has been used to identify the polycyclic aromatic hydrocarbons obtained in the MDA reaction after condense them at the reactor outlet using a cooled trap. The mixture was analyzed by GC-MS on an Agilent 6890N gas chromatograph coupled to a mass spectrometer Agilent 5973N Mass Selective Detector.

3.6. Catalytic evaluation of methane dehydroaromatization

Methane dehydroaromatization experiments were carried out in two different types of reactors: a continuous down-flow fixed bed quartz reactor (FBR) with an inner diameter of 15 mm at 700 °C, and a catalytic membrane quartz reactor (CMR) with an inner diameter of 17 mm at 710 °C and 1.2 bar of pressure. The CMR has been used with a tubular membrane one-close-end (BZCY72) in order to perform the catalytic-electrochemical experiments and also with a quartz tube one-close-end to perform the catalytic experiments that are comparable to the FBR experiments.

3.6.1. Fixed Bed Reactor

In Figure 22 it is shown a simplified scheme of the reaction system used to perform the catalytic experiments using the Fixed Bed Reactor that consists of three zones (from left to right): the gas supply zone, the reaction zone and the analysis zone. Briefly, in the gas supply zone there were six flow mass controllers for different gases, both from pressurized line gases (H₂, N₂, Ar) and from pressurized gas cylinders. Each line was equipped with a non-return valve and then the lines were separated in two zones with three lines each of them. Moreover, each of these two zones were equipped with a three-way valve and a gas bubbler that allowed saturate the corresponding gas/gases with any liquid, if this was not necessary the gas bubbler was bypassed. Then a four-way

pneumatic valve (VN1) allowed supply the gas/gases to the FBR from both zones independently.

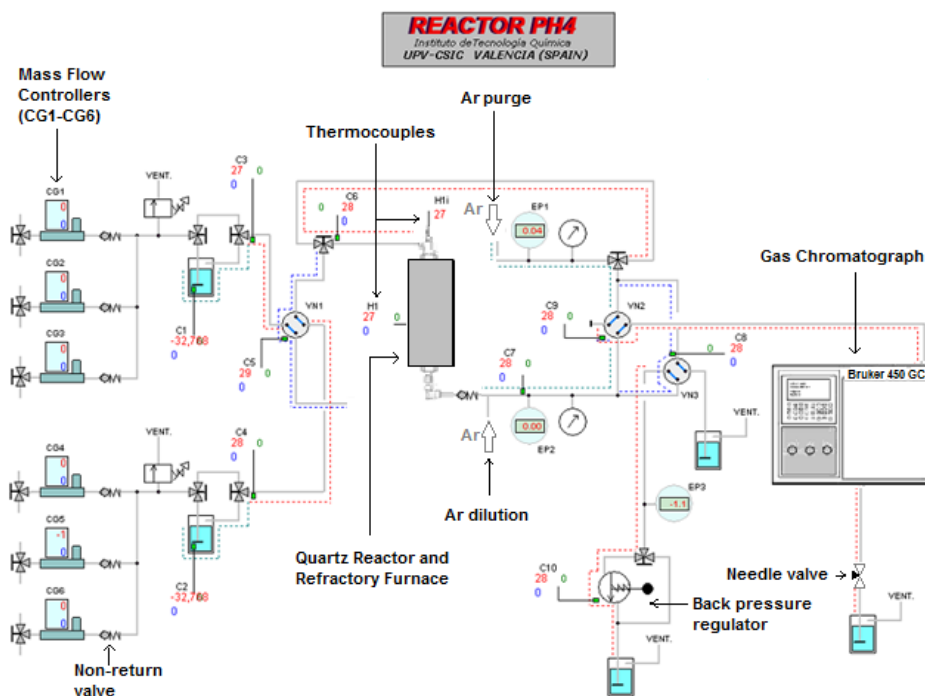


Figure 22. Simplified scheme of the “Reactor PH4”, the reaction system used to perform the catalytic experiments using the Fixed Bed Reactor.

The reaction zone consisted of a quartz reactor with an inner diameter of 15 mm and a refractory furnace with a maximum working temperature of 1100 °C. The FBR was placed in such a way that the catalyst bed was located over the quartz frit in the 2 cm isotherm zone of the refractory furnace (Figure 23). The temperature was controlled with a PID controller integrated in the “Reactor PH4” system via one thermocouple located in the furnace. Other thermocouple placed inside the reactor ensured the correct temperature on it. The methane flow went from top to bottom of the FBR. Furthermore, in the reaction zone there was a three-way valve that allowed bypass the reactor. Reactor downstream all the gas conductions (lines) were heated at 150 °C to

avoid the condensation of heavy aromatics. In addition, at the reactor outlet there was an Argon inlet with a flow of $200 \text{ mL} \cdot \text{min}^{-1}$, thus diluting the reactor outlet stream, before this inlet there was a non-return valve. Then the reactor outlet splits into two branches, one was carried to the gas chromatograph (Bruker 450 GC) through a four-way pneumatic valve (VN2) and the other was vented to the outside, in the latter there was a manual adjusted back pressure regulator.

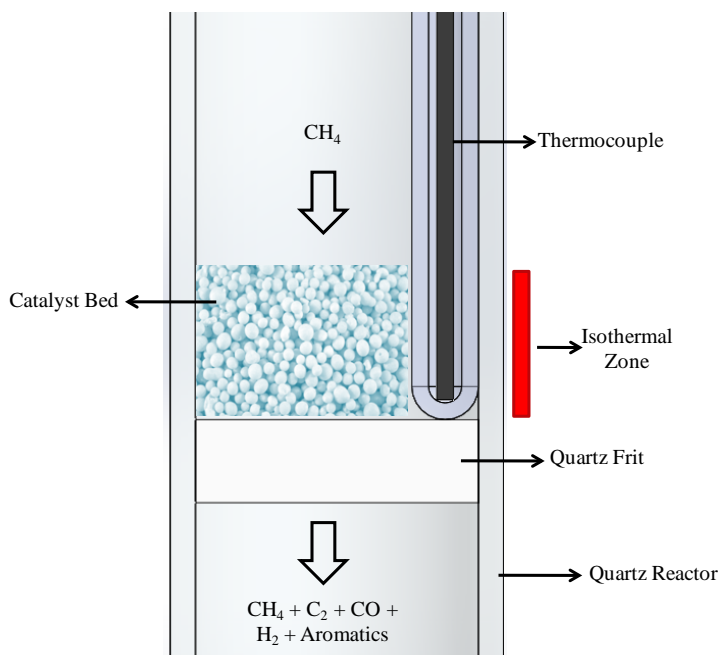


Figure 23. Scheme of the Fixed Bed Reactor (FBR).

In the analysis zone, the VN2 four-way pneumatic valve was kept in the position that allowed supply the reactor outlet stream to the GC during a specific time, after that, the VN2 position was changed to vent this stream entirely and the GC was fed with Ar to purge it. The gaseous components of the reactor outlet stream that were analyzed with the Bruker GC were CH_4 , N_2 , H_2 , CO, ethane, ethylene, benzene, naphthalene and toluene. Moreover, the GC

outlet was vented to the outside through a needle valve that allowed adjust the outlet flow and after the needle valve a glass rotameter was placed to check it.

The thermocouples employed in this system were type K (Inconel® alloy 600, with a diameter of 1 mm) and they were never in contact with the gases inside the reactor. Furthermore, the mass flow controllers and the rotameter were previously calibrated for the different gases that were used in the MDA reaction, for the calibration a bubble flowmeter was used as it allows the real flow measurement.

3.6.1.1. Experimental procedure

Briefly, in a typical experiment 0.6 g of catalyst were diluted with 1.953 g of silicon carbide (SiC) and loaded to the reactor, an additional SiC bed (3.745 g) was placed on top of the catalyst fixed bed. The silicon carbide is an inert that was used to improve the methane and heat diffusion in the catalyst, and it was tested that not participates in this reaction. The catalysts were pre-treated in situ in a flow of Ar ($50 \text{ mL}\cdot\text{min}^{-1}$) from room temperature up to $700 \text{ }^\circ\text{C}$, and kept at this temperature for 30 min. Then, the flow of Ar was switched by the feed gas mixture comprising CH_4 and N_2 (internal standard) in a volumetric ratio of 9.5:0.5 at a flow of $15 \text{ mL}\cdot\text{min}^{-1}$, being the space velocity of $1500 \text{ mL}\cdot\text{h}^{-1}\cdot\text{g}_{\text{cat}}^{-1}$ ($1425 \text{ mL}_{\text{CH}_4}\cdot\text{h}^{-1}\cdot\text{g}_{\text{cat}}^{-1}$) or 900 h^{-1} for the catalyst prepared with the HZSM-5 zeolite and 562.5 h^{-1} for the catalyst prepared with the MCM-22 zeolite. Moreover, a flow of $200 \text{ mL}\cdot\text{min}^{-1}$ of Ar was introduced at the reactor outlet to dilute the reaction products. Finally, the experiments were carried out at 1.2 bar of pressure.

The unconverted methane and the formed products were separated and analyzed on line at different times on stream using a gas chromatograph Bruker 450-GC equipped with five packed columns, one capillary column and three detectors. The Channel 1 is endowed with two packed columns (one Molsieve

5A and one Hayesep Q) connected to one Thermal Conductivity Detector (TCD) that allows separate and quantify H₂. Moreover, the Channel 2 is equipped with three packed columns (one Molsieve 13X, one Hayesep Q and one Hayesep N) connected to the other TCD that allows separate and quantify H₂, CO₂, C₂H₄, C₂H₆, O₂, N₂, CH₄ and CO. And the Channel 3 is endowed with one capillary column (WCOT BR-1) connected to one Flame Ionization Detector (FID) to separate and quantify CH₄, C₂H₄, C₂H₆, C₆H₆, C₇H₈ and C₁₀H₈. All the products analyzed with the GC were previously identified with the analysis of commercial standards, both in gaseous form and in liquid form. The former were directly injected by the loops of the valves of each GC channel, while the latter were injected manually in the GC with a calibrated syringe of 10 µL.

For the purpose of knowing which heavy aromatic products were obtained in this reaction, in addition to the results obtained with the data recorded in the Bruker GC, during one experiment carried out with 3% (wt.) Mo/HZSM-5 catalyst (CBV3020 zeolite) a trap was placed at the reactor outlet using ice to keep it cool, and thus some aromatic products were condensed. The condensed residue was dissolved with toluene and then it was analyzed with a GC-MS. This was done twice during the same experiment, the first time after 1 h of MDA reaction and the second time after 10 h on stream. The chromatograms obtained are shown in Figure 24 and Figure 25, respectively. As seen, the main product was the naphthalene, followed by the 2-methylnaphthalene. The other products were in lower extent, including an aliphatic series from very heavy products. After 10 h of reaction (Figure 25) some products were reduced considerably, such as the biphenyl and the 2-ethenylnaphthalene. These products were formed on the zeolite surface and they are considered coke precursors, being briefly detailed in Table 4.

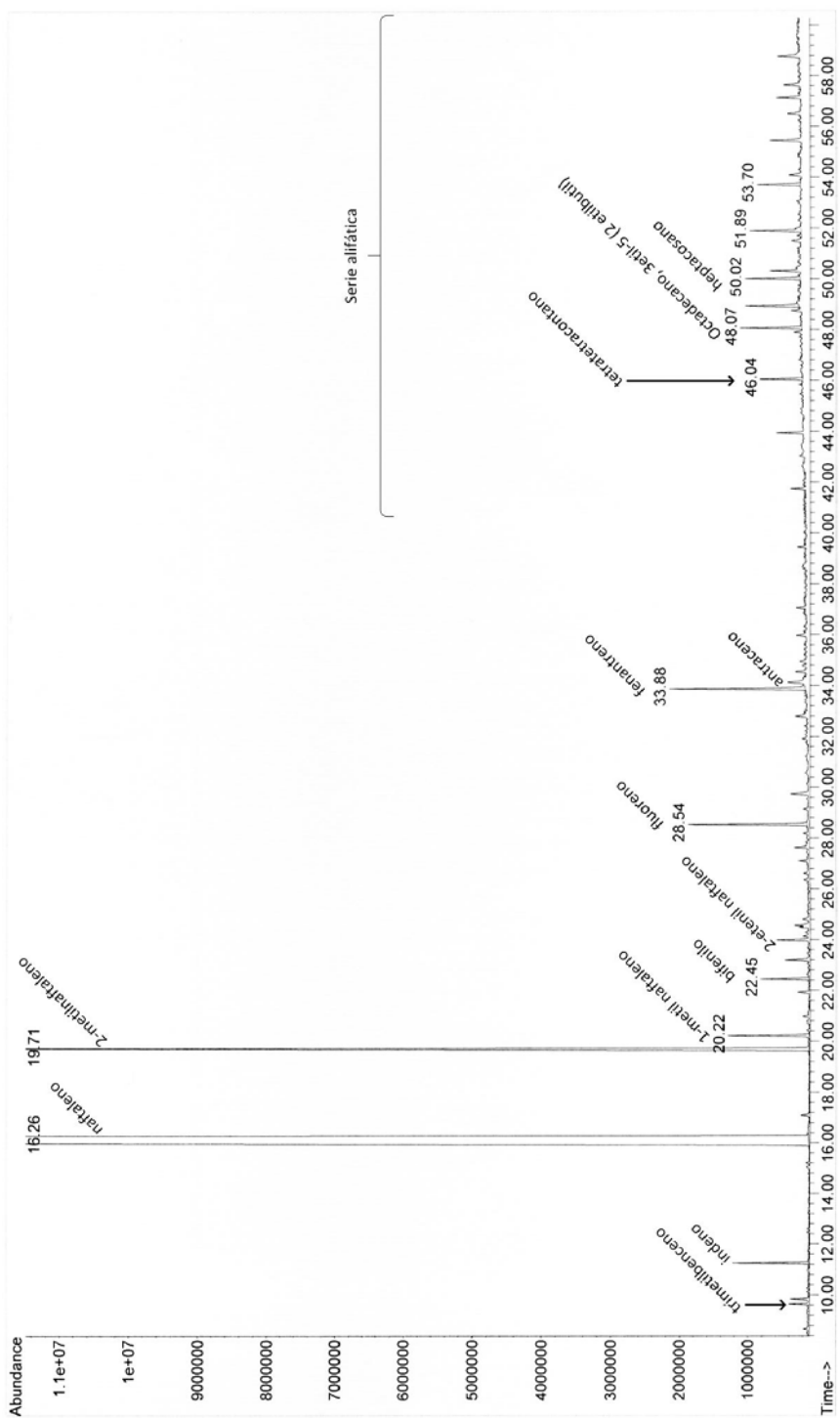


Figure 24. Chromatogram of MDA products over 3% (wt.) Mo/CBV3020 after 1 h of reaction (detail of heavy products).

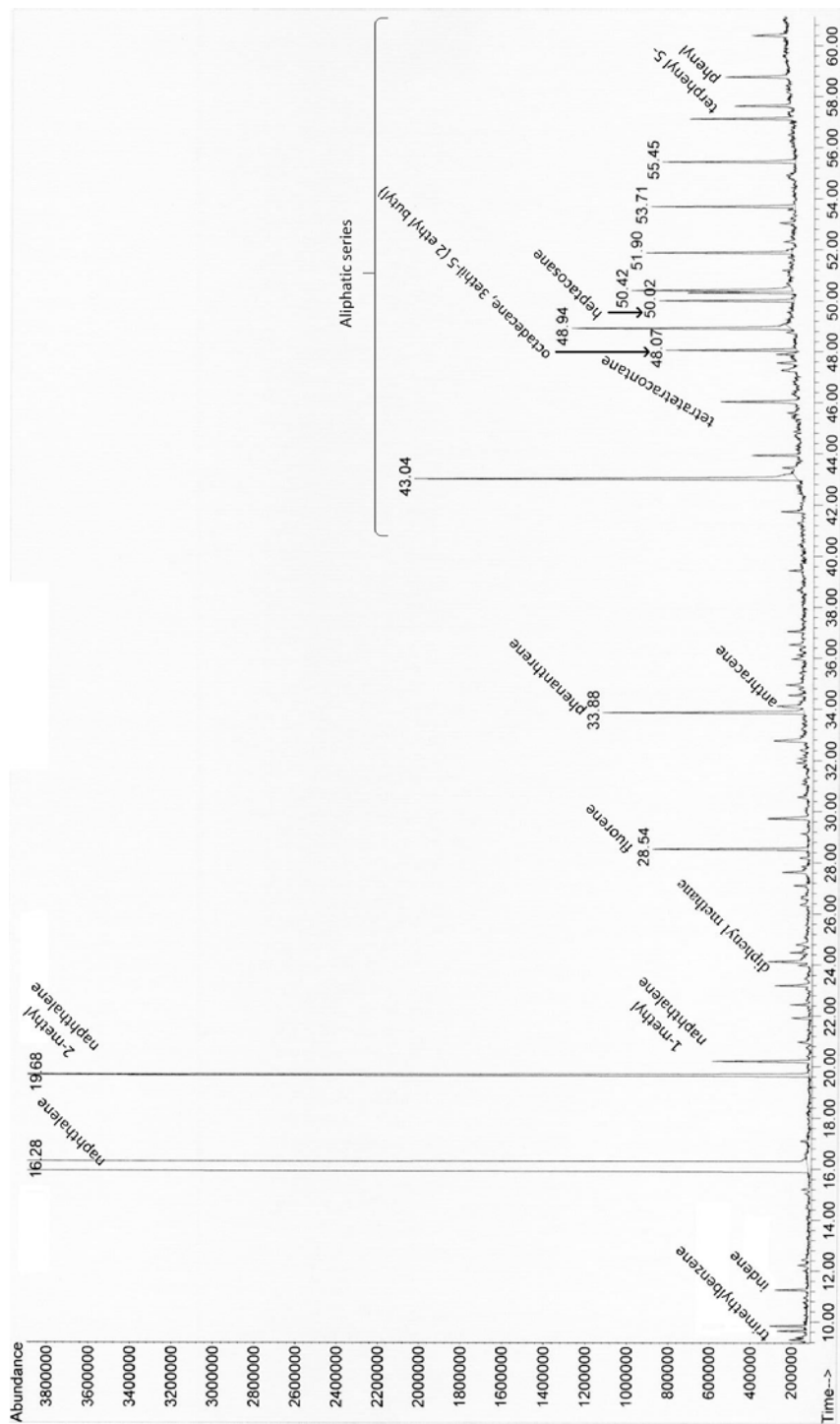


Figure 25. Chromatogram of MDA products over 3% (wt.) Mo/CBV3020 after 10 h of reaction (detail of heavy products).

Table 4. Products obtained in the chromatograms showed in Figure 24 and Figure 25.

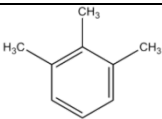
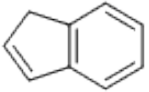
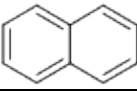
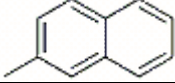
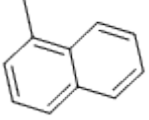
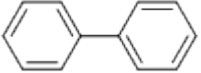
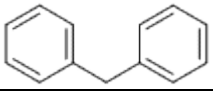
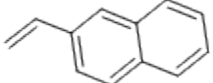
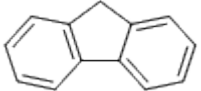
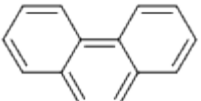
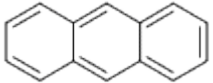
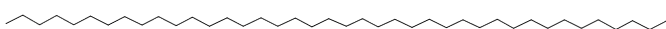
Name	Molecular formula	Structure
1,2,3-trimethylbenzene	C_9H_{12}	
indene	C_9H_8	
naphthalene	$C_{10}H_8$	
2-methyl naphthalene	$C_{11}H_{10}$	
1-methyl naphthalene	$C_{11}H_{10}$	
biphenyl	$C_{12}H_{10}$	
diphenyl methane	$C_{13}H_{12}$	
2-ethenyl naphthalene	$C_{12}H_{10}$	
fluorene	$C_{13}H_{10}$	
phenanthrene	$C_{14}H_{10}$	
anthracene	$C_{14}H_{10}$	
Tetratetracontane	$C_{44}H_{90}$	

Table 4 (Continued). Products obtained in the chromatograms showed in Figure 24 and Figure 25.

octadecane 3-ethyl-5 (2-ethylbutyl)	$C_{26}H_{54}$	
Heptacosane	$C_{27}H_{56}$	
terphenyl, 5-phenyl	$C_{24}H_{18}$	

Additionally, in order to obtain quantitative results from the Bruker GC data was necessary to use correction factors that were dependent on the compound response to the corresponding detector. In this work the response factors of each compound have been determined experimentally using an Ar flow of $200 \text{ mL} \cdot \text{min}^{-1}$ after the reactor (the same dilution used during the MDA reaction). On the one hand, N_2 and CH_4 (Channel 2, TCD) were calibrated with different flows of the feed gas mixture ($CH_4:N_2$, 9.5:0.5 vol. ratio) using N_2 as internal standard, and their response factors were calculated in the following way:

$$RF_i = \frac{A_i}{C_i}; \quad \text{e.g. for } N_2 \text{ is } RF_{N_2} = \frac{A_{N_2}}{C_{N_2}} \quad (\text{Channel 2}) \quad (25)$$

$$RF_{CH_4} = \frac{A_{CH_4}/A_{N_2}}{C_{CH_4}/C_{N_2}} \quad (\text{Channel 2}) \quad (26)$$

$$C_i = \frac{F_i}{F_{Ar} + F_T} \cdot 100 \quad (27)$$

where “*i*” is the corresponding gas, “*RF*” is the response factor, “*A*” is the chromatographic area ($\mu\text{V}\cdot\text{min}$), “*C*” is the concentration (%) and “*F*” is the flow ($\text{mL}\cdot\text{min}^{-1}$), moreover “ F_{Ar} ” is the Ar flow to dilute ($200 \text{ mL}\cdot\text{min}^{-1}$) and “ F_T ” is the total flow of the gas mixture used. At the same time the CH_4 was calibrated in the Channel 3 (FID) using the same gas mixture and the response factor was calculated with the Equation 25.

Moreover H_2 , C_2H_4 , C_2H_6 and CO were calibrated with different flows of a gas mixture with other gases, like N_2 , CH_4 , CO_2 and C_3 hydrocarbons. On the one hand, the response factor of the H_2 (Channel 1, TCD) was calculated with the Equation 25 and the response factors of the C_2 hydrocarbons separately (Channel 3, FID) and CO (Channel 2, TCD) were calculated using CH_4 as internal standard (Equations 28 and 29, respectively); it is understood that the chromatographic area of methane (A_{CH_4}) is different depending on the chromatograph Channel (due to the different detectors):

$$RF_{C_2} = \frac{A_{C_2}/A_{\text{CH}_4}}{C_{C_2}/C_{\text{CH}_4}} \quad (\text{Channel 3}) \quad (28)$$

$$RF_{CO} = \frac{A_{CO}/A_{\text{CH}_4}}{C_{CO}/C_{\text{CH}_4}} \quad (\text{Channel 2}) \quad (29)$$

Finally, the aromatic compounds (benzene, toluene and naphthalene) were calibrated individually. For this purpose, a specific amount of the aromatic compound was introduced in one of the bubblers of the “Reactor PH4” system,

passing through it a flow of the feed gas mixture ($\text{CH}_4:\text{N}_2$, 9.5:0.5 vol. ratio), and all the conductions downstream of the bubbler were heated at 150 °C to avoid the condensation of the aromatic compound. In the case of benzene and toluene was necessary to cool them, introducing the bubbler inside a beaker with H_2O deionized and ice under stirring. Nevertheless, it was necessary to heat the naphthalene since at room temperature is solid, introducing the bubbler inside a beaker with H_2O deionized under stirring, and avoiding during the calibration time the naphthalene condensation in the glass walls of the bubbler. For the three aromatic compounds a thermocouple type K was put within the aromatic compound to control the temperature using a septum to avoid any leakage. Furthermore, it was necessary to calculate the required temperature to reach a specific aromatic vapor pressure and also the gas mixture ($\text{CH}_4:\text{N}_2$, 9.5:0.5 vol. ratio) flow to get an aromatic concentration as close as possible to the maximum concentration obtained on the MDA reaction.

The Antoine equation [18] was used to calculate the benzene vapor pressure at 12 °C (285 K) (Equation 30), from this was possible calculate both the flow (Equation 31) and the concentration of benzene (Equation 32) using a specific flow of the gas mixture $\text{CH}_4:\text{N}_2$ ($10 \text{ mL} \cdot \text{min}^{-1}$):

$$\ln P = 15.9 - \frac{2788.51}{285 - 52.36} \rightarrow P_{C_6H_6} = 0.066 \text{ atm} \quad (30)$$

$$F_{AC} = \frac{n_{AC} \cdot R \cdot T}{P_T} \quad (31)$$

$$C_{AC} = \frac{F_{AC}}{F_{Ar} + F_{AC} + F_{GM}} \cdot 100 \quad (32)$$

where “AC” is the corresponding aromatic compound, “ F_{GM} ” is the gas mixture $\text{CH}_4:\text{N}_2$ flow ($10 \text{ mL} \cdot \text{min}^{-1}$) and “ F_{Ar} ” is the Ar flow to dilute ($200 \text{ mL} \cdot \text{min}^{-1}$).

In the case of toluene its vapor pressure at 1 °C (274 K) was calculated using the Equation 33 [19], and as with the benzene the flow (Equation 31) and

the concentration of toluene (Equation 32) were calculated using a specific flow of the gas mixture CH₄:N₂ (10 mL·min⁻¹):

$$\log P = 6.1528 - \frac{1376.81}{274 - 51.1} \rightarrow P_{C_7H_8} = 9.34 \cdot 10^{-3} \text{ atm} \quad (33)$$

In the case of naphthalene its vapor pressure at 67 °C (340 K) was calculated using the Equation 34 [20], and then the flow (Equation 31) and the concentration of naphthalene (Equation 32) were calculated using a specific flow of the gas mixture CH₄:N₂ (45 mL·min⁻¹):

$$\log P = -\left(\frac{3801}{340}\right) + 13.8 \rightarrow P_{C_{10}H_8} = 0.00412 \text{ atm} \quad (34)$$

Thus, the response factors of the aromatic hydrocarbons separately (Channel 3, FID) were calculated using CH₄ as internal standard (Equation 35):

$$RF_{AC} = \frac{A_{AC}/A_{CH_4}}{C_{AC}/C_{CH_4}} \quad (\text{Channel 3}) \quad (35)$$

In addition, the methane conversion and the selectivities of the different products were evaluated on carbon basis. First it was necessary to calculate the molar concentration of all the compounds, for this the chromatographic areas and the response factors (calculated as abovementioned) were used. The molar concentration “*C_m*” (molar %) was calculated using the Equation 36 for H₂ (Channel 1, TCD), N₂ (Channel 2, TCD) and CH₄ (Channel 3, FID):

$$Cm_i = \frac{A_i}{RF_i} \quad (36)$$

Moreover, the molar concentration “*C_m*” (molar %) was calculated using the Equation 37 for CH₄ (Channel 2, TCD) and the Equation 38 for CO (Channel 2, TCD):

$$Cm_{CH_4} = \frac{A_{CH_4} \cdot Cm_{N_2}}{A_{N_2} \cdot RF_{CH_4}} \quad (\text{Channel 2}) \quad (37)$$

$$Cm_{CO} = \frac{A_{CO} \cdot Cm_{CH_4}}{A_{CH_4} \cdot RF_{CO}} \quad (\text{Channel 2}) \quad (38)$$

The methane conversion “ X_{CH_4} ” was calculated using the Equation 39, with the feed methane molar concentration “ $Cm_{CH_4}^{in}$ ” (Equation 37), that was obtained in the Channel 2 and was measured before the beginning of MDA reaction at room temperature, and the methane molar concentration obtained during the MDA reaction “ $Cm_{CH_4}^{out}$ ” (Equation 37):

$$X_{CH_4} = \frac{Cm_{CH_4}^{in} - Cm_{CH_4}^{out}}{Cm_{CH_4}^{in}} \cdot 100 \quad (39)$$

For ethylene, ethane, benzene, toluene and naphthalene (Channel 3, FID), the molar concentration “ Cm ” (molar %) was calculated using the Equation 40, in all the cases the “ Cm_{CH_4} ” used was that obtained for the Channel 2, that was very similar to the molar concentration calculated for the methane in the Channel 3 due to the use of N_2 as internal standard to calculate it:

$$Cm_i = \frac{A_i \cdot [Cm_{CH_4} (\text{Channel 2})]}{[A_{CH_4} (\text{Channel 3})] \cdot RF_i} \quad (\text{Channel 3}) \quad (40)$$

For the calculation of the selectivities (Equation 41) of the different products on carbon basis it was needed the previous calculation of the molar flows of each of them and of the methane reacted “ CH_4R ” (Equation 42):

$$S_i = \frac{nc \cdot W_i}{W_{CH_4R}} \cdot 100 \quad (41)$$

$$W_{CH_4R} = W_{CH_4}^{in} - W_{CH_4}^{out} \quad (42)$$

where “ S_i ” is the corresponding product selectivity, “ nc ” is the number of carbons, “ W_i ” is the molar flow ($\text{mol}\cdot\text{min}^{-1}$) and “ W_{CH_4R} ” is the molar flow of the methane reacted.

Furthermore, the molar flow of carbonaceous deposits (coke) was obtained as the difference between the carbon in the feed ($W_{CH_4}^{in}$) and the carbon in the products (unreacted CH_4 , CO and hydrocarbons analyzed) at the reactor outlet (W_C). The coke estimated from GC analysis is composed by undetected carbon products such as different types of carbon (amorphous and graphitic) that are deposited on the catalyst, and heavy aromatic products such those detailed in Table 4 that are in lesser extent. The subscript “ hc ” indicates hydrocarbon:

$$W_{Coke} = W_{CH_4}^{in} - W_C \quad (43)$$

$$W_C = W_{CO} + \sum nc \cdot W_{hc} \quad (44)$$

Finally the yield (Y_i) of the products was obtained using the Equation 45 and the flow ($\text{mL}\cdot\text{min}^{-1}$) of any product can be calculated with the Equation 46:

$$Y_i = \frac{S_i \cdot X_{CH_4}}{100} \quad (45)$$

$$F_i = \frac{Cm_i \cdot (F_T + F_{Ar})}{100} \quad (46)$$

In addition, the extrudated catalysts used in the experiments performed with the FBR were prepared according to the procedure described in the section 3.3.2. It should be noted that the Si-containing binder (Silres) left a silica-like residue after its calcination in air at $500\text{ }^\circ\text{C}$. Therefore in order to avoid the dilution of the catalyst was necessary to do a correction of the catalyst mass used in each experiment with the following equations:

$$PZ = \frac{mZ'}{mZ' + (mS \cdot RS)} \cdot 100 \quad (47)$$

$$mC = \frac{mZ}{(PZ/100)} \quad (48)$$

where “PZ” is the zeolite percentage that has the catalyst prepared (%), “mZ'” is the zeolite mass used to prepare the catalyst (g), “mS” is the Silres mass (g), “RS” is the silica-like residue that the Silres leaves after the calcination, “mC” is the catalyst mass needed to avoid the dilution (g) and “mZ” is the zeolite mass that would have if the catalyst would not have Silres.

3.6.1.2. Different operating conditions

In some experiments different operating conditions were varied to study the performance of the MDA reaction, these were: the co-feeding of H₂, H₂O and CO₂, the catalyst activation, the catalyst regeneration with H₂ and the use of the same space velocity but changing both the catalyst amount and the feed gas mixture flow. It should be noted that in these experiments the HZSM-5 zeolite refers to the CBV3024E commercial zeolite and the HMCM-22 zeolite has a Si/Al ratio equal to 15.

3.6.1.2.1. Use of different co-feeding gas in the MDA reaction with the FBR

3.6.1.2.1.1. Co-feeding of 6% of H₂

In order to co-feed H₂ it was necessary to use other feed gas mixture comprising CH₄, H₂ and N₂ (internal standard) in a volumetric ratio of 8.9:0.6:0.5 at a flow of 15 mL·min⁻¹, being the space velocity of 1500 mL·h⁻¹·g_{cat}⁻¹ (1335 mL_{CH₄}·h⁻¹·g_{cat}⁻¹). These experiments were carried out with the gas mixture with H₂ since the beginning of the MDA reaction, in dry conditions and with a total time on stream (TOS) of 17 h.

3.6.1.2.1.2. Co-feeding of H₂O

However, for the co-feeding of H₂O the feed gas was CH₄:N₂ (9.5:0.5 vol. ratio) at a flow of 15 mL·min⁻¹, being the space velocity of 1500 mL·h⁻¹·g_{cat}⁻¹. As abovementioned in the section 2.5.3., a H₂O vapor concentration that results beneficial for MDA reaction should be lower than 1.7%. In order to perform these experiments different saturated aqueous salt solutions were prepared and put inside one of the bubblers of the “Reactor PH4” system. Each of them was used at room temperature using a thermocouple type K within the saturated aqueous salt solution to control the temperature, using a septum to avoid any leakage (the temperature was different depending on the day, therefore the H₂O vapor concentration might be slightly different despite use the same saturated aqueous salt solution). Because of the need to keep the experiment in oxygen free conditions, previous to start the MDA reaction it was necessary to degas the saturated aqueous salt solution during 30 min with the feed gas mixture at room temperature and through the bypass keep it isolated.

In particular, the salts employed to prepare the saturated aqueous solutions were potassium carbonate and potassium acetate. The H₂O vapor concentration was ascertained from the H₂O vapor pressure of the corresponding saturated aqueous salt solution, at a given temperature, which was calculated using the Equation 49:

$$P_{SS} = \frac{RH_{SS}}{100} \cdot P_W \quad (49)$$

where “ P_{SS} ” is the H₂O vapor pressure of the saturated aqueous salt solution (atm), “ RH_{SS} ” is the relative humidity (%) of the saturated aqueous salt solution at a given temperature [21], and “ P_W ” is the H₂O vapor pressure (atm) at a given temperature [22].

In the experiments carried out with the 6% (wt.) Mo/HZSM-5 catalyst, the feed gas mixture (CH₄:N₂, 9.5:0.5 vol. ratio) was introduced in the bubbler

with both saturated aqueous salt solutions separately after 1 h of MDA reaction in dry conditions, achieving the following H₂O vapor concentrations:

- Potassium carbonate: $C_{PCS} = 1.08\%$ (at 21.5 °C), with a TOS in wet conditions of 16 h.
- Potassium acetate: $C_{PAS} = 0.90\%$ (at 30 °C), with a TOS in wet conditions of 62 h.

While in the experiments done with the 6% (wt.) Mo/HMCM-22 catalyst, the feed gas mixture was introduced in the bubbler with the saturated aqueous solution of potassium carbonate after different times of MDA reaction in dry conditions: 1, 3, 4 and 5 h. And after that, one experiment with the potassium acetate solution was performed introducing the feed gas after 3 h of MDA reaction in dry conditions. The H₂O vapor concentrations obtained were the following:

- Potassium carbonate: $C_{PCS} = 1.08\%$ (at 21.5 °C) when the humidification was produced after 1, 3, 4 and 5 h of MDA reaction in dry conditions, with a TOS in wet conditions of 16.50, 14, 19 and 63 h respectively.
- Potassium acetate: $C_{PAS} = 0.86\%$ (at 29 °C), with a TOS in wet conditions of 64 h.

3.6.1.2.1.3. Co-feeding of 2% of CO₂

For the co-feeding of CO₂ one different feed gas mixture was used comprising:

- CH₄, CO₂ and N₂ (internal standard) in a volumetric ratio of 9.3:0.2:0.5 at a flow of 15 mL·min⁻¹, being the space velocity of 1500 mL·h⁻¹·g_{cat}⁻¹ (1395 mL_{CH₄}·h⁻¹·g_{cat}⁻¹).

The 6% (wt.) Mo/HZSM-5 catalyst was tested in two experiments with this gas mixture, in one of them this mixture was used since the beginning of

the MDA reaction in dry conditions, with a TOS of 17 h. While in the other experiment, during the first hour of MDA reaction the feed gas mixture was composed by CH₄:N₂ (9.5:0.5 vol. ratio) and after this time the gas mixture with 2% of CO₂ was introduced for 61.50 h, throughout the total TOS are dry conditions.

Furthermore, the 6% (wt.) Mo/HMCM-22 catalyst was tested in one experiment, in which during the first 3 h of MDA reaction the feed gas mixture used did not have CO₂ (CH₄:N₂, 9.5:0.5 vol. ratio), and after this TOS the gas mixture with 2% of CO₂ was introduced for 68 h, throughout the total TOS are dry conditions.

3.6.1.2.2. Use of different catalyst activation on MDA reaction with the FBR

3.6.1.2.2.1. Pre-coking of the 6% (wt.) Mo/HZSM-5 catalyst

1,2,4-trimethylbenzene was used to pre-coke the 6% (wt.) Mo/HZSM-5 catalyst, thus it was put inside one of the bubblers of the “Reactor PH4” system and was heated up to 51 °C. All the conductions downstream of the bubbler were heated at 150 °C to avoid the condensation of the aromatic compounds. In addition, a thermocouple type K was used within the 1,2,4-trimethylbenzene (TMB) to control the temperature, using a septum to avoid any leakage. Because of the need to keep the experiment in oxygen free conditions, previous to start the MDA reaction it was necessary to degas the TMB during 30 min with Ar at room temperature and through the bypass keep it isolated. Then the experiment was carried out using the standard conditions up to 600 °C, when the Ar flow (50 mL·min⁻¹) was introduced in the TMB during 4 h and, after the pre-coking, the MDA reaction continues to follow the usual conditions for 17 h bypassing the bubbler.

The Antoine equation [18] was used to calculate the 1,2,4-trimethylbenzene vapor pressure at 51 °C (324 K) (Equation 50).

$$\ln P = 16.219 - \frac{3622.58}{324 - 64.59} \rightarrow P_{TMB} = 0.0125 \text{ atm} \quad (50)$$

3.6.1.2.2.2. Catalyst activation with a gas mixture of CH₄:H₂, 1:4 (vol. ratio)

In situ catalyst activation, before catalytic testing, enables to produce a material with suitable catalytic activity. In this case, the catalyst was pre-carburized and pre-reduced aiming to achieve the species more stable and active on MDA reaction (as abovementioned in the section 2.5.1.), using a gas mixture of CH₄:H₂, in a volumetric ratio of 1:4. After the activation the reaction was carried out with the feed gas mixture of CH₄:N₂ (9.5:0.5 vol. ratio) for 17 h, and the different activation conditions were as follows:

- 6% (wt.) Mo/HZSM-5 catalyst: in one experiment the catalyst was pre-carburized and pre-reduced for 1 h up to 700 °C and kept at this temperature during 2 h. While in other experiment the catalyst was pre-carburized and pre-reduced during 4 h up to 700 °C and kept at this temperature for 2 h.
- 6% (wt.) Mo/HMCM-22 catalyst: one experiment in which the catalyst was pre-carburized and pre-reduced for 1 h up to 700 °C and kept at this temperature during 2 h.

3.6.1.2.3. Catalyst regeneration with H₂ using the FBR

Different catalyst regenerations with H₂ were carried out after a specific TOS in dry conditions using both the 6%Mo/HZSM-5 and the 6%Mo/MCM-22 catalysts. Firstly, for the 6% (wt.) Mo/HZSM-5 catalyst, the regeneration took place after 19.70 h of MDA reaction, the feed gas mixture of CH₄:N₂, 9.5:0.5

(vol. ratio) was switched by pure H₂ (100 mL·min⁻¹) for 2 h. Then the feed gas mixture was introduced again during 68.70 h.

Moreover, the regeneration with H₂ was done in one experiment performed with the 6% (wt.) Mo/HZSM-5 catalyst in wet conditions. In particular, during the first hour the MDA reaction was carried out in dry conditions, then the feed gas mixture was introduced in a bubbler with the saturated aqueous solution of potassium carbonate, reaching a H₂O vapor concentration of 1.08% at 21.5 °C, during 38.70 h. Then the catalyst regeneration with H₂ (100 mL·min⁻¹) was done for 2 h in dry conditions and, after that, the feed gas mixture was introduced again during 69 h in wet conditions.

However, with the 6% (wt.) Mo/HMCM-22 catalyst, one experiment was carried out with two cycles of regeneration with H₂ (100 mL·min⁻¹ for 2 h), the first regeneration was carried out after 24.33 h and the second after 22 h from the first regeneration. Then the MDA reaction continued during 110.33 h until total catalyst deactivation.

3.6.1.2.4. Use of different space velocity and change the catalyst amount and the feed gas flow using the same space velocity (1500 mL·h⁻¹·g_{cat}⁻¹) with the FBR

3.6.1.2.4.1. Use of different space velocity with the 6% (wt.) Mo/MCM-22 catalyst

In this experiment, the catalyst amount was 0.6 g and the feed gas flow of CH₄:N₂ (9.5:0.5 vol. ratio) was 8.35 mL·min⁻¹ instead of 15 mL·min⁻¹, being the space velocity 835 mL·h⁻¹·g_{cat}⁻¹ (313.12 h⁻¹), (793.25 mL_{CH₄}·h⁻¹·g_{cat}⁻¹) instead of 1500 mL·h⁻¹·g_{cat}⁻¹. The catalyst was diluted with 2.77 g of silicon carbide (SiC) and loaded to the reactor, an additional SiC bed (3.745 g) was

placed on top of the catalyst fixed bed. The catalyst was pre-treated in situ in a flow of Ar ($50 \text{ mL}\cdot\text{min}^{-1}$) from room temperature up to $700 \text{ }^\circ\text{C}$, and kept at this temperature for 30 min. Then, the flow of Ar was switched by the feed gas mixture. As stated above, it was introduced a flow of $200 \text{ mL}\cdot\text{min}^{-1}$ of Ar at reactor outlet to dilute the reaction products.

3.6.1.2.4.2. Change the catalyst amount and the feed gas flow using the same space velocity with the 6% (wt.) Mo/HZSM-5 catalyst

In this experiment, the catalyst amount was 1.8 g instead of 0.6 g, and the feed gas flow of $\text{CH}_4:\text{N}_2$ (9.5:0.5 vol. ratio) was $45 \text{ mL}\cdot\text{min}^{-1}$ instead of $15 \text{ mL}\cdot\text{min}^{-1}$, maintaining the space velocity at $1500 \text{ mL}\cdot\text{h}^{-1}\cdot\text{g}_{\text{cat}}^{-1}$ (871 h^{-1}), ($1425 \text{ mL}_{\text{CH}_4}\cdot\text{h}^{-1}\cdot\text{g}_{\text{cat}}^{-1}$). The catalyst was diluted with 1.953 g of silicon carbide (SiC) and loaded to the reactor, an additional SiC bed (3.745 g) was placed on top of the catalyst fixed bed. The catalyst was pre-treated in situ in a flow of Ar ($50 \text{ mL}\cdot\text{min}^{-1}$) from room temperature up to $700 \text{ }^\circ\text{C}$, and kept at this temperature for 30 min. Then, the flow of Ar was switched by the feed gas mixture.

3.6.2. Catalytic Membrane Reactor

In order to perform the catalytic-electrochemical experiments using a tubular membrane one-close-end (BZCY72) to remove H_2 from the MDA reaction side and thus displace the equilibrium, obtaining an increase of benzene yield, it was necessary to design and develop a tailored catalytic membrane reactor and perform several changes in the "Reactor PH4" system. It should be noted that the 6% (wt.) Mo/HMCM-22 (Si/Al=15) catalyst was used in all the experiments performed with the CMR.

3.6.2.1. Catalytic Membrane Reactor with continuous H₂ removal through BaZr_{0.7}Ce_{0.2}Y_{0.1}O_{3-δ} tubular membranes

In Figure 26 it is depicted a simplified scheme of the new reaction system used to perform the catalytic-electrochemical experiments using the tailored Catalytic Membrane Reactor (CMR) that consisted of four zones: the gases supply zone, the reaction zone, the analysis zone and the voltammetry zone. Briefly, in the gas supply zone there were six flow mass controllers for different gases, both from pressurized line gases (H₂, N₂, Ar) and from pressurized gas cylinders. Each line was equipped with a non-return valve and then the lines were separated in two zones with three lines each of them. Moreover, each of these two zones were endowed with a three-way valve and a gas bubbler that allowed saturate the corresponding gas/gases with any liquid, if this was not necessary the gas bubbler was bypassed. Then a four-way pneumatic valve (VN1) allowed supply independently the gas/gases to the two inlets of the CMR: the MDA reaction inlet (outside the tubular membrane) and the sweep inlet (inside the tubular membrane).

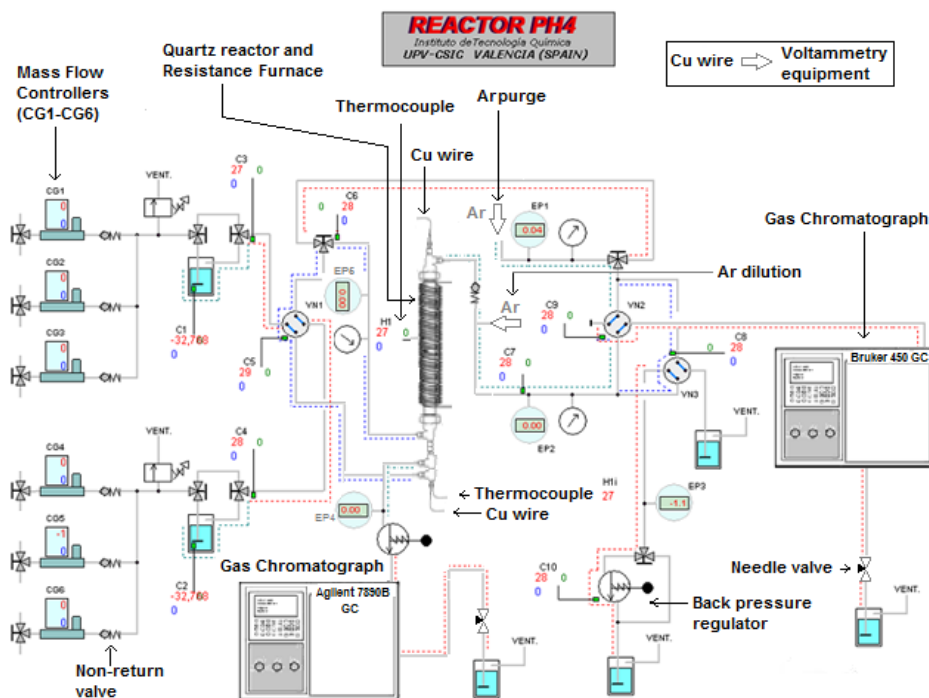


Figure 26. Simplified scheme of the new “Reactor PH4”, reaction system used to perform the catalytic-electrochemical experiments using the Catalytic Membrane Reactor.

The reaction zone (Figure 27 and Figure 28) consisted of a quartz reactor with an inner diameter of 17 mm and a coiled resistance furnace with a maximum working temperature of 750 °C. The methane flow went from bottom to top of the CMR. The tubular membrane (BZCY72) had an external diameter of 10 mm and it was concentrically placed inside of the CM reactor using a stainless steel fitting that also allowed isolate the MDA reaction side from the sweep side by a Viton® o-ring, thus avoiding any leakage. In this case was necessary to put quartz wool in the MDA reaction side around the membrane (~3.5 mm of circular hollow ring), each time in order to place over it the catalyst bed. In addition, the anode had to be painted on the tubular membrane electrolyte at the suitable position to face the catalyst (Figure 28). The catalyst

bed and the tubular membrane (BZCY72) were placed in such a way that they were in the 4 cm isotherm zone of the coiled resistance furnace. The temperature was also controlled with a PID controller integrated in the “Reactor PH4” system via one thermocouple placed in the furnace. Other thermocouple located inside the reactor ensured the correct temperature on it.

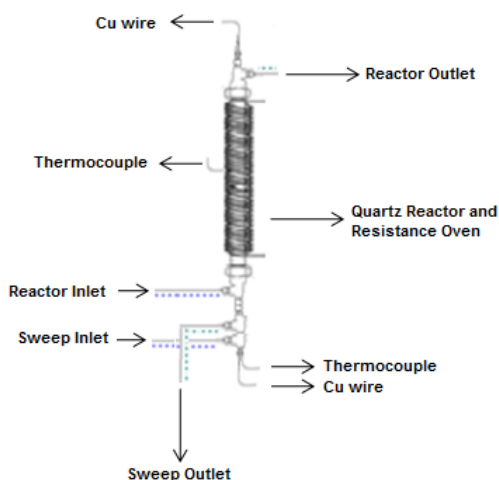


Figure 27. CMR reaction zone enlargement.

Furthermore, in the reaction zone (Figure 26) there was a three-way valve that allowed bypass the reactor. The pressure at the reactor inlet was monitored with a manometer in order to avoid any overpressure inside the reactor. Reactor downstream all the gas conductions (lines) were heated at 150 °C to avoid the condensation of heavy aromatics. In addition, at the reactor outlet there was an Argon inlet with a flow of 200 mL·min⁻¹, thus diluting the reactor outlet stream, before this inlet there was a non-return valve. Then the reactor outlet split into two branches, one was carried to the gas chromatograph (Bruker 450 GC) through a four-way pneumatic valve (VN2), automated with the “Reactor PH4”, and the other was vented to the outside, in the latter there was a manual adjusted back pressure regulator.

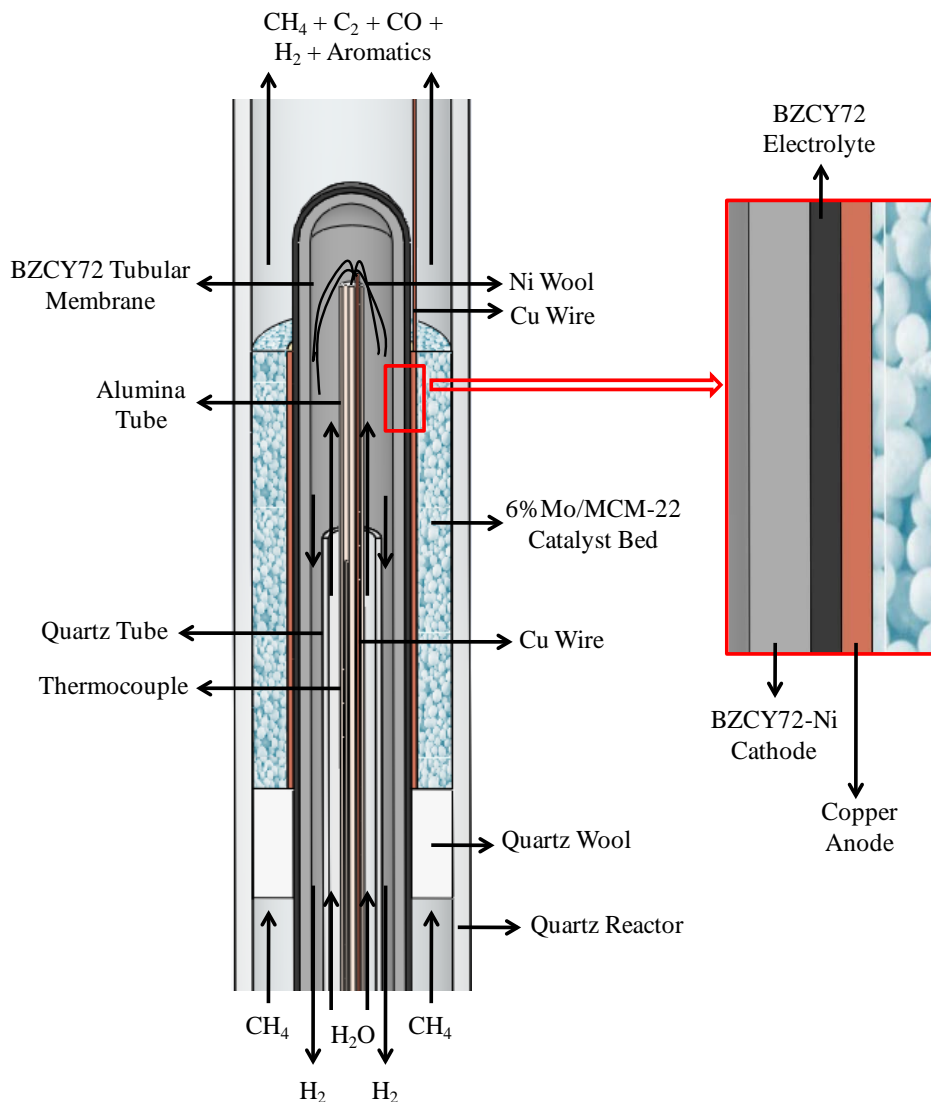


Figure 28. Scheme of the Catalytic Membrane Reactor (CMR).

Additionally, the sweep inlet (Figure 27 and Figure 28) consisted of a gas mixture comprising H_2 and Ar (0.5:9.5 vol. ratio) at a flow of $60 \text{ mL} \cdot \text{min}^{-1}$. This gas mixture was introduced in a bubbler with a saturated aqueous salt solution to work in wet conditions and it was fed at the top inside the tubular membrane by a quartz tube. Then the sweep outlet was carried to the gas

chromatograph (Agilent 7890B GC). Moreover, the GC outlet was vented to the outside through a needle valve that allowed adjust the outlet flow. Before the Agilent GC there was a manual adjusted back pressure regulator.

Thus, there were two different analysis zones (Figure 26): the CMR outlet analysis zone and the sweep outlet analysis zone. In the CMR outlet analysis zone the VN2 four-way pneumatic valve was kept in the position that allowed supply the reactor outlet stream to the GC during a specific time, after that, the VN2 position was changed to vent this stream entirely and the GC was fed with Ar to purge it. Moreover, the GC outlet was vented to the outside through a needle valve that allowed adjust the outlet flow and after the needle valve a glass rotameter was placed to check it.

In order to apply a given current to pump H_2 electrochemically from the anode (MDA reaction side) to the cathode (sweep side) a voltammetry equipment (Solartron Analytical, 1470E CellTest System) was used, following these electrode reactions [23]:



Therefore, two copper (Cu) wires were needed to transport the current applied: one inside the tubular membrane (BZCY72) to contact the cathode in the sweep side and the other outside the tubular membrane to contact the anode in the MDA reaction side. The Cu lead wire at the bottom of the CMR was introduced in an alumina tube inside the tubular membrane up to almost the top of it (Figure 28), this side of the Cu lead wire was connected to nickel wool to facilitate the contact with the cathode, that was the inner wall of the tubular membrane (BZCY72), with this Cu wire the current was applied to the electrochemical cell. Further, the Cu lead wire at the top of the CMR was also introduced in an alumina tube inside the quartz reactor and was coiled to the

anode. Moreover the voltage obtained was measured with the voltammetry equipment.

The information concerning the thermocouples, the mass flow controllers and the rotameter employed in the CMR is the same that for the FBR (section 3.6.1.).

3.6.2.1.1. Experimental procedure

Briefly, in a typical experiment 1.8 g of catalyst were diluted with 1.953 g of SiC and loaded to the reactor, over an additional SiC bed (1.872 g) placed on top of the quartz wool. Because of the tubular membrane the maximum heating rate was of $2\text{ }^{\circ}\text{C}\cdot\text{min}^{-1}$, the furnace took ~ 6 h from room temperature up to $710\text{ }^{\circ}\text{C}$. The catalysts were pre-treated in situ in a flow of Ar ($50\text{ mL}\cdot\text{min}^{-1}$) from room temperature up to $600\text{ }^{\circ}\text{C}$ (~ 5 h) and then, the catalysts were pre-carburized and pre-reduced using a gas mixture of $\text{CH}_4:\text{H}_2$ (1:4 vol. ratio) up to $710\text{ }^{\circ}\text{C}$ (1 h), and kept at this temperature for 2 h. After the catalyst activation, this gas mixture was switched by the feed gas mixture $\text{CH}_4:\text{N}_2$ (9.5:0.5 vol. ratio) at a flow of $45\text{ mL}\cdot\text{min}^{-1}$, being the space velocity of $1500\text{ mL}\cdot\text{h}^{-1}\cdot\text{g}_{\text{cat}}^{-1}$ ($1425\text{ mL}_{\text{CH}_4}\cdot\text{h}^{-1}\cdot\text{g}_{\text{cat}}^{-1}$) or 871 h^{-1} . Moreover, it was introduced a flow of $200\text{ mL}\cdot\text{min}^{-1}$ of Ar at reactor outlet to dilute the reaction products and the experiments were carried out at 1.2 bar of pressure.

Furthermore, in the sweep side a gas mixture of $\text{H}_2:\text{Ar}$ (0.5:9.5 vol. ratio) was fed at a flow of $60\text{ mL}\cdot\text{min}^{-1}$ in wet conditions throughout the experiment, using a saturated aqueous solution of potassium acetate at room temperature. The H_2O vapor concentration used in each experiment was calculated as abovementioned in the section 3.6.1.2.1.2. and it is detailed in Table 5, there were slight variations due to the changes at the room temperature.

Table 5. H_2O vapor concentration used in the experiments performed with H_2 removal through BZCY72 tubular membranes.

Tubular membrane	H_2O temperature ($^{\circ}C$)	H_2O vapor concentration (%)
TM-1	33	1.04
TM-2	31	0.95
TM-3	31	0.95
TM-4	30	0.90
TM-5	30	0.90

The unconverted methane and the formed products were separated and analyzed on line at different TOS using the same gas chromatograph Bruker 450-GC that in the section 3.6.1.1. (FBR).

Moreover, the H_2 content in the sweep side in the test performed with the Tubular Membrane “2” (TM-2) was analyzed using a micro-GC Varian CP-4900 endowed with different modules: Molsieve 5A, PoraPlot-Q glass capillary and CP-Sil modules. Nevertheless in the other four experiments with tubular membranes, the H_2 content in the sweep side was analyzed using a gas chromatograph Agilent 7890B-GC equipped with different columns: two Molsieve 13X, two Porapak Q and one HP-PLOT-Q; and three detectors, two TCD and one FID, this GC was also used to detect any leakage of CH_4 from the reaction side.

In order to obtain quantitative results from the Agilent GC data (sweep side) was necessary to use correction factors that were dependent on the compound response to the corresponding detector. In this work the response factors of the compounds have been determined experimentally. On the one hand, CH_4 (TCD and FID) was calibrated with different concentrations of the feed gas mixture ($CH_4:N_2$, 9.5:0.5 vol. ratio). Furthermore, H_2 (TCD) was calibrated using different concentrations of the gas mixture $H_2:Ar$, 0.5:9.5 (vol. ratio).

In this section, the same calculations employed in the experimental procedure of the FBR (section 3.6.1.1.) were used to obtain quantitative results from the Bruker GC data (reaction side). However, all the tested tubular membranes had a very small leakage of CH₄ from the reaction side to the sweep side. This CH₄ was quantified in the micro-GC Varian and in the Agilent GC as is explained below, and while its molar concentration was equal to or less than 0.15% these data were used quantitatively to complete the data obtained with the Bruker GC in the reaction side. In particular, for the Agilent GC (sweep side), the response factors, the molar concentrations, etc., of H₂ and CH₄ were calculated using the equations previously shown for the Bruker GC.

The H₂ analyzed in the sweep side had three origins: the H₂ included in the gas mixture, the H₂ pumped from the reaction side to the sweep side applying a specific current to the electrochemical cell and the H₂ produced by the water splitting reaction in sweep side. On one hand, the H₂ included in the gas mixture was measured before the beginning of MDA reaction at room temperature, and its molar concentration “ $Cm_{H_2}^{in}$ ” was calculated using the Equation 36. Thus the molar concentration of the H₂ produced in the sweep side “ Cm_{H_2P} ” was calculated with the Equation 51, being “ $Cm_{H_2}^{out}$ ” the molar concentration of the H₂ analyzed by the Agilent GC during the MDA reaction calculated using the Equation 36.

$$Cm_{H_2P} = Cm_{H_2}^{out} - Cm_{H_2}^{in} \quad (51)$$

Then the molar flow (mol·min⁻¹) of the H₂ pumped (or removed) “ W_{H_2R} ” from the reaction side (anode) to the sweep side (cathode) was calculated using the Equation 52. The CO molar flow is equivalent to the molar flow of the H₂ produced by the water splitting reaction in sweep side ($W_{CO} = W_{H_2WS}$).

$$W_{H_2R} = W_{H_2P} - W_{CO} \quad (52)$$

The three H₂ flows (mL·min⁻¹), that is to say, the H₂ flow produced in the sweep side (F_{H_2P}), the H₂ flow removed (F_{H_2R}) from the reaction side (anode) to the sweep side (cathode) and the H₂ flow produced by the water splitting reaction (F_{H_2WS}) in sweep side were calculated using the Equation 31.

Moreover, the Faradaic efficiency describes the efficiency with which a charge (e⁻) is transferred in a system facilitating an electrochemical reaction and it was calculated using the Equation 53:

$$FE (\%) = \frac{\text{Output current}}{\text{Input current}} \cdot 100 \quad (53)$$

$$\text{Output current (A)} = \frac{2 \cdot W_{H_2P} \cdot 96485.33}{60} \quad (54)$$

Where “*Input current*” is the current applied with the Solartron to the electrochemical cell (A); “96485.33” is the Faraday constant (C·mol⁻¹) and it is well known that A = C·s⁻¹.

In addition, the H₂ extracted (%) from the reaction side expresses the ratio of the extracted H₂ to the formed H₂, while the O₂ injected (%) expresses the ratio of O₂ injected to the total molar flow on the reaction side. These parameters can be calculated using the following equations:

$$H_2 \text{ Extracted } (\%) = \frac{F_{H_2P}}{F_{H_2P} + F_{H_2MDA}} \cdot 100 \quad (55)$$

$$O_2 \text{ Injected } (\%) = \frac{(F_{CO}/2)}{F_T} \cdot 100 \quad (56)$$

where “ F_{H_2P} ” is the H₂ flow produced in the sweep side, “ F_{H_2MDA} ” is the H₂ flow produced in the MDA reaction side and “ F_T ” is the feed gas mixture flow, CH₄:N₂, at reaction side.

3.6.2.1.2. Operating conditions of each experiment with CMR-TM

It should be noted that the currents applied with Solartron and the total duration of the experiments were different for each tubular membrane.

Tubular membrane 1 (TM-1): with 4 cm of Copper anode. The operating conditions were those described in the section 3.6.2.1.1. (710 °C) and the different currents were applied directly to the cell without an ascending current ramp. The current applied, the current density and the TOS for each of them are shown in Table 6:

Table 6. Current densities used with TM-1 at different TOS.

Current applied (A)	Current density (mA/cm ²)	Time on stream (h)
open circuit voltage (O.C.V.)	-	5
0.5	~40	4
O.C.V.	-	1
0.5	~40	4
O.C.V.	-	1
0.5	~40	12
O.C.V.	-	1
0.5	~40	12
O.C.V.	-	1
0.5	~40	12
O.C.V.	-	1
0.5	~40	12
O.C.V.	-	1
0.5	~40	2.33
	TOTAL TOS:	69.33

Tubular membrane 2 (TM-2): with 4 cm of Mo₂C/Cu/BZCY72 anode and gold. The operating conditions were those described in the section 3.6.2.1.1., although the temperature was lower (700 °C) and the different currents were applied directly to the cell without an ascending current ramp.

The different currents applied, the current densities and the TOS for each of them were the following:

Table 7. Current densities used with TM-2 at different TOS.

Current applied (A)	Current density (mA/cm ²)	Time on stream (h)
O.C.V.	-	5
0.5	~40	2
O.C.V.	-	1
1	~80	2
O.C.V.	-	1
1.5	~119	2
O.C.V.	-	1
0.5	~40	4
O.C.V.	-	1
1	~80	4
O.C.V.	-	0.67
	TOTAL TOS:	23.67

Tubular membrane 3 (TM-3): with 4 cm of Copper anode. The operating conditions were those described in the section 3.6.2.1.1., except for the temperature that in this experiment was 720 °C, and the different currents were applied directly to the cell without an ascending current ramp. The different currents applied, the current densities and the TOS for each of them are detailed in the following table:

Table 8. Current densities used with TM-3 at different TOS.

Current applied (A)	Current density (mA/cm ²)	Time on stream (h)
O.C.V.	-	5
0.5	~40	4
O.C.V.	-	1
0.75	~60	4
O.C.V.	-	1
0.5	~40	12
O.C.V.	-	1
0.75	~60	12

Table 8 (Continued). Current densities used with TM-3 at different TOS.

Current applied (A)	Current density (mA/cm ²)	Time on stream (h)
O.C.V.	-	1
0.5	~40	12
O.C.V.	-	1
0.75	~60	12
O.C.V.	-	1
0.5	~40	24
O.C.V.	-	6
	TOTAL TOS:	97

Tubular membrane 4 (TM-4): with 4 cm of Copper anode. 2.4 g of catalyst were diluted with 1.953 g of silicon carbide (SiC) and the mixture was placed on top of the quartz wool. After the catalyst activation, the gas mixture for this was switched by the feed gas mixture CH₄:N₂ (9.5:0.5 vol. ratio) at a flow of 60 mL·min⁻¹ and a H₂ flow of 6 mL·min⁻¹ was added (10% of H₂). The other reactions conditions were kept as in a typical experiment described in the section 3.6.2.1.1. (710 °C) and the different currents were applied directly to the cell without an ascending current ramp. The different currents applied, the current densities and the TOS for each of them are shown in the following table:

Table 9. Current densities used with TM-4 at different TOS

Current applied (A)	Current density (mA/cm ²)	Time on stream (h)
O.C.V.	-	5
0.5	~40	4
O.C.V.	-	1
0.75	~60	4
O.C.V.	-	1
0.5	~40	12
O.C.V.	-	1
0.75	~60	12
O.C.V.	-	3
	TOTAL TOS:	43

Tubular membrane 5 (TM-5): with 4 cm of Copper anode. The operating conditions were those described in the section 3.6.2.1.1. (710 °C) and the first current was applied to the cell using an ascending current ramp of $1.39 \text{ mA}\cdot\text{min}^{-1}$ for 3 h, while in the other steps the currents were applied using an ascending current ramp of $75 \text{ mA}\cdot\text{min}^{-1}$ for 10 min. The current applied, the current density and the TOS for each of them are shown in the following table:

Table 10. Current densities used with TM-5 at different TOS.

Current applied (A)	Current density (mA/cm^2)	Time on stream (h)
-	-	3
Ramp from 0 up to 0.75 A	↑	3
0.75	~60	9
O.C.V.	-	1.50
Ramp from 0 up to 0.75 A	↑	0.17
0.75	~60	12
O.C.V.	-	1.50
Ramp from 0 up to 0.75 A	↑	0.17
0.75	~60	12
O.C.V.	-	1.50
Ramp from 0 up to 0.75 A	↑	0.17
0.75	~60	12
O.C.V.	-	1.50
Ramp from 0 up to 0.75 A	↑	0.17
0.75	~60	12
O.C.V.	-	1.50
	TOTAL TOS:	71.18

3.6.2.2. Catalytic Membrane Reactor with Quartz Tube (CMR-QT)

The reaction system used was very similar than that explained in the previous section (3.6.2.1.) depicted in Figure 26, but a quartz tube one-close-end was employed (Figure 29) instead of using a tubular membrane (BZCY72).

Therefore the sweep side, that includes the voltammetry equipment and the Agilent GC, has not been used in these experiments. Due to the coiled resistance furnace the maximum heating rate was of $4\text{ }^{\circ}\text{C}\cdot\text{min}^{-1}$, then the furnace took 3 h from room temperature up to $700\text{ }^{\circ}\text{C}$. The CMR-QT is considered as a FBR, thereby the results obtained using the former were entirely comparable to the latter.

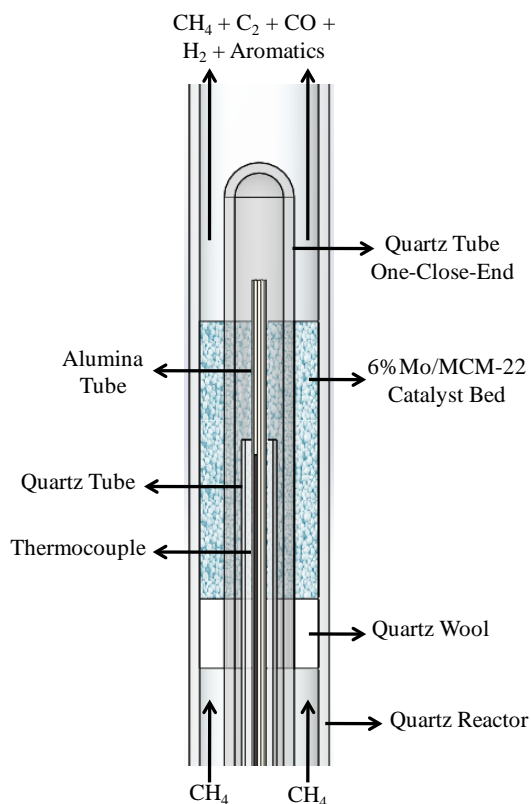


Figure 29. Scheme of the CM Reactor with Quartz Tube (CMR-QT).

3.6.2.2.1. Experimental procedure

Briefly, in a typical experiment 1.8 g of catalyst were diluted with 1.953 g of SiC and loaded to the reactor, over an additional SiC bed (1.872 g) placed on top of the quartz wool. The catalysts were pre-treated in situ in a flow

of Ar ($50 \text{ mL}\cdot\text{min}^{-1}$) from room temperature up to $480 \text{ }^\circ\text{C}$ ($\sim 2 \text{ h}$) and then, the catalysts were pre-carburized and pre-reduced using a gas mixture of $\text{CH}_4:\text{H}_2$ (1:4 vol. ratio) up to $710 \text{ }^\circ\text{C}$ (1 h), and kept at this temperature for 2 h. After the catalyst activation, this gas mixture was switched by the feed gas mixture $\text{CH}_4:\text{N}_2$ (9.5:0.5 vol. ratio) at a flow of $45 \text{ mL}\cdot\text{min}^{-1}$, being the space velocity of $1500 \text{ mL}\cdot\text{h}^{-1}\cdot\text{g}_{\text{cat}}^{-1}$ ($1425 \text{ mL}_{\text{CH}_4}\cdot\text{h}^{-1}\cdot\text{g}_{\text{cat}}^{-1}$) or 871 h^{-1} . Moreover, a flow of $200 \text{ mL}\cdot\text{min}^{-1}$ of Ar was introduced at reactor outlet to dilute the reaction products. The experiments were carried out at 1.2 bar of pressure.

The unconverted methane and the formed products were separated and analyzed on line at different TOS using the same gas chromatograph Bruker 450-GC that in the section 3.6.1.1. (FBR). In this section, the same calculations employed in the experimental procedure of the FBR (section 3.6.1.1.) were used in order to obtain quantitative results from the GC data.

Nevertheless, it should be noted that in the experiments carried out with the extrudated catalysts these were prepared according to the procedure described in the section 3.3.2. Moreover, in order to avoid the dilution of the catalyst due to the silica-like residue left by the Silres was necessary to do a correction of the catalyst mass according to the Equations 47 and 48 (section 3.6.1.1.).

3.6.2.2.2. Different operating conditions

In some experiments different operating conditions were varied to study the performance of the MDA reaction, these were: the space velocity, the temperature and the use of H_2 as co-feeding using different concentrations.

3.6.2.2.2.1. Use of different space velocities with the CMR-QT

In these experiments, two different space velocities were used:

- 750 mL·h⁻¹·g_{cat}⁻¹: 1.6 g of catalyst were diluted with 1.953 g of SiC and loaded to the reactor, over an additional SiC bed (1.872 g) placed on top of the quartz wool. And 20 mL·min⁻¹ of the feed gas mixture of CH₄:N₂, 9.5:0.5 (vol. ratio).
- 3000 mL·h⁻¹·g_{cat}⁻¹: 0.9 g of catalyst were diluted with 1 g of SiC and loaded to the reactor, over an additional SiC bed (1.872 g) placed on top of the quartz wool. And 45 mL·min⁻¹ of the feed gas mixture of CH₄:N₂, 9.5:0.5 (vol. ratio).

3.6.2.2.2.2. Co-feeding of H₂ using the CMR-QT

In these experiments different H₂ concentrations were used:

- 6% of H₂: during the first 3 h of MDA reaction the feed gas mixture used was CH₄:N₂, 9.5:0.5 (vol. ratio) with a space velocity of 1500 mL·h⁻¹·g_{cat}⁻¹ (1425 mL_{CH₄}·h⁻¹·g_{cat}⁻¹), and then it was switched by the gas mixture CH₄:H₂:N₂, 8.9:0.6:0.5 (vol. ratio) using a flow of 48 mL·min⁻¹ for 13 h, maintaining the methane space velocity of 1424 mL_{CH₄}·h⁻¹·g_{cat}⁻¹ (1600 mL·h⁻¹·g_{cat}⁻¹).
- 10% of H₂: as in the previous experiment during the first 3 h of MDA reaction the feed gas mixture used was CH₄:N₂, 9.5:0.5 (vol. ratio) with a space velocity of 1500 mL·h⁻¹·g_{cat}⁻¹ (1425 mL_{CH₄}·h⁻¹·g_{cat}⁻¹), and then this flow was kept and 4.5 mL·min⁻¹ of H₂ were added for 30 h in dry conditions.
- Different concentrations of H₂ without and with addition of H₂O: during the first 3 h of MDA reaction the feed gas mixture used was CH₄:N₂, 9.5:0.5 (vol. ratio) with a space velocity of 1500 mL·h⁻¹·g_{cat}⁻¹ (1425 mL_{CH₄}·h⁻¹·g_{cat}⁻¹). Then this flow (45 mL·min⁻¹) was kept and four different flows of H₂ were added for 4 h each of them, obtaining the following concentrations of H₂: 20% (9 mL·min⁻¹), 15% (6.75 mL·min⁻¹), 10% (4.5 mL·min⁻¹) and

5% ($2.25 \text{ mL}\cdot\text{min}^{-1}$). After these four steps in dry conditions, a catalyst regeneration with H_2 ($17 \text{ mL}\cdot\text{min}^{-1}$) was done during 1 h. Then the feed gas mixture flow ($45 \text{ mL}\cdot\text{min}^{-1}$) was introduced again and the previous steps with H_2 were repeated in wet conditions, using a saturated aqueous solution of potassium hydroxide, obtaining a H_2O vapor concentration of 0.288% at $28 \text{ }^\circ\text{C}$ (calculated as abovementioned in section 3.6.1.2.1.2.).

3.7. References

- [1] <http://www.iza-structure.org/databases/>.
- [2] S.Q. Ma, X.G. Guo, L.X. Zhao, S. Scott, X.H. Bao, *J. Energy Chem.*, 22 (2013) 1-20.
- [3] A. Corma, C. Corell, J. Perezpariente, *Zeolites*, 15 (1995) 2-8.
- [4] E. Benazzi, J.L. Guth, L. Rouleau, IM-5 zeolite, method of preparation and catalytic applications thereof., WO 98/17581, 1998.
- [5] A. Corma, M. Puche, F. Rey, G. Sankar, S.J. Teat, *Angewandte Chemie-International Edition*, 42 (2003) 1156-1159.
- [6] T. Boix, M. Puche, M.A. Cambor, A. Corma, Synthetic porous crystalline material ITQ-13, its synthesis and use, US 6,471,941 B1, 2002.
- [7] S.B. Hong, H.-K. Min, C.-H. Shin, P.A. Cox, S.J. Warrender, P.A. Wright, *Journal of the American Chemical Society*, 129 (2007) 10870-10885.
- [8] J.L. Casci, M.D. Shanon, Zeolite Nu-85, US5,385,718, 1995.
- [9] F. Kiesslich, Catalyst for the dehydroaromatization of methane and mixtures containing methane, US 2011/0124933 A1, 2011.
- [10] W.G. Coors, *Advances in ceramics – synthesis and characterization, processing and specific applications; chap.21: co-ionic conduction in protonic ceramics of the solid solution, $\text{BaCexZry-xY-yO3-\delta}$; part I: fabrication and microstructure.*, in, InTech, 2011.
- [11] S. Ricote, N. Bonanos, A. Manerbino, W.G. Coors, *International Journal of Hydrogen Energy*, 37 (2012) 7954-7961.
- [12] J.-H. Li, X.-Z. Fu, J.-L. Luo, K.T. Chuang, A.R. Sanger, *Electrochemistry Communications*, 15 (2012) 81-84.

- [13] P.R.S. Jackson, D.J. Young, D.L. Trimm, *Journal of Materials Science*, 21 (1986) 4376-4384.
- [14] S. Brunauer, P.H. Emmett, E. Teller, *Journal of the American Chemical Society*, 60 (1938) 309-319.
- [15] Y. Waseda, E. Matsubara, K. Shinoda, *X-Ray Diffraction Crystallography*, Springer-Verlag Berlin Heidelberg, 2011.
- [16] M. Newville, *Fundamentals of XAFS*, in, Consortium for Advanced Radiation Sources, University of Chicago, Chicago, 2004.
- [17] C.A. Emeis, *Journal of Catalysis*, 141 (1993) 347-354.
- [18] R.C. Reid, J.M. Prausnitz, T.K. Sherwood, *The properties of gases and liquids*, McGraw-Hill, 1977.
- [19] W.Y. Shiu, K.C. Ma, *Journal of Physical and Chemical Reference Data*, 29 (2000) 41-130.
- [20] A. DelleSite, *Journal of Physical and Chemical Reference Data*, 26 (1997) 157-193.
- [21] L. Greenspan, *Journal of Research of the National Bureau of Standards Section a-Physics and Chemistry*, 81 (1977) 89-96.
- [22] L. Haar, J.S. Gallagher, G.S. Kell, *NBS/NRC Steam Tables: Thermodynamic and Transport Properties and Computer Programs for Vapor and Liquid States of Water in SI units*, Hemisphere Publishing Corporation, New York, 1984.
- [23] H. Matsumoto, S. Hamajima, H. Iwahara, *Solid State Ionics*, 145 (2001) 25-29.

Chapter 4.

EFFECT OF THE ZEOLITE ON MDA REACTION

4. Effect of the zeolite on MDA reaction

4.1. Different HZSM-5 zeolites with 3% (wt.) of Mo

The preliminary investigation was carried out to study the performance on MDA reaction of different HZSM-5 zeolites, with different crystal sizes and Si/Al ratios, which are summarized in Table 11. These characteristics are detailed in Table 2 (section 3.2.1.), in which it can be observed that the BET surface area and the micropore volume are very similar among the different zeolites. The 3% (wt.) Mo/HZSM-5 catalyst was selected because of the good performance that possesses on MDA reaction, which has been published by many research groups.

Table 11. Crystal sizes and Si/Al ratios of the different HZSM-5.

Zeolite	Crystal size (μm)	Si/Al
CBV3020	~0.1	15
CBV8020	~0.5-1	40
CBV5020	~0.1	25
TZP302H	~1-2	10
TZP322	~0.1	10
CBV3024E	~0.1-0.25	15

Figure 30 shows the XRD patterns of the 3%Mo/HZSM-5 catalysts before the MDA reaction. As seen, the Mo species are highly dispersed inside the channels and on the zeolite surface, as concluded from the absence of diffraction peaks related to the Mo species (expected at 27.3° , 25.7° , 12.8° and 39° for the most common MoO_3 phases).

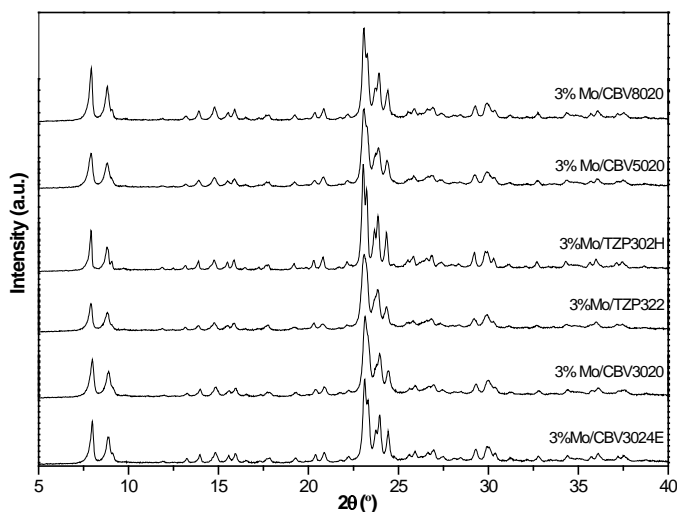


Figure 30. XRD patterns of 3%Mo/HZSM-5 catalysts before the MDA reaction.

The experiments were carried out according to the procedure described in the section 3.6.1.1. As can be observed in Figure 31.a, the methane conversion for the six catalysts with 3% (wt.) of Mo exhibits the same trend, a big decrease during the first 4 h of the reaction due to the quick growth of carbonaceous deposits, and a slighter reduction at longer times. The carbonaceous deposits are accumulated over time on both the Brønsted acid sites of the zeolite and the Mo sites, being mainly the former the responsible of the catalyst deactivation [1]. In particular, the two catalysts with higher Si/Al ratio have a lower methane conversion throughout the time on stream (TOS) than the other catalysts, as the Brønsted acidity is lower for them [2]. Moreover, it was assumed that the quasi-steady state was reached after 9 h of MDA reaction.

In addition, the H_2 flow normalized per gram of catalyst is shown in Figure 31.b. As with the methane conversion the six catalysts show the same trend, the first point obtained is the maximum H_2 flow and then it drops throughout the time on stream. Due to the reduction and carburization of $(Mo_2O_5)^{2+}$ species by methane to MoC_x [3], that takes place during the first hour

of MDA reaction under non oxidative conditions [4, 5], H_2 is produced in greater extent during this time as happened with coke.

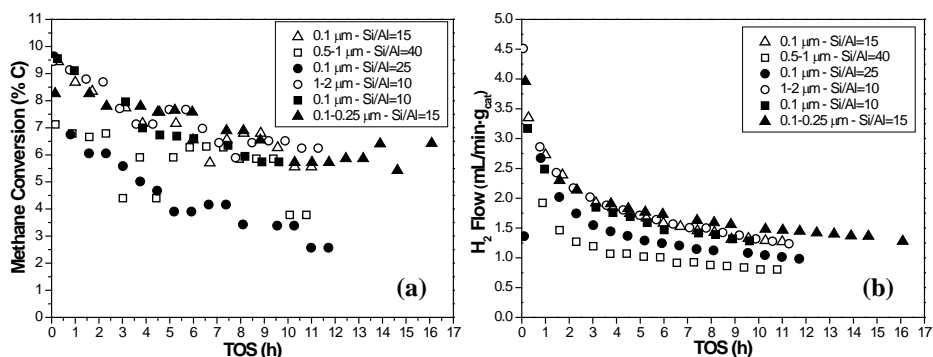


Figure 31. Effect of the HZSM-5 zeolite on the (a) methane conversion and (b) H_2 flow of 3%Mo/HZSM-5 catalysts versus the TOS at 700 °C.

Table 12. Effect of the HZSM-5 zeolite on the selectivity to main products after 9 h on stream of 3%Mo/HZSM-5 catalysts.

Zeolite	Crystal Size (μm) – Si/Al of HZSM-5	Selectivity (% C)				
		C_6H_6	C_2	C_7H_8	$C_{10}H_8$	Coke
CBV3020	0.1 – 15	44.8	9.8	3.9	12.0	29.5
CBV8020	0.5-1 – 40	15.7	6.4	1.3	5.6	71.0
CBV5020	0.1 – 25	39.8	12.4	3.4	14.6	29.8
TZP302H	1-2 – 10	38.0	7.0	2.9	14.1	38.0
TZP322	0.1 – 10	45.3	8.9	3.5	13.8	28.5
CBV3024E	0.1-0.25 – 15	65.3	7.6	5.6	18.6	2.9

The selectivity to main products of MDA reaction after 9 h on stream for the different 3%Mo/HZSM-5 catalysts, at 700 °C, 1.2 bar and $1500 \text{ mL} \cdot \text{h}^{-1} \cdot \text{g}_{\text{cat}}^{-1}$, is given in Table 12. The selectivities of the three aromatics (benzene, toluene and naphthalene) are the highest for the catalyst with the CBV3024E zeolite (0.1-0.25 μm and Si/Al=15), while the coke selectivity is the lowest. Conversely, the coke selectivity for the catalyst with the CBV8020

zeolite (0.5-1 μm and Si/Al=40) is by far the highest, being its selectivity to the other products (ethane, ethylene, benzene, toluene and naphthalene) the lowest after 9 h of MDA reaction. The selectivities obtained are very similar for the CBV3020 (0.1 μm and Si/Al=15) and TZP322 (0.1 μm and Si/Al=15) zeolites.

Figure 32.a illustrates the benzene yield versus the TOS for the different 3%Mo/HZSM-5 catalysts. The catalyst with the CBV3024E zeolite (0.1-0.25 μm and Si/Al=15) shows the highest and most stable benzene yield throughout the time on stream, which is ascribed to both the high methane conversion and the high benzene selectivity obtained with this zeolite. The maximum benzene yield for 3%Mo/CBV3024E is around 4.70% and is reached at 2.33 h of MDA reaction. Nevertheless, the benzene yield is lower for the catalysts with the CBV8020 (0.5-1 μm and Si/Al=40) and CBV5020 (0.1 μm and Si/Al=25) zeolites over time. For the former this is ascribed to its low methane conversion and benzene selectivity, but for the latter is mainly due to its low methane conversion. Additionally, the other three catalysts exhibit a benzene yield very similar, especially the catalysts with the CBV3020 (0.1 μm and Si/Al=15) and TZP322 (0.1 μm and Si/Al=10) zeolites.

Moreover, in Figure 32.b the benzene yield is depicted versus the methane conversion. The catalysts with CBV3024E (0.1-0.25 μm and Si/Al=15) and CBV3020 (0.1 μm and Si/Al=15) zeolites show the highest benzene yield for the whole conversion range. These are very similar although slightly higher for the catalyst with CBV3024E zeolite, therefore it is assumed that the best HZSM-5 is the CBV3024E zeolite. The other zeolites follow the same trend that is shown in Figure 32.a. Thus, the catalyst with the CBV8020 (0.5-1 μm and Si/Al=40) zeolite exhibits the lowest benzene yield. While, the results for the catalysts with the TZP322 (0.1 μm and Si/Al=10) and TZP302H (1-2 μm and Si/Al=10) zeolites are very similar, however for the former are slightly higher than for the latter.

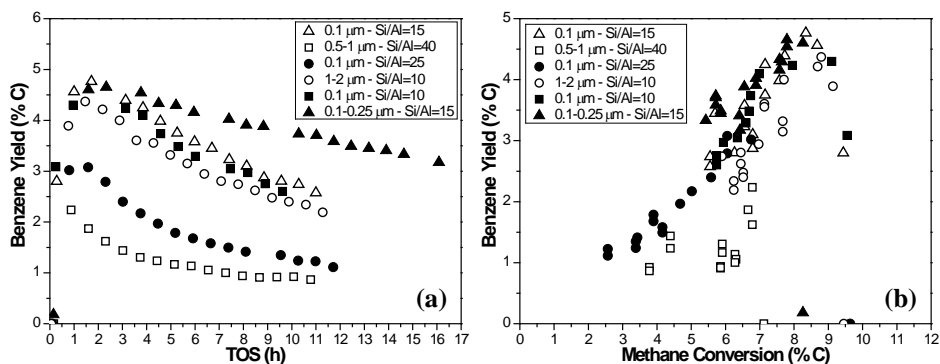


Figure 32. Effect of the HZSM-5 zeolite on the (a) benzene yield versus the TOS and (b) benzene yield versus the methane conversion of 3%Mo/HZSM-5 catalysts at 700°C.

In the following table the TGA results obtained for the spent catalysts are shown. Due to the different duration of each experiment carried out with these catalysts the amount of coke is normalized per hour, thus obtaining the average coke formation rate that is also detailed in this table. The zeolites that are used to prepare the catalysts with 3% (wt.) of Mo are listed according to the average coke formation rate in descending order: CBV5020 (0.1 μm , Si/Al=25), CBV8020 (0.5-1 μm , Si/Al=40), TZP322 (0.1 μm , Si/Al=10), CBV3020 (0.1 μm , Si/Al=15), TZP302H (1-2 μm , Si/Al=10) and CBV3024E (0.1-0.25 μm , Si/Al=15). It should be noted that the catalyst prepared with the CBV3024E zeolite shows the lowest amount of coke and average coke formation rate, in agreement with the lowest coke selectivity obtained after 9 h on stream (Table 12). Moreover, the ratio between the amount of coke ($\text{g} \cdot \text{g}_{\text{cat}}^{-1}$) and the accumulated benzene moles is exhibited in this table. This is a new parameter defined to show the effectiveness of a catalyst regarding the coke deposition and benzene formation. As seen, the catalyst prepared with the zeolite CBV8020 (0.5-1 μm , Si/Al=40) produces the highest amount of coke per accumulated benzene mole, followed by the zeolite CBV5020 (0.1 μm , Si/Al=25). Both zeolites have the higher Si/Al ratios, therefore it is inferred that

these values of Si/Al ratio (40 and 25 respectively) are detrimental for the MDA performance. The catalysts prepared with the zeolites TZP302H (1-2 μm , Si/Al=10), CBV3020 (0.1 μm , Si/Al=15) and TZP322 (0.1 μm , Si/Al=10) produce an intermediate amount of coke per accumulated benzene mole. While the catalyst with the CBV3024E zeolite (0.1-0.25 μm , Si/Al=15) exhibits the lowest amount of coke per accumulated benzene mole.

Table 13. TGA results of spent 3% (wt.) Mo/HZSM-5 catalysts.

Crystal Size (μm) – Si/Al of HZSM-5	TOS (h)	Average Coke Formation Rate ($\text{g}\cdot\text{g}_{\text{cat}}^{-1}\cdot\text{h}^{-1}$)	Amount of Coke ($\text{g}\cdot\text{g}_{\text{cat}}^{-1}$)	$\text{g}\cdot\text{g}_{\text{cat}}^{-1}\cdot\text{mol}_{\text{benz.}}^{-1}$
0.1 μm – 15	11.0	0.0065	0.072	29
0.5-1 μm – 40	10.8	0.0078	0.084	97
0.1 μm – 25	11.7	0.0084	0.098	70
1-2 μm – 10	11.3	0.0057	0.064	28
0.1 μm – 10	9.6	0.0075	0.072	32
0.1-0.25 μm – 15	16.0	0.0044	0.070	19

Note: The differences observed between the amount of coke and the coke selectivity (Table 12) after listing them in descending order are due to the different times on stream at which these parameters are given, as the coke selectivity shown corresponds to that after 9 h on stream, while the amount of coke is determined after the total duration of the different experiments. This should be applied hereafter for the coke selectivity and the amount of coke (TGA).

4.1.1. Effect of the Si/Al ratio

The effect of the Si/Al ratio was studied using three catalysts with the same crystal size ($\sim 0.1 \mu\text{m}$) and different Si/Al ratios: 10, 15 and 25, corresponding to the zeolites TZP322, CBV3020 and CBV5020, respectively. As seen in Figure 33, the benzene selectivity after 9 h on stream decreases as the Si/Al ratio increases. However, an opposite trend is observed for the C_2 hydrocarbons selectivity. This can be ascribed to the higher number of Brønsted acid sites for the zeolites with lower Si/Al ratio, which favors the MDA reaction. Additionally, the highest methane conversion is obtained for the

catalyst with intermediate Si/Al ratio (CBV3020 zeolite). While for this catalyst, the naphthalene and coke selectivities are lower than for the other catalysts.

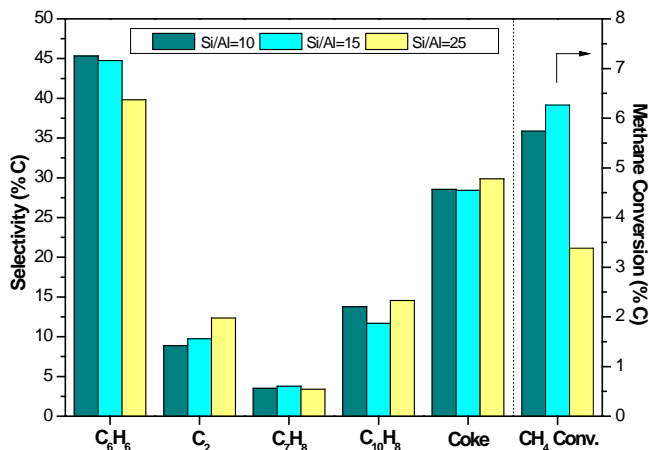


Figure 33. Effect of the Si/Al ratio of 3%Mo/HZSM-5 catalyst on the selectivity to main products and the methane conversion after 9 h on stream.

4.1.2. Effect of the crystal size

The effect of the crystal size was studied for two catalysts with the same Si/Al ratio (10) and different crystal sizes: ~ 0.1 and $\sim 1-2$ μm , corresponding to the zeolites TZP322 and TZP302H, respectively. As can be observed in Figure 34, the selectivity to benzene, C₂ hydrocarbons and toluene after 9 h on stream is higher for the catalyst with a crystal size of ~ 0.1 μm (TZP322 zeolite), that at least for benzene this is in agreement with the results shown in Figure 32. Nevertheless, as abovementioned in the section 2.5., Zhang et al. [6] obtained that both the methane conversion and the benzene selectivity were slightly higher on the HZSM-5 with 1 μm than on the HZSM-5 with 0.07 μm , as over the latter is easily extracted the framework aluminum and, moreover, the Mo is located mainly on the external surface, reducing therefore the shape selectivity. Contrarily in this work, the catalyst with a crystal size of 0.1 μm (TZP322

zeolite) performs slightly better than the catalyst with a crystal size of 1-2 μm (TZP302H zeolite) on the MDA reaction. This may have different reasons, i.e. distinct crystal morphology, different Mo dispersion, etc.

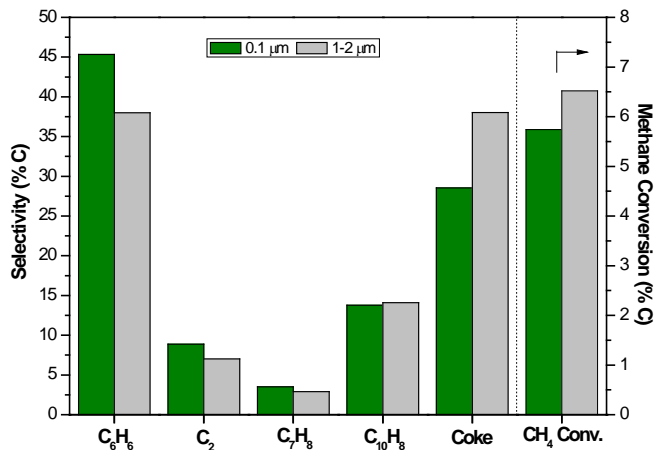


Figure 34. Effect of the crystal size of 3%Mo/HZSM-5 catalyst on the selectivity to main products and the methane conversion after 9 h on stream.

4.2. Effect of the Mo content on the best HZSM-5

The effect of the Mo content was studied on the best HZSM-5 zeolite, i.e., CBV3024E. According to Ma et al. [7], the highest aromatics formation rate and the lowest coke formation rate were obtained with 6% (wt.) Mo/HZSM-5 catalyst, after evaluating different Mo loadings: 2, 6 and 10%. Therefore, in this work two Mo contents were studied, 3 and 6% (wt.) on HZSM-5 zeolite. The experiments were carried out according to the procedure described in the section 3.6.1.1. Figure 35 depicts the methane conversion for the catalysts with 3% and 6% (wt.) of Mo. Both catalysts exhibit the same trend, being the highest for the 6% (wt.) Mo/HZSM-5 catalyst over time.

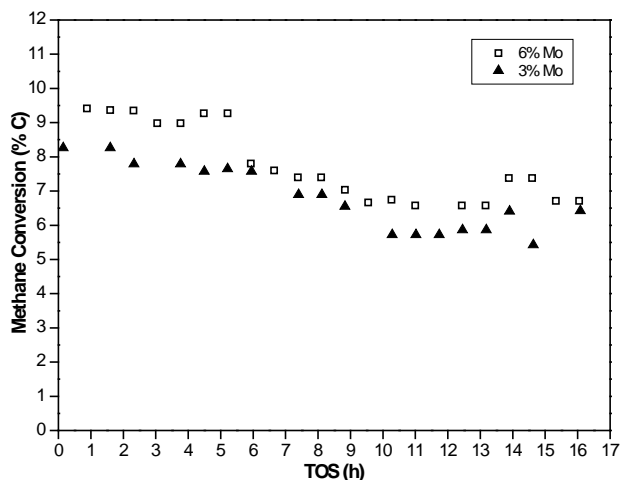


Figure 35. Effect of the Mo content of the Mo/HZSM-5 catalysts on the methane conversion versus the TOS at 700 °C.

The selectivity to main products of MDA reaction and the H_2 flow normalized per gram of catalyst after 9 h (quasi-steady state) on stream for the 3% and 6% (wt.) Mo/HZSM-5 catalysts, at 700 °C, $1500 \text{ mL}\cdot\text{h}^{-1}\cdot\text{g}_{\text{cat}}^{-1}$ and 1.2 bar, are detailed in Table 14. The selectivities are very similar, being the benzene and coke selectivities higher for the catalyst with 6% (wt.) of Mo than for the catalyst with 3% (wt.) of Mo. Conversely, the naphthalene, toluene and C_2 selectivities are higher for the catalyst with 3% (wt.) of Mo than for that with 6% (wt.) of Mo.

Table 14. Effect of the Mo content of the Mo/HZSM-5 catalysts on the selectivity to main products and the H_2 flow after 9 h on stream.

Mo Content (%)	Selectivity (% C)					H_2 Flow (mL/min·g _{cat})
	C_6H_6	C_2	C_7H_8	$C_{10}H_8$	Coke	
3	65.3	7.6	5.6	18.6	2.9	1.5
6	67.2	7.1	5.0	16.4	4.3	1.7

Figure 36.a displays the benzene yield versus the TOS for the catalysts with 3% and 6% (wt.) of Mo. The catalyst with 6% (wt.) of Mo shows the

highest benzene yield throughout the time on stream, due to both its high benzene selectivity and high methane conversion. The maximum benzene yield for this catalyst is 5.63% and it is reached at 2.33 h on stream. In addition, Figure 36.b depicts the benzene yield versus the methane conversion for both catalysts. As seen, the catalyst with 6% of Mo exhibits the highest benzene yield for almost the whole conversion range.

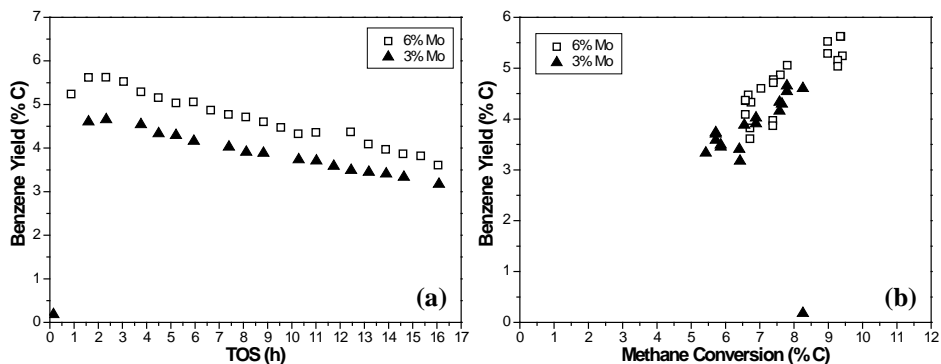


Figure 36. Effect of the Mo content of the Mo/HZSM-5 catalysts on the (a) benzene yield versus the TOS and (b) benzene yield versus the methane conversion.

The effect of the Mo content on the catalytic performance after 2.33 h of MDA reaction at 700 °C, 1.2 bar and $1500 \text{ mL} \cdot \text{h}^{-1} \cdot \text{g}_{\text{cat}}^{-1}$ for the catalysts with 3% and 6 % (wt.) of Mo is illustrated in Figure 37. This specific time on stream was selected since the maximum benzene yield was obtained at this TOS for both catalysts. As seen, both the methane conversion and the benzene yield show a significant increase with increasing Mo content in the range of 3-6%, while the naphthalene and the coke yields slightly increase. Nevertheless, the toluene and the C_2 hydrocarbons yields are almost constant in the Mo loading range of 3-6%.

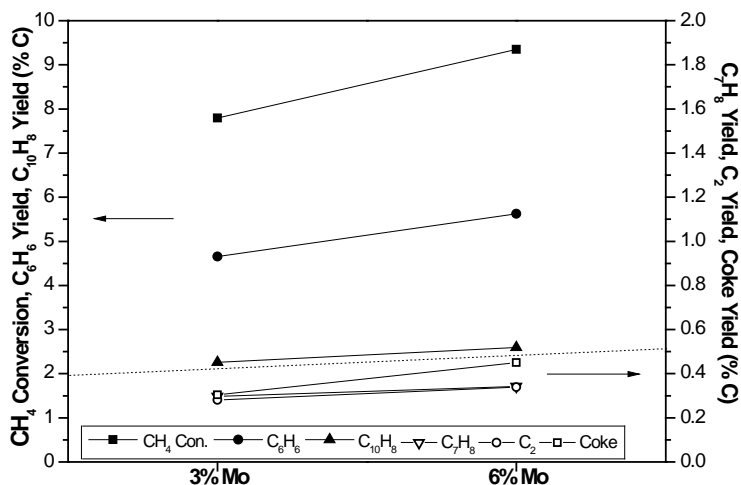


Figure 37. Effect of the Mo content on the catalytic performance after 2.33 h of MDA reaction.

Table 15 shows the TGA results obtained for the spent catalysts. Even though the duration of both experiments was the same (16 h), the amount of coke is also normalized per hour, thus obtaining the average coke formation rate, in order to be able to compare with the other experiments. The lowest amount of coke, average coke formation rate and amount of coke ($\text{g} \cdot \text{g}_{\text{cat}}^{-1}$) per accumulated benzene mole are obtained with the 6% (wt.) Mo/HZSM-5 catalyst.

Table 15. TGA results of spent 3% and 6% (wt.) Mo/HZSM-5 catalysts.

Mo content (%)	TOS (h)	Average Coke Formation Rate ($\text{g} \cdot \text{g}_{\text{cat}}^{-1} \cdot \text{h}^{-1}$)	Amount of Coke ($\text{g} \cdot \text{g}_{\text{cat}}^{-1}$)	$\text{g} \cdot \text{g}_{\text{cat}}^{-1} \cdot \text{mol}_{\text{benz.}}^{-1}$
3	16	0.0044	0.070	19
6	16	0.0031	0.049	11

Figure 38 shows the XRD patterns of the 3% and 6% (wt.) Mo/HZSM-5 catalysts before and after the MDA reaction. As seen, the diffraction peaks of the catalyst with 6% of Mo have a slightly lower intensity than those of the catalyst with 3% of Mo before MDA reaction. Moreover, in order to verify that

the conditions of the MDA reaction did not damage the HZSM-5 structure, the XRD patterns of the 3% and 6% (wt.) Mo/HZSM-5 catalysts were recorded after 16 h on stream. The diffraction peaks of the spent catalysts have a slightly lower intensity than those of the catalysts before the reaction. In general, the zeolite appears to be unaltered after MDA testing for 16 h.

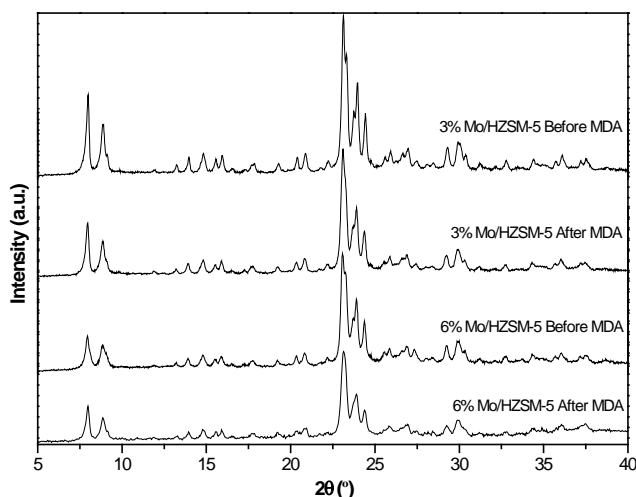


Figure 38. XRD patterns of 3% and 6% (wt.) Mo/HZSM-5 catalysts before and after MDA reaction.

4.3. Different zeolites versus the best HZSM-5 with 3% (wt.) Mo

The effect of the topology and the channel dimensions of the zeolite were studied over the catalytic activity on the MDA reaction using different zeolites, whose characteristics are detailed in Table 16, and with a 3% (wt.) of Mo. The zeolites employed range from small pore (8 MR) to large pore (12 MR). Moreover, the topology was studied since the different zeolites have unidirectional, bidirectional or tridirectional channels. All the zeolites employed had a similar Si/Al ratio, in the range 10-15.6, except for the ITQ-13 and the HZSM-22 zeolites.

Table 16. Different zeolites used to prepare the catalysts with 3% (wt.) Mo.

Zeolite	Channels system	Channels (MR)	Si/Al		S _{BET} (m ² /g)	Pore size (Å)
HZSM-5	Tridirectional	10 x 10	15		405	5.3 x 5.6 5.1 x 5.5
IM-5	Tridirectional	10 x 10	12		350	5.5 x 5.6 5.3 x 5.4 5.3 x 5.9 4.8 x 5.4 5.1 x 5.3
TNU-9	Tridirectional	10 x 10	14		400	5.6 x 5.5 5.4 x 5.5
ITQ-13	Tridirectional	9 x 10	Si/Ge	(Si+Ge)/Al	360	4.0 x 4.8 4.8 x 5.3 4.7 x 5.1
			13	39		
Chabazite	Tridirectional	8 x 8	10		550	3.8 x 3.8
HZSM-22	Unidirectional	10	37.08		--	4.6 x 5.7
NU-87	Bidirectional	10 x 12	15.6		479	4.8 x 5.7
NU-85	--	--	10.2		466	--
Mazzite	Unidirectional	12	13.7		566	7.4 x 7.4 3.1 x 3.1
Beta	Tridirectional	12 x 12	12.5		730	7.6 x 6.4 5.6 x 5.6
Mordenite	Unidirectional	12	10		422.8	6.5 x 7.0

The experiments were carried out according to the procedure described in the section 3.6.1.1. Table 17 shows the methane conversion and the selectivity to main products after 9 h on stream, at 700 °C, 1.2 bar and 1500 mL·h⁻¹·g_{cat}⁻¹, for the catalysts with 3% (wt.) of Mo. The highest methane conversion and the highest benzene, toluene and naphthalene selectivities are obtained for the 3% (wt.) Mo/HZSM-5 catalyst, as well as the lowest coke selectivity. It should be noted that the coke selectivity is higher than 50% for the other catalysts. Moreover, apart from the catalyst prepared with the HZSM-5 zeolite, after 9 h on stream, only the catalysts prepared with IM-5, TNU-9, NU-85 and Beta present selectivity to benzene. The channel dimensions and the topology of the NU-85 are still unknown, however the other four zeolites have tridirectional channels and are medium pore zeolites (10 MR), except for Beta

(12 MR), therefore this topology and the medium pore size are beneficial for the MDA reaction.

The catalyst prepared with Chabazite has smaller pore than HZSM-5 and, in spite of possessing tridirectional channels, shows worse performance in MDA reaction. Thus appearing that the reduction in pore size is detrimental by blocking the diffusion of the aromatic compounds, since the kinetic diameter of benzene molecule is roughly 5 Å [8]. In addition, the catalysts prepared with the zeolites that possess unidirectional or bidirectional channels, even when they have medium pore (HZSM-22), large pore (Mazzite, Mordenite) or simultaneously medium and large pore (NU-87), exhibit worse MDA performance than the catalysts with tridirectional channels.

Table 17. Effect of zeolite on the methane conversion and selectivity to main products after 9 h on stream of the catalysts with 3% (wt.) of Mo.

Zeolite	CH ₄ Conversion (% C)	Selectivity (% C)				
		C ₆ H ₆	C ₂	C ₇ H ₈	C ₁₀ H ₈	Coke
HZSM-5	5.72	65.32	7.66	5.55	18.58	2.89
IM-5	4.90	15.35	3.79	1.36	3.57	75.93
ITQ-13	2.46	0.00	6.52	0.00	0.00	93.48
TNU-9	4.01	22.91	7.06	2.65	2.66	64.72
Chabazite	4.36	0.00	7.96	0.00	0.00	92.04
ZSM-22	1.99	0.00	0.00	0.00	7.41	92.59
NU-87	2.94	0.00	4.73	0.00	0.00	95.27
NU-85	1.65	6.83	3.95	0.00	0.00	89.22
Mazzite	1.74	0.00	15.24	0.00	0.00	84.76
Beta	5.68	9.31	4.00	0.00	0.82	85.87
Mordenite	2.51	0.00	7.90	0.00	0.00	92.10

In Figure 39.a it can be observed that the highest benzene yield is obtained with the catalyst prepared using the HZSM-5 zeolite over time and for the whole conversion range (Figure 39.b). Regarding the other zeolites studied,

as may be inferred from Table 17, the TNU-9 and IM-5 zeolites show higher benzene yield, in that order, throughout the time on stream (Figure 39.a) and almost for the whole conversion range (Figure 39.b). On the contrary, the lowest benzene yield is obtained using the HZSM-22 and Chabazite zeolites.

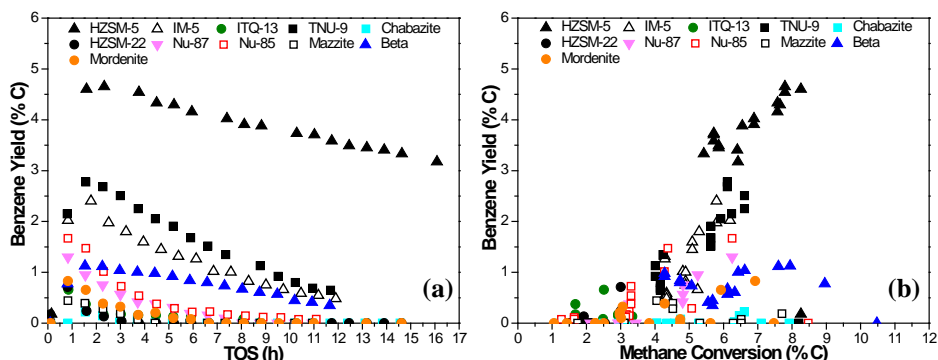


Figure 39. Effect of the zeolite of the 3%Mo/zeolite catalysts on the (a) benzene yield versus the TOS and (b) benzene yield versus the methane conversion.

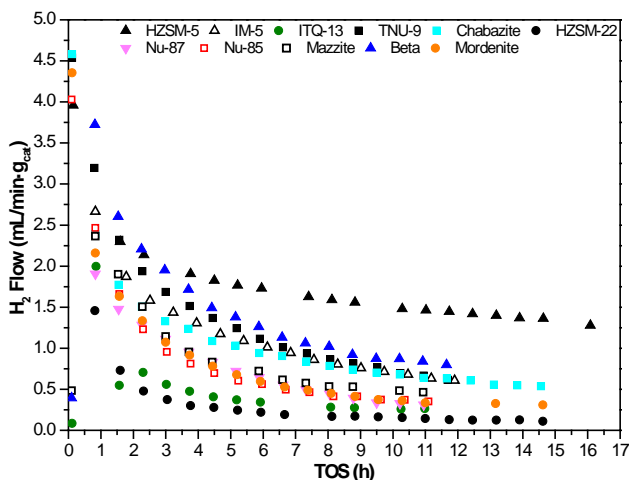


Figure 40. Effect of the zeolite of the 3%Mo/zeolite catalysts on the H₂ flow versus the TOS at 700 °C.

Finally, Figure 40 depicts the H₂ flow normalized per gram of catalyst for the eleven catalysts with 3% (wt.) of Mo. As seen, all the catalysts exhibit

the same trend, the first point obtained is the maximum H₂ flow and then it drops throughout the time on stream. This parameter has a direct relationship with the methane conversion for each catalyst.

The TGA results obtained for the spent catalysts are shown in Table 18. The zeolites used to prepare the catalysts with 3% (wt.) of Mo are listed according to the average coke formation rate in descending order: Beta, Chabazite, TNU-9, Mordenite, Mazzite, IM-5, NU-87, NU-85, ITQ-13, HZSM-5 and HZSM-22. Nevertheless, by focusing on the ratio between the amount of coke ($\text{g}\cdot\text{g}_{\text{cat}}^{-1}$) and the accumulated benzene moles, it is observed that the catalyst prepared with the Chabazite zeolite produces by far the highest amount of coke per accumulated benzene mole, followed in lesser extent by those prepared with the Mazzite and Mordenite zeolites. While, the lowest ratio is obtained for the catalyst prepared with the HZSM-5 zeolite.

Table 18. TGA results of spent 3% (wt.) Mo/zeolite catalysts.

Zeolite	TOS (h)	Average Coke Formation Rate ($\text{g}\cdot\text{g}_{\text{cat}}^{-1}\cdot\text{h}^{-1}$)	Amount of Coke ($\text{g}\cdot\text{g}_{\text{cat}}^{-1}$)	$\text{g}\cdot\text{g}_{\text{cat}}^{-1}\cdot\text{mol}_{\text{benz.}}^{-1}$
HZSM-5	16.0	0.0044	0.0702	19
IM-5	11.9	0.0082	0.0979	107
ITQ-13	11.0	0.0061	0.0673	623
TNU-9	11.7	0.0105	0.1228	99
Chabazite	14.6	0.0106	0.1537	7321
HZSM-22	15.4	0.0033	0.0507	873
NU-87	11.0	0.0070	0.0763	355
NU-85	11.1	0.0063	0.0696	198
Mazzite	10.9	0.0083	0.0903	1368
Beta	11.7	0.0153	0.1784	304
Mordenite	14.6	0.0100	0.1463	1170

4.4. MCM-22 versus the best HZSM-5 with 6% (wt.) Mo

The HZSM-5 and HMCM-22 zeolites have a pore aperture of 10 member rings (10 MR) and therefore are close to the kinetic diameter of benzene molecule, around 5 Å [8]. In this work, the Mo content selected to compare the HZSM-5 and HMCM-22 zeolites was 6% (wt.), since with this content the best performance on MDA reaction was reached for both zeolites [7, 9]. In Table 19, the topology and the channel dimensions of these zeolites are summarized. Concretely, two MCM-22 zeolites were used, one with a Si/Al ratio of 15 and another with a Si/Al ratio of 25, in order to analyze the effect of the acidity on this zeolite. The experiments were carried out according to the procedure described in the section 3.6.1.1.

Table 19. Topology and channel dimensions of the HZSM-5 and MCM-22 zeolites used to prepare the catalysts with 6% of Mo.

Zeolite	Channels system	Channels	Pore size (Å)
HZSM-5	Tridirectional	10 x 10 MR	5.3 x 5.6 5.1 x 5.5
MCM-22	Bidirectional	10 x 10 MR	4.1 x 5.1
	Tridirectional super cage system → 12 MR Interconnected by 10 MR windows		4.0 x 5.5

Table 20 details the selectivity to main products and the methane conversion of MDA reaction after 9 h on stream for the 6%Mo/zeolite catalysts, at 700 °C, 1.2 bar and 1500 mL·h⁻¹·g_{cat}⁻¹. The highest methane conversion and benzene selectivity are obtained for the 6% (wt.) Mo/MCM-22 catalyst (Si/Al=15), as well as the lowest C₂ hydrocarbons selectivity. Furthermore, with this catalyst the toluene, naphthalene and coke selectivities are intermediate between the other two catalysts. While the toluene selectivity is very similar for the three catalysts, the naphthalene selectivity is much higher for the catalyst prepared with the HZSM-5, due to the unique pore structure and the suitable

acid strength distribution of the MCM-22 [9]. Moreover, the coke selectivity is much higher for the catalyst prepared with the MCM-22 (Si/Al=25).

Regarding the two catalysts prepared with the MCM-22 zeolite with different acidity, it can be observed that the aromatics selectivity (Table 20) is higher for the catalyst with a Si/Al ratio of 15. However, the C₂ hydrocarbons and coke selectivities are lower for this catalyst, which is ascribed to its higher concentration of Brønsted acid sites.

Table 20. Effect of the zeolite on the selectivity to main products and methane conversion after 9 h on stream of 6%Mo/zeolite catalysts.

Zeolite	Selectivity (% C)					Methane Conversion (% C)
	C ₆ H ₆	C ₂	C ₇ H ₈	C ₁₀ H ₈	Coke	
HZSM-5 (Si/Al=15)	67.2	7.1	5.0	16.4	4.3	6.7
MCM-22 (Si/Al=15)	82.1	3.3	3.7	5.2	5.7	8.1
MCM-22 (Si/Al=25)	53.2	5.5	2.2	4.1	35.0	4.7

Figure 41.a illustrates the benzene yield for the catalysts with 6 % (wt.) of Mo. The 6%Mo/MCM-22 catalyst with a Si/Al ratio of 15 shows the highest benzene yield over time, which is ascribed to its high benzene selectivity and high methane conversion. The maximum benzene yield for 6%Mo/MCM-22 (Si/Al=15) is around 7.06% and it is reached at 4.61 h of MDA reaction. This catalyst also exhibits the most stable benzene yield throughout the time on stream, since shows a 1.6-fold decrease in the average deactivation rate with respect to the 6%Mo/HZSM-5 catalyst.

Moreover, in Figure 41.b the benzene yield versus the methane conversion is depicted for each catalyst. As seen, the 6%Mo/MCM-22 catalyst with a Si/Al ratio of 15 exhibits the highest benzene yield for the whole conversion range. It should be pointed out that the MDA performance obtained with the 6%Mo/MCM-22 catalyst with a Si/Al ratio of 25 is worse than that reported by Liu et al. [10].

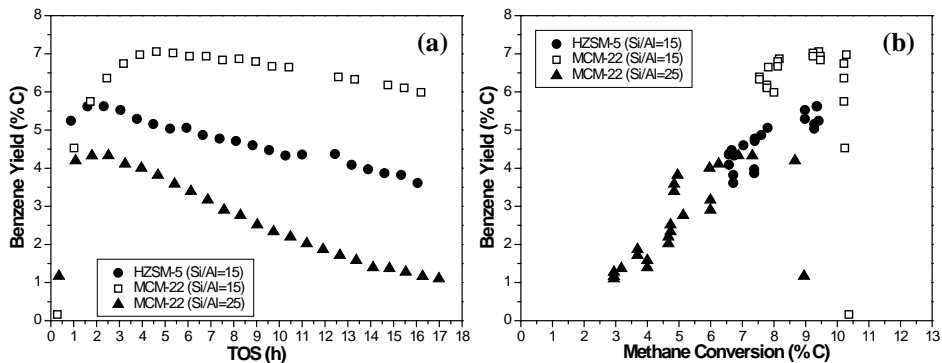


Figure 41. Effect of the zeolite of 6%Mo/zeolite catalysts on the (a) benzene yield versus the TOS and (b) benzene yield versus methane conversion.

Figure 42 displays the H_2 flow normalized per gram of catalyst for the catalysts with 6% (wt.) of Mo. First points of H_2 flow are higher due to the H_2 production by coking the fresh catalyst, and then this is progressively reduced over time. The zeolites that were used to prepare these catalysts are listed according to the H_2 flow normalized per gram of catalyst in descending order: MCM-22 (Si/Al=15), HZSM-5, MCM-22 (Si/Al=25).

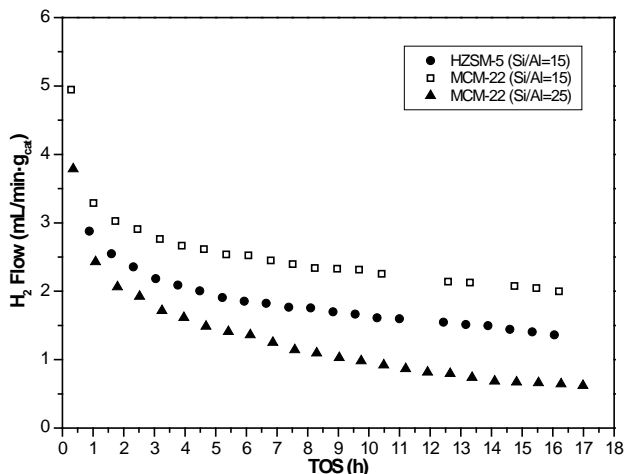


Figure 42. Effect of the zeolite of 6%Mo/zeolite catalysts on the H_2 flow versus the TOS at 700 °C.

The MCM-22 zeolite used to prepare the 6%Mo/MCM-22 catalysts (Si/Al ~ 15) was synthesized using a little bit of seeding, as described in the section 3.2.2., in a teflon-lined stainless steel autoclave of 600 mL. While, the “seeding” used is the MCM-22 zeolite synthesized in teflon-lined stainless steel autoclaves of 60 mL. The thin platelet morphology of the synthesized MCM-22 zeolites, with a Si/Al ~ 15, is shown in the following FE-SEM images (Figure 43, Figure 44 and Figure 45).

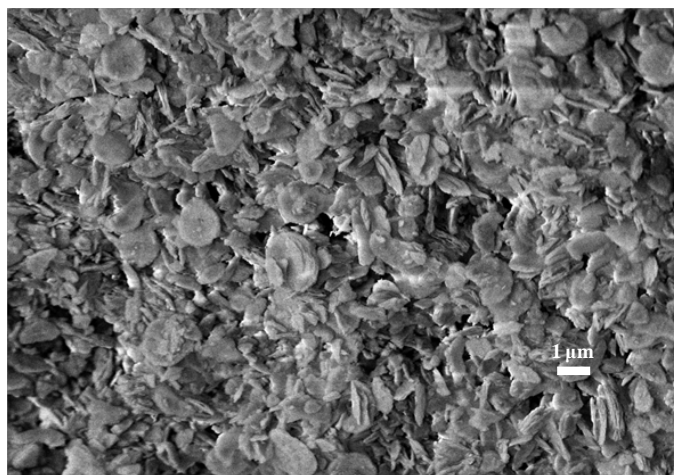


Figure 43. FE-SEM image of the MCM-22 zeolite (Si/Al ~ 15) synthesized without seeding.

The MCM-22 synthesized without seeding (Figure 43) appears in the form of round and thin platelets with a diameter of 1-2 μm and a thickness much lower. However, the MCM-22 synthesized with seeding (Figure 44 and Figure 45) exhibits smaller and thinner platelets than the former, with a diameter $\leq 1 \mu\text{m}$ (Figure 44), which are composed by nanoplatelets with a diameter of 0.1-0.2 μm , as can be observed in Figure 45.

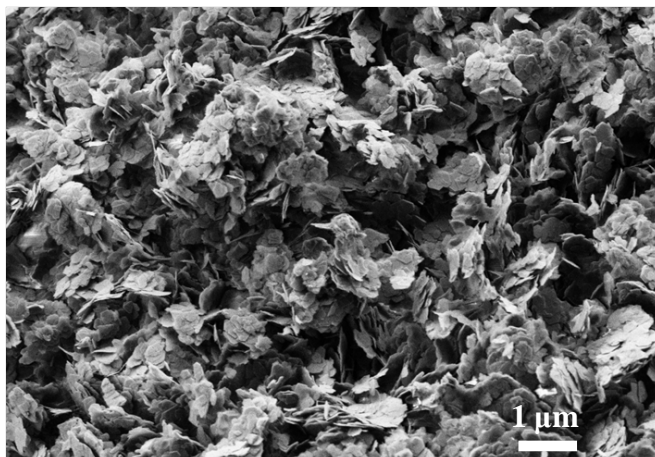


Figure 44. FE-SEM image of the MCM-22 zeolite (Si/Al ~ 15) synthesized using seeding.

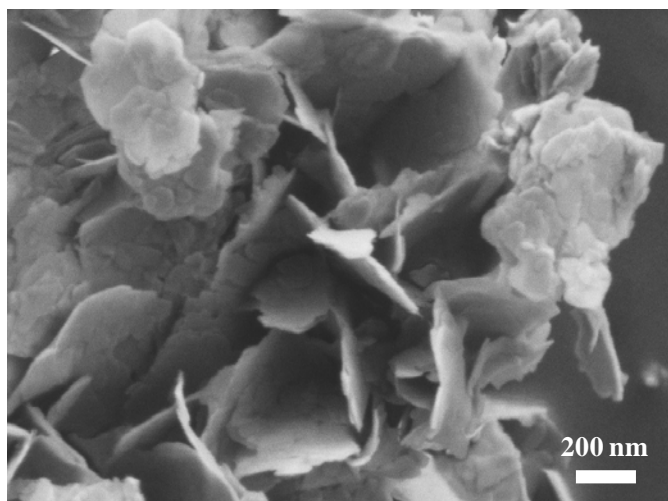


Figure 45. Enlarged FE-SEM image of the MCM-22 zeolite (Si/Al ~ 15) synthesized using seeding.

Moreover, Figure 46 shows the morphology of the 6% Mo/MCM-22 catalyst prepared as mentioned in the section 3.3.1.1., in powder form. The appearance of both the catalyst and the zeolite (Figure 44) is similar, observing platelets with a diameter $< 1 \mu\text{m}$ (Figure 46) composed by nanoplatelets with a diameter of $0.1\text{-}0.2 \mu\text{m}$ (Figure 47). Furthermore, the Mo content of the catalyst

(6% wt.) was confirmed by FE-SEM/EDS and ICP. It should be noted that EDS analysis was recorded in the whole image of Figure 46.

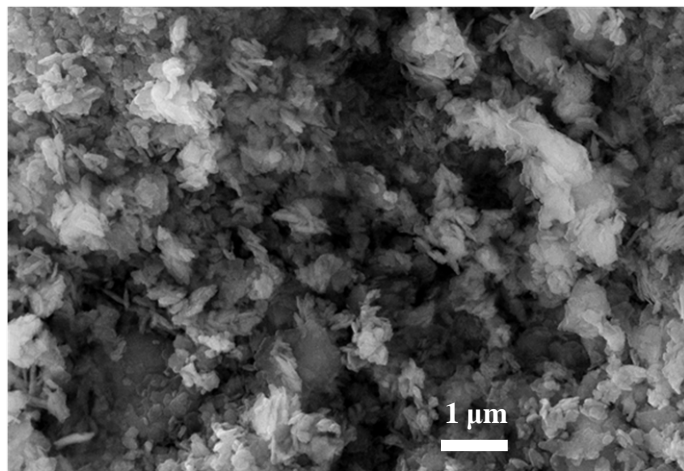


Figure 46. FE-SEM image of the 6% Mo/MCM-22 catalyst (powder).

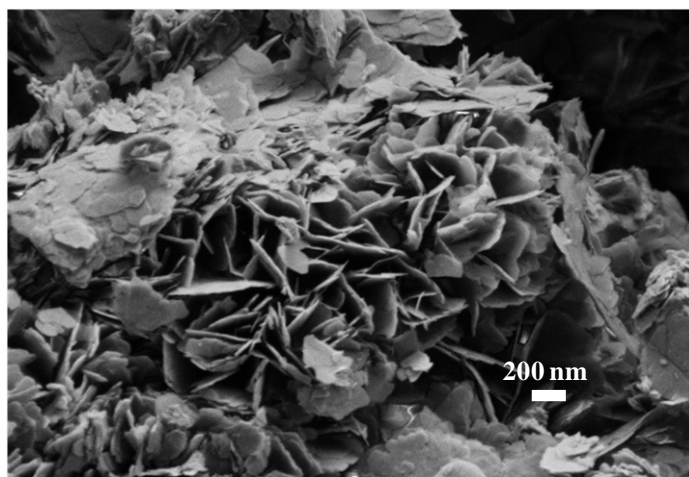


Figure 47. Enlarged FE-SEM image of the 6% Mo/MCM-22 catalyst (powder).

Table 21 summarizes the TGA results, the catalysts prepared using the MCM-22 zeolites accumulate higher amount of coke than the catalyst prepared with the HZSM-5 zeolite. The unique pore structure and the super cages presence in the catalysts prepared with the MCM-22 zeolite, abovementioned in

the section 2.5, are the responsible for this high coke accumulation. In the case of the 6%Mo/MCM-22 catalyst with a Si/Al ratio of 15, this high coke accumulation appears that not affect substantially the catalytic activity. While, the 6%Mo/MCM-22 catalyst with Si/Al = 25 produces the highest amount of coke per accumulated benzene mole.

Table 21. TGA results of spent 6% (wt.) Mo/zeolite catalysts.

Zeolite	TOS (h)	Average Coke Formation Rate ($\text{g} \cdot \text{g}_{\text{cat}}^{-1} \cdot \text{h}^{-1}$)	Amount of Coke ($\text{g} \cdot \text{g}_{\text{cat}}^{-1}$)	$\text{g} \cdot \text{g}_{\text{cat}}^{-1} \cdot \text{mol}_{\text{benz.}}^{-1}$
HZSM-5 (Si/Al=15)	16.0	0.0031	0.0490	11
MCM-22 (Si/Al=15)	16.9	0.0078	0.1325	21
MCM-22 (Si/Al=25)	17.0	0.0041	0.0698	24

The Mo introduction in the HZSM-5 and HMCM-22 zeolites followed by the calcination in air reduces both the surface area and the pore volume [9, 11]. As can be observed in Table 22, the surface area of the HZSM-5 and the MCM-22 zeolites (Si/Al=15) was reduced ca. 25% and 17.80%, respectively, after the loading of the 6% (wt.) of Mo. In addition, the micropore volume also decreased in both zeolites after the incorporation of the 6% (wt.) of Mo, 27.50% and 23% for the HZSM-5 and MCM-22, respectively.

Further, the surface area and the micropore volume of both catalysts were measured after 16 h of MDA reaction (Table 22) in order to confirm the higher coke accumulation capacity of the MCM-22 zeolite. The BET surface area for the 6%Mo/HZSM-5 and 6%Mo/MCM-22 catalysts decreased roughly 19.41% and 46.60%, respectively. Moreover, the micropore volume also was reduced in both catalysts after the MDA experiments, ca. 15.52% and 53% for 6%Mo/HZSM-5 and 6%Mo/MCM-22 catalysts, respectively.

Table 22. BET surface area and micropore volume for the 6% (wt.) Mo/zeolite catalysts (Si/Al=15) before and after MDA reaction.

Zeolite	S_{BET} (m^2/g)			Micropore volume (cm^3/g)		
	Without Mo	With 6% (wt.) Mo		Without Mo	With 6% (wt.) Mo	
		Before MDA	After MDA		Before MDA	After MDA
HZSM-5	370	277	223	0.160	0.116	0.098
MCM-22	485	399	213	0.196	0.151	0.071

Furthermore, the temperature programmed oxidation technique (TPO) was employed over both spent catalysts to determine the nature and location of the carbonaceous species on them. The CO_2 in part contributes to the signal at $m/z = 28$, therefore this contribution was removed from the total intensity at $m/z = 44$ to obtain the signal that corresponds to the CO_2 . Then, in order to depict the CO_x ($\text{CO} + \text{CO}_2$) signal versus the temperature (Figure 48), the signal corresponding to CO was added to that of CO_2 .

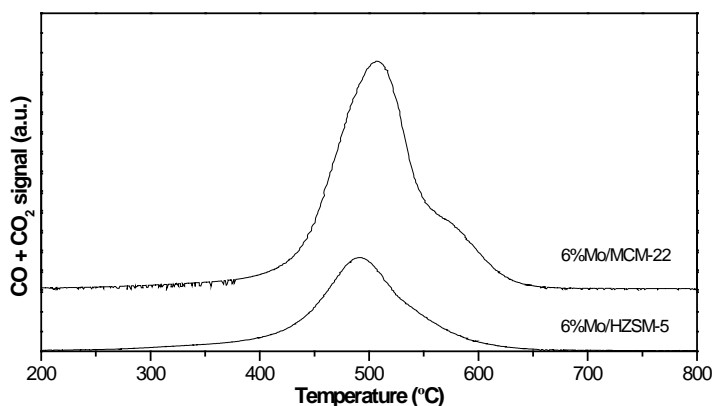


Figure 48. TPO profiles of carbon species over spent 6%Mo/HZSM-5 and 6%Mo/MCM-22 catalysts (Si/Al=15). Same scale of Y-axis.

As can be observed in Figure 48, two peaks can be distinguished in the CO_x profiles, i.e., a peak at lower (peak 1) and a peak at higher temperature

(peak 2), which are attributed to the carbon related to Mo species and to the carbon associated with the Brønsted acid sites, respectively.

The TGA results (Table 21) indicate that the 6%Mo/MCM-22 catalyst accumulates more than the double amount of coke than the 6%Mo/HZSM-5 catalyst. Furthermore, the TPO profiles were deconvoluted by using a Gauss curve-fitting method and the area of each peak and the corresponding percentage were calculated. These percentages were used to determine the corresponding amount of each type of coke (Table 23). Thus, it can be concluded that on the 6%Mo/HZSM-5 catalyst, the coke related to Mo species and the coke associated with Brønsted acid sites (aromatic-type carbon) are roughly 63.4% and 61.1% lower than on the 6%Mo/MCM-22 catalyst, respectively.

Moreover, the temperature at maximum of both peaks (Table 23) is similar for both catalysts, which points out that the coke characteristics (particle size, morphology, etc.) may be similar between them [12]. Furthermore, the peak corresponding to the carbidic-like carbon from Mo carbide species is not observed since it is covered by the Mo-associated coke at longer times (> 10 min) [1, 13, 14].

Table 23. Results of the deconvoluted TPO profiles of carbon species over 6%Mo/HZSM-5 and 6%Mo/MCM-22 catalysts (Si/Al=15).

Catalyst	Temperature at maximum (°C)		Percentage (%)		Amount of coke (g·g _{cat} ⁻¹)	
	Peak 1	Peak 2	Peak 1	Peak 2	Peak 1	Peak 2
6%Mo/HZSM-5	491	576	81.63	18.37	0.0400	0.0090
6%Mo/MCM-22	503	587	82.52	17.48	0.1093	0.0232

By focusing on the 6%Mo/MCM-22 catalyst (Si/Al=15), the acidic properties of this were determined by FTIR of adsorbed pyridine. In Table 24 the acidity obtained for the MCM-22 zeolite (abovementioned in the section

3.2.2) and for the 6%Mo/MCM-22 catalyst is detailed. As seen, after loading of 6% of Mo in the MCM-22 zeolite the Brønsted acidity was reduced for the three temperatures, while the Lewis acidity was barely decreased. These results are in agreement with those shown by Ma et al. [15]. The Mo reacted mainly with Brønsted acid sites (framework aluminum), thus being better distributed into the channels of the MCM-22 zeolite.

Table 24. Acidity of the synthesized MCM-22 and 6%Mo/MCM-22 catalyst.

	Acidity ($\mu\text{mol pyridine/g}$)					
	Brønsted ($^{\circ}\text{C}$)			Lewis ($^{\circ}\text{C}$)		
	150	250	350	150	250	350
MCM-22	74	47	31	30	19	16
6%Mo/MCM-22	47	31	18	30	18	15

Furthermore, in order to verify that the conditions of the MDA reaction did not damage the MCM-22 structure, the XRD patterns of the 6% (wt.) Mo/MCM-22 catalyst were recorded after 16 h of MDA reaction. As seen in Figure 49, the diffraction peaks of the spent catalyst present a lower intensity than those of the catalyst before the MDA reaction. The XRD patterns of the 6% (wt.) Mo/HZSM-5 catalyst are shown in Figure 38.

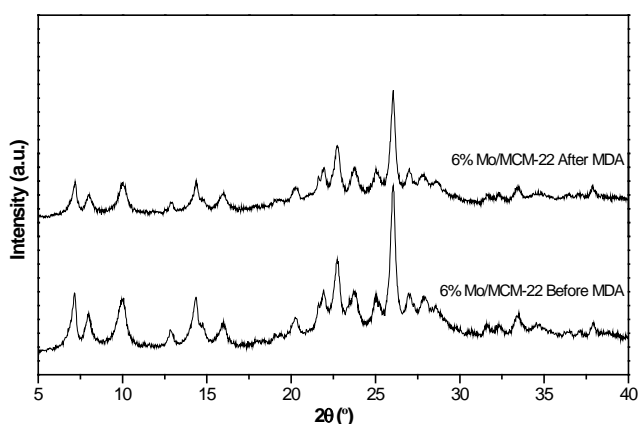


Figure 49. XRD patterns of 6% (wt.) Mo/MCM-22 catalyst before and after MDA reaction.

4.5. Conclusions

The MDA performance is strongly related to the characteristics of the zeolite employed. Firstly, in the study carried out among different HZSM-5 with tridirectional channels and medium pore size (10 MR), it can be concluded that the Si/Al ratio and the crystal size of the zeolite play a significant role in the MDA performance. Specifically, the 3%Mo/HZSM-5 catalysts with higher Si/Al ratio (40 and 25) exhibited lower methane conversion throughout the time on stream than the other catalysts, since the Brønsted acidity is lower for them. Nonetheless, the highest and most stable benzene yield over time was obtained for one of the catalysts with an intermediate Si/Al ratio (CBV3024E, Si/Al=15), therefore this zeolite was the best HZSM-5 tested.

Moreover, by focusing on three catalysts with the same crystal size (~0.1 μm) and different Si/Al ratios (10, 15 and 25) the benzene selectivity after 9 h of MDA reaction decreased as the Si/Al ratio increased. While an opposite trend was observed for the C₂ hydrocarbons selectivity, since for a low Si/Al ratio the concentration of the Brønsted acid sites is higher. Further, by comparing catalysts with a Si/Al ratio equal to 10, the catalyst with a crystal size of 0.1 μm performed better on the MDA reaction than the catalyst with a crystal size of 1-2 μm .

Regarding the Mo content, it affects notably the MDA performance, i.e. the methane conversion and the benzene yield exhibited a significant increase with increasing Mo content in the range of 3-6%, while the naphthalene and the coke yields slightly increased. Furthermore, by means of the TGA results it was calculated the average coke formation rate and the lowest was obtained with the 6% (wt.) Mo/HZSM-5 catalyst. Concretely, the maximum benzene yield for 3% (wt.) and 6% (wt.) Mo/CBV3024E were around 4.70% and 5.63%, respectively, both reached at 2.33 h of MDA reaction.

In addition, the topology and the channel dimensions of the zeolite have a notable influence on the MDA performance. In a first screening of different zeolite topologies with 3% (wt.) of Mo, the highest benzene yield was obtained with the catalyst prepared with the HZSM-5 zeolite (CBV3024E), that possesses tridirectional channels and medium pore (10 MR). Moreover, after 9 h on stream, only the catalysts prepared with HZSM-5, IM-5, TNU-9, NU-85 and Beta zeolites had selectivity to benzene. Except for Beta (12 MR) and NU-85 (still unknown), the other three zeolites have tridirectional channels and are medium pore zeolites (10 MR), therefore this topology and the medium pore size were beneficial for the MDA reaction.

Further, by comparing the best HZSM-5 (CBV3024E) and the MCM-22 zeolites with 6% (wt.) of Mo, it can be said that the highest benzene yield was obtained for the 6%Mo/MCM-22 catalyst (Si/Al=15) throughout the time on stream, which was ascribed to its high benzene selectivity and methane conversion. Moreover, the benzene yield for the 6%Mo/MCM-22 catalyst was more stable over time, since exhibited a 1.6-fold decrease in the average deactivation rate with respect to the 6%Mo/HZSM-5 catalyst. In particular, the maximum benzene yield for this catalyst was around 7.06% and was reached at 4.61 h of MDA reaction. Therefore, the unique pore structure of the MCM-22 zeolite, that consists of two independent pore system (as abovementioned in the section 2.5.): a smaller 2D (two-dimensional), with an aperture of 10 member rings (10 MR), sinusoidal pore system (4.1 x 5.1 Å), and a larger 3D (three-dimensional), with an aperture of 12 member rings (12 MR), super cage system interconnected by 10 MR windows (4.0 x 5.5 Å) [16], was beneficial for the MDA performance. Indeed, so far the 6%Mo/MCM-22 was the best catalyst tested for the MDA reaction.

Finally, it is confirmed that the BET surface area and the micropore volume were reduced after loading 6% (wt.) of Mo in HZSM-5 and MCM-22

zeolites. Furthermore after 16 h of MDA reaction both the BET surface area and the micropore volume also were decreased. Therefore, with these results, and those of TGA and TPO, it is verified that the MCM-22 zeolite possesses higher coke accumulation capacity than the HZSM-5 zeolite. Moreover, it is corroborated that the Mo reacts preferentially with the Brønsted acid sites (framework aluminum) of the MCM-22 zeolite by FTIR of adsorbed pyridine, thus being better distributed into the channels of this zeolite.

4.6. References

- [1] H.M. Liu, X.H. Bao, Y.D. Xu, *Journal of Catalysis*, 239 (2006) 441-450.
- [2] S.T. Liu, L. Wang, R. Ohnishi, M. Ichikawa, *Journal of Catalysis*, 181 (1999) 175-188.
- [3] R.W. Borry, Y.H. Kim, A. Huffsmith, J.A. Reimer, E. Iglesia, *Journal of Physical Chemistry B*, 103 (1999) 5787-5796.
- [4] F. Solymosi, A. Erdohelyi, A. Szoke, *Catalysis Letters*, 32 (1995) 43-53.
- [5] D.J. Wang, J.H. Lunsford, M.P. Rosynek, *Topics in Catalysis*, 3 (1996) 289-297.
- [6] W.P. Zhang, D. Ma, X.W. Han, X.M. Liu, X.H. Bao, X.W. Guo, X.S. Wang, *Journal of Catalysis*, 188 (1999) 393-402.
- [7] D. Ma, Y.Y. Shu, X.H. Bao, Y.D. Xu, *Journal of Catalysis*, 189 (2000) 314-325.
- [8] E. Bartsch, H. Bertagnolli, G. Schulz, P. Chieux, *Berichte Der Bunsen-Gesellschaft-Physical Chemistry Chemical Physics*, 89 (1985) 147-156.
- [9] Y.Y. Shu, D. Ma, L.Y. Xu, Y.D. Xu, X.H. Bao, *Catalysis Letters*, 70 (2000) 67-73.
- [10] L. Liu, D. Ma, H.Y. Chen, H. Zheng, M.J. Cheng, Y.D. Xu, X.H. Bao, *Catalysis Letters*, 108 (2006) 25-30.
- [11] L.Y. Chen, L.W. Lin, Z.S. Xu, X.S. Li, T. Zhang, *Journal of Catalysis*, 157 (1995) 190-200.
- [12] C.A. Querini, S.C. Fung, *Appl. Catal. A-Gen.*, 117 (1994) 53-74.
- [13] D. Ma, D.Z. Wang, L.L. Su, Y.Y. Shu, Y. Xu, X.H. Bao, *Journal of Catalysis*, 208 (2002) 260-269.

[14] W.P. Ding, S.Z. Li, G.D. Meitzner, E. Iglesia, *Journal of Physical Chemistry B*, 105 (2001) 506-513.

[15] D. Ma, Y.Y. Shu, X.W. Han, X.M. Liu, Y.D. Xu, X.H. Bao, *Journal of Physical Chemistry B*, 105 (2001) 1786-1793.

[16] <http://www.iza-structure.org/databases/>.

Chapter 5.

EFFECT OF THE CATALYST ACTIVATION ON MDA REACTION

5. Effect of the catalyst activation on MDA reaction

5.1. 6% (wt.) Mo/HZSM-5 catalyst

Different activations procedures (detailed in section 3.6.1.2.2.) over the 6% (wt.) Mo/HZSM-5 catalyst have been carried out in order to improve the MDA reaction performance: pre-coking of the catalyst with 1.25% of 1,2,4-trimethylbenzene (1,2,4-TMB) and activation with a gas mixture of CH₄:H₂, 1:4 (vol. ratio) [1] in which the catalyst was pre-carburized and pre-reduced. In the following table the type of activation and the code used are summarized:

Table 25. Type of catalyst activation and code used in MDA reaction.

Code	Activation Gas	Type of activation
Standard	Ar	0.5 h at 700 °C
TMB	1.25% of 1,2,4-TMB	4 h at 600 °C
CH₄:H₂ (1 h)	CH ₄ :H ₂ , 1:4 (vol. ratio)	1 h up to 700 °C and 2 h at 700 °C
CH₄:H₂ (4 h)	CH ₄ :H ₂ , 1:4 (vol. ratio)	4 h up to 700 °C and 2 h at 700 °C

The experiment performed with the standard catalyst activation was carried out according to the procedure described in the section 3.6.1.1. The catalyst was prepared using the HZSM-5 zeolite (CBV3024E) impregnated with a 6% (wt.) of Mo. Table 26 details the methane conversion and the selectivity to main products of MDA reaction after 9 h on stream obtained for the different activation procedures, at 700 °C, 1.2 bar and 1500 mL·h⁻¹·g_{cat}⁻¹. The lowest methane conversion and coke selectivity are obtained with the standard activation procedure, by coking the zeolite and carburizing the Mo during the first 3 h on methane stream. Nonetheless, when the catalyst was pre-carburized and pre-reduced using a gas mixture of CH₄:H₂, 1:4 (vol. ratio) during 1 h up to

700 °C and it was kept at this temperature for 2 h (code “CH₄:H₂ (1 h)”), the benzene selectivity obtained is the highest and the coke selectivity is very low, near to the lowest. However, the C₂ hydrocarbons, toluene and naphthalene selectivities are very similar in all cases.

Table 26. Effect of the 6%Mo/HZSM-5 catalyst activation on the methane conversion and the selectivity to main products after 9 h on stream.

Code	Methane Conversion (% C)	Selectivity (% C)				
		C ₆ H ₆	C ₂	C ₇ H ₈	C ₁₀ H ₈	Coke
Standard	6.66	67.15	7.12	5.03	16.44	4.25
TMB	8.07	49.20	5.53	3.74	12.03	29.50
CH₄:H₂ (1 h)	8.32	69.16	5.33	4.76	13.04	7.04
CH₄:H₂ (4 h)	9.00	54.67	3.76	3.45	13.47	24.65

The trend observed in Table 26 is confirmed in Figure 50 that depicts the benzene yield achieved for the different activation procedures. The highest benzene yield throughout the time on stream is obtained in the experiment in which the catalyst was pre-carburized and pre-reduced using a gas mixture of CH₄:H₂, 1:4 (vol. ratio) during 1 h up to 700 °C and kept at this temperature for 2 h (code CH₄:H₂ (1 h)). In particular, the maximum benzene yield reached is around 6.21% at 3.23 h of MDA reaction. It should be pointed out that these results are slightly higher than those obtained using the same gas mixture during 4 h up to 700 °C and kept at this temperature for 2 h (code CH₄:H₂ (4 h)). In addition, in both cases the benzene yield is more stable over time, since these experiments show a 2-fold and 2.4-fold decrease in the average deactivation rate with respect to the experiment performed using the standard activation, respectively. Finally, the detrimental effect that involves the pre-coking of the catalyst with 1.25% of 1,2,4-TMB on the MDA performance might be due to the higher formation of carbonaceous deposits that were blocking the channels of the zeolite since the beginning of the experiment. These results show that the

pre-carburization and pre-reduction of the 6%Mo/HZSM-5 catalyst using a gas mixture of CH₄:H₂, 1:4 (vol. ratio) during 1 h up to 700°C and kept at this temperature for 2 h (code CH₄:H₂ (1 h)) was beneficial for the performance of the MDA reaction. This treatment enables the pre-carburization of Mo species and the simultaneous pre-reduction of these MoC_x species [1-3].

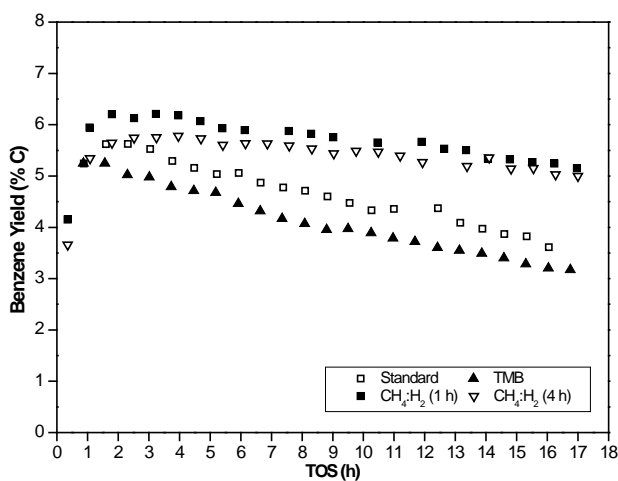


Figure 50. Effect of the 6%Mo/HZSM-5 catalyst activation on the benzene yield versus the TOS at 700 °C and 1.2 bar.

Figure 51.a confirms the results observed in Figure 50, i.e., the accumulated benzene moles are higher for the two activation procedures that use a gas mixture of CH₄:H₂, 1:4 (vol. ratio) than using the other catalyst activations. In particular, the highest accumulated benzene moles are obtained for the catalyst activated with “CH₄:H₂ (1 h)” procedure, achieving a maximum of 0.01038 mol·g_{cat}⁻¹ after 17 h on stream. The lowest accumulated benzene moles are reached by the “TMB” procedure.

Additionally, Figure 51.b depicts the effect of the catalyst activation on the H₂ flow normalized per gram of catalyst obtained during the MDA reaction. As seen, the highest H₂ flow is reached by the catalysts activated using a gas mixture of CH₄:H₂, 1:4 (vol. ratio). While the lowest H₂ flow is achieved with

the catalyst activated with the standard and the “TMB” procedures. The H_2 flow is higher during the first stages of the MDA reaction due to (i) the reduction and carburization of $(Mo_2O_5)^{2+}$ species by methane to MoC_x [4] under non oxidative conditions [5, 6] and (ii) the coking of the most active Brønsted acid sites, especially on the external surface of the zeolite.

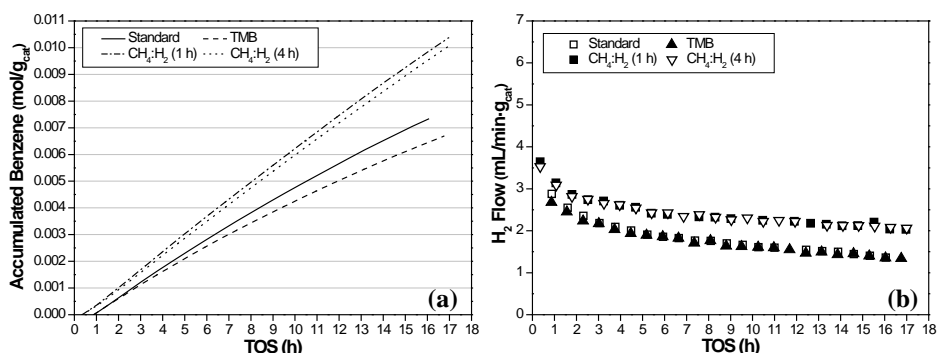


Figure 51. Effect of the 6%Mo/HZSM-5 catalyst activation on the (a) accumulated benzene moles and (b) H_2 flow versus the TOS at 700 °C.

Table 27 shows the TGA results obtained for the spent 6%Mo/HZSM-5 catalysts using the different activations. The activation procedures are listed according to the amount of coke in descending order: TMB, standard, $CH_4:H_2$ (1 h) and $CH_4:H_2$ (4 h). The highest average coke formation rate and amount of coke per accumulated benzene mole are produced by the “TMB” procedure, followed by the standard activation. While the procedures “ $CH_4:H_2$ (1 h)” and “ $CH_4:H_2$ (4 h)” show a similar and lower coke formation rate and amount of coke per accumulated benzene mole. Thus confirming that the Mo species obtained using a gas mixture of $CH_4:H_2$, 1:4 (vol. ratio) are more stable and active for MDA reaction [1-3], being the first coking process more selective.

Table 27. TGA results of spent 6%Mo/HZSM-5 catalysts activated with different procedures.

Code	TOS (h)	Average Coke Formation Rate ($\text{g} \cdot \text{g}_{\text{cat}}^{-1} \cdot \text{h}^{-1}$)	Amount of Coke ($\text{g} \cdot \text{g}_{\text{cat}}^{-1}$)	$\text{g} \cdot \text{g}_{\text{cat}}^{-1} \cdot \text{mol}_{\text{benz.}}^{-1}$
Standard	16.0	0.0031	0.0490	11
TMB	16.8	0.0066	0.1112	28
CH ₄ :H ₂ (1 h)	17.0	0.0027	0.0467	7
CH ₄ :H ₂ (4 h)	17.0	0.0022	0.0372	6

5.2. 6% (wt.) Mo/MCM-22 catalyst

The 6% (wt.) Mo/MCM-22 catalyst was pre-carburized and pre-reduced using the best activation conditions found for the 6% (wt.) Mo/HZSM-5 catalyst (detailed in section 3.6.1.2.2.3.). The results of this experiment were compared with those achieved using the standard activation method, which was done according to the procedure described in the section 3.6.1.1. The catalysts were prepared using the MCM-22 zeolite (Si/Al=15) and impregnated with a 6% (wt.) of Mo. Table 28 shows the methane conversion and the selectivity to main products after 9 h on stream at 700 °C, 1.2 bar and 1500 mL·h⁻¹·g_{cat}⁻¹. As seen, the lowest methane conversion and coke selectivity are obtained using the standard activation method. However, the aromatics selectivities are slightly lower for the catalyst activated with “CH₄:H₂ (1 h)” procedure. The C₂ hydrocarbon selectivity is very similar for both activation procedures.

Table 28. Effect of the 6%Mo/MCM-22 catalyst activation on the methane conversion and the selectivity to main products after 9 h on stream.

Code	Methane Conversion (% C)	Selectivity (% C)				
		C ₆ H ₆	C ₂	C ₇ H ₈	C ₁₀ H ₈	Coke
Standard	8.12	82.12	3.28	3.68	5.26	5.66
CH ₄ :H ₂ (1 h)	8.89	79.52	3.31	3.07	4.64	9.46

Figure 52.a depicts the benzene yield over time for both experiments. The highest benzene yield throughout the time on stream is obtained when the catalyst was pre-carburized and pre-reduced using a gas mixture of $\text{CH}_4:\text{H}_2$, 1:4 (vol. ratio). The maximum benzene yield reached is around 7.35% and is reached at 3.95 h of MDA reaction. In spite of the improvement obtained with this activation, the relative effect is lower on the 6% (wt.) Mo/MCM-22 catalyst than on the 6% (wt.) Mo/HZSM-5 catalyst (Figure 50). The benzene yield obtained with this activation is slightly more stable, because it exhibits a 1.3-fold decrease in the average deactivation rate with respect to that activated using the standard procedure. Moreover, Figure 52.b shows that the highest accumulated benzene moles are reached by the 6% (wt.) Mo/MCM-22 catalyst activated using the “ $\text{CH}_4:\text{H}_2$ (1 h)” procedure, achieving a maximum of $0.01235 \text{ mol} \cdot \text{g}_{\text{cat}}^{-1}$ after 17 h on stream.

As with the case with the 6% Mo/HZSM-5 catalyst, these results show that the pre-carburization and pre-reduction of the 6% Mo/MCM-22 catalyst using a gas mixture of $\text{CH}_4:\text{H}_2$, 1:4 (vol. ratio) was favorable for the MDA performance since the Mo species became slightly more stable and active for MDA reaction [1-3].

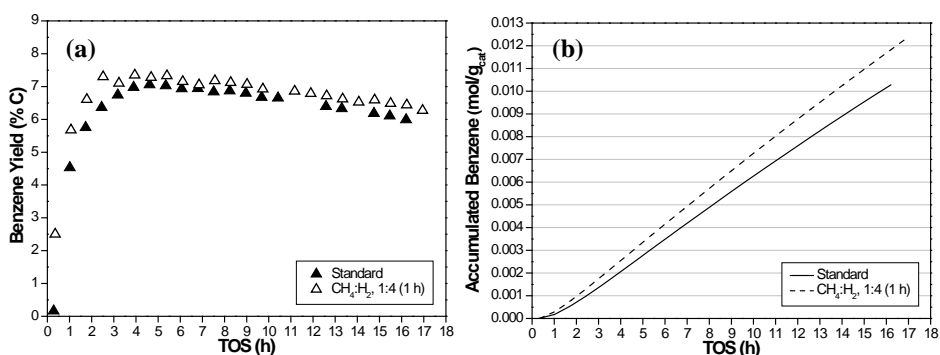


Figure 52. Effect of the 6% Mo/MCM-22 catalyst activation on the (a) benzene yield and (b) accumulated benzene moles versus the TOS at 700 °C.

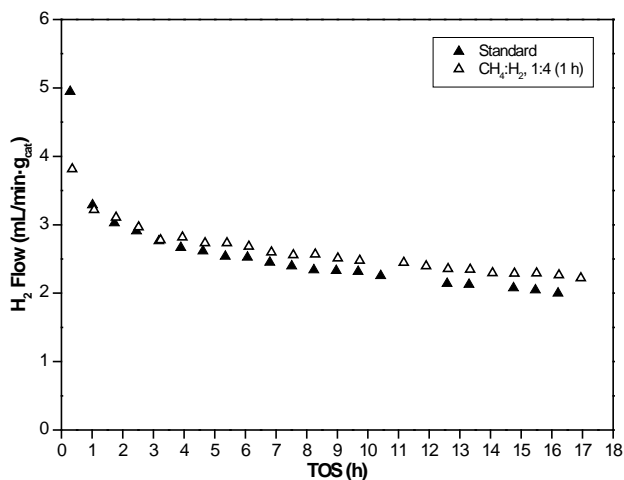


Figure 53. Effect of the 6%Mo/MCM-22 catalyst activation on the H₂ flow versus the TOS at 700 °C and 1.2 bar.

Figure 53 illustrates the effect of the 6%Mo/MCM-22 catalyst activation on the H₂ flow normalized per gram of catalyst. The H₂ flow is slightly higher for the catalyst activated using a gas mixture of CH₄:H₂, 1:4 (vol. ratio), which is in line with the benzene yield results.

Table 29 details the TGA results obtained for the spent 6%Mo/MCM-22 catalysts activated using different procedures. As seen, both the average coke formation rate and the amount of coke are much lower for the catalyst pre-carburized and pre-reduced using a gas mixture of CH₄:H₂, 1:4 (vol. ratio) during 1 h up to 700 °C and kept at this temperature for 2 h. Moreover, the amount of coke per accumulated benzene mole is almost halved for the catalyst activated using this gas mixture.

Table 29. TGA results of spent 6%Mo/MCM-22 catalysts activated with different procedures.

Code	TOS (h)	Average Coke Formation Rate (g·g _{cat} ⁻¹ ·h ⁻¹)	Amount of Coke (g·g _{cat} ⁻¹)	g·g _{cat} ⁻¹ ·mol _{benz.} ⁻¹
Standard	16.9	0.0078	0.1325	21
CH ₄ :H ₂ (1 h)	17.0	0.0046	0.0776	10

Figure 54 depicts the CO_x profiles obtained by TPO technique, in which two peaks can be differentiated, i.e., a peak at lower (peak 1) and a peak at higher temperature (peak 2).

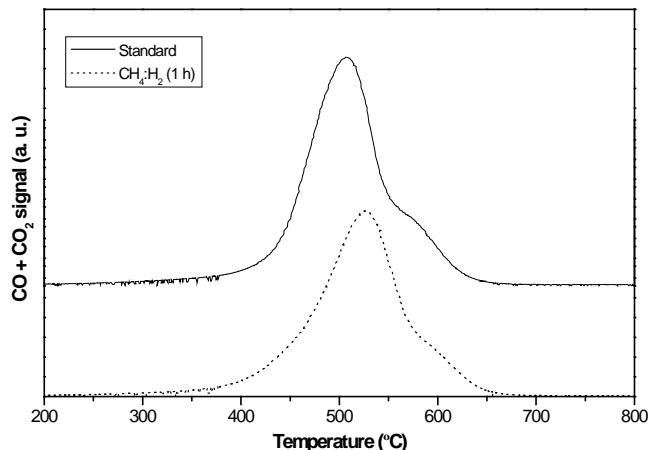


Figure 54. TPO profiles of carbon species over 6%Mo/MCM-22 catalysts activated with different procedures. Same scale of Y-axis.

As stated in the section 4.4., the amount of each type of coke was ascertained (Table 30). In the catalyst activated using the “ $\text{CH}_4:\text{H}_2$ (1 h)” method, the coke related to Mo species is reduced ca. 38.69% and the coke associated with Brønsted acid sites (aromatic-type carbon) is decreased roughly 59.07% with respect to the catalyst activated with the standard procedure. Concretely, the catalyst activated with the standard procedure is deactivated a bit faster than the catalyst activated using the “ $\text{CH}_4:\text{H}_2$ (1 h)” procedure, since the catalyst deactivation is presumably caused by the deposition of the aromatic-type coke on the Brønsted acid sites [7]. Therefore, the catalyst activation using the “ $\text{CH}_4:\text{H}_2$ (1 h)” method leads to a slightly better MDA performance.

The coke characteristics (particle size, morphology, etc.) may be different between both catalysts [8], since the temperature at maximum of both

peaks (Table 30) is slightly higher for the catalyst activated with the “CH₄:H₂ (1 h)” procedure than for the standard method.

Table 30. Results of the deconvoluted TPO profiles of carbon species over 6%Mo/MCM-22 catalysts activated with different procedures.

Code	Temperature at maximum (°C)		Percentage (%)		Amount of coke (g·g _{cat} ⁻¹)	
	Peak 1	Peak 2	Peak 1	Peak 2	Peak 1	Peak 2
Standard	503	587	82.52	17.48	0.1093	0.0232
CH ₄ :H ₂ (1 h)	521	612	87.78	12.22	0.0681	0.0095

5.3. Conclusions

The catalyst activation used is particularly relevant in the performance of the MDA reaction. The different activation procedures applied to the 6%Mo/HZSM-5 catalyst revealed that the catalyst activation can be positive or not. In particular, the pre-coking of the catalyst with 1.25% of 1,2,4-TMB for 4 h at 600 °C was detrimental for the MDA performance probably due to the higher formation of carbonaceous deposits that were obstructing the zeolite channels since the beginning of the experiment. However, the other two activation methods employed with this catalyst were beneficial for the MDA performance. Concretely, by using a gas mixture of CH₄:H₂, 1:4 (vol. ratio) during 1 h up to 700 °C and kept at this temperature for 2 h, the 6%Mo/HZSM-5 catalyst was pre-carburized and pre-reduced, obtaining the best performance on MDA reaction, that is to say, the highest benzene yield and stability throughout the time on stream. These results and those obtained by TGA verified that the Mo species formed during the catalyst activation with this gas mixture are more stable and active for MDA reaction [1-3]. The maximum benzene yield was around 6.21% reached at 3.23 h of MDA reaction, while for the catalyst activated with the standard procedure the maximum benzene yield

was 5.63% reached at 2.33 h on stream. In addition, by using this activation the benzene yield was more stable throughout the time on stream, showing a 2-fold decrease in the average deactivation rate with respect to the standard activation. Nevertheless, these results were slightly higher than those obtained using the same gas mixture during 4 h up to 700 °C and kept at this temperature for 2 h.

The best activation procedure found for the 6%Mo/HZSM-5 catalyst ($\text{CH}_4:\text{H}_2$, 1:4 (1 h)) was tested over the 6%Mo/MCM-22 catalyst, thereby resulting in the highest benzene yield over time. However, the magnitude of the improvement was lower in the 6%Mo/MCM-22 catalyst than in the 6%Mo/HZSM-5 catalyst, i.e., only a relative increase of 4% in the maximum benzene yield was reached. Moreover, with this activation the benzene yield was slightly more stable, showing a 1.3-fold decrease in the average deactivation rate with respect to the catalyst activated using the standard procedure.

In addition, by the TGA results it can be inferred that the 6%Mo/MCM-22 catalyst pre-carburized and pre-reduced using a gas mixture of $\text{CH}_4:\text{H}_2$, 1:4 (vol. ratio) accumulates lower amount of coke, nearly half, than the catalyst activated using the standard method. Furthermore, from TPO analysis, it can presumably be assumed that the catalyst activated with the standard method was deactivated faster than the catalyst activated using the “ $\text{CH}_4:\text{H}_2$ (1 h)” procedure since it presents more quantity of coke associated with the Brønsted acid sites of the zeolite (aromatic-type coke) [7].

5.4. References

- [1] H. Ma, Kojima, R., Kikuchi, S., Ichikawa, M., *Journal of Natural Gas Chemistry*, 14 (2005) 129-139.
- [2] H.M. Liu, W.J. Shen, X.H. Bao, Y.D. Xu, *Journal of Molecular Catalysis a-Chemical*, 244 (2006) 229-236.
- [3] H.M. Liu, X.H. Bao, Y.D. Xu, *Journal of Catalysis*, 239 (2006) 441-450.

- [4] R.W. Borry, Y.H. Kim, A. Huffsmith, J.A. Reimer, E. Iglesia, *Journal of Physical Chemistry B*, 103 (1999) 5787-5796.
- [5] F. Solymosi, A. Erdohelyi, A. Szoke, *Catalysis Letters*, 32 (1995) 43-53.
- [6] D.J. Wang, J.H. Lunsford, M.P. Rosynek, *Topics in Catalysis*, 3 (1996) 289-297.
- [7] D. Ma, Y.Y. Shu, M.J. Cheng, Y.D. Xu, X.H. Bao, *Journal of Catalysis*, 194 (2000) 105-114.
- [8] C.A. Querini, S.C. Fung, *Appl. Catal. A-Gen.*, 117 (1994) 53-74.

Chapter 6.

EFFECT OF THE SPACE VELOCITY ON MDA REACTION

6. Effect of the space velocity on MDA reaction

6.1. Effect of the 6% (wt.) Mo/HZSM-5 catalyst amount and the feed gas flow using a space velocity of $1500 \text{ mL}\cdot\text{h}^{-1}\cdot\text{g}_{\text{cat}}^{-1}$

Different catalysts amounts and feed gas flows were used over the 6% (wt.) Mo/HZSM-5 catalyst (detailed in section 3.6.1.2.4.2.). Briefly, two different experiments were carried out using 0.6 and 1.8 g of the 6% (wt.) Mo/HZSM-5 catalyst with 15 and 45 $\text{mL}\cdot\text{min}^{-1}$ of the feed gas flow ($\text{CH}_4:\text{N}_2$ in a volumetric ratio of 9.5:0.5), respectively. The catalyst was prepared using the HZSM-5 zeolite (CBV3024E) impregnated with a 6% (wt.) of Mo. Since the reactor geometry was maintained, the length of the catalyst bed was varied.

Table 31 summarizes the selectivity to main products after 9 h on stream at 700 °C, 1.2 bar and $1500 \text{ mL}\cdot\text{h}^{-1}\cdot\text{g}_{\text{cat}}^{-1}$. The lowest coke selectivity is achieved using 0.6 g of the catalyst and 15 $\text{mL}\cdot\text{min}^{-1}$ of the feed gas flow, while the naphthalene selectivity using these conditions is the highest obtained, almost the double. However, the benzene, toluene and C_2 selectivities are very similar for both experiments.

Table 31. Effect of the 6%Mo/HZSM-5 catalyst amount and the feed gas flow on the selectivity to main products after 9 h on stream at $1500 \text{ mL}\cdot\text{h}^{-1}\cdot\text{g}_{\text{cat}}^{-1}$.

Conditions	Selectivity (% C)				
	C_6H_6	C_2	C_7H_8	C_{10}H_8	Coke
0.6 g, 15 mL/min feed	67.15	7.12	5.03	16.44	4.25
1.8 g, 45 mL/min feed	67.14	7.21	5.08	8.37	12.20

In Figure 55 the methane conversion and the aromatics yield are depicted versus the time on stream. In both experiments the results obtained are very similar, thus indicating that the external diffusion effects appears to be insignificant [1, 2].

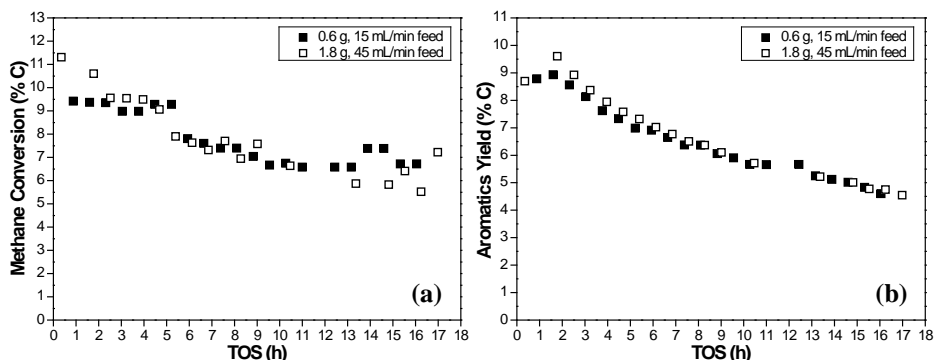


Figure 55. Effect of the 6%Mo/HZSM-5 catalyst amount and the feed gas flow on the (a) methane conversion and (b) aromatics yield versus the TOS.

However, by focusing on each aromatic hydrocarbon yield separately, the benzene yield (Figure 56.a) using higher feed gas flow at constant space velocity is higher than for lower feed gas flow, as with the toluene yield (Figure 56.c). On the contrary, the naphthalene yield (Figure 56.d) achieved using higher feed gas flow at constant space velocity is lower than using lower feed gas flow. Among these aromatic hydrocarbons, the benzene is the most interesting product, therefore these results indicate that the MDA performance is improved using higher feed gas flow rates at constant space velocity, being this space velocity $1500 \text{ mL}\cdot\text{h}^{-1}\cdot\text{g}_{\text{cat}}^{-1}$ [3]. These results may be related to thermo-fluid dynamic effects of this complex reaction process. Hence, the mass transfer effects from bulk gas phase to external surface of the catalyst may be negligible using these reaction conditions.

Nevertheless, the benzene yield obtained is slightly more stable using lower feed gas flow at constant space velocity, because it shows a 1.5-fold

decrease in the average deactivation rate, which is associated with the lower coke deposition rate. Moreover, the benzene yield (Figure 56.b) is also higher for almost the whole conversion range for the experiment carried out using higher gas flow rates.

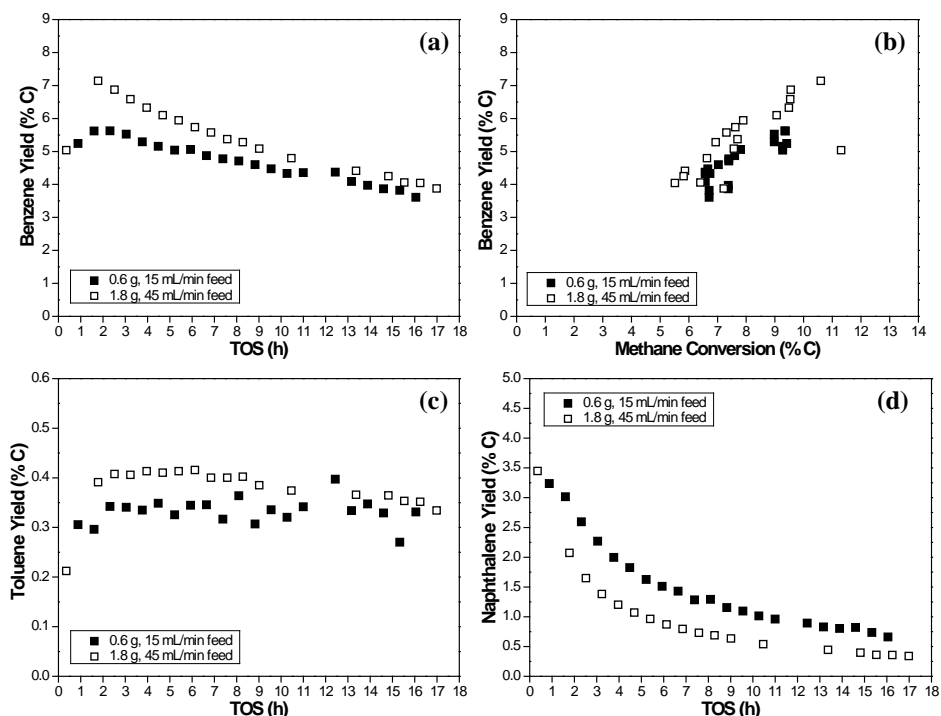


Figure 56. Effect of the 6%Mo/HZSM-5 catalyst amount and the feed gas flow on the (a) benzene yield versus the TOS, (b) benzene yield versus the methane conversion, (c) toluene and (d) naphthalene yields versus the TOS at 700 °C.

Table 32 details the TGA results obtained for the spent catalysts. Both the amount of coke and the average coke formation rate are lower using 0.6 g of catalyst and 15 mL·min⁻¹ of the feed gas. However, the amount of coke (g·g_{cat}⁻¹) per accumulated benzene mole is almost three times higher using the lower feed gas flow. These TGA results are in agreement with the previous remark that the benzene yield obtained with 0.6 g of catalyst and 15 mL·min⁻¹ of the feed gas mixture is more stable, that is, its decay of catalytic activity is slower.

Table 32. TGA results of spent 6%Mo/HZSM-5 catalysts.

Conditions	TOS (h)	Average Coke Formation Rate ($\text{g} \cdot \text{g}_{\text{cat}}^{-1} \cdot \text{h}^{-1}$)	Amount of Coke ($\text{g} \cdot \text{g}_{\text{cat}}^{-1}$)	$\text{g} \cdot \text{g}_{\text{cat}}^{-1} \cdot \text{mol}_{\text{benz.}}^{-1}$
0.6 g, 15 mL/min	16.0	0.0031	0.049	11
1.8 g, 45 mL/min	17.0	0.0040	0.068	4

6.2. Effect of the space velocity on MDA reaction using the 6% (wt.) Mo/MCM-22 catalyst

6.2.1. Effect of the space velocity using the standard activation

In these experiments the catalysts were not pre-carburized and pre-reduced before the MDA reaction. The experiment with a space velocity of $1500 \text{ mL} \cdot \text{h}^{-1} \cdot \text{g}_{\text{cat}}^{-1}$ ($2.4 \text{ s} \cdot \text{g}_{\text{cat}} \cdot \text{mL}^{-1}$) was carried out according to the procedure described in the section 3.6.1.1., and the other with a space velocity of $835 \text{ mL} \cdot \text{h}^{-1} \cdot \text{g}_{\text{cat}}^{-1}$ ($4.3 \text{ s} \cdot \text{g}_{\text{cat}} \cdot \text{mL}^{-1}$) was done according to the procedure detailed in the section 3.6.1.2.4.1. In both experiments the amount of catalyst was constant and the feed gas flow was varied. The catalyst was prepared using the MCM-22 zeolite (Si/Al=15) impregnated with a 6% (wt.) of Mo.

Table 33 summarizes the methane conversion and the selectivity to main products after 9 h on stream at 700 °C and 1.2 bar. The lowest methane conversion and coke selectivity are obtained using a space velocity of $1500 \text{ mL} \cdot \text{h}^{-1} \cdot \text{g}_{\text{cat}}^{-1}$, while the highest C₂ and aromatics selectivities are achieved with this space velocity. In agreement with Shu et al. [3], it can be said that at lower space velocity (longer contact time) the coke deposition is favored by the condensation of the aromatic hydrocarbons.

Table 33. Effect of the space velocity on the methane conversion and the selectivity to main products after 9 h on stream of 6%Mo/HZSM-5 catalyst.

Space Velocity (mL/h·g _{cat})	Methane Conversion (% C)	Selectivity (% C)				
		C ₆ H ₆	C ₂	C ₇ H ₈	C ₁₀ H ₈	Coke
835	10.03	69.82	2.43	2.22	4.44	21.09
1500	8.12	82.12	3.28	3.68	5.26	5.66

Moreover, in Figure 57 the benzene yield for both space velocities is shown. As seen, the benzene yield reached using a space velocity of 1500 mL·h⁻¹·g_{cat}⁻¹ is higher during the first 6 h on stream, then this is very similar for both space velocities during 3 h. However, after 9 h on stream the benzene yield achieved using 835 mL·h⁻¹·g_{cat}⁻¹ is higher and more stable than with 1500 mL·h⁻¹·g_{cat}⁻¹. It should be pointed out that with a space velocity of 835 mL·h⁻¹·g_{cat}⁻¹ the maximum benzene yield takes about 8 h more to reach. In particular, the maximum benzene yield obtained is around 7.35% (at 12.65 h) and 7.05% (at 4.62 h) using a space velocity of 835 and 1500 mL·h⁻¹·g_{cat}⁻¹, respectively.

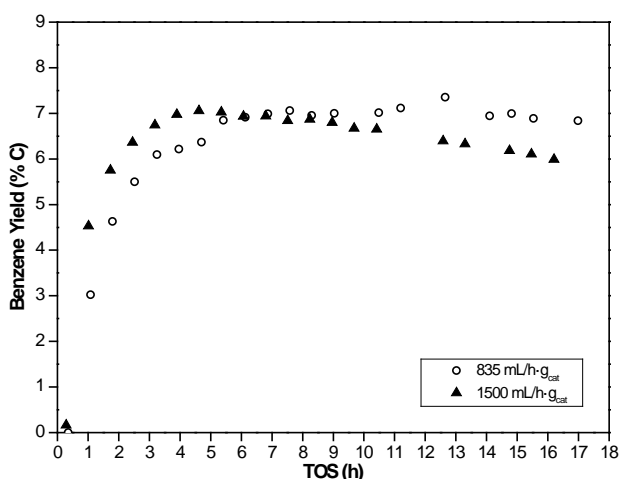


Figure 57. Effect of the space velocity on the benzene yield versus the TOS of the 6%Mo/MCM-22 catalyst at 700 °C and 1.2 bar (standard activation).

However, the accumulated benzene moles normalized per gram of catalyst (Figure 58.a) obtained with a space velocity of $1500 \text{ mL}\cdot\text{h}^{-1}\cdot\text{g}_{\text{cat}}^{-1}$ are higher than those achieved using $835 \text{ mL}\cdot\text{h}^{-1}\cdot\text{g}_{\text{cat}}^{-1}$ over time, being almost the double after 16 h on stream, 0.0103 and $0.0061 \text{ mol}\cdot\text{g}_{\text{cat}}^{-1}$, respectively. This is attributed to the higher feed gas flow used for $1500 \text{ mL}\cdot\text{h}^{-1}\cdot\text{g}_{\text{cat}}^{-1}$. Regarding stability, it appears that the decay rate is directly related to the methane conversion magnitude and, therefore, the coke formation rate (for a given catalyst). Figure 58.b depicts the H_2 flow normalized per gram of catalyst obtained during the MDA reaction. As can be observed, the H_2 flow reached with a space velocity of $1500 \text{ mL}\cdot\text{h}^{-1}\cdot\text{g}_{\text{cat}}^{-1}$ is higher than that obtained with $835 \text{ mL}\cdot\text{h}^{-1}\cdot\text{g}_{\text{cat}}^{-1}$ throughout the time on stream, as expected from the higher feed flow used for $1500 \text{ mL}\cdot\text{h}^{-1}\cdot\text{g}_{\text{cat}}^{-1}$.

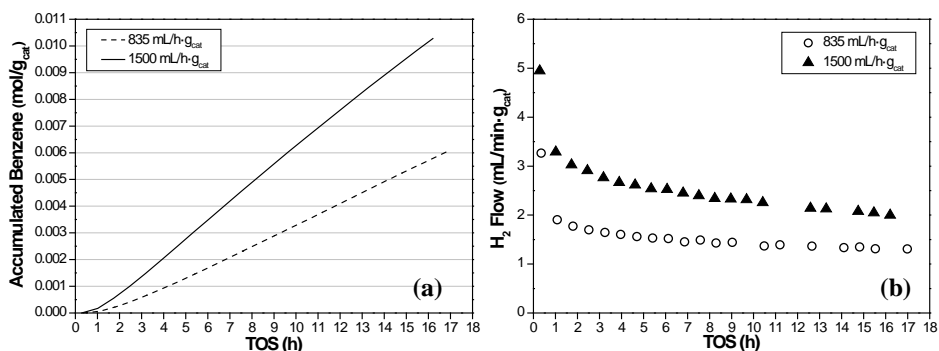


Figure 58. Effect of the space velocity on the (a) accumulated benzene moles and (b) H_2 flow versus the TOS of the 6%Mo/MCM-22 catalyst at 700°C (standard activation).

TGA results are detailed in Table 34, both the average coke formation rate and the amount of coke are much lower using a space velocity of $835 \text{ mL}\cdot\text{h}^{-1}\cdot\text{g}_{\text{cat}}^{-1}$, thus confirming that with this space velocity the catalytic activity is slowed down. Nevertheless, by focusing on the amount of coke ($\text{g}\cdot\text{g}_{\text{cat}}^{-1}$) per accumulated benzene mole there is barely difference between them, being slightly lower for the experiment performed at $1500 \text{ mL}\cdot\text{h}^{-1}\cdot\text{g}_{\text{cat}}^{-1}$.

Table 34. TGA results of spent 6%Mo/MCM-22 catalysts (standard activation) using different space velocities.

Space Velocity ($\text{mL}\cdot\text{h}^{-1}\cdot\text{g}_{\text{cat}}^{-1}$)	TOS (h)	Average Coke Formation Rate ($\text{g}\cdot\text{g}_{\text{cat}}^{-1}\cdot\text{h}^{-1}$)	Amount of Coke ($\text{g}\cdot\text{g}_{\text{cat}}^{-1}$)	$\text{g}\cdot\text{g}_{\text{cat}}^{-1}\cdot\text{mol}_{\text{benz.}}^{-1}$
835	17	0.0047	0.080	22
1500	17	0.0078	0.132	21

6.2.2. Effect of the space velocity using the new activation

In this section the catalysts were pre-treated in situ in a flow of Ar ($50 \text{ mL}\cdot\text{min}^{-1}$) from room temperature up to $480 \text{ }^\circ\text{C}$ ($\sim 2 \text{ h}$) and then, the catalysts were pre-carburized and pre-reduced using a gas mixture of $\text{CH}_4:\text{H}_2$, 1:4 (vol. ratio) up to $700 \text{ }^\circ\text{C}$ during 1 h, and kept at this temperature for 2 h. In particular, the experiment with a space velocity of $1500 \text{ mL}\cdot\text{h}^{-1}\cdot\text{g}_{\text{cat}}^{-1}$ was carried out according to the procedure described in the section 3.6.2.2.1., and the others with space velocities of 750 and $3000 \text{ mL}\cdot\text{h}^{-1}\cdot\text{g}_{\text{cat}}^{-1}$ were done according to the procedure detailed in the section 3.6.2.2.1. The catalyst was prepared using the MCM-22 zeolite (Si/Al=15) impregnated with a 6% (wt.) of Mo.

In Figure 59 the methane conversion and the H_2 flow normalized per gram of 6%Mo/MCM-22 catalyst obtained using different space velocities are depicted. The methane conversion (Figure 59.a) is higher over time for the experiments carried out at 750 and $1500 \text{ mL}\cdot\text{h}^{-1}\cdot\text{g}_{\text{cat}}^{-1}$, although for the former it is slightly scattered. Moreover, the highest H_2 flow (Figure 59.b) is achieved with $3000 \text{ mL}\cdot\text{h}^{-1}\cdot\text{g}_{\text{cat}}^{-1}$ and the lowest with $750 \text{ mL}\cdot\text{h}^{-1}\cdot\text{g}_{\text{cat}}^{-1}$. This is ascribed to the higher feed gas flow used and the higher ethylene (throughout the time on stream) and benzene (first 3 h on stream) selectivities obtained using

$3000 \text{ mL}\cdot\text{h}^{-1}\cdot\text{g}_{\text{cat}}^{-1}$. In this case, the trend observed between both parameters is rather different.

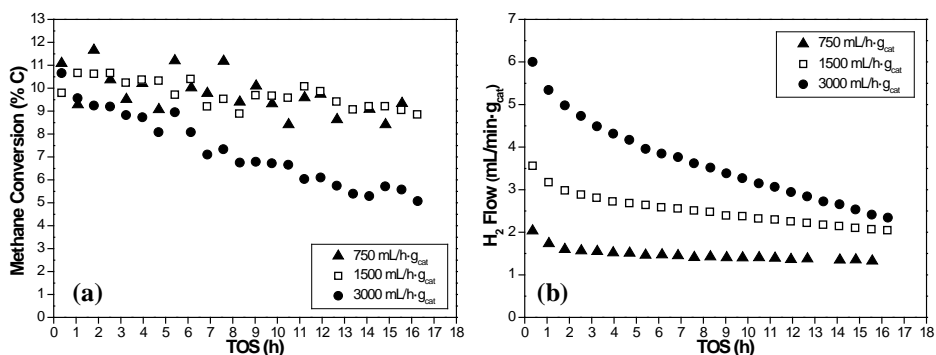


Figure 59. Effect of the space velocity on the (a) methane conversion and (b) H_2 flow versus the TOS of the 6%Mo/MCM-22 catalyst (new activation) at 700 °C.

Table 35 shows that the toluene and naphthalene selectivities increase as the space velocity decreases. However, the lowest benzene and C_2 selectivities are obtained using $1500 \text{ mL}\cdot\text{h}^{-1}\cdot\text{g}_{\text{cat}}^{-1}$, contrary to the coke selectivity.

Table 35. Effect of the space velocity on the selectivity to main products after 9 h on stream of 6%Mo/MCM-22 catalyst.

Space Velocity ($\text{mL}/\text{h}\cdot\text{g}_{\text{cat}}$)	Selectivity (% C)				
	C_6H_6	C_2	C_7H_8	C_{10}H_8	Coke
750	71.17	3.82	3.23	6.07	15.71
1500	69.83	2.13	2.83	3.78	21.43
3000	73.01	4.21	1.42	3.60	17.76

The benzene yield (Figure 60.a) obtained with a space velocity of $3000 \text{ mL}\cdot\text{h}^{-1}\cdot\text{g}_{\text{cat}}^{-1}$ is the lowest and less stable over time. Furthermore, during the first 6 h of MDA reaction the benzene yield reached using $1500 \text{ mL}\cdot\text{h}^{-1}\cdot\text{g}_{\text{cat}}^{-1}$ is higher than with $750 \text{ mL}\cdot\text{h}^{-1}\cdot\text{g}_{\text{cat}}^{-1}$, and then, this is very similar to both space velocities for 3 h. While after 9 h on stream, the benzene yield achieved using

750 mL·h⁻¹·g_{cat}⁻¹ is higher and more stable than with 1500 mL·h⁻¹·g_{cat}⁻¹. In particular, the benzene yield for 750 mL·h⁻¹·g_{cat}⁻¹ exhibits a 2.9-fold and 5.5-fold decrease in the average deactivation rate with respect to the experiments carried out at 1500 and 3000 mL·h⁻¹·g_{cat}⁻¹, respectively. The maximum benzene yields reached are 7.36% (at 11.22 h), 7.25% (at 4.68 h) and 6.46% (at 2.52 h) using 750, 1500 and 3000 mL·h⁻¹·g_{cat}⁻¹, respectively. It should be pointed out that with a space velocity of 750 mL·h⁻¹·g_{cat}⁻¹ the maximum benzene yield takes about 6.50 h more to reach. This behavior is very similar to that observed previously (Figure 57), but it is slightly faster due to the catalyst activation and the higher catalyst amount and feed gas flow used. However, the accumulated benzene moles normalized per gram of catalyst (Figure 60.b) increases as the space velocity increases, as expected, being 0.0055, 0.0115 and 0.0166 mol·g_{cat}⁻¹ for 750, 1500 and 3000 mL·h⁻¹·g_{cat}⁻¹, respectively.

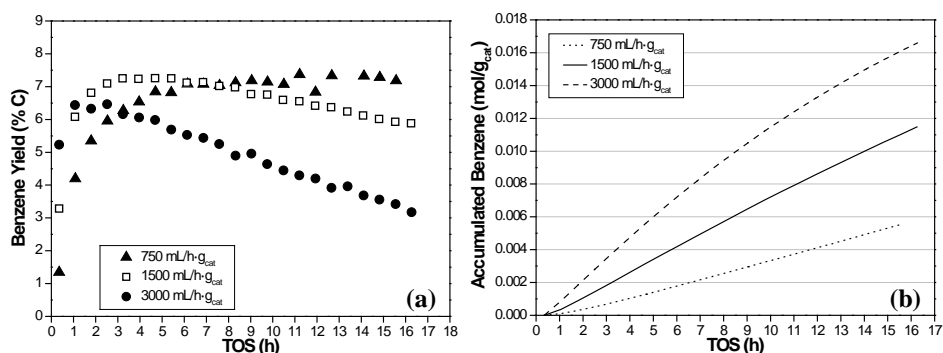


Figure 60. Effect of the space velocity on the (a) benzene yield and (b) accumulated benzene moles versus the TOS of the 6%Mo/MCM-22 catalyst (new activation) at 700 °C.

The effect of the space velocity on the catalytic performance after 2.50 h on stream at 700 °C and 1.2 bar for the 6 %Mo/MCM-22 catalyst is shown in Figure 61. This specific time corresponds to the half of TOS at which the maximum benzene yield was reached for the experiment run at 1500 mL·h⁻¹·g_{cat}⁻¹[3]. The highest methane conversion and yields of benzene

and toluene are obtained using $1500 \text{ mL}\cdot\text{h}^{-1}\cdot\text{g}_{\text{cat}}^{-1}$, as with the lowest C_2 yield. Therefore the oligomerization of the C_2 species appears more effective on the Brønsted acid sites at this space velocity. The lowest methane conversion is obtained at $3000 \text{ mL}\cdot\text{h}^{-1}\cdot\text{g}_{\text{cat}}^{-1}$, thus suggesting that at higher space velocities the methane might not have enough time to react with the active sites of the catalyst. In addition, the lowest benzene yield is obtained at $750 \text{ mL}\cdot\text{h}^{-1}\cdot\text{g}_{\text{cat}}^{-1}$, whereas using this space velocity the highest coke, naphthalene and C_2 yields are obtained. This indicates that at lower space velocities the aromatics condensation is facilitated and it helps out with the rising of the coke deposition [3].

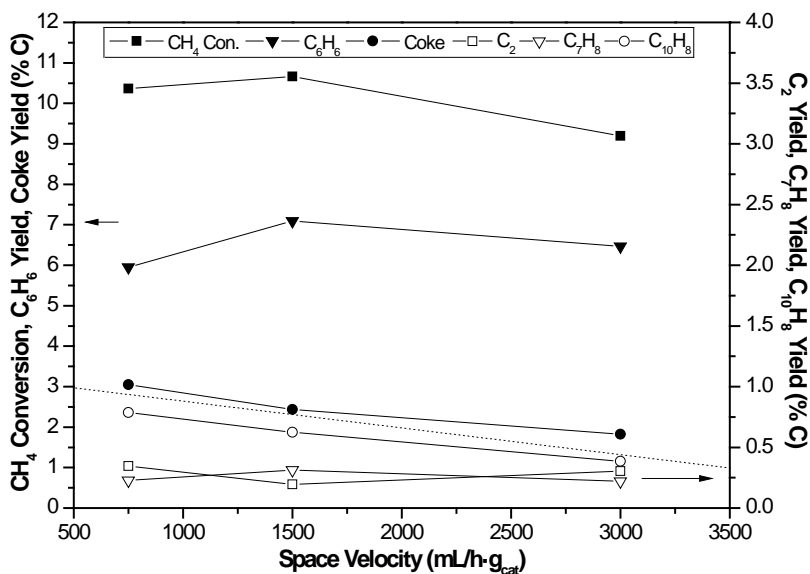


Figure 61. Effect of the space velocity on the catalytic performance after 2.50 h of MDA reaction.

Table 36 details the TGA results obtained for the spent catalysts at different space velocities. The space velocities that are used in the three experiments are listed according to the average coke formation rate and amount of coke in descending order: 1500 , 3000 and $750 \text{ mL}\cdot\text{h}^{-1}\cdot\text{g}_{\text{cat}}^{-1}$. However, these

TGA results and the benzene yield obtained (Figure 60.a) support that with a space velocity of $750 \text{ mL}\cdot\text{h}^{-1}\cdot\text{g}_{\text{cat}}^{-1}$ the catalytic activity is slowed down. Additionally, these point out to the conclusion that with a space velocity of $3000 \text{ mL}\cdot\text{h}^{-1}\cdot\text{g}_{\text{cat}}^{-1}$ the decay of the catalytic activity is not merely due to the accumulation of coke on the catalyst, but this may be ascribed to other thermo-fluid dynamic factors, such as, the nature of coke deposits and the detrimental location of these deposits which may be blocking the access to the zeolite channels. Nonetheless, it can be said that using $750 \text{ mL}\cdot\text{h}^{-1}\cdot\text{g}_{\text{cat}}^{-1}$ the highest amount of coke ($\text{g}\cdot\text{g}_{\text{cat}}^{-1}$) per accumulated benzene mole is obtained, whereas it is almost halved for 1500 and 3000 $\text{mL}\cdot\text{h}^{-1}\cdot\text{g}_{\text{cat}}^{-1}$, being slightly lower for the experiment performed using the former.

Table 36. TGA results of spent 6%Mo/MCM-22 catalysts (new activation) using different space velocities.

Space Velocity ($\text{mL}\cdot\text{h}^{-1}\cdot\text{g}_{\text{cat}}^{-1}$)	TOS (h)	Average Coke Formation Rate ($\text{g}\cdot\text{g}_{\text{cat}}^{-1}\cdot\text{h}^{-1}$)	Amount of Coke ($\text{g}\cdot\text{g}_{\text{cat}}^{-1}$)	$\text{g}\cdot\text{g}_{\text{cat}}^{-1}\cdot\text{mol}_{\text{benz}}^{-1}$
750	16.3	0.0060	0.098	11
1500	16.3	0.0072	0.117	6
3000	16.3	0.0065	0.105	7

The CO_x ($\text{CO} + \text{CO}_2$) signals (from TPO technique) versus the temperature are illustrated in Figure 62. By focusing on the TPO results (Table 37), it can be said that on the catalyst used at $750 \text{ mL}\cdot\text{h}^{-1}\cdot\text{g}_{\text{cat}}^{-1}$, the coke associated with Mo species and the coke related to Brønsted acid sites (aromatic-type carbon) are ca. 13.93% and around 17.64% lower than on the catalyst tested at $1500 \text{ mL}\cdot\text{h}^{-1}\cdot\text{g}_{\text{cat}}^{-1}$, respectively. Therefore, the TGA and TPO results confirm that with a space velocity of $750 \text{ mL}\cdot\text{h}^{-1}\cdot\text{g}_{\text{cat}}^{-1}$ the catalytic activity is slowed down. Moreover, on the catalyst tested at $3000 \text{ mL}\cdot\text{h}^{-1}\cdot\text{g}_{\text{cat}}^{-1}$ the coke related to Mo species is reduced roughly 8.22% and the coke associated with Brønsted acid sites (aromatic-type carbon) is decreased ca. 18.75% with respect to the catalyst used at $1500 \text{ mL}\cdot\text{h}^{-1}\cdot\text{g}_{\text{cat}}^{-1}$. These TPO

results verify that the worse MDA performance obtained using a space velocity of

$3000 \text{ mL}\cdot\text{h}^{-1}\cdot\text{g}_{\text{cat}}^{-1}$ is not due to the accumulation of coke on the catalyst. But these reinforced the hypothesis abovementioned, that is to say, the nature of coke may be slightly different for the catalyst tested at $3000 \text{ mL}\cdot\text{h}^{-1}\cdot\text{g}_{\text{cat}}^{-1}$, due to the difference among the temperature at maximum of both peaks (Table 37) for this catalyst with respect to the other catalysts. While, for the catalysts tested at 750 and $1500 \text{ mL}\cdot\text{h}^{-1}\cdot\text{g}_{\text{cat}}^{-1}$ the temperature at maximum of both peaks is almost alike, being the coke characteristics (particle size, morphology, etc.) for them likely very similar [4].

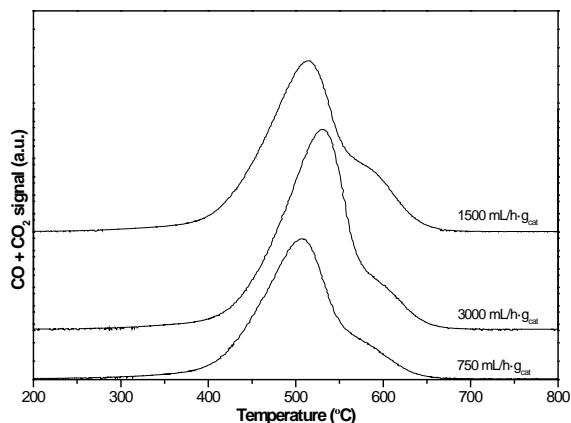


Figure 62. TPO profiles of carbon species over 6%Mo/MCM-22 catalysts tested using different space velocities (new activation). Same scale of Y-axis.

Table 37. Results of the deconvoluted TPO profiles of carbon species over 6%Mo/MCM-22 catalysts tested at different space velocities (new activation).

Space Velocity ($\text{mL}\cdot\text{h}^{-1}\cdot\text{g}_{\text{cat}}^{-1}$)	Temperature at maximum ($^{\circ}\text{C}$)		Percentage (%)		Amount of coke ($\text{g}\cdot\text{g}_{\text{cat}}^{-1}$)	
	Peak 1	Peak 2	Peak 1	Peak 2	Peak 1	Peak 2
750	501	597	86.31	13.69	0.0842	0.0133
1500	508	601	86.10	13.90	0.1004	0.0162
3000	522	615	87.50	12.50	0.0922	0.0132

6.3. Conclusions

The space velocity employed has a great influence on the performance of the MDA reaction. Furthermore, even maintaining the same space velocity ($1500 \text{ mL}\cdot\text{h}^{-1}\cdot\text{g}_{\text{cat}}^{-1}$) but changing the catalyst amount (in the range 0.6-1.8 g) and the feed gas flow (in the range $15\text{-}45 \text{ mL}\cdot\text{min}^{-1}$) the results obtained in the MDA reaction are slightly affected. Although the methane conversion and the aromatics yield are very similar over time, the benzene and toluene yields are higher for the higher catalyst amount and feed gas flow, whereas the naphthalene yield is lower. Thus indicating that at $1500 \text{ mL}\cdot\text{h}^{-1}\cdot\text{g}_{\text{cat}}^{-1}$ the best MDA performance is reached using 1.8 g of catalyst and $45 \text{ mL}\cdot\text{min}^{-1}$ of feed gas flow. This may be ascribed to thermo-fluid dynamic effects instead of external diffusion effects. However, with the higher catalyst amount and feed gas flow the benzene yield is slightly less stable, but the amount of coke per accumulated benzene mole is almost three times lower.

Moreover, after testing different space velocities over the 6%Mo/MCM-22 catalyst activated using the standard and the new procedure, the results obtained are in concordance. The highest methane conversion and benzene and toluene yields, and the lowest C_2 yield are achieved for the experiment carried out at $1500 \text{ mL}\cdot\text{h}^{-1}\cdot\text{g}_{\text{cat}}^{-1}$, after 2.5 h on stream. This implies that using $1500 \text{ mL}\cdot\text{h}^{-1}\cdot\text{g}_{\text{cat}}^{-1}$ the C_2 species may be oligomerized in a more efficient way on the Brønsted acid sites. Furthermore, at $3000 \text{ mL}\cdot\text{h}^{-1}\cdot\text{g}_{\text{cat}}^{-1}$, $700 \text{ }^\circ\text{C}$ and 1.2 bar appears that the methane conversion decay is faster than at 750 and $1500 \text{ mL}\cdot\text{h}^{-1}\cdot\text{g}_{\text{cat}}^{-1}$, due to the lower interaction between the methane and the active sites of the catalyst. While at $750 \text{ mL}\cdot\text{h}^{-1}\cdot\text{g}_{\text{cat}}^{-1}$ the aromatic hydrocarbons condensation is easier and hence the carbonaceous deposits increase.

Additionally, the use of space velocities lower than $1500 \text{ mL}\cdot\text{h}^{-1}\cdot\text{g}_{\text{cat}}^{-1}$, such as 750 and $835 \text{ mL}\cdot\text{h}^{-1}\cdot\text{g}_{\text{cat}}^{-1}$, involves a slowdown in the catalytic activity since the maximum benzene yields take about 6.5 and 8 h more to reach,

respectively. In this case, the lower time required by the experiment with lower space velocity ($750 \text{ mL}\cdot\text{h}^{-1}\cdot\text{g}_{\text{cat}}^{-1}$) may be directly related to the new catalyst activation. These results are in agreement with those of TGA and TPO for these catalysts.

6.4. References

- [1] G. Emig, R. Dittmeyer, Handbook of Heterogeneous Catalysis, in, 1997, pp. 1235.
- [2] E. Peris, Estudio de catalizadores microporosos Mo/Zeolita en la reacción de deshidroaromatización de metano, in: Instituto de Tecnología Química (CSIC), Universidad Politécnica de Valencia, Valencia, 2015, pp. Chapter 4; Page 119.
- [3] Y.Y. Shu, D. Ma, L.Y. Xu, Y.D. Xu, X.H. Bao, Catalysis Letters, 70 (2000) 67-73.
- [4] C.A. Querini, S.C. Fung, Appl. Catal. A-Gen., 117 (1994) 53-74.

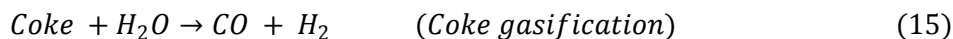
Chapter 7.

EFFECT OF THE CO-FEEDING GAS ON MDA REACTION

7. Effect of the co-feeding gas on MDA reaction

7.1. Effect of co-feeding H₂O

H₂O has been added to methane feed aiming to improve the stability of Mo/zeolite catalysts on MDA reaction, via the H₂O reaction with the carbonaceous deposits (reforming reaction) [1, 2]. In particular, as abovementioned in the section 2.5.3., H₂O vapor concentration that results beneficial for MDA reaction should be lower than 1.7% for the 6%Mo/HZSM-5 catalyst.



7.1.1. Thermodynamic study of co-feeding H₂O

A preliminary thermodynamic study on the chemical equilibrium of the MDA reaction with co-feeding H₂O was done in order to highlight the thermodynamic limitations of this complex process. The thermodynamic equilibrium was calculated using the databases of Aspen Plus V8.8, taking into account the different species that could be formed, i. e., methane, H₂O, H₂, ethylene, ethane, benzene, toluene, naphthalene, CO and CO₂, at 700 °C and 1 bar. The coke formation was not considered since if it was included in the thermodynamic calculations, the coke was the main and almost unique product of the MDA reaction, thus indicating that the coke inhibition by

kinetic control is crucial. The results shown in this study are in agreement with those obtained by Bijani et al. [3].

In Figure 63 the equilibrium methane conversion is depicted versus the H₂O vapor concentration in the methane feed. The equilibrium methane conversion without co-feeding H₂O is roughly 12.55%, but this decreases as H₂O vapor concentration in the feed increases up to 7%, reaching around 9.23% of methane conversion. However, from this H₂O vapor concentration the methane conversion begins to rise, achieving ca. 19.81% for a H₂O vapor concentration of 20%.

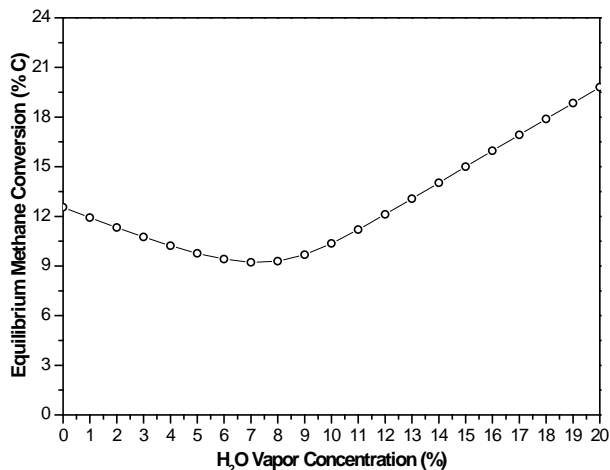


Figure 63. Effect of the H₂O vapor concentration in the methane feed on the equilibrium methane conversion at 700 °C and 1 bar.

Figure 64 displays the equilibrium selectivities to aromatics (benzene, toluene and naphthalene), C₂ hydrocarbons, CO and CO₂ versus the H₂O vapor concentration in the feed. Regarding the selectivities to aromatics, these decrease as the H₂O vapor concentration increases, being the naphthalene selectivity the highest up to 3% of H₂O co-fed, from which the benzene selectivity is the highest. Further, the selectivities to benzene, naphthalene and toluene are lower than 1% for 11, 9 and 6% of H₂O vapor concentration in the

feed, respectively. On the contrary, the equilibrium selectivities to ethylene and ethane slightly increase as the H₂O vapor concentration increases up to 6 and 7%, respectively, from which both selectivities decrease. Additionally, the equilibrium selectivities to CO and CO₂ increase as the H₂O vapor concentration increases. It should be pointed out that the CO selectivity is slightly reduced from 19% of H₂O co-fed, thus rising the formation of CO₂ following the water gas shift (WGS) reaction shown in Equation 57 [3]. Moreover, the increase in the H₂O vapor concentration in the feed also leads to an increment in the H₂ formed (not shown).

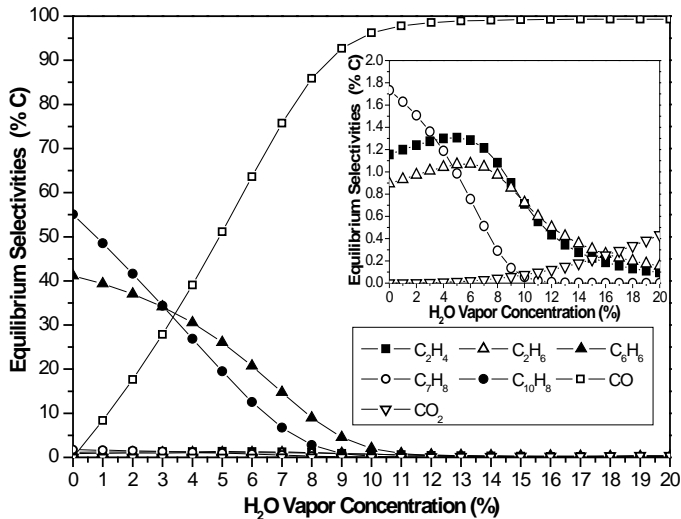


Figure 64. Effect of the H₂O vapor concentration in the methane feed on the equilibrium selectivities to aromatics, C₂, CO and CO₂ at 700 °C and 1 bar. Inset figure shows an enlarged version of the C₂, toluene and CO₂ selectivities.

Therefore, it can be said that thermodynamically the co-feeding of H₂O, at 700 °C and 1 bar, benefits the methane reforming reaction (Equation 13), the coke gasification (Equation 15) and the WGS reaction (Equation 57) at the

expense of the MDA reaction. In particular, the WGS reaction is mainly favored at high H₂O vapor concentrations in the feed.

7.1.2. Effect of co-feeding H₂O over 6% (wt.) Mo/HZSM-5 catalyst on MDA reaction

In order to perform these experiments, saturated aqueous solutions of potassium carbonate and potassium acetate were used. The experiments were carried out according to the procedure described in the section 3.6.1.2.1.2. with the standard activation of the catalysts. In these the feed gas mixture was introduced in the bubbler with both saturated salt solutions separately after 1 h of MDA reaction in dry conditions, to achieve a H₂O vapor concentration of 1.08% and 0.9%, respectively. The experiments without H₂O were carried out according to the procedure described in the section 3.6.1.1. The catalysts were prepared using the HZSM-5 zeolite (CBV3024E, Si/Al=15) impregnated with a 6% (wt.) of Mo.

In the following table the methane conversion and the selectivity to main products after 9 h on stream, at 700 °C, 1.2 bar and 1500 mL·h⁻¹·g_{cat}⁻¹, are shown. The methane conversion and the CO selectivity increase as H₂O co-fed increases, contrary to the aromatics selectivities. Carbon monoxide (CO) was obtained due to the methane reforming reaction and coke gasification (Equations 13, 14 and 15). The CO selectivity is higher for higher H₂O vapor concentration, which is very closely related to the lower coke selectivity obtained by adding 1.08% of H₂O than that obtained by the addition of 0.9%. These results are consistent with the previous thermodynamic study shown in section 7.1.1., except for the methane conversion and with the difference that the benzene is the major product among the aromatics instead of the naphthalene due to the shape selectivity of the catalyst. Moreover, the CO selectivity reached after 9 h on stream by adding 1.08% of H₂O surpass that

exhibited in Figure 64 (thermodynamic study). The higher methane conversion and CO selectivity obtained experimentally may be ascribed to the presence of coke deposits on the catalyst, which react with the H₂O co-fed (Equation 15) forming CO and H₂, since the CO resulting of this reaction has not been included in the thermodynamic calculations. What is more, the C₂ hydrocarbons selectivity is lower for higher H₂O vapor concentration, which is in disagreement with the thermodynamic results, although the C₂ selectivities obtained experimentally are higher than those shown in Figure 64.

Table 38. Effect of co-feeding H₂O on the methane conversion and the selectivity to main products after 9 h on stream of 6%Mo/HZSM-5 catalyst.

H ₂ O co-fed (%)	Methane Conversion (% C)	Selectivity (% C)					
		C ₆ H ₆	C ₂	C ₇ H ₈	C ₁₀ H ₈	Coke	CO
0	6.66	67.16	7.12	5.03	16.44	4.25	0.00
0.90	7.17	47.43	4.30	2.96	12.09	28.53	4.69
1.08	8.03	35.91	3.74	1.92	8.02	18.50	31.91

Figure 65 illustrates the effect of the H₂O addition to the methane feed on the benzene yield and the accumulated benzene moles normalized per gram of catalyst over time. In the experiments in which H₂O was added, the solid symbols correspond to the results in dry conditions (catalyst activation period) and the open symbols to the results in wet conditions. As seen, the highest benzene yield (Figure 65.a) during 16 h on stream is obtained for the experiment carried out in dry conditions, and among the experiments done in wet conditions the highest benzene yield is reached with 0.9% of H₂O. These results are in agreement with those obtained by Liu et al. [1], in which case they determined that the Mo species are partially re-oxidized, by means of the use of Mo K-edge XAFS studies, therefore the benzene yield is lower in the experiments carried out by adding H₂O. Moreover, the methane reforming reaction is thermodynamically favored in the experiments performed by co-

feeding H_2O , reaching higher selectivity to CO in detriment to the aromatics selectivities, in particular to benzene. Furthermore, the value of the accumulated benzene moles normalized per gram of catalyst (Figure 65.b) is higher at least during 16 h for the experiment run in dry conditions over time. Between the experiments carried out by co-feeding H_2O , the value of the accumulated benzene moles is higher for the experiment with lower H_2O vapor concentration in the feed (0.9%). Thereby, these results are in concordance with those of benzene yield.

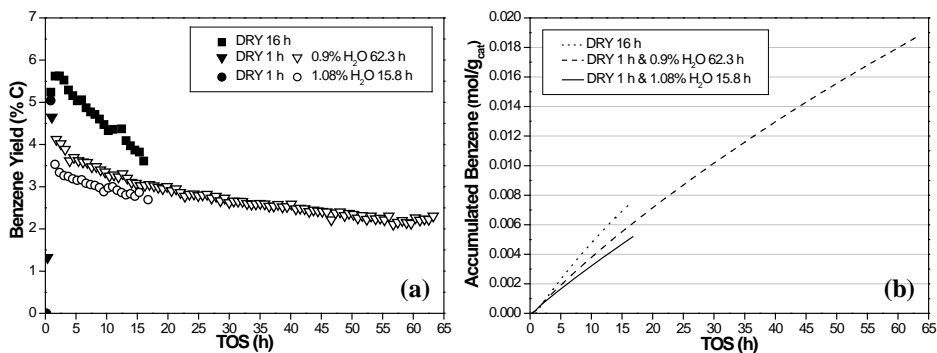


Figure 65. Effect of the H_2O addition to the methane feed on the (a) benzene yield and (b) accumulated benzene moles versus the TOS of 6%Mo/HZSM-5 catalyst at 700 °C.

Nevertheless, paying attention to Figure 65.a, both experiments carried out in wet conditions (after 1 h in dry conditions) are more stable than that performed exclusively in dry conditions, since the experiments carried out by adding 1.08% and 0.9% of H_2O show a 2.7 and 2-fold decrease in the average deactivation rate with respect to that performed in dry conditions. Moreover, it should be noted that the experiment carried out by adding 1.08% of H_2O exhibits a 1.4-fold decrease in the average deactivation rate with respect to that performed by co-feeding 0.9% of H_2O .

Figure 66 displays the effect of co-feeding H_2O on the H_2 flow normalized per gram of catalyst. As can be observed, the H_2 flow obtained is

higher in the experiments carried out by adding H₂O, and among these experiments it is higher with the addition of 1.08% of H₂O than with 0.9%. H₂ flow is directly related to the catalyst activity, that is to say, the methane conversion, and reflects the positive effect of H₂O on stability. Moreover, as happens with CO selectivity and in agreement with the thermodynamic results shown in the previous section, the H₂ flow increases as the H₂O vapor concentration in the feed increases.

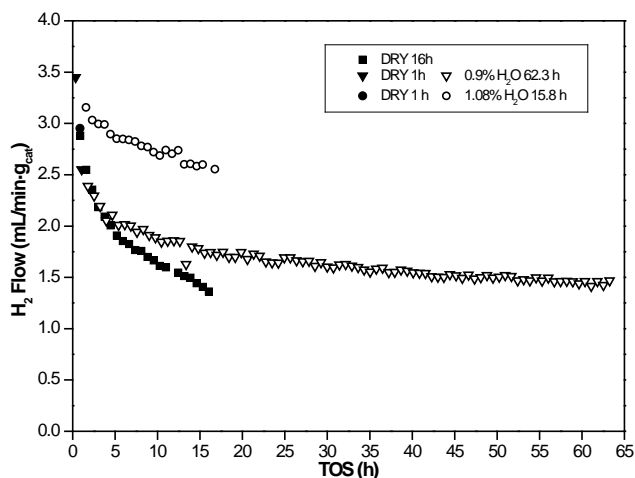


Figure 66. Effect of co-feeding H₂O on the H₂ flow versus the TOS of 6%Mo/HZSM-5 catalyst at 700 °C.

Table 39 shows the TGA results for the spent catalysts with and without the addition of H₂O. The amount of H₂O co-fed to the methane feed is listed according to the amount of coke in descending order: 0.9, 0 and 1.08%. In particular, it can be said that in the longest experiment (almost 4 times), 0.9% of H₂O, the catalyst accumulates more coke, but not even the double, therefore the coke accumulation is not linear with the time on stream, that is to say, the accumulation of coke decreases as time on stream increases. Hence, for the longest experiment the average coke formation rate and the amount of coke ($\text{g} \cdot \text{g}_{\text{cat}}^{-1}$) per accumulated benzene mole are lower than for the shorter ones.

Nonetheless, by focusing on the TGA results for the spent catalysts with similar TOS, 0 and 1.08% of H₂O, both the amount of coke and the average coke formation rate are lower for the experiment done by adding 1.08% of H₂O due to the coke gasification reaction. Although for this experiment the amount of coke (g·g_{cat}⁻¹) per accumulated benzene mole is higher than for the experiment carried out in dry conditions, thus reflecting the MDA performance worsening with the addition of H₂O for shorter times on stream.

Table 39. TGA results of spent 6%Mo/HZSM-5 catalysts with and without addition of H₂O.

H ₂ O co-fed (%)	TOS (h)	Average Coke Formation Rate (g·g _{cat} ⁻¹ ·h ⁻¹)	Amount of Coke (g·g _{cat} ⁻¹)	g·g _{cat} ⁻¹ ·mol _{benz.} ⁻¹
0	16.0	0.0031	0.049	11
0.90	63.3	0.0010	0.062	6
1.08	16.8	0.0026	0.043	14

7.1.3. Effect of co-feeding H₂O over 6% (wt.) Mo/MCM-22 catalyst on MDA reaction

7.1.3.1. Effect of co-feeding 1.08% of H₂O after different times on stream in dry conditions for the 6% (wt.) Mo/MCM-22 catalyst

The experiments were carried out according to the procedure described in the section 3.6.1.2.1.2 with the standard activation, in which the feed gas was introduced in the bubbler with the potassium carbonate saturated solution after different times on stream in dry conditions: 1, 3, 4 and 5 h, achieving a H₂O vapor concentration of 1.08%. The experiment without H₂O was done according to the procedure described in the section 3.6.1.1. The catalysts were prepared using the MCM-22 zeolite (Si/Al=15) impregnated with a 6% (wt.) of Mo.

Table 40 details the methane conversion and the selectivity to main products after 9 h on stream at 700 °C, 1.2 bar and 1500 mL·h⁻¹·g_{cat}⁻¹. The lowest methane conversion is reached for the experiment in which the 1.08% of H₂O was added after 3 h on stream in dry conditions and it is very similar to that obtained for the experiment run entirely in dry conditions. This is opposite to the results shown in the previous thermodynamic study, but it may be attributed to the coke deposits present on the catalyst, which were not included in that study. However, the highest aromatics selectivities and the lowest coke selectivity are reached for the experiment carried out exclusively in dry conditions. Among the experiments performed in wet conditions, the benzene selectivity is higher for that in which the 1.08% of H₂O was added after 3 h on stream in dry conditions. While, the coke selectivity is the lowest for this experiment. Moreover, the highest CO selectivity is obtained by introducing the H₂O after 1 h of MDA reaction in dry conditions. The C₂ hydrocarbons selectivity is very similar for the five experiments.

Table 40. Effect of co-feeding 1.08% of H₂O after different TOS in dry conditions on the methane conversion and the selectivity to main products after 9 h on stream of 6%Mo/MCM-22 catalyst.

TOS in dry conditions (h)	CH ₄ Conversion (% C)	Selectivity (% C)					
		C ₆ H ₆	C ₂	C ₇ H ₈	C ₁₀ H ₈	Coke	CO
~ 17	8.12	82.12	3.28	3.68	5.26	5.66	0.00
1	8.74	26.27	3.60	0.57	1.66	32.32	35.56
3	7.95	45.72	2.65	0.72	1.53	24.52	24.84
4	8.34	34.43	2.40	1.69	2.44	32.87	26.17
5	8.55	35.81	3.65	1.55	1.58	29.27	28.14

Figure 67 depicts the effect of co-feeding 1.08% of H₂O after different TOS on the benzene yield. As stated above, in the experiments in which H₂O was added, the solid symbols correspond to the results in dry conditions and the

open symbols to the results in wet conditions. The benzene yield obtained in dry conditions is the highest for the different experiments and it is almost equal, thus demonstrating the reproducibility of these experiments. However, at the moment in which the 1.08% of H₂O was added to the methane feed, the benzene yield drops drastically, reaching the highest benzene yield for the experiment in which the H₂O was added after 3 h on stream in dry conditions. The required carburization of the Mo species that are present in the catalyst to achieve a good MDA performance has to be carried out in dry conditions. Therefore, it can be deduced that 1 h in dry conditions is not enough time to carburize entirely the Mo species. Furthermore, 4 and 5 h in dry conditions are sufficient time to carburize entirely the Mo species and coke the most acidic Brønsted sites, but these species have accumulated more quantity of carbonaceous deposits than with 3 h in dry conditions. Thereby, it can be concluded that the time required in dry conditions to obtain the Mo species more active for MDA reaction is of 3 h.

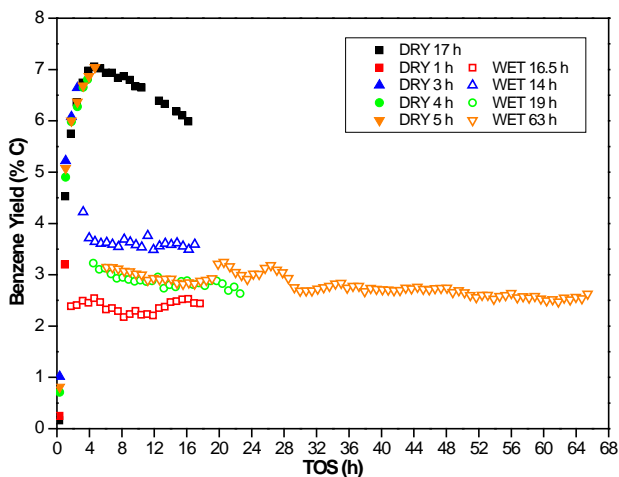


Figure 67. Effect of the addition of 1.08% of H₂O to the methane feed after different periods of time in dry conditions on the benzene yield versus the TOS of 6%Mo/MCM-22 catalyst at 700 °C.

It should be pointed out that the stability is greater for the experiments performed in wet conditions. In particular, the experiment carried out by adding 1.08% of H₂O after 3 h of MDA reaction in dry conditions exhibits a 5.1-fold decrease in the average deactivation rate with respect to that performed entirely in dry conditions. Moreover, by focusing on the experiments carried out in wet conditions, the experiment performed by adding 1.08% of H₂O after 3 h of MDA reaction in dry conditions shows a 1.6-fold decrease in the average deactivation rate with respect to those carried out by adding H₂O after 4 and 5 h of MDA reaction in dry conditions.

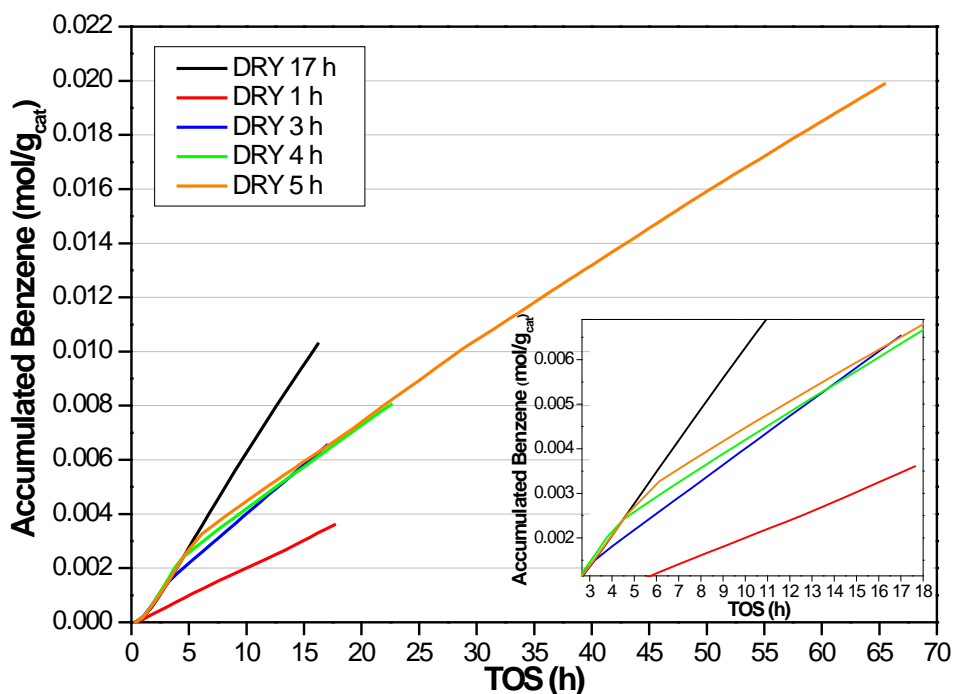


Figure 68. Effect of co-feeding 1.08% of H₂O after different periods of time in dry conditions on the accumulated benzene moles versus the TOS of 6%Mo/MCM-22 catalyst at 700 °C. Inset figure shows an enlarged version.

The accumulated benzene moles normalized per gram of catalyst are illustrated in Figure 68. The highest value of accumulated benzene moles is

reached in dry conditions for 17 h on stream, while the lowest value is obtained by adding 1.08% of H_2O after 1 h in dry conditions. For the other three experiments in wet conditions, a change in the slopes (inset Figure 68) of the accumulated benzene moles is observed to lower values after the introduction of 1.08% of H_2O to the feed, being the largest slope, i.e. benzene productivity, that achieved by co-feeding H_2O after 3 h. For this experiment the accumulated benzene moles even slightly exceed those obtained by adding 1.08% of H_2O after 4 and 5 h.

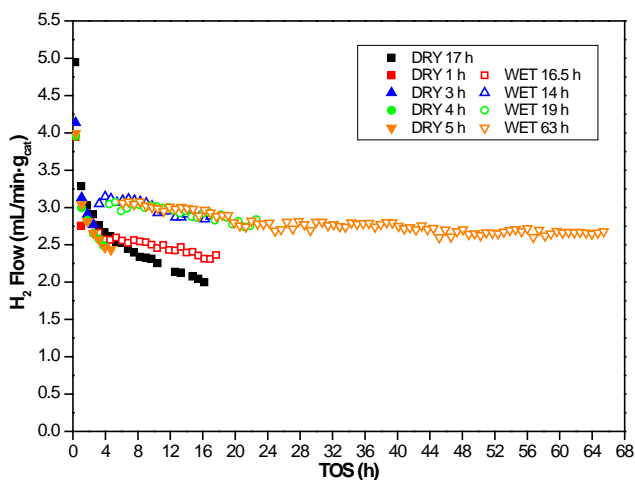


Figure 69. Effect of co-feeding 1.08% of H_2O after different periods of time in dry conditions on the H_2 flow versus the TOS of 6%Mo/MCM-22 catalyst.

Figure 69 displays the effect of co-feeding 1.08% of H_2O after different times on stream on the H_2 flow normalized per gram of catalyst. The H_2 flow is higher in the experiments carried out by adding H_2O , and among these experiments, it is higher for the experiments in which the H_2O was added after 3, 4 and 5 h of MDA reaction in dry conditions. This increment in the H_2 flow is attributed to the methane reforming reaction and coke gasification with H_2O (Equation 13 and Equation 15) and it is in agreement with the abovementioned thermodynamic results. Moreover, this increment in the H_2 flow is also

detrimental for the performance of the MDA reaction due to the equilibrium shift that takes place.

Table 41 shows the TGA results obtained for the spent catalysts with and without addition of 1.08% of H₂O. The amount of coke for the catalysts tested in wet conditions is lower than for the catalyst run exclusively in dry conditions. Concretely, the amount of coke for the catalyst spent by adding H₂O after 5 h in dry conditions is higher than for the other three catalysts tested in wet conditions, since it is the longest experiment. Therefore, using a H₂O concentration of 1.08% the coke is effectively reduced on the 6%Mo/MCM-22 catalyst. Moreover, by focusing on the experiments with a similar total TOS, it can be said that the addition of 1.08% of H₂O to the feed after 3 h in dry conditions leads to lower amount of coke ($\text{g}\cdot\text{g}_{\text{cat}}^{-1}$) per accumulated benzene mole than the addition of H₂O after 1 h in dry conditions. Nevertheless, by adding the H₂O after 3 h in dry conditions the amount of coke ($\text{g}\cdot\text{g}_{\text{cat}}^{-1}$) per accumulated benzene mole is slightly higher than for the experiment run entirely in dry conditions. For the longer experiments, in which the H₂O was added after 4 and 5 h in dry conditions, this ratio is lower than for the other three experiments, especially for the longest one, achieving the lowest amount of coke per accumulated benzene mole.

Table 41. TGA results of spent 6%Mo/MCM-22 catalysts with and without addition of 1.08% of H₂O after different periods of time in dry conditions.

TOS in dry conditions (h)	Total TOS (h)	Average Coke Formation Rate ($\text{g}\cdot\text{g}_{\text{cat}}^{-1}\cdot\text{h}^{-1}$)	Amount of Coke ($\text{g}\cdot\text{g}_{\text{cat}}^{-1}$)	$\text{g}\cdot\text{g}_{\text{cat}}^{-1}\cdot\text{mol}_{\text{benz.}}^{-1}$
~ 17	~ 17	0.0078	0.132	21
1	17.6	0.0046	0.081	38
3	17	0.0055	0.094	24
4	22.6	0.0040	0.091	19
5	65.4	0.0019	0.121	10

7.1.3.2. Effect of co-feeding 1.08% and 0.86% of H_2O over 6% (wt.) Mo/MCM-22 catalyst

The experiments were carried out according to the procedure described in the section 3.6.1.2.1.2 with the standard activation of the catalysts, in which the feed gas was introduced in a bubbler with the saturated aqueous salt solutions, potassium carbonate and potassium acetate, separately after 3 h of MDA reaction in dry conditions, reaching a H_2O vapor concentration of 1.08% and 0.86%, respectively. Furthermore, the experiment without H_2O was carried out according to the procedure described in the section 3.6.1.1. The catalysts were prepared using the MCM-22 zeolite (Si/Al=15) impregnated with a 6% (wt.) of Mo.

Table 42. Effect of co-feeding H_2O on the methane conversion and the selectivity to main products after 9 h on stream of 6%Mo/MCM-22 catalyst.

H_2O co-fed (%)	CH_4 Conversion (% C)	Selectivity (% C)					
		C_6H_6	C_2	C_7H_8	$C_{10}H_8$	Coke	CO
0	8.12	82.12	3.29	3.68	5.26	5.65	0.00
0.86	9.88	53.01	2.51	2.27	3.02	33.49	5.70
1.08	7.95	45.72	2.66	0.72	1.54	24.52	24.84

Table 42 summarizes the methane conversion and the selectivity to main products after 9 h on stream at 700 °C, 1.2 bar and $1500 \text{ mL} \cdot \text{h}^{-1} \cdot \text{g}_{\text{cat}}^{-1}$. In this case, the highest methane conversion and coke selectivity are obtained by adding 0.86% of H_2O . However, the aromatics selectivities decreases as the H_2O vapor concentration in the feed increases, in contrast to the CO selectivity. As with the 6%Mo/HZSM-5 catalyst (section 7.1.2.), the CO selectivity obtained by co-feeding 1.08% of H_2O after 9 h on stream is higher than that shown in the thermodynamic study (section 7.1.1.) and this may be related to the coke present on the catalyst (not considered in this study), which through

Equation 15 reacts with H_2O forming CO and H_2 . Furthermore, the C_2 hydrocarbons selectivity is also lower by adding H_2O to the feed.

Figure 70 depicts the effect of co-feeding H_2O on the benzene yield and the accumulated benzene moles normalized per gram of catalyst. The highest benzene yield (Figure 70.a) during 16 h on stream is obtained in the experiment carried out entirely in dry conditions, and among the experiments done in wet conditions the highest benzene yield is obtained with 0.86% of H_2O . As with the 6%Mo/HZSM-5 catalyst (section 7.1.2.), the results obtained are in agreement with those achieved by Liu et al. [1]. The benzene yield is lower for the experiments carried out by adding H_2O , due to the lower benzene selectivity. Furthermore, it can be assumed that this partial re-oxidation undergone by the Mo species increases as the amount of H_2O added to the methane feed increases, hence the MDA performance is worse by adding 1.08% of H_2O than by adding 0.86%. In addition to this fact, the methane reforming reaction and coke gasification are thermodynamically favored instead of MDA reaction as the H_2O vapor concentration rises, thus increasing the CO selectivity at the expense of the aromatics selectivities. Moreover, both experiments carried out in wet conditions (after 3 h in dry conditions) are more stable than that performed exclusively in dry conditions, as the experiments carried out by adding 1.08% and 0.86% of H_2O exhibit a 5.1 and 3-fold decrease in the average deactivation rate with respect to that performed in dry conditions, respectively. Further, it should be noted that the experiment carried out by adding 1.08% of H_2O is more stable than that performed by adding 0.86% of H_2O , since the former shows a 1.7-fold decrease in the average deactivation rate with respect to the latter.

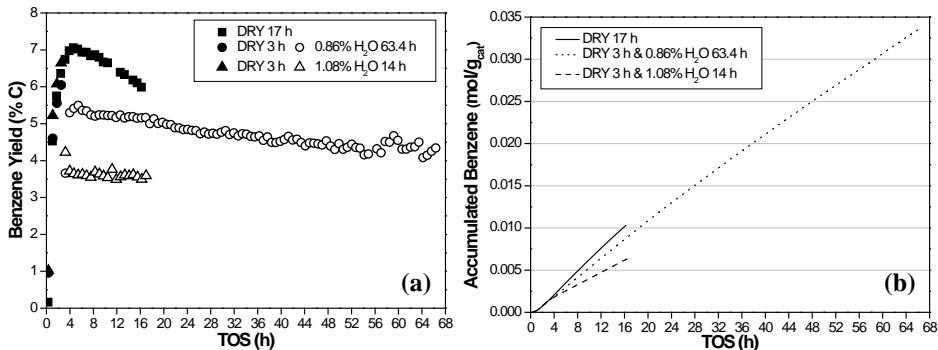


Figure 70. Effect of co-feeding H₂O on the (a) benzene yield and (b) accumulated benzene moles versus the TOS of 6%Mo/MCM-22 catalyst.

By focusing on the accumulated benzene moles normalized per gram of catalyst (Figure 70.b), these are higher for the experiment performed entirely in dry conditions. Among the experiments run by adding H₂O to the feed, the value of the accumulated benzene moles is higher for the experiment with lower H₂O vapor concentration, i. e., 0.86% of H₂O. Moreover, the accumulated benzene moles obtained by co-feeding 0.86% of H₂O increases with the time on stream in an almost linear way.

Figure 71 shows the effect of the H₂O addition on the H₂ flow normalized per gram of catalyst. The highest H₂ flow is obtained for the experiment carried out by adding 1.08% of H₂O. While the H₂ flow is very similar for the other two experiments, although after approximately 11 h on stream it is higher for the experiment carried out by adding 0.86% of H₂O. As abovementioned, this increment in the H₂ flow is ascribed to the methane reforming reaction and coke gasification (Equation 13 and Equation 15).

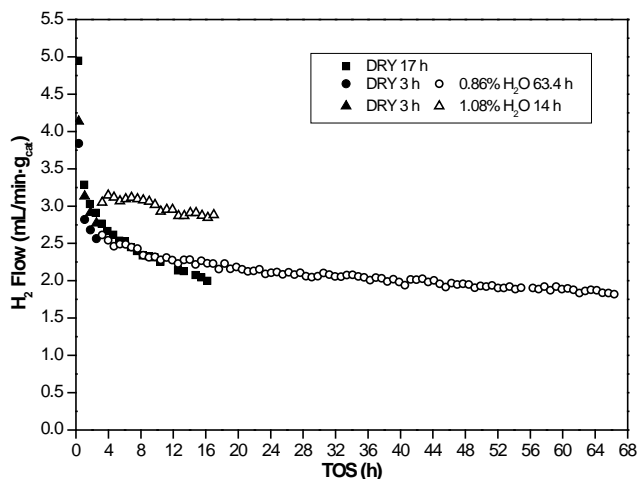


Figure 71. Effect of the H₂O addition to the methane feed on the H₂ flow versus the time on stream of 6%Mo/MCM-22 catalyst at 700 °C and 1.2 bar.

The Mo K-edge XANES spectra of some of the 6%Mo/MCM-22 catalysts employed in this work are shown in Figure 72, by comparing these with three reference compounds, i.e., Mo foil, Mo₂C and MoO₃. As the absorption edge energy rises, the oxidation state of the material increases. Therefore, the Mo foil exhibits the lowest absorption edge energy since it is the most reduced material. Moreover, the Mo K-edge energies detailed in Table 43 were selected as the energy at half of the height of the total absorption edge [4]. Thereby, there is a good linear correlation among the Mo K-edge energy and the formal oxidation state of the reference compounds. The spectrum of the fresh catalyst is very similar to that of MoO₃, even the pre-edge, thereby it is assumed that the majority of the Mo centers in this catalyst are as Mo⁶⁺. However, the spectra of the spent catalysts, in dry and wet (0.86% of H₂O) conditions, show K-edge energies between the Mo₂C and MoO₃ energies. Hence these catalysts have different species of Mo as Mo²⁺, Mo⁴⁺ and Mo⁶⁺, that could co-exist in the material. Nevertheless, the K-edge energy is slightly higher for the catalyst tested in wet conditions (0.86% of H₂O), thus indicating that this catalyst is slightly more oxidized than the catalyst spent in dry conditions [5].

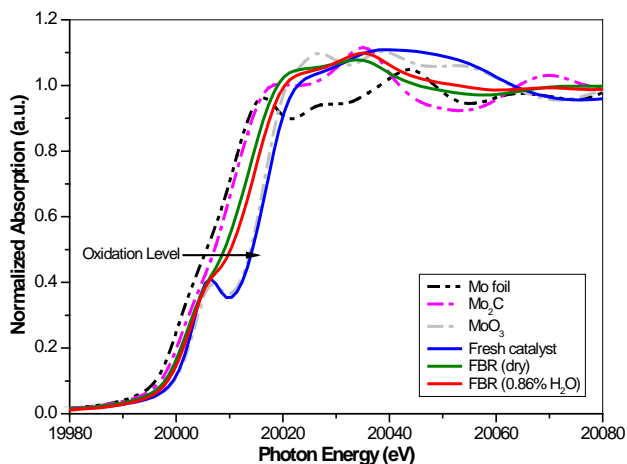


Figure 72. XANES spectra at Mo K-edge of Mo foil, Mo_2C , MoO_3 and 6%Mo/MCM-22 catalysts before and after MDA in dry and wet conditions.

Furthermore, an approximation of the formal oxidation state of the 6%Mo/MCM-22 catalysts can be ascertained using the abovementioned linear correlation among the Mo K-edge energy and the formal oxidation state of the reference compounds, which are shown in Table 43.

Table 43. Experimental XANES results of Mo foil, Mo_2C , MoO_3 and 6%Mo/MCM-22 catalysts before and after MDA in dry and wet conditions.

Sample	Mo K-edge energy (eV)	Formal oxidation state
Mo foil	20005	0
Mo_2C	20007	+2
MoO_3	20014	+6
Fresh catalyst	20014	+6
FBR (dry)	20009	+2.8
FBR (0.86% H_2O)	20010	+3.4

Further, Figure 73 displays the Mo3d spectra of the 6%Mo/MCM-22 catalysts before and after MDA reaction in dry and wet conditions (0.86% H_2O)

by XPS technique. These XPS spectra verify that there is certain amount of Mo species located on the external surface of the three catalysts.

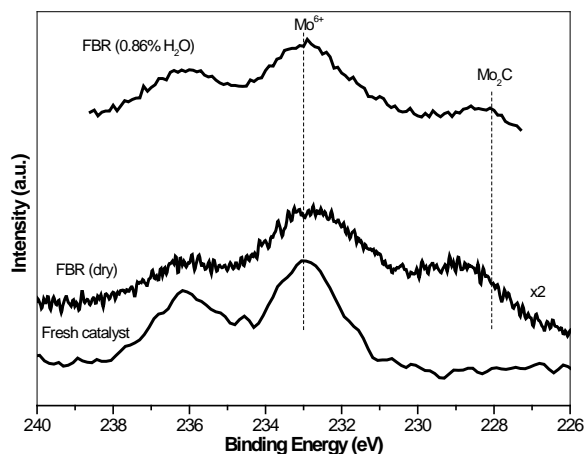


Figure 73. XPS Mo 3d_{5/2} and 3d_{3/2} spectra of 6%Mo/MCM-22 catalysts before and after MDA reaction in dry and wet conditions.

Moreover, Table 44 details the chemical state of Mo species on the surface of these catalysts. The binding energies employed are shown as a footnote in Table 44. The concentration of Mo species on the surface is different for the three catalysts, being entirely Mo⁶⁺ species for the fresh catalyst. While the spent catalysts exhibit Mo⁶⁺, Mo⁵⁺/Mo⁴⁺ and Mo²⁺ species. Concretely, the spent catalyst in wet conditions (0.86% H₂O) shows higher concentration of Mo⁶⁺ species than the spent catalyst in dry conditions, almost the double. Thus, revealing that some of the Mo species were re-oxidized when the experiment was carried out by co-feeding 0.86% of H₂O [5]. Therefore, these XPS results corroborate those obtained by XANES for the same catalysts.

Table 44. Surface oxidation state of Mo by XPS* on 6%Mo/MCM-22 catalysts before and after MDA reaction in dry and wet conditions.

Sample	Mo ⁶⁺ (%)	Mo ⁵⁺ / Mo ⁴⁺ (%)	Mo ₂ C (Mo ²⁺) (%)
Fresh catalyst	100	0	0
FBR (dry)	39	17	44
FBR (0.86% H ₂ O)	75	13	12

* Mo⁶⁺ (BE = 233.1 eV [6]), Mo⁵⁺ (BE = 234.4 eV [6]), Mo⁴⁺ (BE = 229.3 eV [7]) and Mo₂C (Mo²⁺) (BE = 227.9 eV [8]).

Table 45. TGA results of spent 6%Mo/MCM-22 catalysts with and without addition of H₂O.

H ₂ O co-fed (%)	TOS (h)	Average Coke Formation Rate (g·g _{cat} ⁻¹ ·h ⁻¹)	Amount of Coke (g·g _{cat} ⁻¹)	g·g _{cat} ⁻¹ ·mol _{benz.} ⁻¹
0	17	0.0078	0.132	21
0.86	66.4	0.0023	0.150	7
1.08	17	0.0055	0.094	24

Table 45 shows the TGA results obtained for the spent 6%Mo/MCM-22 catalysts with and without addition of H₂O. The amount of H₂O co-fed is listed according to the amount of coke in descending order: 0.86, 0 and 1.08. As stated above, in the longest experiment (66 h), with the addition of 0.86% of H₂O, the catalyst accumulates more coke than in the short experiments. Nevertheless, as abovementioned, the coke accumulation is not linear with the time on stream, that is to say, the accumulation of coke decreases as time on stream increases. Moreover, by focusing on the TGA results for the spent catalysts with the addition of 0 and 1.08% of H₂O, in which the TOS is alike, both the amount of coke and the average coke formation rate are lower for the experiment done with 1.08% of H₂O due to the coke gasification. Additionally, the amount of coke (g·g_{cat}⁻¹) per accumulated benzene mole is slightly higher for the experiment run co-feeding 1.08% of H₂O than for the experiment carried out

in dry conditions throughout the time on stream. Nonetheless, for the longest experiment performed by adding 0.86% of H₂O this ratio is the lowest obtained.

The TGA results are in agreement with the results of elemental analysis, BET surface area and micropore volume of the three catalysts after the MDA reaction, being the latter detailed in Table 46. The BET surface area and the micropore volume of the 6%Mo/MCM-22 catalyst before the MDA reaction (section 4.4.; Table 22) is of 399 m²·g⁻¹ and 0.151 cm³·g⁻¹, respectively. However, after the three experiments both the BET surface area and the micropore volume are reduced, being the most reduced those corresponding to the longest experiment (66.4 h), 0.86% of H₂O, which has the highest amount of coke accumulated. Moreover, by focusing on the BET surface area and micropore volume of the spent catalysts with the same TOS, 0 and 1.08% of H₂O, both are higher for the catalyst tested by adding 1.08% of H₂O, therefore the coke is effectively reduced by co-feeding 1.08% of H₂O.

Table 46. BET surface area and micropore volume for the spent 6%Mo/MCM-22 catalysts with and without addition of H₂O.

H ₂ O co-fed (%)	TOS (h)	S _{BET} (m ² /g)	Micropore volume (cm ³ /g)
0	17	213.10	0.071
0.86	66.4	173.21	0.053
1.08	17	282.01	0.102

Figure 74 depicts the CO_x profiles obtained by TPO technique for the spent catalysts by co-feeding 0, 0.86 and 1.08% of H₂O after 3 h on stream in dry conditions. Moreover, the TPO results for these catalysts are given in Table 47.

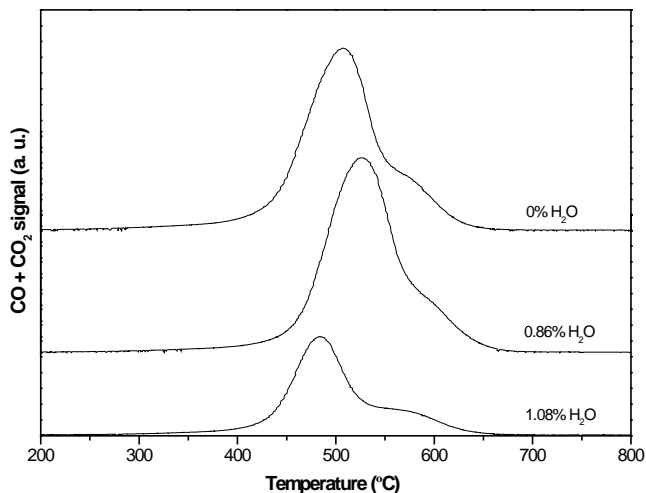


Figure 74. TPO profiles of carbon species over 6%Mo/MCM-22 catalysts after MDA reaction by co-feeding 0, 0.86 and 1.08% of H₂O. Same scale of Y-axis.

By focusing on the experiments with the same TOS, 0 and 1.08% of H₂O, it can be concluded that the coke related to Mo species is ca. 40.8% lower on the catalyst tested by adding 1.08% of H₂O, while the coke associated with Brønsted acid sites (aromatic-type carbon) relatively increased around 19.7% with respect to the catalyst without H₂O addition. These TPO results agree to the TGA and N₂ sorption (BET surface area and micropore volume) results, since the reduction suffered by the coke associated with Mo species is almost double than the increment observed for the coke related to Brønsted acid sites, thus balancing the amount of coke. Furthermore, for the longest experiment (66.4 h), 0.86% of H₂O, it can be said that both types of coke increase with respect to the catalyst used in dry conditions. Concretely, the coke associated with Mo species increases around 13.4% and the coke related to Brønsted acid sites (aromatic-type carbon) rises roughly 2.6%. These TPO results also verify the TGA and N₂ sorption results abovementioned.

The coke characteristics (particle size, morphology, etc.) may be different among the three catalysts [9], because of the different temperature at

maximum of both peaks in TPO (Table 47). The differences may be related to the different times on stream and with the co-feeding of H₂O. In particular, for the longest experiment in which 0.86% of H₂O is co-fed, the temperature at maximum of both peaks is higher than for the experiment run in dry conditions. While for the experiment performed by adding 1.08% of H₂O and with the same TOS that the experiment done without H₂O, the temperature at maximum of both peaks is lower than for the latter.

Table 47. Results of the deconvoluted TPO profiles of carbon species over 6%Mo/MCM-22 catalysts with and without addition of H₂O.

H ₂ O co-fed (%)	TOS (h)	Temperature at maximum (°C)		Percentage (%)		Amount of coke (g·g _{cat} ⁻¹)	
		Peak 1	Peak 2	Peak 1	Peak 2	Peak 1	Peak 2
0	17	503	587	82.52	17.48	0.1093	0.0232
0.86	66.4	566	605	84.16	15.84	0.1262	0.0238
1.08	17	482	524	69.18	30.82	0.0647	0.0288

In addition, experiments of temperature-programmed desorption of ammonia (NH₃ TPD) were also done to study the variation of acidity before and after MDA reaction with and without addition of H₂O to the methane feed. Figure 75 depicts the NH₃-TPD profiles of 6%Mo/MCM-22 catalysts before and after MDA reaction with and without addition of H₂O. In general, it is known that the NH₃-TPD profile of the 6%Mo/MCM-22 catalyst can be deconvoluted into three peaks [10, 11], a peak at low temperature that is assigned to the desorption of the physisorbed NH₃ species and/or NH₃ adspecies residing on non-exchangeable cationic sites, a peak at medium temperature that is attributed to the desorption of NH₃ adspecies adsorbed on exchangeable protonic sites, that is, Brønsted acid sites, and a peak at high temperature that corresponds to strong Lewis acid sites. As can be observed in the NH₃-TPD profiles (Figure 75), the amount of acid sites was lower for the three spent catalysts, specifically, the concentration of acid sites desorbed at low and

medium temperature decreased, especially for both catalysts tested with addition of H₂O.

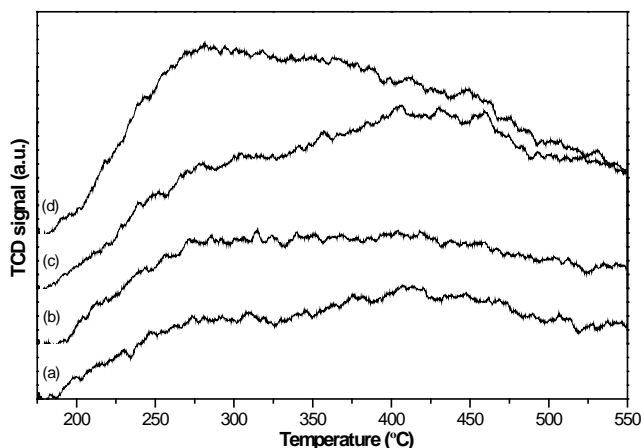


Figure 75. NH₃-TPD profiles of 6%Mo/MCM-22 catalysts after MDA reaction by co-feeding (a) 0.86%, (b) 1.08% and (c) 0% of H₂O, and (d) before MDA reaction. Same scale of Y-axis.

Table 48. Acidity of 6%Mo/MCM-22 catalysts before and after MDA reaction with and without addition of H₂O determined by NH₃-TPD.

6%Mo/MCM-22 Catalyst	TOS (h)	NH ₃ - uptake (μmol/g)	T _{max} (°C)
Before MDA reaction	-	526	281
After MDA with 0% H ₂ O co-fed	17	398	406
After MDA with 0.86% H ₂ O co-fed	66.4	295	407
After MDA with 1.08% H ₂ O co-fed	17	387	286

The NH₃ uptake at 175 °C and the maximum temperature (T_{max}) are detailed in Table 48. The acidity for the catalysts in descending order is as follows: the catalyst before MDA reaction, the spent catalyst without H₂O addition and the spent catalysts by co-feeding 1.08% (TOS = 17 h) and 0.86% of H₂O (TOS = 66.4 h). Concretely, by comparing the spent catalysts tested with the addition of 0 and 1.08% of H₂O, in which the TOS is alike, the acidity

of both catalysts is very similar. But the acid strength distribution is different due to the difference between the maximum temperatures, which may be due to the different conditions of each experiment [10, 11], that is, the co-feeding or not of H₂O.

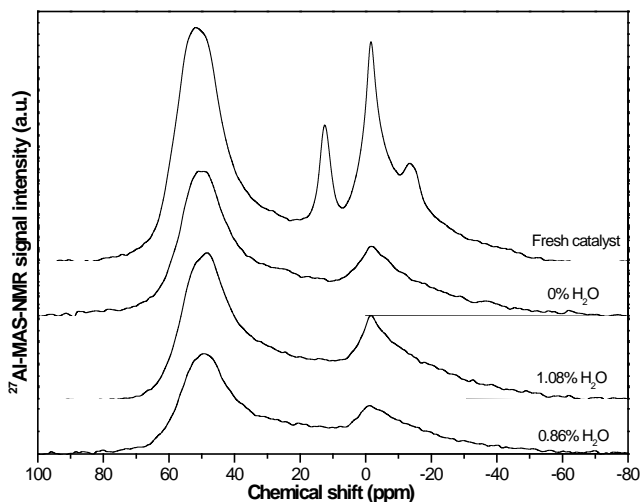


Figure 76. ²⁷Al MAS NMR spectra of fresh and spent 6%Mo/MCM-22 catalyst by co-feeding 0, 0.86 and 1.08% of H₂O. Same scale of Y-axis.

In order to obtain information about the aluminum environment on the 6%Mo/MCM-22 catalyst, ²⁷Al MAS NMR technique was used to differentiate the state of the aluminum atom in the zeolite. Solid-state ²⁷Al MAS NMR spectra of the fresh and spent 6%Mo/MCM-22 catalysts, with co-feeding 0, 0.86 and 1.08% of H₂O, are illustrated in Figure 76. For the fresh catalyst, four different peaks can be observed, according to Ma et al. [12] the peak at ca. 50 ppm is ascribed to tetrahedral framework aluminum, the peak at roughly 0 ppm is assigned to extraframework octahedral aluminum, the peak at around 14 ppm is attributed to hydrated aluminum molybdate and the peak at ca. -14 ppm is ascribed to non-hydrated aluminum molybdate, as with the Mo/HZSM-5 catalyst [13], being the latter two caused by the aluminum framework extraction by the Mo during the catalyst preparation. Moreover, the

peak recorded at roughly 50 ppm is composed by the signals of aluminum located at different tetrahedral sites [11, 12].

The three spent catalysts show a decrease in the intensity of peaks related to framework (~ 50 ppm) and extraframework (~ 0 ppm) aluminum, while the peak ascribed to hydrated aluminum molybdate (~ 14 ppm) disappears upon MDA testing. This reduction in the intensity of the ^{27}Al MAS NMR spectrum (Figure 76) may be attributed to the displacement of H_2O and oxygen by the coke in the channels of the zeolite, hence the electric-field gradient increases around aluminum thus causing quadrupolar shifts [14]. Furthermore, the high reaction temperature employed (700°C) intensifies the interaction between the Mo and the framework aluminum, distorting the zeolite lattice. Moreover, it is supposed that the disappearance of the peak attributed to hydrated aluminum molybdate occurs since part of the coke is deposited over the aluminum molybdate crystallites, thereby preventing their rehydration. Nevertheless, the peak at -14 ppm assigned to aluminum molybdate is also not observed in the ^{27}Al MAS NMR spectrum, but it is likely associated with the shoulder of the peak at ca. 0 ppm ascribed to extraframework octahedral aluminum, since the coke accumulated over the aluminum molybdate causes a distortion of its symmetry [12, 15].

In particular, for the spent 6%Mo/MCM-22 catalysts with the addition of H_2O to the feed, the ^{27}Al MAS NMR spectra (Figure 76) obtained are very similar to that of the spent catalyst without H_2O addition, especially the spectrum of the catalyst used by co-feeding 1.08% of H_2O , despite having less coke accumulated (Table 45). Therefore, the addition of 1.08% of H_2O is not detrimental for the framework aluminum. Moreover, the longest experiment (66.4 h) run by co-feeding 0.86% of H_2O exhibits a ^{27}Al MAS NMR spectrum with an intensity more reduced than the other spectra. This may be attributed to the higher amount of coke accumulated on this catalyst, since the displacement

of H₂O and oxygen may worsen by the coke in the channels of the zeolite, causing a higher electric-field gradient around aluminum with the associated quadrupolar shifts [14], than in the catalysts with less coke accumulated. Furthermore, these both concentrations of H₂O added to the methane feed are lower than the detrimental concentration of H₂O obtained by Liu et al. [1], higher than 2.20%.

7.2. Effect of co-feeding H₂

H₂ has been added to methane feed aiming to improve the stability of Mo/zeolite catalysts on MDA reaction, focusing on the H₂ reaction with carbonaceous deposits [2, 16, 17].

7.2.1. Thermodynamic study of co-feeding H₂

As with the H₂O addition, a thermodynamic study was carried out with co-feeding H₂ using the same databases and experimental conditions, with the difference that H₂O, CO and CO₂ were not considered like species that could be formed. Further, the results obtained in this study are in concordance with those exhibited by Bijani et al. [3].

Figure 77 displays the equilibrium methane conversion as a function of the H₂ concentration in the feed. The equilibrium methane conversion markedly decreases as the H₂ concentration in the feed increases, being lower than 1% from 28% of H₂ concentration.

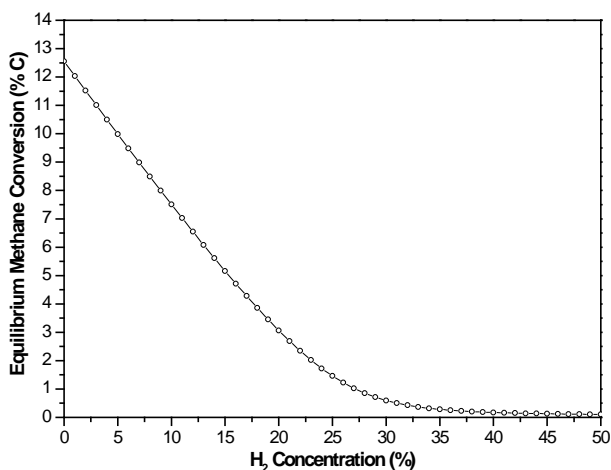


Figure 77. Effect of the H_2 concentration in the methane feed on the equilibrium methane conversion at 700 °C and 1 bar.

The effect of the H_2 concentration in the feed on the equilibrium selectivities to aromatics and C_2 hydrocarbons is shown in Figure 78. The naphthalene selectivity decreases as the H_2 concentration increases and it is the highest up to 10% of H_2 co-fed. However, the benzene selectivity increases as the H_2 concentration in the feed increases up to 26% of H_2 co-fed, reaching 63.5%. The increment experimented by the benzene selectivity up to its maximum may be ascribed to the reduction in the naphthalene selectivity, and the decrease of the benzene selectivity may be related to the increase suffered by the C_2 selectivities. Since the latter are almost stable up to 12% of H_2 co-fed, from which they become higher, although they have a more marked increase from 26% of H_2 co-fed. The lowest aromatic selectivity is for toluene, which is rather stable for all the H_2 concentrations studied. Moreover, the H_2 formed drastically drops as the H_2 concentration rises (not shown).

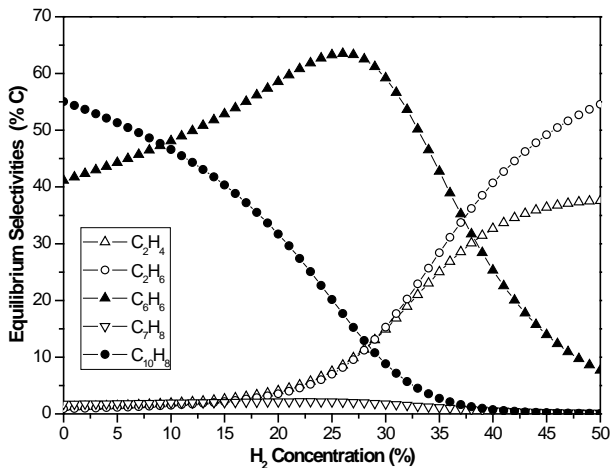


Figure 78. Effect of the H_2 concentration in the methane feed on the equilibrium selectivities to aromatics and C_2 hydrocarbons at 700 °C and 1 bar.

Thus, it can be concluded that thermodynamically the addition of H_2 to the feed, at 700 °C and 1 bar, appears to be detrimental for the MDA performance, especially due to the noted decrease suffered by the methane conversion.

7.2.1.1. Thermodynamic study of co-feeding H_2 without and with the addition of H_2O

In this study, besides the co-feeding of H_2 the addition of H_2O to the methane feed was considered for two H_2O vapor concentrations, 1 and 2%. As stated above, the thermodynamic equilibrium was calculated using the databases of Aspen Plus V8.8 and the previous experimental conditions (700 °C and 1 bar). Furthermore, the species included that could be formed were methane, H_2O , H_2 , ethylene, ethane, benzene, toluene, naphthalene, CO and CO_2 .

Figure 79 depicts the effect of co-feeding H_2 and H_2O on the equilibrium methane conversion. As seen, the equilibrium methane conversion is drastically reduced as the H_2 concentration increases, as abovementioned.

Moreover, the equilibrium methane conversion is almost not affected by the H_2O addition to the feed until this reaches similar values to the H_2O co-fed ($\leq 2\%$), coinciding with higher H_2 concentrations than 20%.

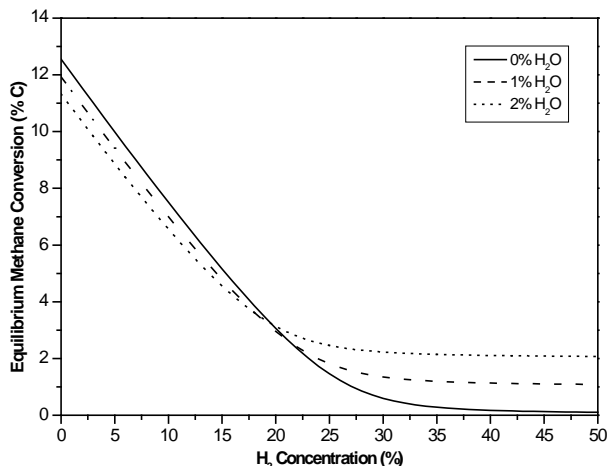


Figure 79. Effect of co-feeding H_2 and H_2O on the equilibrium methane conversion at 700 °C and 1 bar.

Figure 80 shows the effect of co-feeding H_2 and H_2O on the equilibrium selectivities to aromatics. For the benzene (Figure 80.a), naphthalene (Figure 80.b) and toluene (Figure 80.c) selectivities the addition of H_2O besides co-feeding H_2 is negative, since the three are reduced, mainly the benzene selectivity. As stated above, the naphthalene selectivity decreases as the H_2 concentration increases, while the benzene and toluene selectivities have a maximum roughly at 26% and 23% of H_2 co-fed, respectively. Moreover, the addition of H_2O leads to a reduction in the selectivity to the three aromatics and, in particular to benzene and toluene the maximums are smoothed, thus reducing in higher extent the benzene selectivity.

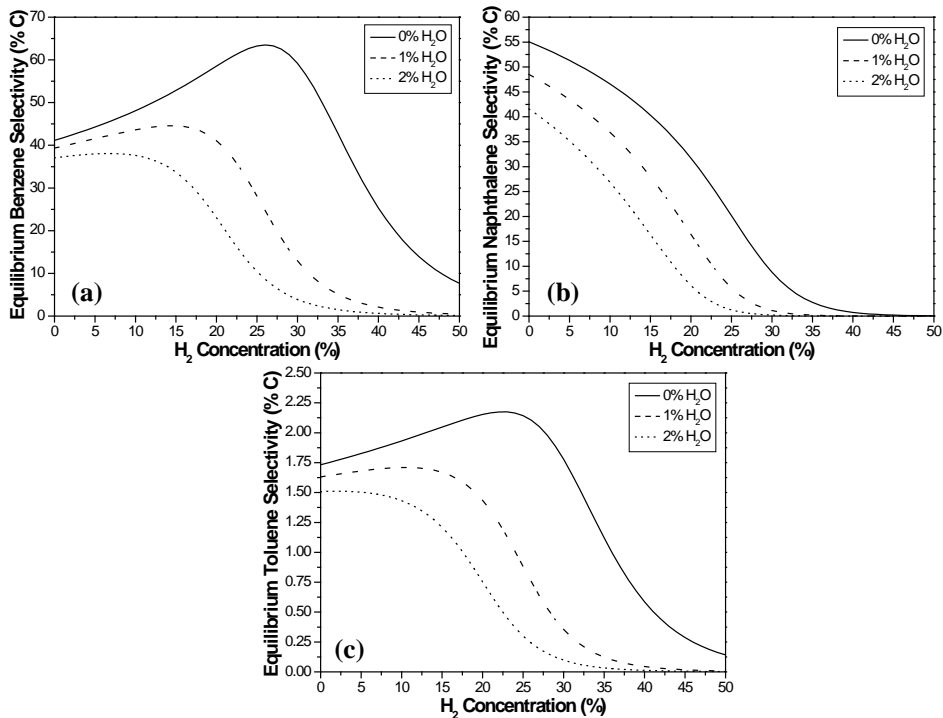


Figure 80. Effect of co-feeding H₂ and H₂O on the equilibrium selectivities to (a) benzene, (b) naphthalene and (c) toluene at 700 °C and 1 bar.

The effect of co-feeding H₂ and H₂O on the equilibrium selectivities to ethylene, ethane, CO and CO₂ is exhibited in Figure 81. The ethylene (Figure 81.a) and ethane (Figure 81.b) selectivities are markedly reduced from ca. 23% of H₂ co-fed with the addition of H₂O to the feed, being lower for higher H₂O vapor concentration. On the contrary, the CO selectivity (Figure 81.c) sharply increases from roughly 20% of H₂ co-fed with the addition of H₂O, coinciding with an equilibrium methane conversion lower than 2%, being higher for higher H₂O vapor concentration. Thus, as abovementioned, the co-feeding of H₂O thermodynamically favors the methane reforming reaction and the coke gasification (Equations 13, 14 and 15) at the expense of the MDA reaction. The CO₂ selectivity (Figure 81.d) behaves like CO selectivity but in a much lower extent, hence it may be considered negligible. Furthermore, the H₂ obtained (not

shown) decreases as the H_2 concentration in the feed increases, achieving higher values for higher H_2O vapor concentrations, especially for H_2 concentrations higher than 20%.

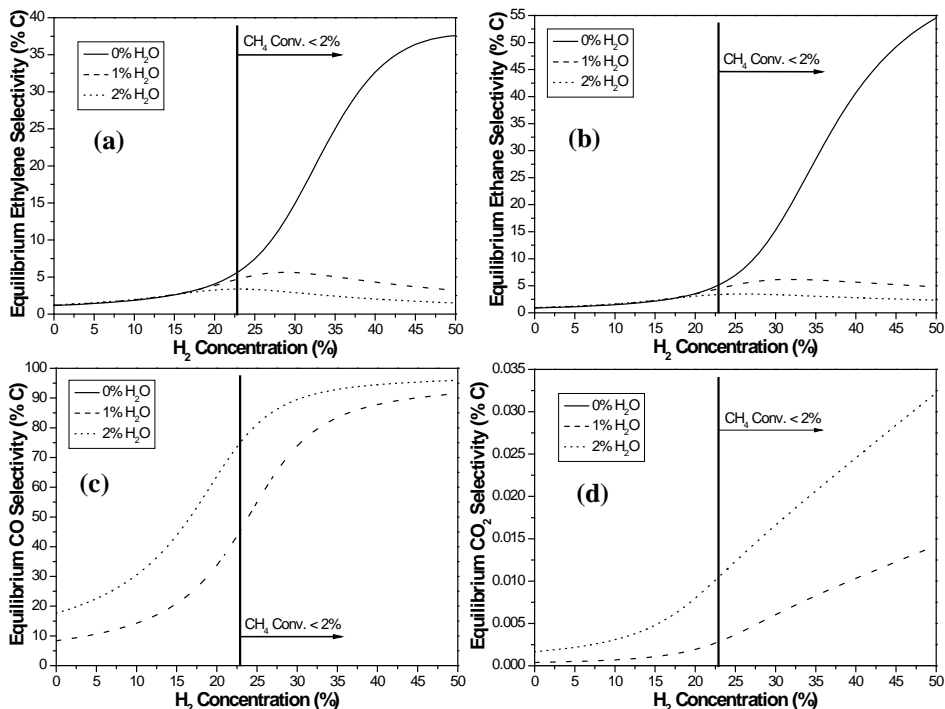
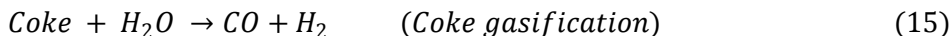
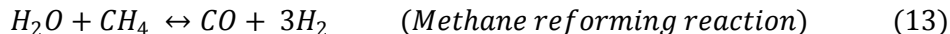


Figure 81. Effect of co-feeding H_2 and H_2O on the equilibrium selectivities to (a) ethylene, (b) ethane, (c) CO and (d) CO_2 at 700 °C and 1 bar.

7.2.2. Effect of co-feeding 6% of H_2 with the standard activation of the catalyst

In order to co-feed H_2 , it was necessary to use other feed gas mixture comprising CH_4 , H_2 and N_2 (internal standard) in a volumetric ratio of

8.9:0.6:0.5 (section 3.6.1.2.1.1.). This H₂ content was selected because it seems proper in view of the results obtained by Ma et al. [17]. The experiments without H₂ were carried out according to the procedure described in the section 3.6.1.1. The catalysts were prepared using the HZSM-5 and MCM-22 zeolites (Si/Al=15) and these were impregnated with a 6% (wt.) of Mo separately.

Table 49. Effect of co-feeding 6% of H₂ on the methane conversion and the selectivity to main products after 9 h on stream of 6%Mo/HZSM-5 and 6%Mo/MCM-22 catalysts.

Zeolite	H ₂ co-fed (%)	CH ₄ Conversion (% C)	Selectivity (% C)				
			C ₆ H ₆	C ₂	C ₇ H ₈	C ₁₀ H ₈	Coke
HZSM-5	0	6.66	67.15	7.12	5.03	16.44	4.25
HZSM-5	6	4.43	49.79	9.79	3.39	7.28	29.76
MCM-22	0	8.12	82.12	3.29	3.68	5.26	5.66
MCM-22	6	6.02	70.00	4.74	2.62	4.33	18.30

Table 26 summarizes the methane conversion and the selectivity to main products after 9 h on stream at 700 °C and 1.2 bar. The methane conversion for 6%Mo/HZSM-5 and 6%Mo/MCM-22 catalysts is lower for the experiments carried out by adding 6% of H₂ to the feed. This trend is agreed with the results shown in the previous thermodynamic study (section 7.2.1.). Moreover, the aromatics selectivities, especially the benzene selectivity, are lower for both catalysts tested by co-feeding 6% of H₂. It should be pointed out that the benzene and toluene selectivities obtained experimentally are higher than those exhibited in the thermodynamic results (Figure 78). While for the naphthalene selectivity is exactly the opposite. This may be ascribed to the shape selectivity of the catalysts. Furthermore, both C₂ and coke selectivities are higher for both catalysts tested by co-feeding 6% of H₂. This notes that the co-feeding of 6% of H₂, at 700 °C and 1.2 bar, appears detrimental for the performance of the MDA reaction due to the equilibrium shift that takes place,

thus reducing the methane conversion and also the effectiveness with which the C_2 species are oligomerized on the Brønsted acid sites of the zeolites to form aromatics, mainly benzene.

The highest benzene yield (Figure 82) is obtained for both catalysts without co-feeding 6% of H_2 . In spite of this detrimental effect of the addition of 6% of H_2 , it should be noted that by co-feeding 6% of H_2 , the benzene yield is slightly more stable throughout the time on stream. Especially for the 6%Mo/MCM-22 catalyst that shows a 2-fold decrease in the average deactivation rate, while the 6%Mo/HZSM-5 catalyst exhibits a 1.3-fold decrease in the average deactivation rate.

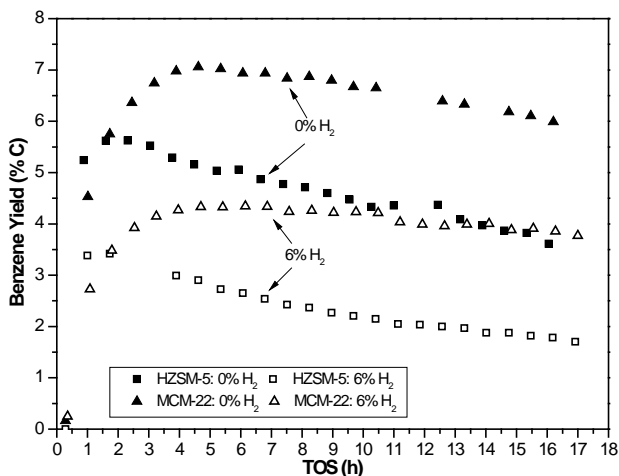


Figure 82. Effect of co-feeding 6% of H_2 on the benzene yield versus the TOS of 6%Mo/HZSM-5 and 6%Mo/MCM-22 catalysts at 700 °C.

Furthermore, the accumulated benzene moles normalized per gram of catalyst (Figure 83.a) are higher for both catalysts without the addition of H_2 . Concretely, these are higher for the 6%Mo/MCM-22 catalyst whether with or without co-feeding 6% of H_2 . Figure 83.b shows the effect of the addition of 6% of H_2 to the feed on the H_2 flow normalized per gram of catalyst. By comparing each catalyst separately, 6%Mo/HZSM-5 and 6%Mo/MCM-22, the highest H_2

flow is obtained, in both cases, without co-feeding 6% of H₂. These results are in agreement with those stated above in the thermodynamic study.

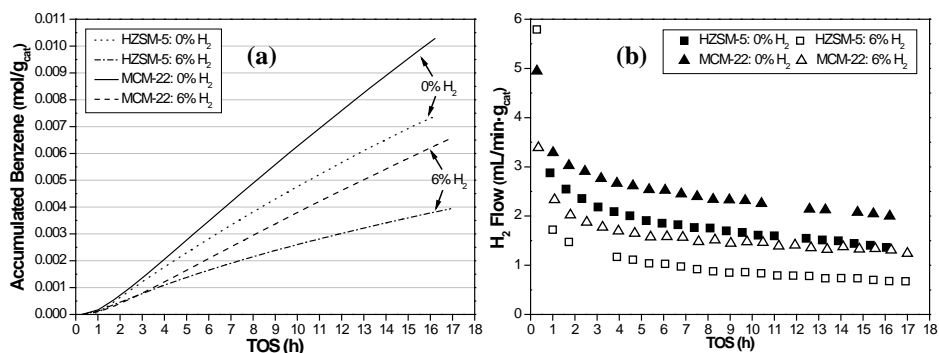


Figure 83. Effect of co-feeding 6% of H₂ on the (a) benzene accumulated and (b) H₂ flow versus the TOS of 6%Mo/HZSM-5 and 6%Mo/MCM-22 catalysts.

Table 50. TGA results of spent 6%Mo/HZSM-5 and 6%Mo/MCM-22 catalysts with and without addition of 6% of H₂ to the methane feed.

Zeolite	H ₂ co-fed (%)	TOS (h)	Average Coke Formation Rate (g·g _{cat} ⁻¹ ·h ⁻¹)	Amount of Coke (g·g _{cat} ⁻¹)	g·g _{cat} ⁻¹ ·mol _{benz.} ⁻¹
HZSM-5	0	16	0.0031	0.049	11
HZSM-5	6	17	0.0011	0.019	8
MCM-22	0	17	0.0078	0.132	21
MCM-22	6	17	0.0035	0.060	15

Table 50 details the TGA results for the spent catalysts with and without co-feeding 6% of H₂. The 6%Mo/MCM-22 catalyst accumulates much more coke than the 6%Mo/HZSM-5 catalyst, irrespective of co-feeding H₂. Moreover, by adding 6% of H₂ to the methane feed, both catalysts accumulate less than half amount of coke than without the H₂ addition. Therefore, it can be concluded that for both catalysts, 6%Mo/HZSM-5 and 6%Mo/MCM-22, the amount of coke is effectively reduced by co-feeding 6% of H₂. Additionally, the amount of coke (g·g_{cat}⁻¹) per accumulated benzene mole is also lower by adding

H₂ for both catalysts, although for the 6%Mo/MCM-22 catalyst the decrease is higher than for the 6%Mo/HZSM-5 catalyst.

In addition, by comparing these TGA results with those obtained in the section 7.1.2. for the 6%Mo/HZSM-5 catalyst and in the section 7.1.3.2. for the 6%Mo/MCM-22 catalyst, in both cases by co-feeding 1.08% of H₂O and with similar TOS, it can be said that the addition of 6% of H₂ removes more efficiently the coke accumulated for both catalysts than the co-feeding of 1.08% of H₂O. Thereby, this highlights the different elimination of coke that takes place by adding H₂ or H₂O.

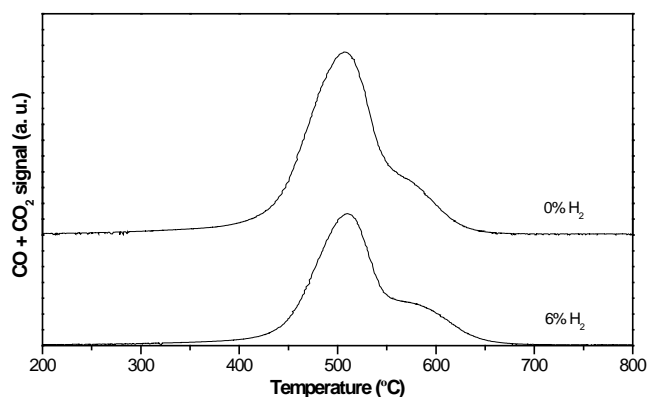


Figure 84. TPO profiles of carbon species over 6%Mo/MCM-22 catalysts without and with co-feeding 6% of H₂. Same scale of Y-axis.

The CO_x signals (from TPO technique) versus the temperature are depicted in Figure 84 for the 6%Mo/MCM-22 catalyst with and without co-feeding 6% of H₂ after 17 h of MDA reaction. Moreover, the TPO results are given in Table 51. For the catalyst tested by co-feeding 6% of H₂, both types of coke are lower than for the catalyst without H₂ addition. In particular, the coke related to Mo species and the coke associated with Brønsted acid sites (aromatic-type carbon) are reduced roughly 58.9% and 35.9%, respectively. Therefore, these results confirm those obtained by TGA, that is to say, the co-feeding of 6% of H₂ reduces both types of coke on the catalyst.

The temperature at maximum of both peaks (Table 51) is almost the same for both catalysts, noting that despite co-feeding H₂ the coke characteristics (particle size, morphology, etc.) may be similar between them [9]. Furthermore, by comparing these TPO results with those shown in the section 7.1.3.2. with the addition of 1.08% of H₂O. It can be inferred that by co-feeding 6% of H₂, the coke associated with the Brønsted acid sites of the 6%Mo/MCM-22 catalyst is more effectively reduced than by adding 1.08% of H₂O. These results are agreed with those reached by Ma et al. [2] for the 6%Mo/HZSM-5 catalyst.

Table 51. Results of the deconvoluted TPO profiles of carbon species over 6%Mo/MCM-22 catalysts without and with co-feeding 6% of H₂.

H ₂ co-fed (%)	TOS (h)	Temperature at maximum (°C)		Percentage (%)		Amount of coke (g·g _{cat} ⁻¹)	
		Peak 1	Peak 2	Peak 1	Peak 2	Peak 1	Peak 2
0	17	503	587	82.52	17.48	0.1093	0.0232
6	17	506	591	75.19	24.81	0.0450	0.0148

7.2.3. Effect of co-feeding H₂ over the 6%Mo/MCM-22 catalyst with the new activation

Further, the co-feeding of H₂ at two concentration levels (6 and 10%) was studied. The addition of H₂ was carried out according to the procedure described in section 3.6.2.2.2. In both experiments the H₂ was added after 3 h of MDA reaction without H₂, since 3 h was the time required to obtain the more active Mo species for MDA reaction, as it was concluded in the section 7.1.3.1. The experiments without H₂ were carried out according to the procedure described in the section 3.6.2.2.1. In all cases, the catalyst was pre-carburized and pre-reduced using a gas mixture of CH₄:H₂, 1:4 (vol. ratio), due to the better results obtained with this new catalyst activation (section 5.2.). The catalysts

were prepared using the MCM-22 zeolite (Si/Al=15) impregnated with a 6% (wt.) of Mo.

Table 52 details the methane conversion and the selectivity to main products after 9 h on stream at 700 °C and 1.2 bar. The methane conversion decreases as the H₂ concentration co-fed increases, this reduction is thermodynamically consistent (section 7.2.1.). Moreover, the lowest benzene selectivity is obtained by co-feeding 10% of H₂, while that reached without the addition of H₂ is very similar to that achieved with 6% of H₂, in the same way as with the toluene selectivity. Nevertheless, the naphthalene selectivity slightly decreases as the H₂ concentration increases. It is worth noting that the benzene and toluene selectivities are higher by adding 6 and 10% of H₂ than those shown in the thermodynamic study (section 7.2.1.), contrary to the naphthalene selectivity. As stated above, these results may be attributed to the shape selectivity of the catalyst. Conversely, the C₂ hydrocarbons selectivity is higher for both catalysts tested by co-feeding H₂. While, the highest coke selectivity is obtained co-feeding 10% of H₂. Thereby, in concordance with the results of the previous section, the co-feeding of 6 and 10% of H₂ affects negatively on the MDA performance, since it reduces the methane conversion and the C₂ oligomerization on the Brønsted acid sites of the zeolites to form aromatics.

Table 52. Effect of co-feeding H₂ on the methane conversion and the selectivity to main products after 9 h on stream of 6%Mo/MCM-22 catalyst.

H ₂ co-fed (%)	CH ₄ Conversion (% C)	Selectivity (% C)				
		C ₆ H ₆	C ₂	C ₇ H ₈	C ₁₀ H ₈	Coke
0	9.70	69.83	2.13	2.83	3.78	21.43
6	7.60	70.62	4.57	2.68	2.75	19.37
10	6.43	56.70	5.03	2.01	2.11	34.15

Figure 85 shows the effect of co-feeding H₂ on the benzene yield and the accumulated benzene moles normalized per gram of catalyst. The benzene

yield (Figure 85.a) obtained without the addition of H_2 is almost equal for the three experiments, pointing out the reproducibility of the experiments. However, at the moment in which the H_2 is added to the methane feed, the benzene yield drops sharply, being this decrease more marked for the experiment with the highest concentration of H_2 (10%). Furthermore, both experiments carried out by adding H_2 (after 3 h of MDA reaction) are slightly more stable than that performed exclusively without the addition of H_2 , showing both experiments a 1.3-fold decrease in the average deactivation rate with respect to the experiment run without co-feeding H_2 . In addition, the accumulated benzene moles per gram of catalyst (Figure 85.b) decrease as the H_2 content in the feed increases. As seen, the accumulated benzene moles are almost alike during the first 3 h on stream without co-feeding H_2 for the three experiments.

Moreover, by comparing the benzene yield results obtained in this section (Figure 85.a) with those obtained in the previous section (Figure 82) for the 6%Mo/MCM-22 catalyst, it can be observed that the new catalyst activation, the use of higher feed flow and catalyst amount, and the addition of 6% of H_2 after 3 h of MDA reaction without addition of H_2 turns out in a better MDA performance of this catalyst by adding 6% of H_2 .

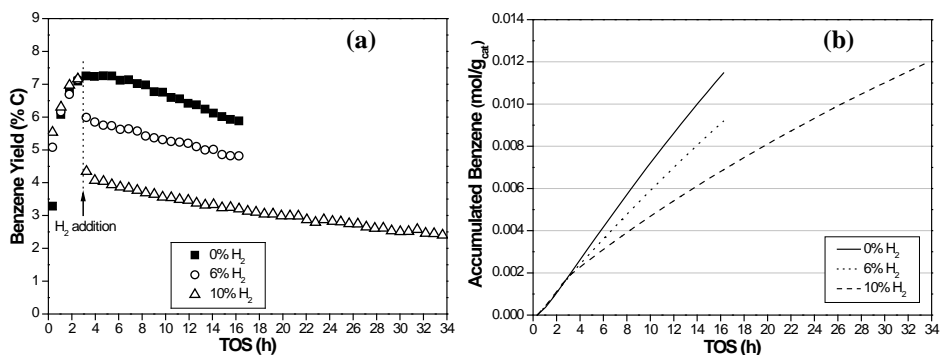


Figure 85. Effect of co-feeding H_2 on the (a) benzene yield and (b) accumulated benzene versus the TOS of 6%Mo/MCM-22 catalysts at 700 °C.

Figure 86 displays the effect of co-feeding H_2 on the H_2 flow normalized per gram of catalyst. The highest H_2 flow is obtained for the experiment carried out without the addition of H_2 , while as increases the H_2 content added the obtained H_2 flow decreases, which is in concordance with the thermodynamic results previously shown.

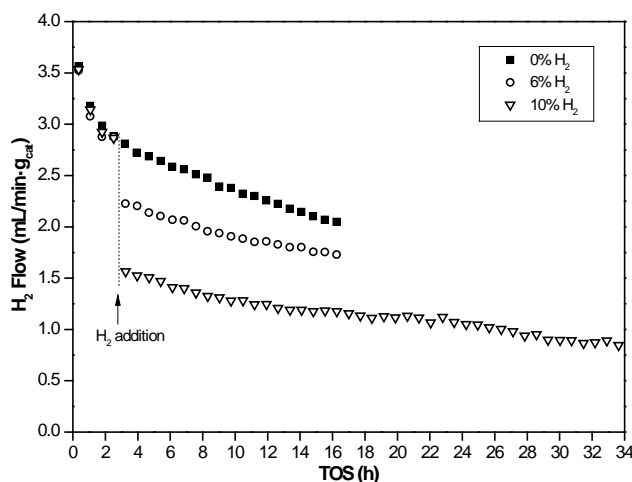


Figure 86. Effect of co-feeding H_2 on the H_2 flow versus the time on stream of 6%Mo/MCM-22 catalysts at 700 °C.

Table 53 summarizes the TGA results obtained for the spent 6%Mo/MCM-22 catalysts with and without addition of H_2 . The amount of coke for the catalysts tested by co-feeding H_2 is lower than for the catalyst without the addition of H_2 , despite the longer duration of the experiment run by co-feeding 10% of H_2 . Hence, the latter accumulates a bit more coke than the catalyst with the addition of 6% of H_2 . By focusing on the TGA results for the catalysts with the same TOS, 0 and 6% of H_2 , both the amount of coke and the average coke formation rate are lower for the experiment with the addition of 6% of H_2 . Thus indicating that by co-feeding 6% of H_2 , the coke deposition on the catalyst is reduced. In addition, the amount of coke ($g \cdot g_{cat}^{-1}$) per accumulated benzene mole is very similar for the three catalysts. Further, by

comparing these results with those obtained in the previous section (Table 50), this ratio is rather low for the catalysts shown in Table 53, that is to say, the new activation of the catalysts, the use of higher feed flow and catalyst amount, and the addition of 6% of H₂ after 3 h of MDA reaction without addition of H₂ leads to much lower coke deposition per accumulated benzene mole.

Table 53. TGA results of spent 6%Mo/MCM-22 catalysts with and without addition of H₂ to the methane feed.

H ₂ co-fed (%)	TOS (h)	Average Coke Formation Rate (g·g _{cat} ⁻¹ ·h ⁻¹)	Amount of Coke (g·g _{cat} ⁻¹)	g·g _{cat} ⁻¹ ·mol _{benz.} ⁻¹
0	16.3	0.0072	0.1166	6
6	16.3	0.0060	0.0977	6
10	33.6	0.0030	0.0997	5

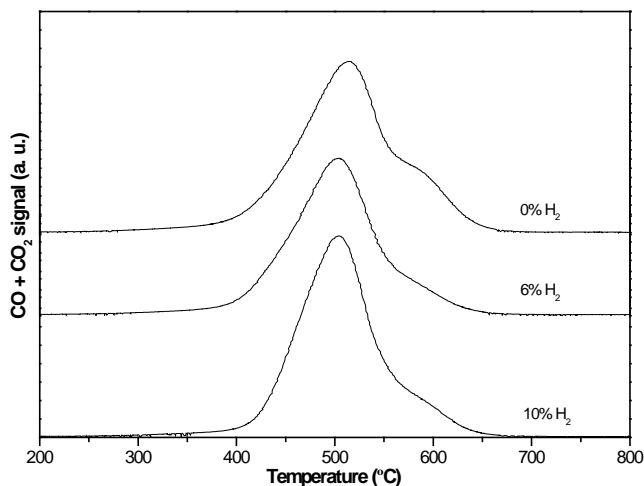


Figure 87. TPO profiles of carbon species over 6%Mo/MCM-22 catalysts after MDA reaction by co-feeding 0, 6 and 10% of H₂. Same scale of Y-axis.

Figure 87 illustrates the CO_x profiles obtained by TPO technique and the results are given in Table 54. For both catalysts tested by co-feeding 6% and 10% of H₂, the amount of coke related to Mo species is reduced ca. 16.2% and

14.5%, respectively, and the amount of coke associated with Brønsted acid sites (aromatic-type carbon) is decreased around 23.4% and 16.5%, respectively, with respect to the catalyst tested without co-feeding H_2 . These TPO results are in agreement with the TGA results, i. e., the co-feeding of 6% and 10% of H_2 reduces the accumulation of both types of coke on the catalyst.

Moreover, the temperature at maximum of both peaks (Table 54) is very similar for the three catalysts, thus indicating that the coke characteristics (particle size, morphology, etc.) may be similar among them [9].

Table 54. Results of the deconvoluted TPO profiles of carbon species over 6%Mo/MCM-22 catalysts with co-feeding 0, 6 and 10% of H_2 .

H_2 co-fed (%)	TOS (h)	Temperature at maximum ($^{\circ}C$)		Percentage (%)		Amount of coke ($g \cdot g_{cat}^{-1}$)	
		Peak 1	Peak 2	Peak 1	Peak 2	Peak 1	Peak 2
0	16.3	508	601	86.10	13.90	0.1004	0.0162
6	16.3	498	598	87.30	12.70	0.0853	0.0124
10	33.6	500	593	86.43	13.57	0.0861	0.0135

7.2.3.1. Effect of co-feeding different concentrations of H_2 without and with H_2O addition

Besides the concentrations of H_2 utilized in the previous section, four different concentrations of H_2 were used at the same experiment, for 4 h each of them, 20, 15, 10 and 5%, respectively. This experiment was carried out without H_2 during the first 3 h, and then a specific flow of H_2 was added to the feed flow to achieve the required concentration of H_2 , as is described in the section 3.6.2.2.2.2. Then, a catalyst regeneration using pure H_2 was done for 1 h, thus restoring almost totally the activity of the catalyst [18], as abovementioned in the section 2.5.2. Moreover, after the catalyst regeneration the same concentrations of H_2 were introduced again in the methane flow for 4 h each of

them, and in addition the feed flow was bubbled in a saturated aqueous potassium hydroxide solution, reaching a H_2O vapor concentration of 0.288%. For further information about the catalyst regeneration using H_2 , Chapter 8 includes a detailed explanation.

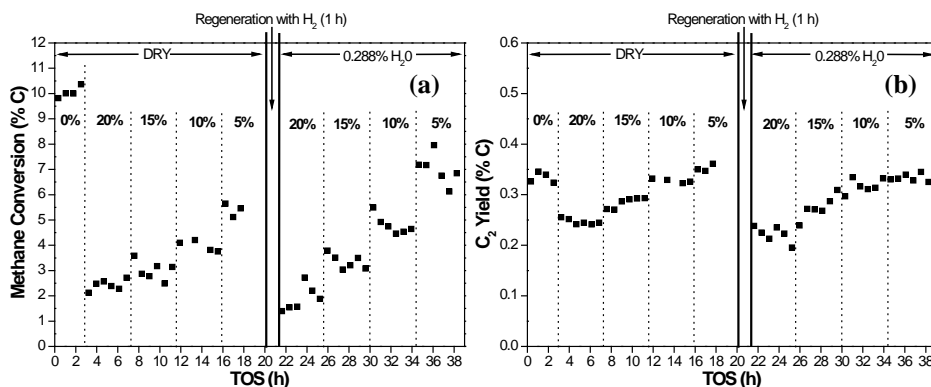


Figure 88. Effect of co-feeding different concentrations of H_2 without and with H_2O addition on the (a) methane conversion and (b) C_2 yield versus the time on stream of 6%Mo/MCM-22 catalyst at 700 °C.

Figure 88 shows the methane conversion and the C_2 yield using different concentrations of H_2 without and with 0.288% of H_2O . As seen, the highest methane conversion (Figure 88.a) is obtained during the first 3 h on stream, without H_2 addition, but the introduction of 20% of H_2 causes a sharp drop on it and then, the methane conversion increases as the concentration of H_2 co-fed decreases. These results are in concordance with those shown in the thermodynamic study (section 7.2.1.1.). Moreover, after the catalyst regeneration and the addition of 0.288% of H_2O , the methane conversion exhibits the same trend but with slightly higher values than in dry conditions for all the concentrations of H_2 except for 20%. In particular, the greater improvement is observed for the co-feeding of 5% of H_2 . Nevertheless, this improvement observed with the addition of H_2O is contrary to that obtained thermodynamically (section 7.2.1.1.), and it may be partly ascribed to the coke

deposits not considered in that study. Further, the methane conversion slightly rises with co-feeding 0.288% of H_2O since the methane reforming reaction and coke gasification (Equations 13, 14 and 15) are facilitated. Regarding the C_2 yield (Figure 88.b), it can be observed that it increases as the concentration of H_2 decreases, which is directly related to the behavior of the methane conversion. Moreover, after the catalyst regeneration and the addition of 0.288% of H_2O , the C_2 yield shows the same trend and slightly lower values.

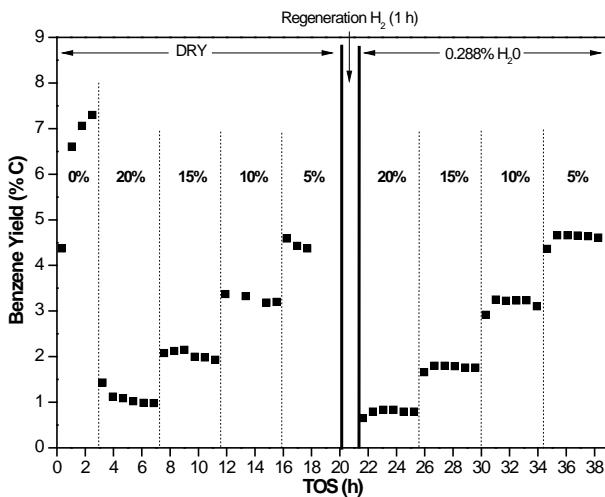


Figure 89. Effect of co-feeding different concentrations of H_2 without and with H_2O addition on the benzene yield versus the TOS of 6%Mo/MCM-22 catalyst.

Figure 89 depicts the effect of co-feeding different concentrations of H_2 without and with the addition of H_2O on the benzene yield. As with the methane conversion, the highest benzene yield is obtained during the first 3 h of MDA reaction without H_2 addition. Nevertheless, the introduction of 20% of H_2 leads to a great decrease in the benzene yield and this rises as the H_2 content co-fed decreases. Furthermore, after the catalyst regeneration and the addition of 0.288% of H_2O , the benzene yield shows the same behavior but it is more stable than in dry conditions for all the concentrations of H_2 . Concretely, by co-feeding 5% of H_2 is slightly higher than in dry conditions. Therefore, the

addition of 5% of H_2 and 0.288% of H_2O to the methane feed turns out in a slightly better MDA performance for the 6%Mo/MCM-22 catalyst than in dry conditions.

The naphthalene and toluene yields are not included because the results reached without and with the addition of 0.288% of H_2O are very similar, and in both cases the introduction of 20% of H_2 causes a big decrease.

Figure 90 exhibits the H_2 flow normalized per gram of catalyst co-feeding different concentrations of H_2 without and with 0.288% of H_2O . The highest H_2 flow is also obtained for the first 3 h on stream without H_2 addition. However, the H_2 flow suffers a sharp reduction by co-feeding 20% of H_2 , and then, the H_2 flow increases as the H_2 concentration co-fed decreases. Further, after the catalyst regeneration and the addition of 0.288% of H_2O , the H_2 flow shows slightly higher values than those obtained in dry conditions. This slight increment in the H_2 flow is due to the methane reforming reaction and coke gasification with the addition of H_2O (Equations 13, 14 and 15), as it happens with the CO formation.

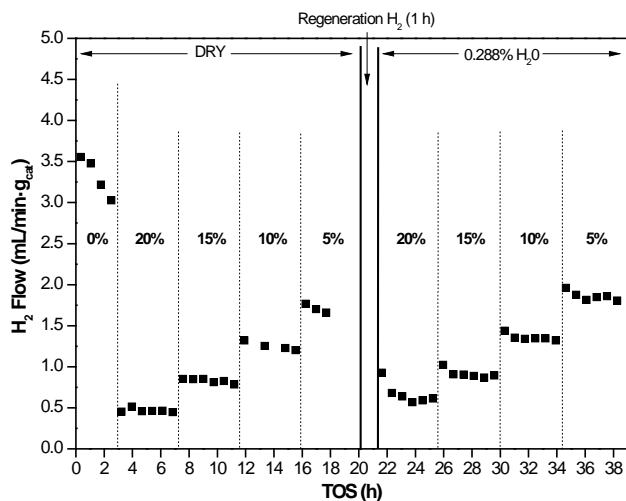


Figure 90. Effect of co-feeding different concentrations of H_2 without and with H_2O addition on the H_2 flow versus the TOS of 6%Mo/MCM-22 catalyst.

Moreover, Figure 91 illustrates the coke and the CO yields by co-feeding different concentrations of H_2 without and with 0.288% of H_2O . The highest coke yield (Figure 91.a) is obtained without co-feeding H_2 , being reduced as the concentration of H_2 co-fed decreases. After the catalyst regeneration and the addition of 0.288% of H_2O , the coke yield exhibits the opposite trend and this slightly increases as the concentration of H_2 co-fed decreases. As abovementioned, CO (Figure 91.b) is obtained during the addition of 0.288% of H_2O owing to the methane reforming reaction and coke gasification (Equations 13, 14 and 15). As seen, CO yield is slightly scattered, appearing almost constant for the different H_2 concentrations co-fed.

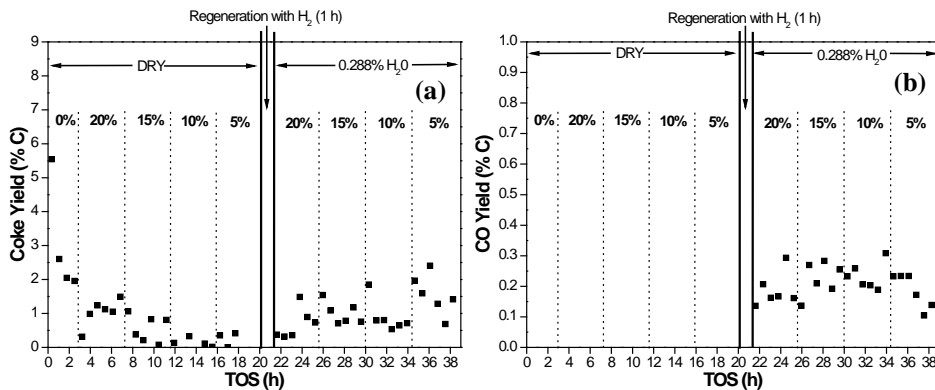


Figure 91. Effect of co-feeding different concentrations of H_2 without and with H_2O addition on the (a) coke yield and (b) CO yield versus the TOS of 6%Mo/MCM-22 catalyst at 700 °C.

The TGA results for the spent 6%Mo/MCM-22 catalysts with the addition of H_2 and without and with co-feeding H_2O are detailed in the following table. The catalyst tested by co-feeding different concentrations of H_2 and 0.288% of H_2O accumulates slightly higher amount of coke than the catalyst tested in dry conditions with co-feeding 10% of H_2 (previous section), even being 5 h longer. Thus, in this case the catalyst regeneration with pure H_2 during 1 h should be also taken into account as a factor that affects positively in

the reduction of coke accumulated, besides the co-feeding of H_2 and H_2O . Moreover, the amount of coke ($g \cdot g_{cat}^{-1}$) per accumulated benzene mole is the same for both catalysts.

Table 55. TGA results of spent 6%Mo/MCM-22 catalysts with co-feeding H_2 and without and with the addition of 0.288% of H_2O .

H_2 & H_2O co-fed (%)	TOS (h)	Average Coke Formation Rate ($g \cdot g_{cat}^{-1} \cdot h^{-1}$)	Amount of Coke ($g \cdot g_{cat}^{-1}$)	$g \cdot g_{cat}^{-1} \cdot mol_{benz.}^{-1}$
10 & 0	33.6	0.0030	0.0997	5
20, 15, 10, 5 & 0.288	38.3	0.0026	0.1013	5

The CO_x profiles obtained by TPO technique are depicted in Figure 92 and the results are shown in Table 56. By comparing the catalyst tested with co-feeding different concentrations of H_2 and 0.288% of H_2O with the catalyst tested entirely in dry conditions by adding 10% of H_2 , it can be said that for the former the coke associated with Mo species increases ca. 4% and the coke related to Brønsted acid sites (aromatic-type carbon) decreases roughly 12% with respect to the latter.

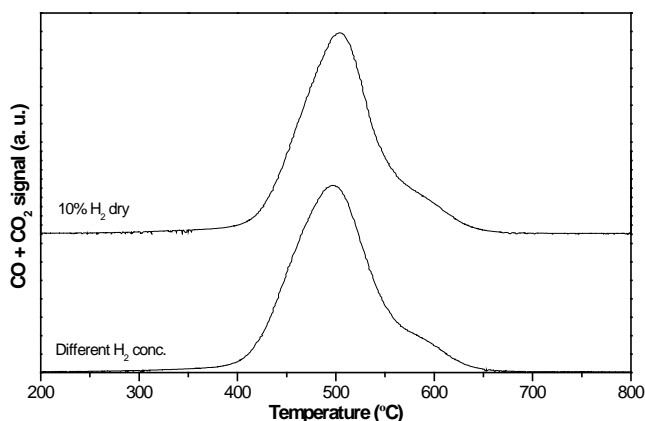


Figure 92. TPO profiles of carbon species over 6%Mo/MCM-22 catalysts after MDA reaction by co-feeding H_2 and without and with co-feeding 0.288% of H_2O . Same scale of Y-axis.

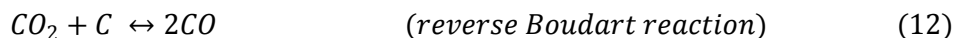
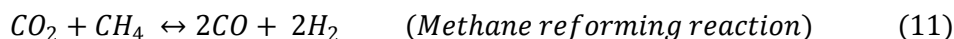
Regarding the coke characteristics (particle size, morphology, etc.) of both catalysts, it can be concluded that these may be similar [9], since the temperature at maximum of both peaks (Table 56) is very similar for both catalysts. Thus, pointing out that the co-feeding of 0.288% of H₂O barely affects the coke characteristics, adding simultaneously H₂ to the methane feed from 5 to 20%.

Table 56. Results of the deconvoluted TPO profiles of carbon species over 6%Mo/MCM-22 catalysts with co-feeding H₂ and without and with the addition of 0.288% of H₂O.

H ₂ & H ₂ O co-fed (%)	TOS (h)	Temperature at maximum (°C)		Percentage (%)		Amount of coke (g·g _{cat} ⁻¹)	
		Peak 1	Peak 2	Peak 1	Peak 2	Peak 1	Peak 2
10 & 0	33.6	500	593	86.43	13.57	0.0861	0.0135
20, 15, 10, 5 & 0.288	38.3	494	592	88.31	11.69	0.0894	0.0118

7.3. Effect of co-feeding CO₂

CO₂ has been added to the methane feed aiming to enhance the stability of Mo/zeolite catalysts in MDA reaction [16, 19, 20], focusing on the CO₂ reaction with the carbonaceous deposits by the methane reforming reaction (Equation 11) and the reverse Boudart reaction (Equation 12):



In order to co-feed a 2% of CO₂, it was necessary to use other feed gas mixture comprising CH₄, CO₂ and N₂ (internal standard) in a volumetric ratio of 9.3:0.2:0.5 (section 3.6.1.2.1.3.). In all cases the catalysts were activated using the standard procedure.

7.3.1. Thermodynamic study of co-feeding CO₂

By using the same and abovementioned databases and experimental conditions that for the co-feeding of H₂ and H₂O, the addition of CO₂ was studied thermodynamically, considering the formation of ethylene, ethane, benzene, toluene, naphthalene, H₂, CO, methane and CO₂.

The equilibrium methane conversion as a function of the CO₂ concentration co-fed is depicted in Figure 93. The equilibrium methane conversion remains almost stable up to 9% of CO₂ co-fed, from which the methane conversion increases strongly.

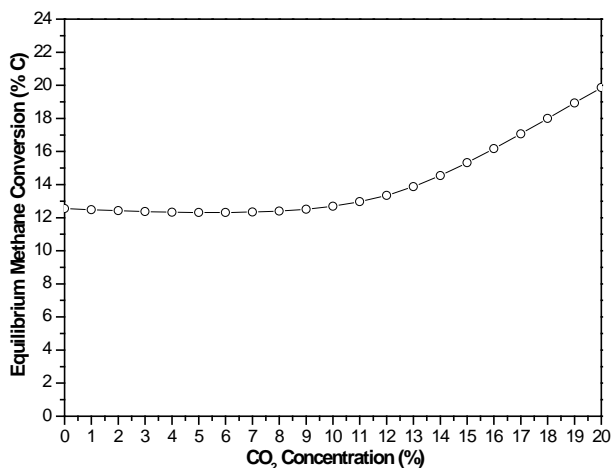


Figure 93. Effect of CO₂ concentration in the methane feed on the equilibrium methane conversion at 700 °C and 1 bar.

The effect of the CO₂ concentration added to the methane feed on the equilibrium selectivities to aromatics, C₂ hydrocarbons and CO is exhibited in Figure 94. The selectivities to aromatics decreases as the CO₂ concentration co-fed rises, being the naphthalene selectivity the highest up to 5% of CO₂, from which the benzene selectivity is higher than the other aromatic selectivities. Concretely, the selectivities to benzene, naphthalene and toluene are lower than

1% for 16, 14 and 6% of CO₂ concentration co-fed, respectively. In addition, the C₂ selectivities also decreases as the CO₂ concentration co-fed increases, being this reduction more marked from 10% of CO₂. On the contrary, the equilibrium selectivity to CO increases as the CO₂ concentration rises, being higher than 90% from 13% of CO₂ co-fed. Further, the increase in the CO₂ concentration added to the feed causes an increment in the H₂ formed (not shown).

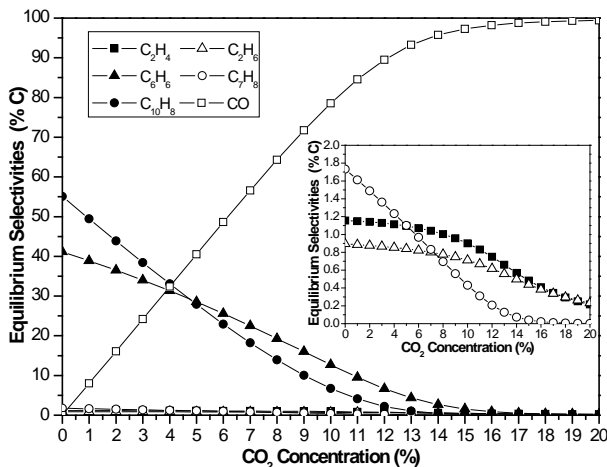


Figure 94. Effect of the CO₂ concentration in the feed on the equilibrium selectivities to aromatics, C₂ hydrocarbons and CO at 700 °C and 1 bar. Inset figure shows an enlarged version of the C₂ and toluene selectivities.

The co-feeding of CO₂, at 700 °C and 1 bar, thermodynamically favors the methane reforming reaction (Equation 11) and the reverse Boudart reaction (Equation 12) in detriment of the MDA reaction.

7.3.2. Effect of co-feeding 2% of CO₂ over 6% (wt.) Mo/zeolite catalysts on MDA reaction

The 6%Mo/HZSM-5 catalyst was tested in two experiments using a gas mixture with 2% of CO₂, in one of them this gas mixture was used since the

beginning of the MDA reaction, and in the other experiment, during the 1st h on stream the feed gas mixture was composed by CH₄:N₂, 9.5:0.5, and after this time the gas mixture with 2% of CO₂ was fed. Furthermore, the 6%Mo/MCM-22 catalyst was tested only co-feeding 2% of CO₂ after 3 h on stream without CO₂. The experiments run exclusively without CO₂ were carried out according to the procedure described in the section 3.6.1.1. The catalysts were prepared using the HZSM-5 and MCM-22 zeolites (Si/Al=15) impregnated with a 6% (wt.) of Mo.

Table 57 details the methane conversion and the selectivity to main products after 9 h on stream, at 700 °C and 1.2 bar, for both catalysts without and with co-feeding 2% of CO₂. For the 6%Mo/MCM-22 catalyst the methane conversion is slightly higher without co-feeding 2% of CO₂. Nevertheless, for the 6%Mo/HZSM-5 catalyst the methane conversion is higher for the catalyst tested by adding 2% of CO₂ after 1 h on stream without CO₂, while the methane conversion is alike for the catalysts tested without and with the addition of 2% of CO₂ since the beginning of the MDA reaction. In general, these results are close to those obtained in the thermodynamic study (section 7.3.1.).

Furthermore, for both catalysts the aromatics and C₂ selectivities are lower by co-feeding 2% of CO₂. In particular, by focusing on the aromatics selectivities, it can be said that the benzene and toluene selectivities obtained experimentally are higher than those exhibited in the previous thermodynamic study (Figure 94), on the contrary the naphthalene selectivity is lower. These results may be due to the shape selectivity of both catalysts. Nonetheless, the CO and coke selectivities are higher by adding 2% of CO₂ for both catalysts. This indicates that the co-feeding of 2% of CO₂ may be detrimental for the performance of the MDA reaction, since the Mo species are partially re-oxidized [16] and, moreover, the methane reforming reaction and the reverse Boudart reaction (Equation 11 and Equation 12) are promoted, being the CO

selectivity slightly higher for the 6%Mo/HZSM-5 catalyst using the gas mixture with 2% of CO₂ since the beginning of the experiment.

Table 57. Effect of co-feeding 2% of CO₂ on the methane conversion and the selectivity to main products after 9 h on stream of 6%Mo/HZSM-5 and 6%Mo/MCM-22 catalysts.

Zeolite	CO ₂ co-fed (%)	CH ₄ Conversion (% C)	Selectivity (% C)					
			C ₆ H ₆	C ₂	C ₇ H ₈	C ₁₀ H ₈	Coke	CO
HZSM-5	0	6.66	67.15	7.12	5.03	16.44	4.26	0.00
HZSM-5	2	6.66	42.97	4.90	1.97	10.92	11.76	27.48
HZSM-5	0% 1 h & 2% 61.5 h	7.94	39.00	3.67	2.17	9.79	20.37	25.00
MCM-22	0	8.12	82.12	3.29	3.68	5.26	5.65	0.00
MCM-22	0% 3 h & 2% 67.5 h	7.86	56.34	3.11	1.99	3.78	7.46	27.32

Figure 95 illustrates the effect of the addition of 2% of CO₂ on the benzene yield. In the experiments in which CO₂ is added, the solid symbols correspond to the results without CO₂ and the open symbols to the results with CO₂. The highest benzene yield is obtained without co-feeding CO₂ for both catalysts during 16 h on stream. Among the experiments done with the addition of 2% of CO₂, the highest benzene yield is obtained for the 6%Mo/MCM-22 catalyst. Moreover, by focusing on the 6%Mo/HZSM-5 catalyst, the benzene yield is slightly higher for the experiment in which the 2% of CO₂ was co-fed after 1 h of MDA reaction without CO₂.

Additionally, the benzene yield obtained by adding CO₂ is more stable throughout the time on stream for both catalysts, which exhibit a 2.1, 2.6 and 2.8-fold decrease in the average deactivation rate with respect to that performed without CO₂ addition, for the 6%Mo/HZSM-5 catalyst tested by adding CO₂ since the beginning and after 1 h on stream, and for the 6%Mo/MCM-22 catalyst tested by co-feeding CO₂ after 3 h on stream, respectively.

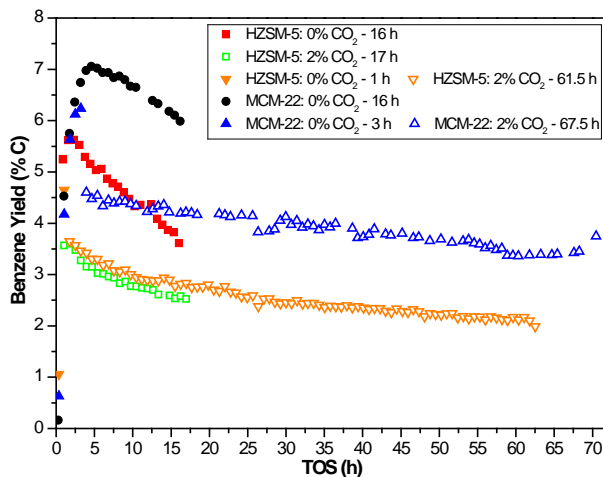


Figure 95. Effect of co-feeding 2% of CO_2 on the benzene yield versus the TOS of 6%Mo/HZSM-5 and 6%Mo/MCM-22 catalysts at 700 °C.

Regarding the accumulated benzene moles (Figure 96.a), the highest is obtained for the 6%Mo/MCM-22 catalyst without co-feeding CO_2 . However, the accumulated benzene moles are almost alike for the 6%Mo/MCM-22 catalyst tested by adding CO_2 and for the 6%Mo/HZSM-5 catalyst without co-feeding CO_2 . Moreover, between the experiments tested by adding CO_2 using the 6%Mo/HZSM-5 catalyst, the accumulated benzene moles are higher by co-feeding CO_2 after 1 h on stream without CO_2 .

Figure 96.b shows the effect of co-feeding 2% of CO_2 on the H_2 flow normalized per gram of catalyst. For the 6%Mo/HZSM-5 catalyst, the H_2 flow is higher and very similar for both experiments performed by adding CO_2 , being slightly higher by co-feeding CO_2 after 1 h on stream without CO_2 . Furthermore, for the 6%Mo/MCM-22 catalyst, the highest H_2 flow is obtained for the experiment performed by co-feeding 2% of CO_2 after 10 h on stream. This increment in the H_2 flow is in agreement with the previous thermodynamic study and it can be ascribed to the methane reforming reaction and the reverse Boudart reaction (Equation 11 and Equation 12), as it happens with the CO

formation. Moreover, this increment in the H_2 flow may be also detrimental for the performance of the MDA reaction due to the equilibrium shift that takes place.

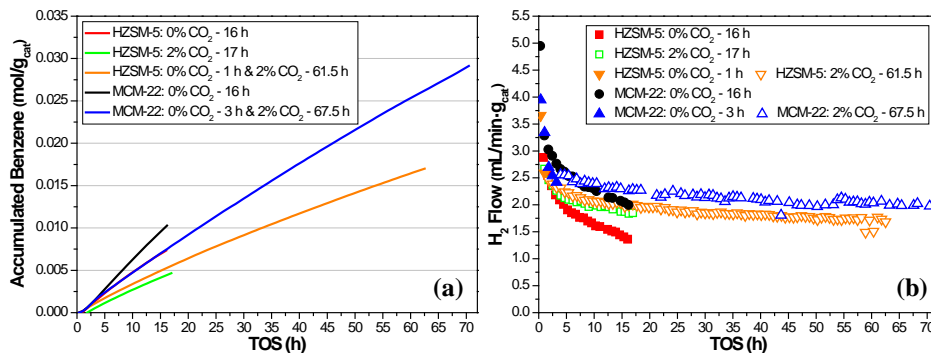


Figure 96. Effect of co-feeding 2% of CO_2 on the (a) accumulated benzene and (b) H_2 flow versus the TOS of 6%Mo/HZSM-5 and 6%Mo/MCM-22 catalysts.

Table 58 summarizes the TGA results for the spent catalysts with and without addition of CO_2 . For the 6%Mo/HZSM-5 catalyst, the highest amount of coke is obtained for the longest experiment, in which 2% of CO_2 was co-fed after 1 h on stream without CO_2 , being almost the double than for the catalyst tested without CO_2 . However, by focusing on the catalysts with a similar TOS (adding 0 and 2% of CO_2 since the beginning of the reaction), the amount of coke and the average coke formation rate are lower by adding 2% of CO_2 due to the methane reforming reaction (Equation 11), the reverse Boudart reaction (Equation 12) and the lower average methane conversion. Further, regarding the amount of coke ($g \cdot g_{cat}^{-1}$) per accumulated benzene mole, it is lower and alike for both catalysts tested co-feeding 2% of CO_2 . Thus, pointing out that the most effective coke suppression for the 6%Mo/HZSM-5 catalyst is achieved co-feeding 2% of CO_2 after 1 h on stream without CO_2 instead of since the beginning of the MDA reaction.

By focusing on the 6%Mo/MCM-22 catalyst, it can be said that the amount of coke is almost the same for both experiments, despite the longest

duration (~ 53.5 h) of the experiment by co-feeding 2% of CO₂. However, the amount of coke (g·g_{cat}⁻¹) per accumulated benzene mole for the catalyst with the addition of CO₂ is three times lower than for the catalyst without co-feeding CO₂. Therefore, these TGA results indicate that the coke removal by adding 2% of CO₂ using the 6%Mo/MCM-22 catalyst is slightly more effective than by using the 6%Mo/HZSM-5 catalyst.

Table 58. TGA results of spent 6%Mo/HZSM-5 and 6%Mo/MCM-22 catalysts without and with co-feeding 2% of CO₂.

Zeolite	CO ₂ co-fed (%)	TOS (h)	Average Coke Formation Rate (g·g _{cat} ⁻¹ ·h ⁻¹)	Amount of Coke (g·g _{cat} ⁻¹)	g·g _{cat} ⁻¹ ·mol _{benz.} ⁻¹
HZSM-5	0	16	0.0031	0.049	11
HZSM-5	2	17	0.0013	0.023	8
HZSM-5	0% 1 h & 2% 61.5 h	62.5	0.0013	0.080	8
MCM-22	0	17	0,0078	0,132	21
MCM-22	0% 3 h & 2% 67.5 h	70.5	0,0019	0,131	7

In addition, Figure 97 displays the CO_x profiles obtained by TPO technique and Table 59 details the TPO results. By focusing on the 6%Mo/HZSM-5 catalyst (Figure 97.a), for the catalyst tested by co-feeding 2% of CO₂ since the beginning of MDA reaction, the coke related to Mo species and the coke associated with Brønsted acid sites decrease with respect to the catalyst tested without CO₂, 56% and 44%, respectively. Nevertheless, for the catalyst tested by co-feeding 2% of CO₂ after 1 h on stream without CO₂ (~ 46.5 h longer), the coke associated with Mo species and the coke related to Brønsted acid sites increase with respect to the catalyst tested without CO₂, 36.3% and 47.7%, respectively. Furthermore, by comparing the TPO results of the 6%Mo/MCM-22 catalysts (Figure 97.b), it can be concluded that for the catalyst tested by co-feeding CO₂, the coke related to Mo species increases 8.5%, while the coke associated with Brønsted acid sites (aromatic-type carbon)

decreases roughly 51.7% with respect to the catalyst tested without CO₂. These TPO results are in agreement with the TGA results previously shown.

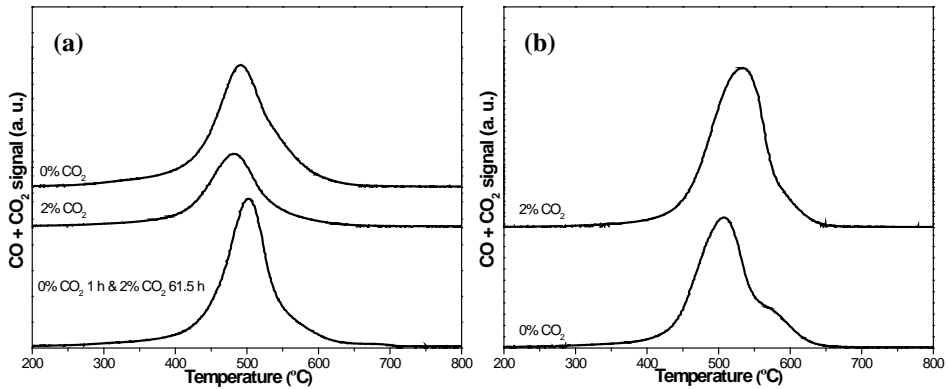


Figure 97. TPO profiles of carbon species over (a) 6%Mo/HZSM-5 and (b) 6%Mo/MCM-22 catalysts after MDA reaction without and with co-feeding 2% of CO₂. Same scale of Y-axis in each graph.

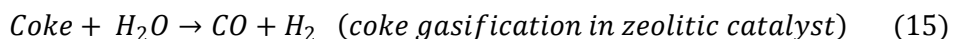
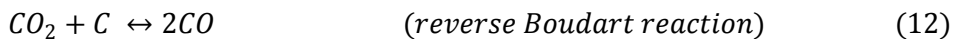
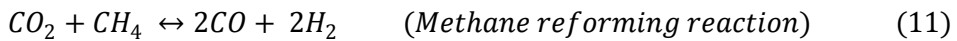
Finally, for the 6%Mo/HZSM-5 catalyst, the temperature at maximum of peak 1 (Table 59) is different for the three catalysts, even though the temperature at maximum of peak 2 is similar among them. This fact points out that the coke characteristics (particle size, morphology, etc.) may be slightly different among them [9]. Moreover, for the spent 6%Mo/MCM-22 catalysts the coke characteristics also may be different, since the temperature at maximum of both peaks is different for both catalysts [9], thus indicating that the co-feeding of CO₂ affects the coke characteristics. Further, it should be noted that for the longest experiments the temperature at maximum of both peaks is higher than for the shortest ones, as with the co-feeding of H₂O.

Table 59. Results of the deconvoluted TPO profiles of carbon species over 6%Mo/HZSM-5 catalysts with and without addition of 2% of CO₂.

Zeolite	CO ₂ co-fed (%)	TOS (h)	Temperature at maximum (°C)		Percentage (%)		Amount of coke (g·g _{cat} ⁻¹)	
			Peak 1	Peak 2	Peak 1	Peak 2	Peak 1	Peak 2
HZSM-5	0	16	491	576	81.63	18.37	0.0400	0.0090
HZSM-5	2	17	480	575	77.73	22.27	0.0176	0.0050
HZSM-5	0% 1 h & 2% 61.5 h	62.5	499	582	78.47	21.53	0.0628	0.0172
MCM-22	0	17	503	587	82.52	17.48	0.1093	0.0232
MCM-22	0% 3 h & 2% 67.2	70.5	527	616	91.44	8.56	0.1195	0.0112

7.4. Conclusions

The addition of H₂O, H₂ and CO₂ separately to the methane feed affects severely the performance of the MDA reaction, regardless of the employed catalyst, 6%Mo/HZSM-5 or 6%Mo/MCM-22. Thermodynamically, for the three cases, the MDA performance is adversely affected, since the methane reforming reaction (Equation 13) and the coke gasification (Equation 15) are favored by co-feeding H₂O. While, the methane reforming reaction (Equation 11) and the reverse Boudart reaction (Equation 12) are promoted by adding CO₂. Moreover, in these two cases, the co-feeding of H₂O [1, 5] and CO₂ [16], the catalysts are partially re-oxidized. However, the co-feeding of H₂ causes a sharp reduction of the methane conversion due to the equilibrium shift.



Firstly, the addition of 1.08, 0.9 and 0.86% of H₂O to the methane feed considerably improves the stability of the 6% Mo/HZSM-5 [1, 2] and 6%Mo/MCM-22 catalysts in MDA reaction, due to the H₂O reaction with the carbonaceous deposits by the methane reforming reaction and coke gasification. Concretely, by adding H₂O the methane conversion, the H₂ flow and the coke and CO selectivities are higher, while the aromatics selectivities are lower than in dry conditions. Therefore, the co-feeding of H₂O results in a worse MDA performance irrespective of the catalyst employed. This occurs not only because the methane reforming reaction and coke gasification are facilitated thermodynamically, but also because the catalysts in wet conditions suffer a partial re-oxidation, which was demonstrated by Liu et al. [1] for the 6% Mo/HZSM-5 by Mo K-edge XAFS studies and by Morejudo et al. [5] for the 6%Mo/MCM-22 catalyst by Mo K-edge XANES studies.

The time on stream at which the H₂O is added to the methane feed appears an important parameter for the MDA reaction, as the carburization of Mo species should be done in dry conditions. In consequence, for the 6%Mo/HZSM-5 catalyst the H₂O was added to the methane feed after 1 h on stream in dry conditions based on previous researches [1, 2]. However, for the 6%Mo/MCM-22 catalyst different times on stream in dry conditions were tested, reaching the best MDA performance for the experiment in which 1.08% of H₂O was co-fed after 3 h on stream in dry conditions. Further, by focusing on the experiments in which different H₂O vapor concentrations were added to the feed, for both the 6%Mo/HZSM-5 catalyst and the 6%Mo/MCM-22 catalyst, the best MDA performance was obtained for the experiments run with the lowest H₂O vapor concentration.

The methane conversion and CO selectivity reached experimentally are higher than those shown in the thermodynamic study. This fact may be attributed to the presence of coke deposits on the catalyst, which are not

included in that study, and to the formation of CO and H₂ by the coke gasification reaction (Equation 15). Moreover, the amount of coke (TGA) accumulated on both catalysts was reduced by co-feeding H₂O for the experiments with a similar TOS, with 0 and 1.08% of H₂O. Nevertheless, for these experiments the amount of coke (g·g_{cat}⁻¹) per accumulated benzene mole was higher for the catalysts tested with the addition of 1.08% of H₂O. Further, the N₂ sorption (BET surface area and micropore volume) and TPO results are in agreement with those obtained by TGA. Concretely, from TPO results it can be ascertained that the coke characteristics (particle size, morphology, etc.) may be different among the three 6%Mo/MCM-22 catalysts [9], tested by adding 0, 0.86 and 1.08% of H₂O, due to both the different duration of the experiments and the co-feeding of H₂O. For these three 6%Mo/MCM-22 catalysts, regarding the NH₃-TPD results obtained, it can be concluded that the amount of acid sites was lower for the three catalysts after testing MDA reaction, mainly for both catalysts tested in wet conditions. Additionally, the ²⁷Al MAS NMR spectra obtained for the 6%Mo/MCM-22 catalysts tested adding 0, 0.86 and 1.08% of H₂O reflect that the addition of these H₂O vapor concentrations to the feed is not detrimental for the framework aluminum.

Secondly, the stability of the 6% Mo/HZSM-5 and 6%Mo/MCM-22 catalysts in MDA reaction is slightly improved by co-feeding 6 and 10% of H₂ due to the suppression of coke formation. For both catalysts the addition of these contents of H₂ to the feed leads to a decrease of the methane conversion, H₂ flow and aromatics selectivities, and an increment of the C₂ and coke selectivities. Thus, the MDA performance is negatively affected by co-feeding 6 and 10% of H₂ because of the equilibrium shift that takes place, which reduces the methane conversion and the effectiveness of C₂ species oligomerization on the Brønsted acid sites of the zeolites to form aromatics. Moreover, for the 6%Mo/MCM-22 catalyst the best MDA performance obtained co-feeding 6% of H₂ was for the H₂ addition after 3 h on stream without H₂, with the new

activation of the catalyst and using higher amount of catalyst and feed gas flow. The TGA results are in concordance with those of TPO, that is to say, the co-feeding of 6 and 10% of H_2 causes a reduction on the amount of coke. In particular, from TPO results of 6%Mo/MCM-22 catalyst, it can be concluded that the addition of H_2 to the feed does not influence on the coke characteristics [9]. Further, the addition of 6% of H_2 to the methane feed reduces more efficiently the coke deposition on both the 6%Mo/HZSM-5 catalyst and the 6%Mo/MCM-22 catalyst, than by co-feeding 1.08% of H_2O . Concretely for the 6%Mo/MCM-22 catalyst, the coke related to the Brønsted acid sites is more successfully reduced, thus supporting the TPO results achieved by Ma et al. for the 6%Mo/HZSM-5 catalyst [2].

Furthermore, the methane conversion, the H_2 flow, the C_2 and aromatics yields (and selectivities) increase as the H_2 content co-fed decreases, from 20, 15, 10 to 5%, while the coke yield decreases. Besides the addition of these concentrations of H_2 , the co-feeding of 0.288% of H_2O leads to the obtaining of very similar methane conversion, C_2 and aromatics yields, however the coke yield exhibits the opposite trend. Moreover, CO is obtained by adding H_2O due to the methane reforming reaction and coke gasification. The TGA and TPO results indicate that both the co-feeding of H_2 and H_2O are beneficial for the reduction on the coke accumulation, besides the regeneration with pure H_2 suffered by the 6%Mo/MCM-22 catalyst. In addition, from the TPO results it can be inferred that the co-feeding of 0.288% of H_2O barely influences on the coke characteristics.

Finally, the addition of 2% of CO_2 to the feed improves the stability of the 6% Mo/HZSM-5 and 6%Mo/MCM-22 catalysts in MDA reaction because of the CO_2 reaction with the accumulated coke by the reverse Boudart reaction (Equation 12). For both catalysts, the methane conversion is slightly affected by co-feeding CO_2 , while the C_2 and aromatics selectivities are decreased, and the

H₂ flow, coke and CO selectivities are increased with respect to the experiment without CO₂. Thereby, the co-feeding of 2% of CO₂ is detrimental for the MDA performance, as on the one hand the methane reforming reaction and the reverse Boudart reaction are thermodynamically promoted and, on the other, the catalysts may suffer a partial re-oxidation [16]. The TGA and TPO results show that the addition of 2% of CO₂ to the feed decrease the amount of coke deposited on the catalysts and also per accumulated benzene mole, especially on the 6%Mo/MCM-22 catalyst. As with the addition of H₂O, from TPO results it can be assumed that the coke characteristics [9] may be affected by the addition of 2% of CO₂, due to both the different duration of the experiments and the co-feeding of CO₂.

For the three cases, the co-feeding of H₂O, H₂ and CO₂, the benzene and toluene selectivities achieved experimentally are higher than those exhibited in the thermodynamic results, whereas the naphthalene selectivity is lower. This is presumably ascribed to the shape selectivity of both catalysts, 6%Mo/HZSM-5 and 6%Mo/MCM-22.

7.5. References

- [1] S.L. Liu, R. Ohnishi, M. Ichikawa, *Journal of Catalysis*, 220 (2003) 57-65.
- [2] H.T. Ma, R. Kojima, S. Kikuchi, M. Ichikawa, *Catalysis Letters*, 104 (2005) 63-66.
- [3] P.M. Bijani, M. Sohrabi, S. Sahebdehfar, *Chemical Engineering & Technology*, 35 (2012) 1825-1832.
- [4] L.W. Li, M.R. Morrill, H. Shou, D.G. Barton, D. Ferrari, R.J. Davis, P.K. Agrawal, C.W. Jones, D.S. Sholl, *Journal of Physical Chemistry C*, 117 (2013) 2769-2773.
- [5] S.H. Morejudo, R. Zanon, S. Escolastico, I. Yuste-Tirados, H. Malerod-Fjeld, P.K. Vestre, W.G. Coors, A. Martinez, T. Norby, J.M. Serra, C. Kjolseth, *Science*, 353 (2016) 563-566.

- [6] C.D. Wagner, W.M. Riggs, L.E. Davis, J.F. Moulder, Handbook of X-ray Photoelectron Spectroscopy, First ed., Physical Electronics Division, Perkin-Elmer Corp., 1979.
- [7] K.S. Kim, W.E. Baitinger, J.W. Amy, N. Winograd, Journal of Electron Spectroscopy and Related Phenomena, 5 (1974) 351-367.
- [8] L. Ovari, J. Kiss, Vacuum, 80 (2005) 204-207.
- [9] C.A. Querini, S.C. Fung, Appl. Catal. A-Gen., 117 (1994) 53-74.
- [10] Y.Y. Shu, D. Ma, L.Y. Xu, Y.D. Xu, X.H. Bao, Catalysis Letters, 70 (2000) 67-73.
- [11] S. Unverricht, M. Hunger, S. Ernst, H.G. Karge, J. Weitkamp, ZEOLITE MCM-22 - SYNTHESIS, DEALUMINATION AND STRUCTURAL CHARACTERIZATION, 1994.
- [12] D. Ma, Y.Y. Shu, X.W. Han, X.M. Liu, Y.D. Xu, X.H. Bao, Journal of Physical Chemistry B, 105 (2001) 1786-1793.
- [13] J.Z. Zhang, M.A. Long, R.F. Howe, Catal. Today, 44 (1998) 293-300.
- [14] R.H. Meinhold, D.M. Bibby, Zeolites, 10 (1990) 146-150.
- [15] O.H. Han, C.Y. Lin, G.L. Haller, Catalysis Letters, 14 (1992) 1-9.
- [16] Z. Liu, M.A. Nutt, E. Iglesia, Catalysis Letters, 81 (2002) 271-279.
- [17] H.T. Ma, R. Ohnishi, M. Ichikawa, Catalysis Letters, 89 (2003) 143-146.
- [18] D. Ma, D.Z. Wang, L.L. Su, Y.Y. Shu, Y. Xu, X.H. Bao, Journal of Catalysis, 208 (2002) 260-269.
- [19] R. Ohnishi, S.T. Liu, Q. Dong, L. Wang, M. Ichikawa, Journal of Catalysis, 182 (1999) 92-103.
- [20] Y.Y. Shu, R. Ohnishi, M. Ichikawa, Journal of Catalysis, 206 (2002) 134-142.

Chapter 8.

EFFECT OF CATALYST REGENERATION WITH H₂ ON MDA REACTION

8. Effect of catalyst regeneration with H₂ on MDA reaction

The regeneration of the spent catalysts after MDA reaction was carried out using pure H₂ since the activity of the catalyst was almost entirely restored [1] (as abovementioned in the section 2.5.2.). This is attributed to the reduction of the coke deposited on both the Mo sites and the Brønsted acid sites of the zeolite, due to the H₂ reaction with carbonaceous deposits [2-4].

The experiments in which the catalyst was regenerated were carried out according to the procedure described in the section 3.6.1.2.3., with standard activation of the catalysts. The catalysts were prepared using the HZSM-5 and MCM-22 zeolites (Si/Al=15) impregnated with a 6% (wt.) of Mo.

8.1. Effect of the 6%Mo/HZSM-5 catalyst regeneration with H₂

The effect of the 6%Mo/HZSM-5 catalyst regeneration with pure H₂ was studied whether in dry conditions or in wet conditions (1.08% of H₂O).

8.1.1. Effect of the 6%Mo/HZSM-5 catalyst regeneration with H₂ in dry conditions

The catalyst regeneration with pure H₂ took place after 19.70 h of MDA reaction. Figure 98 depicts the effect of catalyst regeneration on the methane conversion and the H₂ flow normalized per gram of catalyst. The catalytic activity is totally restored after the regeneration with pure H₂, since both the methane conversion (Figure 98.a) and the H₂ flow (Figure 98.b) rise after this, reaching almost the first values.

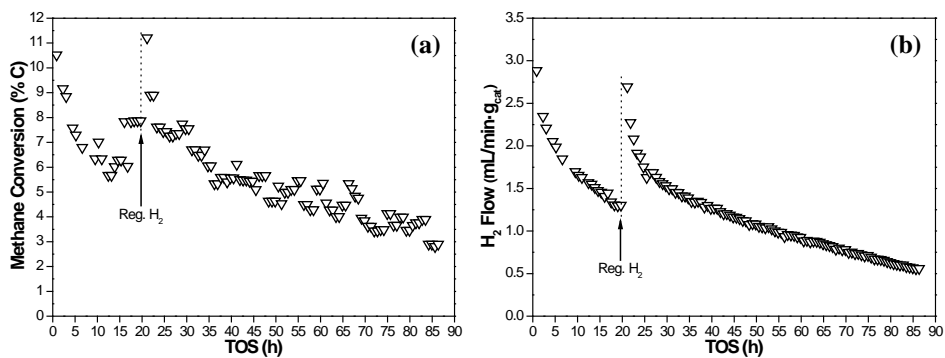


Figure 98. Effect of the 6%Mo/HZSM-5 catalyst regeneration with H₂ in dry conditions on the (a) methane conversion and (b) H₂ flow versus the TOS.

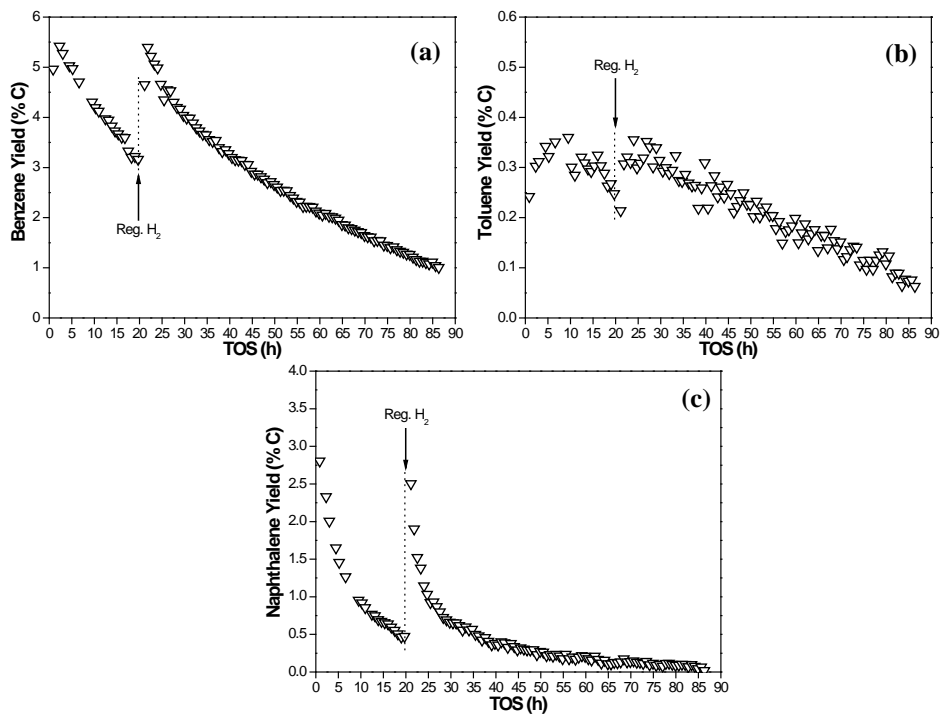


Figure 99. Effect of the 6%Mo/HZSM-5 catalyst regeneration with H₂ in dry conditions on the (a) benzene, (b) toluene and (c) naphthalene yields versus the TOS at 700 °C.

As with the methane conversion and H₂ flow, the benzene, toluene and naphthalene yields are almost completely reestablished after the catalyst regeneration with H₂ (Figure 99). Moreover, the benzene yield (Figure 99.a) decreases a little more slowly than before the catalyst regeneration. Nonetheless, the decays of the toluene (Figure 99.b) and naphthalene (Figure 99.c) yields follow practically the same trend than before the regeneration with H₂.

In addition, Figure 100 illustrates the effect of catalyst regeneration with pure H₂ on the C₂ and coke yields. The C₂ yield (Figure 100.a) after the catalyst regeneration suffers a drop up to its first values and then increases more quickly than before it, until the 35th h on stream, reaching a plateau around 0.6% for 20 h, and from which the C₂ yield decreases slightly. In the same way, the coke yield (Figure 100.b) after the catalyst regeneration decreases almost up to its starting values, thus rising slightly slower than before it.

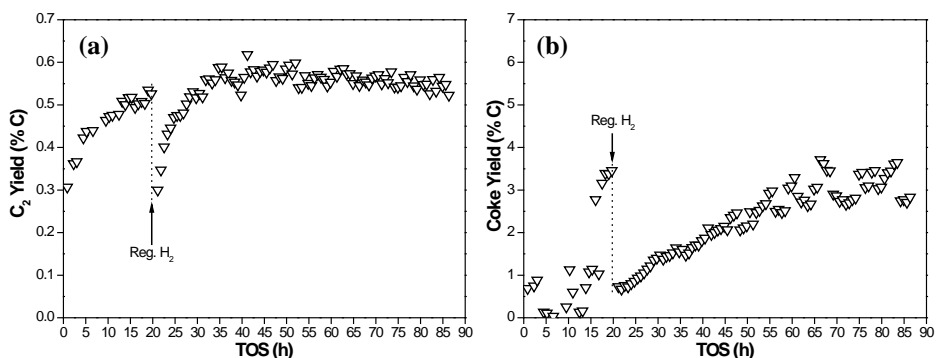


Figure 100. Effect of the 6%Mo/HZSM-5 catalyst regeneration with H₂ in dry conditions on the (a) C₂ and (b) coke yields versus the TOS at 700 °C.

The amount of coke obtained by TGA for the spent 6%Mo/HZSM-5 catalyst after 86.4 h of MDA reaction in dry conditions is detailed in Table 60.

Table 60. TGA results of spent 6%Mo/HZSM-5 catalyst subjected to a regeneration with pure H₂ after 19.70 h on stream in dry conditions.

TOS (h)	Average Coke Formation Rate (g·g _{cat} ⁻¹ ·h ⁻¹)	Amount of Coke (g·g _{cat} ⁻¹)	g·g _{cat} ⁻¹ ·mol _{benz.} ⁻¹
86.4	0.0013	0.108	7

8.1.2. Effect of the 6%Mo/HZSM-5 catalyst regeneration with H₂ in wet conditions

After 1 h of MDA reaction in dry conditions the feed gas mixture (CH₄:N₂, 9.5:0.5 vol. ratio) was introduced in the bubbler with the saturated aqueous solution of potassium carbonate, achieving a H₂O vapor concentration of 1.08%. The catalyst regeneration with pure H₂ was done after 38.70 h on stream in wet conditions, though the regeneration was carried out exclusively in dry conditions.

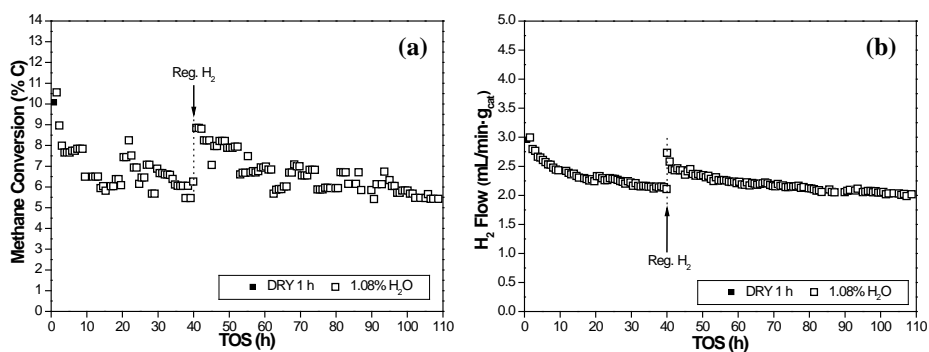


Figure 101. Effect of the 6%Mo/HZSM-5 catalyst regeneration with H₂ in wet conditions on the (a) methane conversion and (b) H₂ flow versus the TOS.

Figure 101 displays the effect of catalyst regeneration on the methane conversion and the H₂ flow normalized per gram of catalyst. After the catalyst regeneration the methane conversion (Figure 101.a) increases up to its first values in wet conditions. Nevertheless, the H₂ flow (Figure 101.b) is not totally

restored after the regeneration, but it is greatly stabilized throughout the time on stream.

Figure 102 shows the effect of catalyst regeneration on the aromatics yields separately. Concretely, the benzene yield (Figure 102.a) is not fully reestablished after the catalyst regeneration, but it is stabilized around 2.5%, almost as before the regeneration. In addition, for the toluene (Figure 102.b) and naphthalene (Figure 102.c) yields the same trend is observed, although the latter slightly decreases throughout the time on stream.

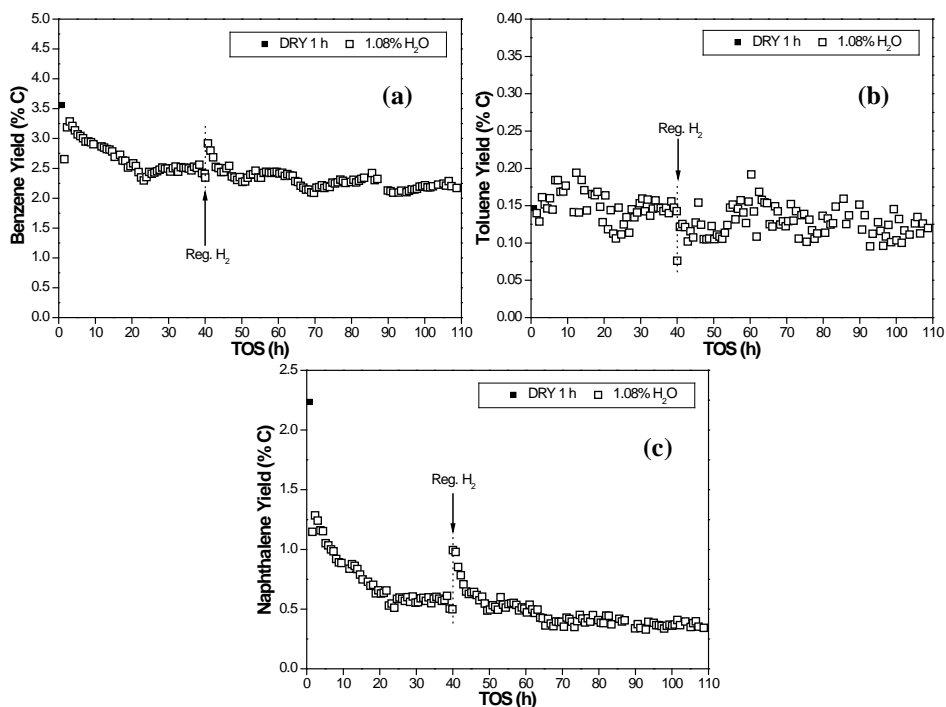


Figure 102. Effect of the 6%Mo/HZSM-5 catalyst regeneration with H_2 in wet conditions on the (a) benzene, (b) toluene and (c) naphthalene yields versus the TOS at 700 °C.

Figure 103 depicts the effect of catalyst regeneration on the C_2 and coke yields in wet conditions. After the catalyst regeneration the C_2 yield (Figure

103.a) decreases, but after that increasing slowly over time. However, the coke yield (Figure 103.b) is very scattered and therefore the catalyst regeneration is barely noticeable.

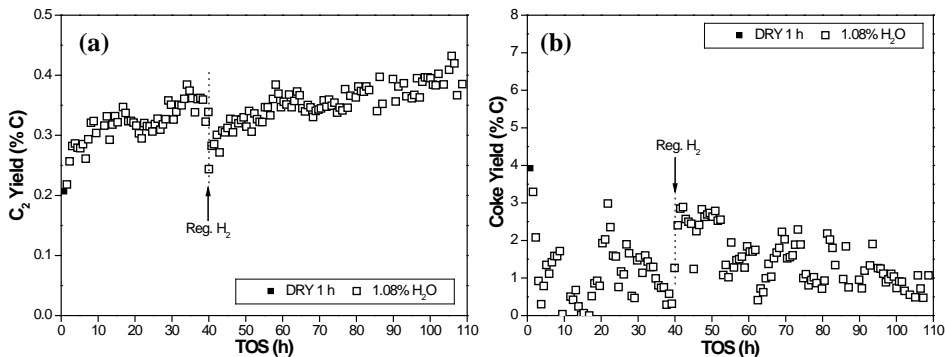


Figure 103. Effect of the 6%Mo/HZSM-5 catalyst regeneration with H_2 in wet conditions on the (a) C_2 and (b) coke yields versus the TOS at 700 °C.

The TGA results for the spent 6%Mo/HZSM-5 catalyst after 107.7 h of MDA reaction in wet conditions are summarized in Table 61.

Table 61. TGA results of spent 6%Mo/HZSM-5 catalyst subjected to a regeneration with pure H_2 after 38.7 h on stream in wet conditions.

Total TOS (h)	Average Coke Formation Rate ($g \cdot g_{cat}^{-1} \cdot h^{-1}$)	Amount of Coke ($g \cdot g_{cat}^{-1}$)	$g \cdot g_{cat}^{-1} \cdot mol_{benz.}^{-1}$
108.7	0.0004	0.042	3

By comparing these TGA results with those obtained in dry conditions (section 8.1.1.), it can be observed that the amount of coke deposited on the catalyst tested by co-feeding 1.08% of H_2O is much lower than on the catalyst used in dry conditions, despite the former is 22.3 h longer. As with the amount of coke ($g \cdot g_{cat}^{-1}$) per accumulated benzene mole, which is lower for the catalyst tested by adding H_2O to the methane feed. This lower coke accumulation is ascribed to the co-feeding of 1.08% of H_2O , because of the H_2O reaction with

the carbonaceous deposits by the methane reforming reaction and coke gasification [2, 5], as stated above in the section 7.1.

8.2. Effect of the 6%Mo/MCM-22 catalyst regeneration with H_2 in dry conditions

Based on the good MDA performance of the 6%Mo/HZSM-5 catalyst after the regeneration with pure H_2 in dry conditions, the 6%Mo/MCM-22 catalyst was also regenerated. In this case, two regenerations with pure H_2 were done at different times on stream in the same experiment. The first regeneration took place after 24.3 h on stream and the second 22 h after the first regeneration. Figure 104 illustrates the effect of catalyst regeneration on the methane conversion and the H_2 flow normalized per gram of catalyst. The methane conversion (Figure 104.a) increases after each regeneration but without reaching its first values. As with the H_2 flow (Figure 104.b), since it is not totally restored after each regeneration.

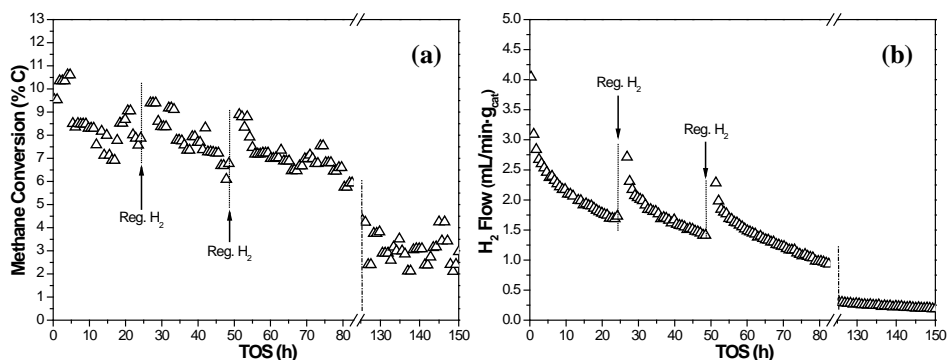


Figure 104. Effect of the 6%Mo/MCM-22 catalyst regeneration with H_2 in dry conditions on the (a) methane conversion and (b) H_2 flow versus the TOS.

The trend observed in Figure 104 is confirmed in Figure 105, i. e., the benzene (Figure 105.a), toluene (Figure 105.b) and naphthalene yields (Figure 105.c) are not entirely reestablished after the different regenerations carried out.

In particular, it should be noted that after the second catalyst regeneration the benzene yield is lower than that obtained just after the first regeneration. This behavior is indicative that for the 6%Mo/MCM-22 catalyst the activity is worse regenerated than for the 6%Mo/HZSM-5 catalyst (Figure 99.a), especially for longer times on stream.

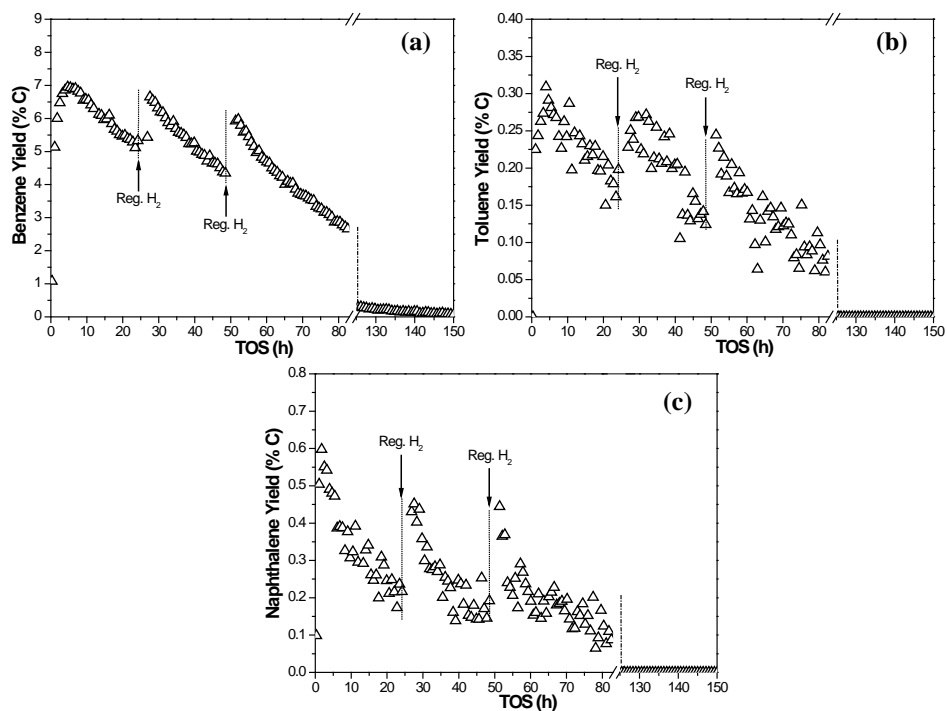


Figure 105. Effect of the 6%Mo/MCM-22 catalyst regeneration with H₂ in dry conditions on the (a) benzene, (b) toluene and (c) naphthalene yields versus the TOS at 700 °C.

Figure 106 shows the effect of catalyst regeneration on the C₂ and coke yields. Both the C₂ yield and the coke yield are scattered and therefore the effect of catalyst regeneration is barely perceptible. Concretely, the C₂ yield appears unchanging after the regenerations that the catalyst suffered by comparing with its starting values.

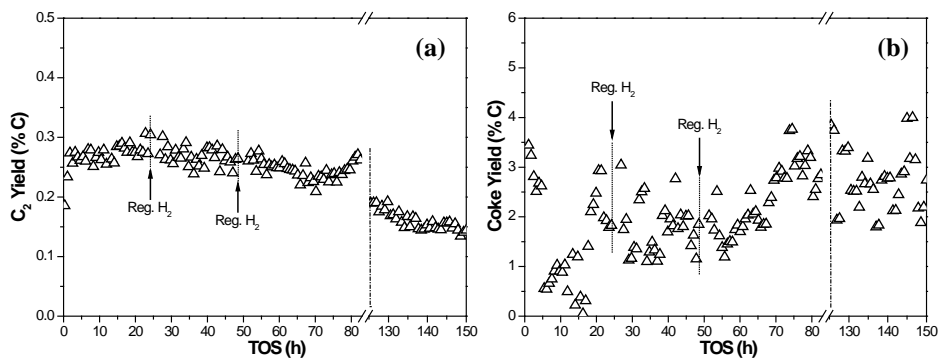


Figure 106. Effect of the 6%Mo/MCM-22 catalyst regeneration with H₂ in dry conditions on the (a) C₂ and (b) coke yields versus the TOS at 700 °C.

In this experiment, it can be observed that after 125 h on stream practically only C₂ hydrocarbons, coke and H₂ are produced in this experiment. Thus, indicating that the 6%Mo/MCM-22 catalyst is almost totally deactivated for the MDA reaction.

Moreover, the TGA results for the spent 6%Mo/MCM-22 catalyst after 159.4 h of MDA reaction in dry conditions, with two regenerations using pure H₂ at 24.3 and 46.3 h, are detailed in Table 62. As abovementioned, this catalyst accumulates much more coke than the 6%Mo/HZSM-5 catalyst. In addition, this experiment is ca. 73 h longer than the experiment carried out using the 6%Mo/HZSM-5 catalyst, about 34.4 h of which the catalyst was deactivated.

Table 62. TGA results of spent 6%Mo/MCM-22 catalyst after two regenerations with pure H₂ after 24.3 and 46.3 h on stream in dry conditions.

Total TOS (h)	Average Coke Formation Rate (g·g _{cat} ⁻¹ ·h ⁻¹)	Amount of Coke (g·g _{cat} ⁻¹)	g·g _{cat} ⁻¹ ·mol _{benz.} ⁻¹
159.4	0.0017	0.273	10

8.3. Conclusions

The catalyst regeneration with pure H₂ was very effective for the 6%Mo/HZSM-5 catalyst after 19.7 h of MDA reaction in dry conditions. Nevertheless, the effectiveness of the 6%Mo/HZSM-5 catalyst regeneration with H₂ in wet conditions was lower than in dry conditions, thus reflecting these results the partial re-oxidation of the Mo species on the catalyst.

Moreover, the catalyst regeneration with pure H₂ was also successful for the 6%Mo/MCM-22 catalyst in the MDA reaction in dry conditions. Although in lesser extent than for the 6%Mo/HZSM-5 catalyst, which may be attributed to the longer time on stream at which the regeneration was done in this experiment, almost 5 h. Furthermore, the second cycle of regeneration with H₂ was less effective than the first, despite taking place in a shorter time, thus indicating that the type of coke deposited may be more difficult to remove by the H₂.

8.4. References

- [1] D. Ma, D.Z. Wang, L.L. Su, Y.Y. Shu, Y. Xu, X.H. Bao, *Journal of Catalysis*, 208 (2002) 260-269.
- [2] H.T. Ma, R. Kojima, S. Kikuchi, M. Ichikawa, *Catalysis Letters*, 104 (2005) 63-66.
- [3] Z. Liu, M.A. Nutt, E. Iglesia, *Catalysis Letters*, 81 (2002) 271-279.
- [4] H.T. Ma, R. Ohnishi, M. Ichikawa, *Catalysis Letters*, 89 (2003) 143-146.
- [5] S.L. Liu, R. Ohnishi, M. Ichikawa, *Journal of Catalysis*, 220 (2003) 57-65.

Chapter 9.

EFFECT OF THE CATALYST MANUFACTURING PROCESS ON MDA REACTION

9. Effect of the catalyst manufacturing process on MDA reaction

9.1. Granulated catalysts obtained by different procedures: 6%Mo/HZSM-5 and 6%Mo/MCM-22

A new catalyst manufacturing process described in the U.S. patent [1] was employed aiming to improve the catalyst properties. The catalysts prepared using this procedure were coded like “Extrudated I”, with the HZSM-5 and the MCM-22 zeolites (Si/Al=15), as detailed in section 3.3.2.1. In this case the code refers to an intermediate step of the manufacturing process, since these catalysts were tested in granulated form after crushing and sieving the extrudates initially obtained. However, the catalysts coded like “Granulated” were prepared by the standard procedure (section 3.3.1.), using also the HZSM-5 and the MCM-22 zeolites (Si/Al=15). The experiments were carried out according to the procedure described in the section 3.6.1.1., with the standard activation of the catalysts.

In the following table the methane conversion and the selectivity to main products after 9 h on stream, at 700 °C, 1.2 bar and $1500 \text{ mL} \cdot \text{h}^{-1} \cdot \text{g}_{\text{cat}}^{-1}$, are shown. For both catalysts the methane conversion is lower for the Extrudated I catalysts. However, toluene and C₂ selectivities are slightly higher for the Extrudated I catalysts. Nonetheless, by focusing on the benzene selectivity the results obtained for both catalysts are opposite, that is, for the 6%Mo/MCM-22 catalyst Extrudated I the benzene selectivity is higher than for the Granulated, while for the 6%Mo/HZSM-5 catalyst Extrudated I it is slightly lower than for the Granulated. On the contrary, the coke selectivity for the 6%Mo/MCM-22 catalyst is lower for the Extrudated I, whereas for the 6%Mo/HZSM-5 catalyst

is higher for the Extrudated I than for the Granulated. Moreover, the naphthalene selectivity is lower for both Extrudated I catalysts.

Table 63. Effect of the catalyst manufacturing process on the methane conversion and the selectivity to main products after 9 h on stream of 6%Mo/HZSM-5 and 6%Mo/MCM-22 catalysts.

Zeolite	Code	CH ₄ Conversion (% C)	Selectivity (% C)				
			C ₆ H ₆	C ₂	C ₇ H ₈	C ₁₀ H ₈	Coke
HZSM-5	Granulated	6.66	67.15	7.12	5.03	16.44	4.25
HZSM-5	Extrudated I	6.00	66.77	8.37	5.70	11.91	7.25
MCM-22	Granulated	8.12	82.12	3.29	3.68	5.26	5.66
MCM-22	Extrudated I	7.55	84.88	3.70	4.85	4.07	2.51

Figure 107 displays the effect of the catalyst manufacturing process on the benzene yield for the 6%Mo/HZSM-5 and 6%Mo/MCM-22 catalysts. By comparing each catalyst separately, for the 6%Mo/HZSM-5 catalyst the highest benzene yield is obtained with the catalyst manufactured by the standard procedure (Granulated) throughout the time on stream. While for the 6%Mo/MCM-22 catalyst, the benzene yield is higher for the catalyst manufactured by the new procedure (Extrudated I) until the 4th h on stream, from which it is lower.

Furthermore, it should be indicated that for the 6%Mo/HZSM-5 catalyst, the stability is barely improved. Nevertheless, the benzene yield obtained for the 6%Mo/MCM-22 catalyst is slightly more stable for the catalyst produced by the standard procedure (Granulated), showing a 1.5-fold decrease in the average deactivation rate with respect to the catalyst manufactured by the new procedure (Extrudated I).

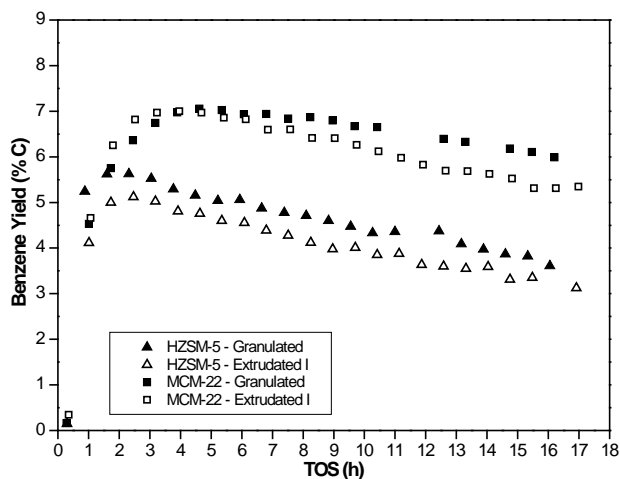


Figure 107. Effect of the catalyst manufacturing process on the benzene yield versus the TOS of 6%Mo/HZSM-5 and 6%Mo/MCM-22 catalysts at 700 °C.

Figure 108 depicts the effect of the catalyst manufacturing process on the accumulated benzene moles and the H_2 flow both normalized per gram of catalyst for the Granulated catalysts, and per gram of zeolite for the Extrudated I catalysts, since in the latter the Si-containing binder (Silres) left a silica-like residue that was necessary to correct. The accumulated benzene moles (Figure 108.a) achieved for the 6%Mo/HZSM-5 catalysts are higher using the Granulated catalyst, thus confirming that the best MDA performance is obtained with this one. However, for the 6%Mo/MCM-22 catalysts, the accumulated benzene moles are slightly higher for the Extrudated I catalyst. Although for the 6%Mo/HZSM-5 catalyst the accumulated benzene moles tend to separate over time, for the 6%Mo/MCM-22 catalyst these appear that will cross with time on stream, thus reversing the results. Therefore, for the 6%Mo/MCM-22 catalysts it is intricate to determine with which catalyst the MDA performance is improved.

Moreover, the H_2 flow is almost the same for both 6%Mo/HZSM-5 catalysts over time. Nonetheless, the H_2 flow is higher for the 6%Mo/MCM-22

catalyst obtained by the standard procedure (Granulated) throughout the time on stream. For both catalysts these results may be ascribed to the methane conversion behavior.

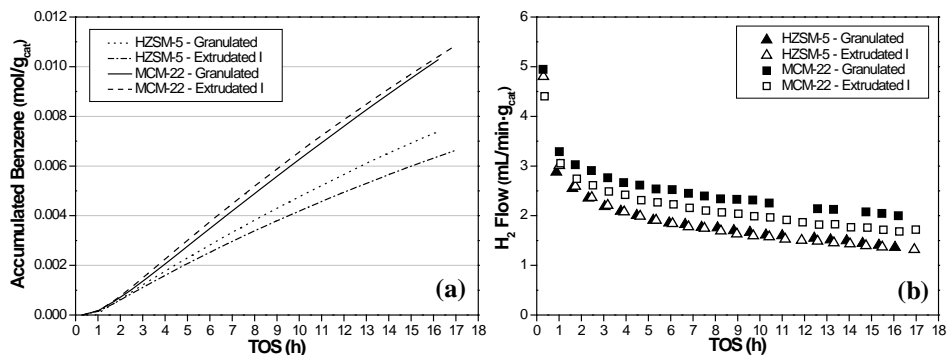


Figure 108. Effect of the catalyst manufacturing process on the (a) accumulated benzene moles and (b) H₂ flow versus the TOS of 6%Mo/HZSM-5 and 6%Mo/MCM-22 catalysts at 700 °C.

Table 64. TGA results of spent 6%Mo/HZSM-5 and 6%Mo/MCM-22 catalysts produced using the standard (Granulated) and the new (Extrudated I) procedure.

Zeolite	Code	TOS (h)	Average Coke Formation Rate (g·g _{cat} ⁻¹ ·h ⁻¹)	Amount of Coke (g·g _{cat} ⁻¹)	g·g _{cat} ⁻¹ ·mol _{benz.} ⁻¹
HZSM-5	Granulated	16	0.0031	0.049	11
HZSM-5	Extrudated I	17	0.0036	0.061	15
MCM-22	Granulated	17	0.0078	0.132	21
MCM-22	Extrudated I	17	0.0045	0.077	12

The TGA results obtained for the spent catalysts using the standard (Granulated) and the new (Extrudated I) manufacturing procedure are summarized in Table 64. The TGA results are opposite for each catalyst, since for the 6%Mo/HZSM-5 catalysts the amount of coke, the average coke formation rate and the amount of coke (g·g_{cat}⁻¹) per accumulated benzene mole

are higher for the catalyst manufactured by the new procedure (Extrudated I). While for the 6%Mo/MCM-22 catalysts these parameters are lower for the Extrudated I catalyst. Hence, the new catalyst manufacturing process affects in a different way the coke accumulation on both catalysts.

In the following figure the CO_x profiles obtained by TPO technique are illustrated and the results are shown in Table 65. For the 6%Mo/HZSM-5 catalyst (Figure 109.a) manufactured by the new procedure (Extrudated I), it can be concluded that the coke associated with Mo species decreases roughly 11% and the coke related to Brønsted acid sites (aromatic-type carbon) rises around 64% with respect to the Granulated (standard procedure). While by focusing on the 6%Mo/MCM-22 catalysts (Figure 109.b), for the Extrudated I the coke related to Mo species and with Brønsted acid sites are reduced ca. 47% and 15%, respectively, with respect to the Granulated. These TPO results are in agreement with the TGA results abovementioned.

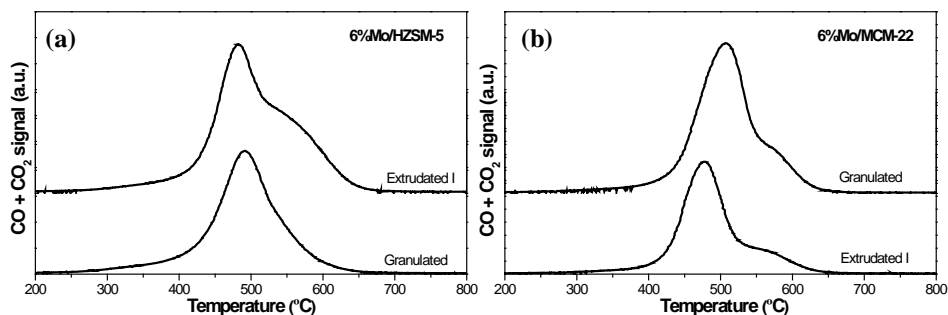


Figure 109. TPO profiles of carbon species over (a) 6%Mo/HZSM-5 and (b) 6%Mo/MCM-22 catalysts after MDA, produced using the standard (Granulated) and the new (Extrudated I) procedure. Same scale of Y-axis.

Moreover, for both the 6%Mo/HZSM-5 and 6%Mo/MCM-22 catalysts, the temperature at maximum of both peaks (Table 65) for the catalysts manufactured by the standard procedure (Granulated) is higher than for the catalysts manufactured by the new procedure (Extrudated I), especially for the

6%Mo/MCM-22 catalyst. Therefore the coke characteristics (particle size, morphology, etc.) are likely different between both catalysts depending on the type of manufacturing process used [2].

Table 65. Results of the deconvoluted TPO profiles of carbon species over 6%Mo/HZSM-5 and 6%Mo/MCM-22 catalysts produced using the standard (Granulated) and the new (Extrudated I) procedure.

Zeolite	Code	TOS (h)	Temperature at maximum (°C)		Percentage (%)		Amount of coke (g·g _{cat} ⁻¹)	
			Peak 1	Peak 2	Peak 1	Peak 2	Peak 1	Peak 2
HZSM-5	Granulated	16	491	576	81.63	18.37	0.0400	0.0090
HZSM-5	Extrudated I	17	480	560	58.93	41.07	0.0357	0.0249
MCM-22	Granulated	17	503	587	82.52	17.48	0.1093	0.0232
MCM-22	Extrudated I	17	475	561	74.58	25.42	0.0575	0.0196

The NH₃-TPD profiles of the 6%Mo/HZSM-5 and 6%Mo/MCM-22 catalysts are depicted in Figure 110, in order to know the extent in which the acidity of the catalysts is affected by the manufacturing process. It is known that the NH₃-TPD profile of the 6%Mo/HZSM-5 catalyst can be deconvoluted into three peaks [3, 4], a peak at high temperature that is attributed to the desorption of NH₃ adsorbed on the acidic hydroxide group $\equiv\text{Si}-\text{OH}-\text{Al}\equiv$, that is, Brønsted acid sites; a peak at low temperature that is assigned to the desorption of the NH₃ adsorbed on weak acid sites; and a peak at medium temperature that is attributed to the desorption of NH₃ adsorbed on acid sites of medium strength. Moreover, it should be noted that for the parent HZSM-5 zeolite only the peaks corresponding to weak (low temperature) and Brønsted (high temperature) acid sites can be observed in the NH₃-TPD profile, and after the Mo incorporation to the HZSM-5 zeolite, the peak corresponding to the medium acid sites appears, decreasing the other both acid sites, but mainly the Brønsted acid sites.

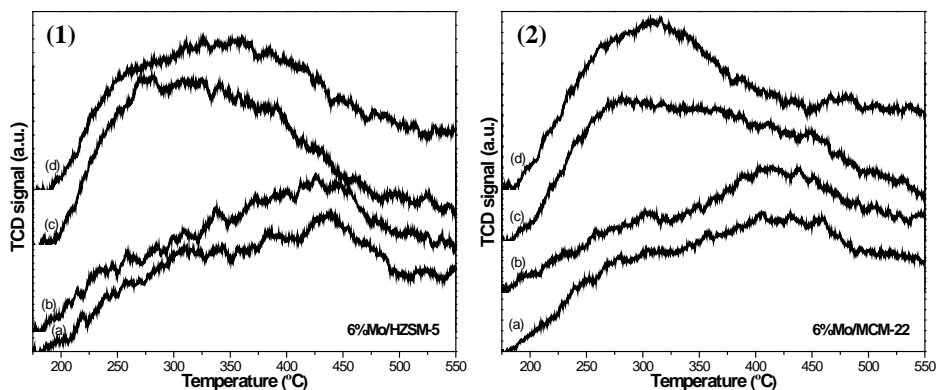


Figure 110. NH_3 -TPD profiles of (1) 6%Mo/HZSM-5 and (2) 6%Mo/MCM-22 catalysts: Granulated (a) after and (c) before MDA reaction; and Extruded I (b) after and (d) before MDA reaction. Same scale of Y-axis.

Concretely, Figure 110.1 exhibits the NH_3 -TPD profiles of 6%Mo/HZSM-5 catalysts manufactured by the standard and the new procedure, before and after MDA reaction. The amount of acid sites was lower for both spent catalysts, being those at low and medium temperature which mainly decreased, obtaining a NH_3 -TPD profile with a TCD signal very similar for the spent Granulated (Figure 110.1.a) and Extruded I (Figure 110.1.b) catalysts. Nonetheless, by focusing on the fresh catalysts, the Granulated (Figure 110.1.c) shows higher amount of weak and medium acid sites and lower amount of Brønsted acid sites than the Extruded I catalyst (Figure 110.1.d).

Furthermore, for the 6%Mo/MCM-22 catalysts (Figure 110.2), as stated above, the NH_3 -TPD profiles can be deconvoluted into three peaks [5, 6]. Briefly, the peak at low temperature corresponds to non-exchangeable cationic sites, the peak at medium temperature to Brønsted acid sites and the peak at high temperatures to Lewis acid sites. The fresh Granulated catalyst (Figure 110.2.c) exhibits slightly higher amount of Brønsted and Lewis acid sites than the fresh Extruded I (Figure 110.2.d). However, the spent catalysts show lower amount of acid sites than the fresh ones, especially those at low and

medium temperature. In addition, the spent Granulated catalyst (Figure 110.2.a) shows slightly higher amount of acid sites than the Extrudated I (Figure 110.2.b).

Moreover, the NH_3 uptake at 175 °C and the maximum temperature (T_{max}) are detailed in Table 66. By focusing on the 6%Mo/HZSM-5 catalysts, the acidity is lower for the catalysts produced by the new procedure (Extrudated I). Nevertheless, for the fresh 6%Mo/MCM-22 catalysts the acidity was slightly higher for the Extrudated I, unlike for the spent catalysts. Further, for the 6%Mo/HZSM-5 Extrudated I catalyst the acid strength distribution is slightly more similar for both the fresh and the spent catalysts than for the Granulated, owing to the lower difference between the maximum temperatures, as with the 6%Mo/MCM-22 catalysts.

Table 66. Acidity of 6%Mo/HZSM-5 and 6%Mo/MCM-22 catalysts before (fresh) and after (spent) MDA reaction using the standard (Granulated) and the new (Extrudated I) procedure determined by NH_3 -TPD.

Catalyst	Code	NH_3 - uptake ($\mu\text{mol/g}$)	T_{max} (°C)
6%Mo/HZSM-5 Fresh	Granulated	470.96	281
6%Mo/HZSM-5 Fresh	Extrudated I	393.33	326
6%Mo/HZSM-5 Spent	Granulated	342.88	436
6%Mo/HZSM-5 Spent	Extrudated I	303.25	426
6%Mo/MCM-22 Fresh	Granulated	526.07	281
6%Mo/MCM-22 Fresh	Extrudated I	547.47	315
6%Mo/MCM-22 Spent	Granulated	398.30	406
6%Mo/MCM-22 Spent	Extrudated I	282.62	404

9.2. Extrudated catalyst obtained by a new procedure: 6%Mo/MCM-22

A new catalyst manufacturing process was implemented aiming to improve the catalyst properties, this process was based on the U.S. patent [1]. The catalyst coded like “Extrudated II” was prepared using this new procedure with the MCM-22 zeolite, as described in the section 3.3.2.2. The manufacturing processes of the Extrudated II and the Extrudated I catalysts differ for the former in: (i) the different moment at which the Mo is incorporated to the zeolite, (ii) the addition of an emulsifier to facilitate the catalyst extrusion, (iii) the reduction of the catalyst calcination steps from 2 to 1, and (iv) the suppression of the shaped of the catalyst in granules, since the catalyst was used as extrudated with a particle size ≤ 1 cm. The catalyst coded like “Granulated” was prepared by the standard procedure (section 3.3.1.). The experiments were carried out according to the procedure described in the section 3.6.2.2.1. with the pre-carburization and pre-reduction of the catalysts.

Table 67 summarizes the selectivity to main products after 9 h on stream at 700 °C, 1.2 bar and $1500 \text{ mL}\cdot\text{h}^{-1}\cdot\text{g}_{\text{cat}}^{-1}$. The highest C_2 and aromatics selectivities are achieved for the Granulated catalyst. However, the highest coke selectivity is obtained for the Extrudated II catalyst, being almost three times higher than for the Granulated. It should be noted that the toluene and naphthalene were not detected over time for the Extrudated II experiment.

Table 67. Effect of the new catalyst manufacturing process on the selectivity to main products after 9 h on stream of 6%Mo/MCM-22 catalysts.

Code	Selectivity (% C)				
	C_6H_6	C_2	C_7H_8	C_{10}H_8	Coke
Granulated	69.83	2.13	2.83	3.78	21.43
Extrudated II	39.61	1.36	0.00	0.00	59.03

Figure 111 displays the effect of the new manufacturing process on the methane conversion and the benzene yield. Both the methane conversion (Figure 111.a) and the benzene yield (Figure 111.b) are rather high for the Granulated catalyst over time, especially the benzene yield. Hence, these results show that the internal diffusion effects are important [7].

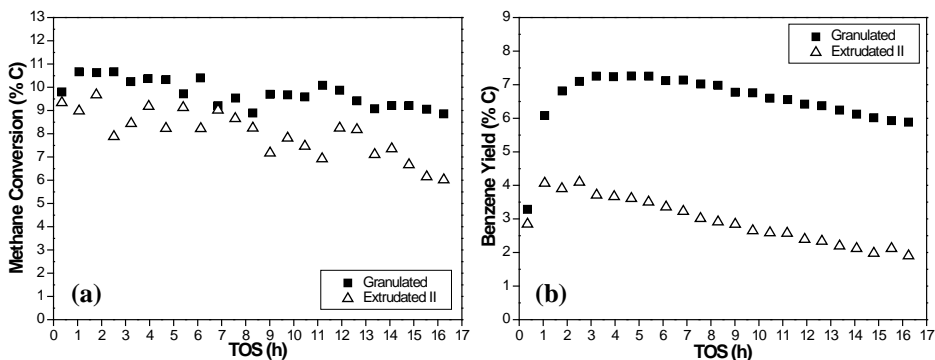


Figure 111. Effect of the new catalyst manufacturing process on the (a) methane conversion and (b) benzene yield versus the TOS of 6%Mo/MCM-22 catalyst at 700 °C.

The internal diffusion influence may be ascribed to the large size of the catalyst particles or the small pore size of the zeolite. In this case, the latter can be excluded since the pore size of the zeolite MCM-22 (section 3.2.2.) is higher than the kinetic diameter of the methane (3.8 Å [8]). However, the size of the Extrudated II particles (≤ 1 cm) is almost two orders of magnitude greater than the size of the Granulated ones (0.025 – 0.042 cm). Therefore, this difference in size can worsen the MDA performance, especially the benzene selectivity, since the mass transfer from the outer surface of the Extrudated II to the active sites within the pores of the catalyst particles may be limiting the MDA process.

Possible complementary ways to improve these results could be: (i) increase the porosity of the Extrudate II by using pore formers, (ii) scale up of the reactor dimensions, and (iii) fine adjustment of the reaction conditions [9].

Indeed, it has been reported that if the size of the catalyst particles remains in the range from 0.010 to 0.085 cm, the internal diffusion effects are insignificant for the MDA performance [10].

The morphology of the “Extrudated II” 6% Mo/MCM-22 catalyst is shown in the FE-SEM images exhibited in Figure 112 and Figure 113. As can be observed, both the axial cross-section (Figure 112) and the radial cross-section (Figure 113) of the “Extrudated II” catalyst exhibit a very similar appearance. In both cases, aggregates of round and thin platelets with a diameter of 1-2 μm and a thickness much lower are shown, these aggregates are bonded together to form the extrudated with some occluded porosity.

Furthermore, the Mo content of the catalyst (6% wt.) was studied by FE-SEM/EDS in inner zones and in zones nearer to the edge of the analyzed samples in order to confirm the correct distribution of the Mo. The Mo content (% wt.) of the zones nearer to the edge was slightly higher than that of the inner zones of the extrudated. Thus, it is supposed a suitable Mo content gradient from 4.5% (inner) to 8% (edge). It should be noted that EDS analyses were recorded in the corresponding whole image.

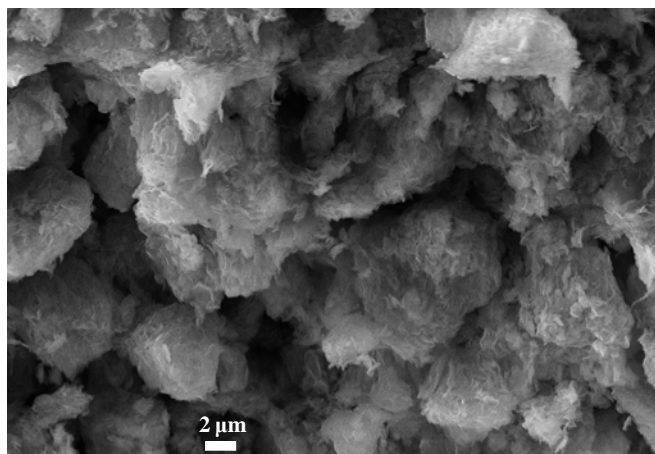


Figure 112. FE-SEM image of the “Extrudated II” 6% Mo/MCM-22 catalyst, showing axial cross-section view.

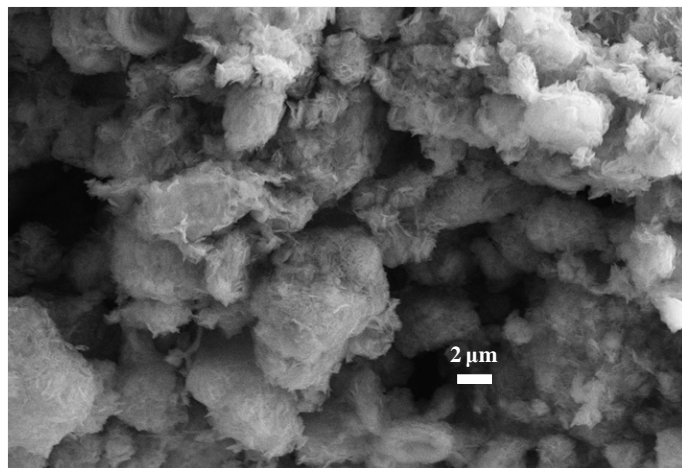


Figure 113. FE-SEM image of the “Extrudated II” 6% Mo/MCM-22 catalyst, showing radial cross-section view.

Moreover, Figure 114 exhibits the “Extrudated II” 6% Mo/MCM-22 catalyst. As seen, the size of the “Extrudate II” particles is ≤ 1 cm.



Figure 114. Picture of the “Extrudated II” 6% Mo/MCM-22 catalyst.

TGA results obtained for the spent catalysts produced using the standard (Granulated) and the new (Extrudated II) manufacturing process are

given in Table 68. For the 6%Mo/MCM-22 Extrudated II catalyst both the average coke formation rate and the amount of coke are lower than for the Granulated, as with the previous section but in lesser extent. Nonetheless, the Extrudated II catalyst (new procedure) exhibits the highest amount of coke per accumulated benzene mole, concretely almost three times higher than for the Granulated.

Table 68. TGA results of spent 6%Mo/MCM-22 catalysts produced using the standard (Granulated) and the new (Extrudated II) procedure.

Code	TOS (h)	Average Coke Formation Rate ($\text{g} \cdot \text{g}_{\text{cat}}^{-1} \cdot \text{h}^{-1}$)	Amount of Coke ($\text{g} \cdot \text{g}_{\text{cat}}^{-1}$)	$\text{g} \cdot \text{g}_{\text{cat}}^{-1} \cdot \text{mol}_{\text{benz.}}^{-1}$
Granulated	16.3	0.0072	0.117	6
Extrudated II	16.3	0.0054	0.088	17

The CO_x ($\text{CO} + \text{CO}_2$) signals (from TPO technique) versus the temperature are depicted in Figure 115 and the results are detailed in Table 69. For the catalyst produced by the new procedure (Extrudated II), the coke related to Mo species decreases ca. 37%, while the coke associated with Brønsted acid sites (aromatic-type carbon) increases roughly 33% with respect to the catalyst manufactured by the standard procedure (Granulated). Thereby, it can be said that these TPO results are in concordance with the TGA results (Table 68).

Besides the abovementioned negative effects ascribed to the internal diffusion, the fact that the coke associated with Brønsted acid sites (aromatic-type carbon) is higher for this catalyst (Extrudated II) than for the Extrudated I catalyst (previous section) is also detrimental for the MDA performance. Since the catalyst deactivation is supposed that it is mainly due to aromatic-type coke on the Brønsted acid sites [11].

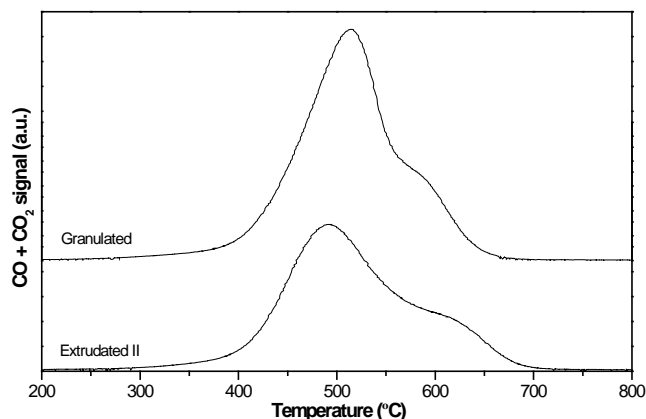


Figure 115. TPO profiles of carbon species over 6%Mo/MCM-22 catalysts after 16.3 h of MDA reaction, produced using the standard (Granulated) and the new (Extrudated II) procedure. Same scale of Y-axis.

For the coke characteristics (particle size, morphology, etc.), it can be concluded that these may be similar between both catalysts, Granulated and Extrudated II, since the temperature at maximum of both peaks (Table 69) is slightly different [2], especially for the Peak 2.

Table 69. Results of the deconvoluted TPO profiles of carbon species over 6%Mo/MCM-22 catalysts produced using the standard (Granulated) and the new (Extrudated II) procedure.

Code	Temperature at maximum (°C)		Percentage (%)		Amount of coke ($\text{g} \cdot \text{g}_{\text{cat}}^{-1}$)	
	Peak 1	Peak 2	Peak 1	Peak 2	Peak 1	Peak 2
Granulated	508	601	86.10	13.90	0.1004	0.0162
Extrudated II	493	605	72.33	27.67	0.0636	0.0243

Figure 116 shows the effect of the manufacturing process on the acidity of the 6%Mo/MCM-22 catalysts. The amount of acid sites was lower for both spent catalysts, being those at low (non-exchangeable cationic sites) and medium (Brønsted acid sites) temperature which mainly decreased. Hence, the NH_3 -TPD profiles are very similar for the spent Extrudated II (Figure 116.a)

and Granulated (Figure 116.b) catalysts. Nevertheless, by focusing on the fresh catalysts, the Granulated (Figure 116.d) shows higher amount of weak and Brønsted acid sites than the Extruded II catalyst (Figure 116.c).

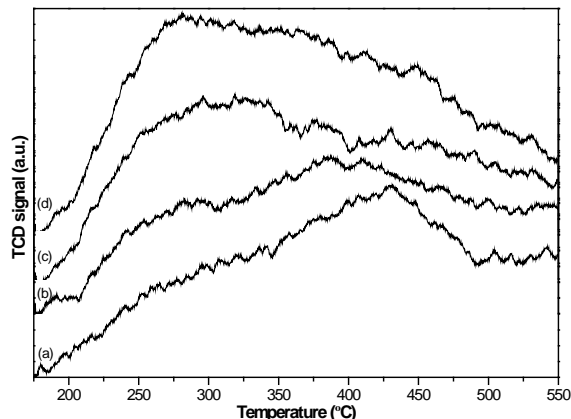


Figure 116. NH_3 -TPD profiles of 6%Mo/MCM-22 catalysts produced using the new procedure (Extruded II) (a) after and (c) before MDA reaction; and the standard procedure (Granulated) (b) after and (d) before MDA reaction. Same scale of Y-axis.

Table 70. Acidity of fresh and spent 6%Mo/MCM-22 catalysts prepared by the standard (Granulated) and the new (Extruded II) procedure determined by NH_3 -TPD.

Catalyst Code	NH_3 - uptake ($\mu\text{mol/g}$)	T_{max} ($^{\circ}\text{C}$)
Fresh Granulated	526.07	281
Fresh Extruded II	543.78	296
Spent Granulated	247.10	382
Spent Extruded II	245.97	429

NH_3 uptake at 175 $^{\circ}\text{C}$ and the maximum temperature (T_{max}) are given in Table 70. For the fresh 6%Mo/MCM-22 catalysts, the acidity was higher for the Extruded II, while for the spent 6%Mo/MCM-22 catalysts the acidity was slightly higher for the Granulated. In addition, it can be inferred that the acid

strength distribution for the fresh and the spent catalysts may be similar owing to the small difference between the maximum temperatures.

9.3. Conclusions

The two new manufacturing processes studied in this work to produce the 6%Mo/HZSM-5 and the 6%Mo/MCM-22 catalysts affect the MDA performance. First of all, a slightly worse MDA performance is reached for the Extrudated I catalysts, both 6%Mo/HZSM-5 and 6%Mo/MCM-22, manufactured using the procedure described in the U.S. patent [1]. Moreover, it can be concluded that this new catalyst manufacturing process affects in a different extent the coke accumulation on both catalysts, as it increases on the 6%Mo/HZSM-5 while on the 6%Mo/MCM-22 decreases. The TGA results are in agreement with those obtained by the TPO technique. The acidity is also influenced in a different way, since for the fresh Granulated 6%Mo/HZSM-5 catalyst the amount of weak and medium acid sites is higher, and the amount of Brønsted acid sites is lower than for the Extrudated I catalyst. However, for the fresh Granulated 6%Mo/MCM-22 catalyst the amount of Brønsted and Lewis acid sites is higher than for the Extrudated I. In addition, in all cases the spent catalysts exhibit lower acidity than the fresh ones.

Secondly, a worse MDA performance is obtained for the 6%Mo/MCM-22 Extrudated II catalyst, produced using the procedure based on the U.S. patent [1]. This may be ascribed to the internal diffusion effects resulting from the largest size of the Extrudated II particles in comparison with the Granulated ones. The MDA performance could be enhanced via the adjustment of the reaction conditions and the reactor dimensions [9], and also increasing the porosity of the Extrudated II catalyst.

In spite of the lower amount of coke exhibited by the Extrudated II catalyst, the amount of coke per accumulated benzene mole is nearly three times

higher than for the Granulated. The TPO results are in concordance with those of TGA. Moreover, the fresh Extrudated II catalyst shows lower amount of weak and Brønsted acid sites than the fresh Granulated. And for both spent catalysts the acidity is lower than for the fresh.

9.4. References

- [1] F. Kiesslich, Catalyst for the dehydroaromatization of methane and mixtures containing methane, US 2011/0124933 A1, 2011.
- [2] C.A. Querini, S.C. Fung, *Appl. Catal. A-Gen.*, 117 (1994) 53-74.
- [3] D. Ma, W.P. Zhang, Y.Y. Shu, X.M. Liu, Y.D. Xu, X.H. Bao, *Catalysis Letters*, 66 (2000) 155-160.
- [4] B. Li, S.J. Li, N. Li, H.Y. Chen, W.J. Zhang, X.H. Bao, B.X. Lin, *Microporous and Mesoporous Materials*, 88 (2006) 244-253.
- [5] Y.Y. Shu, D. Ma, L.Y. Xu, Y.D. Xu, X.H. Bao, *Catalysis Letters*, 70 (2000) 67-73.
- [6] S. Unverricht, M. Hunger, S. Ernst, H.G. Karge, J. Weitkamp, *ZEOLITE MCM-22 - SYNTHESIS, DEALUMINATION AND STRUCTURAL CHARACTERIZATION*, 1994.
- [7] G. Emig, R. Dittmeyer, *Handbook of Heterogeneous Catalysis*, in, 1997, pp. 1235.
- [8] D.W. Breck, *Zeolite Molecular Sieves: Structure, Chemistry and Use*, p. 636, New York, 1973.
- [9] Coorstek, Inc. Private Communication, in, 2014.
- [10] E. Peris, Estudio de catalizadores microporosos Mo/Zeolita en la reacción de deshidroaromatización de metano, in: Instituto de Tecnología Química (CSIC), Universidad Politécnica de Valencia, Valencia, 2015, pp. Chapter 4; Page 119.
- [11] D. Ma, D.Z. Wang, L.L. Su, Y.Y. Shu, Y. Xu, X.H. Bao, *Journal of Catalysis*, 208 (2002) 260-269.

Chapter 10.

EFFECT OF H₂ REMOVAL THROUGH BaZr_{0.7}Ce_{0.2}Y_{0.1}O_{3-δ} TUBULAR MEMBRANES ON MDA REACTION

10. Effect of H₂ removal through BaZr_{0.7}Ce_{0.2}Y_{0.1}O_{3-δ} tubular membranes on MDA reaction

The MDA process has different drawbacks that make difficult its commercial application. Firstly, it is limited by thermodynamics reaching an equilibrium conversion of ~ 12% in typical conditions for MDA [1]. Secondly, the catalyst is quickly deactivated due to the growth of carbonaceous deposits on its surface [2, 3]. These limitations cannot be surpassed only by the catalytic sites, but by removing H₂ [4-6] or supplying oxygen [7] using selective membranes, these constraints can be overcome due to the shift of the thermodynamic equilibrium. Nevertheless, the H₂ extraction or the O₂ injection separately results in faster catalyst deactivation and higher production of carbon monoxide, respectively.

In this work, the development and application of a novel catalytic membrane reactor for intensification of the MDA process is shown [8], which is driven by a tailored electrochemical co-ionic proton and oxide ion conducting BaZr_{0.7}Ce_{0.2}Y_{0.1}O_{3-δ} (BZCY72) tubular membrane. Five experiments were carried out following the experimental procedure described in the sections 3.6.2.1.1. and 3.6.2.1.2. The 6%Mo/MCM-22 catalyst was pre-reduced and pre-carburized using a gas mixture of CH₄:H₂, 1:4 (vol. ratio). Furthermore, the results exhibited for the CMR-TM (CMR- Tubular Membrane) can be compared with both the CMR-QT (CMR- Quartz Tube) and the FBR results, indistinctly.

10.1. Effect of H₂ removal through BaZr_{0.7}Ce_{0.2}Y_{0.1}O_{3-δ} tubular membrane on MDA reaction

First of all, the CMR-TM-1 experiment (using the Tubular Membrane “1” and 4 cm of copper anode) is compared with one CMR-QT experiment carried out at 710 °C (section 3.6.2.2.1.). As stated above, the electrode reactions [9] that take place when a direct current is imposed externally to pump H₂ electrochemically from the anode (MDA reaction side) to the cathode (sweep side) are as follows:



Figure 117 illustrates the effect of the H₂ removal through BZCY72 TM-1 on the methane conversion and the H₂ flow normalized per gram of catalyst. The methane conversion (Figure 117.a) achieved for both experiments is very similar during the first 5 h on stream, in which the H₂ was not removed. Nonetheless, the methane conversion for the CMR-TM-1 is higher over time than for the CMR-QT when 40 mA·cm⁻² are imposed externally, since the H₂ removal from the reaction side causes the shift of the thermodynamic equilibrium. Moreover, the methane conversion for the CMR-TM-1 is much more stable than for the CMR-QT, reaching 11.50% and 4.2% after roughly 44 h on stream, respectively.

The highest H₂ flow (Figure 117.b) is obtained for the CMR-TM-1 experiment from the 9th h on stream. As with the methane conversion, the H₂ flow for the CMR-TM-1 shows higher stability than for the CMR-QT, achieving 2.42 and 0.72 mL·min⁻¹·g_{cat}⁻¹ after ~ 44 h on stream, respectively. Further, the H₂ flow is slightly increased when the current density is not imposed to the cell, due to the non-removal of H₂ from the reaction side.

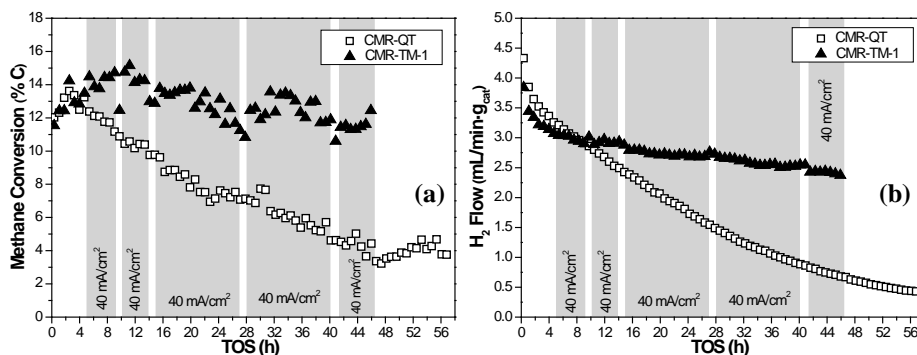


Figure 117. Effect of the H₂ removal through BZCY72 TM-1 on the (a) methane conversion and (b) H₂ flow versus the TOS of 6%Mo/MCM-22 catalyst at 710 °C. Shaded areas indicate when H₂ is extracted.

Table 71 shows the effect of the H₂ removal through BZCY72 TM-1 on the selectivity to main products after 9 h on stream by imposing 40 mA·cm⁻² at 710 °C, 1.2 bar and 1500 mL·h⁻¹·g_{cat}⁻¹. Benzene, C₂ and toluene selectivities are lower for the CMR-TM-1. On the contrary, naphthalene and coke selectivities are slightly higher for the CMR-TM-1. Moreover, in this experiment carbon monoxide (CO) was obtained.

Table 71. Effect of the H₂ removal through BZCY72 TM-1 on the selectivity to main products after 9 h on stream of 6%Mo/MCM-22 catalyst.

H ₂ removal from reaction side	Selectivity (% C)					
	C ₆ H ₆	C ₂	C ₇ H ₈	C ₁₀ H ₈	Coke	CO
No (CMR-QT)	71.10	3.16	2.73	3.50	19.51	0.00
Yes (CMR-TM-1)	68.71	2.13	2.70	4.33	19.67	2.46

Concretely, the carbon monoxide was obtained since the electrolyte of the tubular membrane (BZCY72) exhibits a low oxide-ionic conduction, and therefore, the H₂O was partially consumed at the cathode (sweep side) by the water splitting reaction (Equation 22). In addition, the oxide ions that pass through the membrane (BZCY72 TM) likely react with H₂ (Equation 23) at the

anode to produce H_2O , which in turn reacts with the coke deposited on the catalyst to form CO and H_2 (Equation 15):

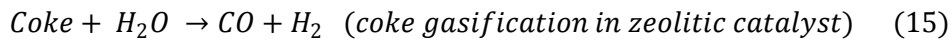
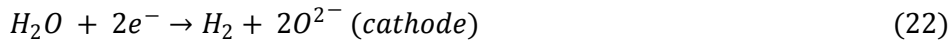


Figure 118 displays a scheme of the reactions involved in the Equations 20, 21, 22, 23 and 15, which take place when a direct current is imposed externally at the CMR using a BZCY72 tubular membrane.

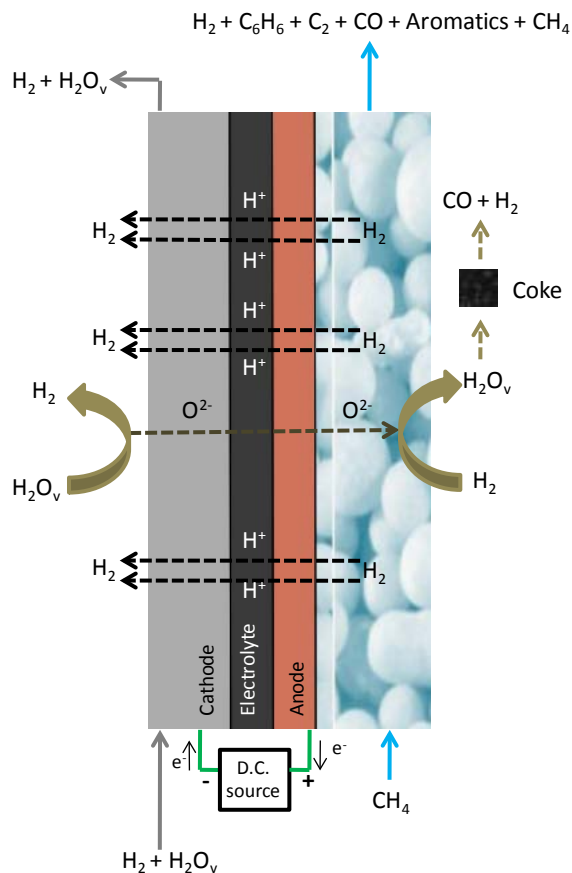


Figure 118. Scheme of electrochemical and side reactions at the CMR using a BZCY72 tubular membrane.

Figure 119 shows the effect of the H₂ removal through BZCY72 TM-1 on the benzene yield by applying 40 mA·cm⁻². The benzene yield obtained for the CMR-TM-1 is the highest throughout the time on stream. It should be noted that until the 20th h on stream this behavior is mainly ascribed to the methane conversion increment, since the benzene selectivity achieved for both experiments is very similar during the first 20 h. While from this TOS, both the benzene selectivity and the methane conversion are higher and more stable for the CMR-TM-1. Therefore, the benzene yield obtained by removing H₂ through TM-1 is more stable, exhibiting a 5-fold decrease in the average deactivation rate with respect to that achieved without H₂ removal (CMR-QT), which is attributed to the coke reaction with the slight amounts of H₂O that are introduced along the catalyst bed in a controlled way as explained before (Equations 22, 23 and 15). In particular, the maximum benzene yield reached for the CMR-QT is 8.74% at ca. 4 h on stream and for the CMR-TM-1 is 10.40% at roughly 11 h on stream.

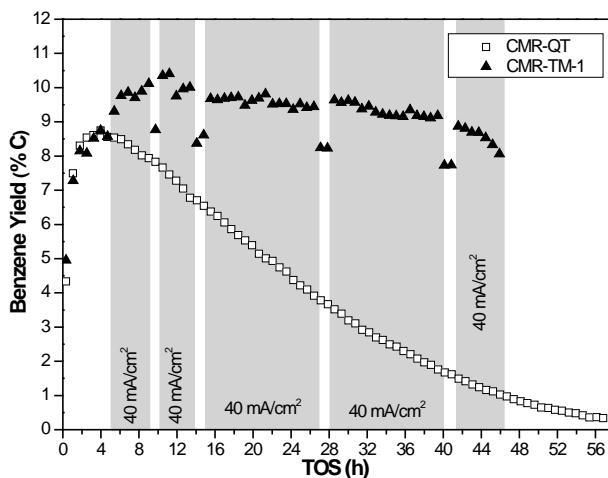


Figure 119. Effect of the H₂ removal through BZCY72 TM-1 on the benzene yield versus the TOS of 6%Mo/MCM-22 catalyst at 710 °C. Shaded areas indicate when H₂ is extracted (Current ON).

For the aromatics yield (Figure 120.a) the same trend that for the benzene yield is observed. Concretely, the maximum aromatics yield obtained for the CMR-QT and for the CMR-TM-1 is 9.72% and 11.70% at roughly 4 and 11 h on stream, respectively. Further, the fact that the aromatics yield was also higher for the CMR-TM-1 than for the CMR-QT when the H_2 extraction current was switched off, points out the lower deactivation during the galvanic mode.

Moreover, the accumulated benzene moles (Figure 120.b) are alike for both experiments during the first 5 h on stream without the H_2 extraction. However, when the current is imposed to the cell, the accumulated benzene moles for the CMR-TM-1 are higher and rise almost linearly over time achieving $\sim 0.044 \text{ mol} \cdot \text{g}_{\text{cat}}^{-1}$ after ca. 45 h on stream. However, the accumulated benzene moles for the CMR-QT reach a plateau of $\sim 0.023 \text{ mol} \cdot \text{g}_{\text{cat}}^{-1}$ after 45 h on stream.

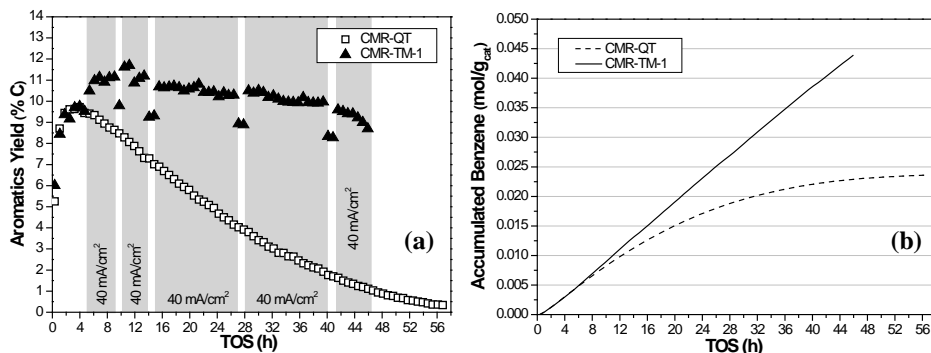


Figure 120. Effect of the H_2 removal through BZCY72 TM-1 on the (a) aromatics yield and (b) accumulated benzene versus the TOS of 6%Mo/MCM-22 catalyst. Shaded areas indicate when H_2 is extracted.

It should be indicated that after 46 h on stream, the tubular membrane TM-1 had an increasing leakage of the CH_4 from the reaction side to the sweep side, being the CH_4 molar concentration in sweep side higher than 0.15% and therefore, the data collected were not used quantitatively.

Figure 121 depicts the total H₂ flux measured in the sweep side and the faradaic efficiency obtained for the CMR-TM-1. When a current density of 40 mA·cm⁻² was applied to the electrochemical cell, both the total H₂ flux and the faradaic efficiency rise with time on stream up to 0.11 mL·min⁻¹·cm⁻² and 38%, respectively. Further, when the same current density was applied for the second time, both the H₂ flux and the faradaic efficiency reach the maximum value of ~ 0.15 mL·min⁻¹·cm⁻² and ~ 53%, respectively. Nonetheless, thereafter both parameters are lower and almost stable, being the H₂ flux roughly 0.09 mL·min⁻¹·cm⁻² and the faradaic efficiency ca. 31%.

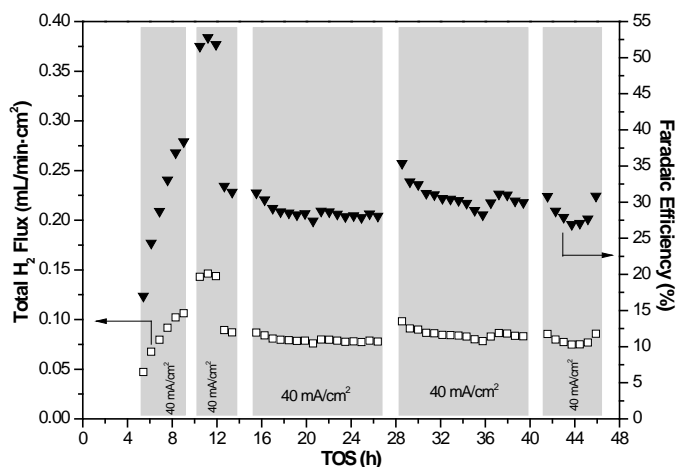


Figure 121. Electrochemical results of BZCY72 TM-1: total H₂ flux in sweep side and faradaic efficiency versus the TOS at 710 °C. Shaded areas indicate when H₂ is extracted.

The total H₂ flux includes the H₂ pumped (removed) from the reaction side to the sweep side (H₂ from protons) and the H₂ produced by the water splitting reaction in the sweep side (H₂ from oxide ions), being the latter equivalent to the CO flux obtained in the reaction side. These H₂ fluxes are illustrated in Figure 122.a. and both are a little bit scattered, being the H₂ from protons substantially higher than the H₂ from oxide ions. Concretely, for the maximum total H₂ flux achieved by TM-1, the H₂ flux from protons is roughly

0.13 mL·min⁻¹·cm⁻² and the H₂ flux from oxide ions is ca. 0.02 mL·min⁻¹·cm⁻². Hence, throughout the time on stream the H₂ flux removed from the reaction side contributes to the total H₂ flux obtained in the sweep side mainly above 80%, thus demonstrating that the proton conduction exhibited by the BZCY72 electrolyte is by far higher than the oxide ion conduction.

Another way of expressing the electrochemical results is shown in Figure 122.b, in which the H₂ extracted¹ and the O₂ injected² are displayed versus the TOS. The maximum H₂ extracted achieved for the BZCY72 TM-1 is around 26% at 11.20 h on stream, coinciding with the TOS at which the maximum methane conversion and, hence, the highest aromatics yield were reached. Nevertheless, the maximum O₂ injected was obtained later, at 28.6 h on stream, being roughly 0.33%.

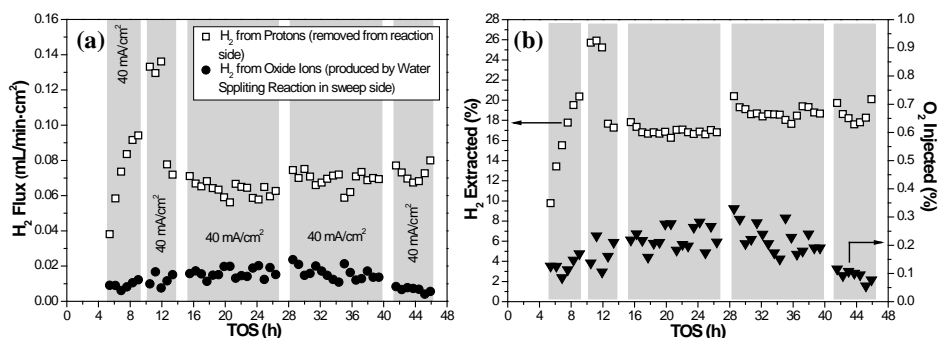


Figure 122. Electrochemical results of BZCY72 TM-1: (a) H₂ fluxes and (b) H₂ extracted and O₂ injected versus the TOS at 710 °C. Shaded areas indicate when H₂ is extracted.

In addition, the theoretical faradaic flux at 40 mA·cm⁻² is roughly 0.28 mL·min⁻¹·cm⁻². Therefore, by comparing this flux with the maximum H₂ flux achieved for the BZCY72 TM-1 (0.15 mL·min⁻¹·cm⁻²), it can be concluded that the latter is deviated from theoretical faradaic flux to lower values. This

¹ H₂ extracted (%) from the reaction side expresses the ratio of the extracted H₂ to the formed H₂.

² O₂ injected (%) expresses the ratio of O₂ injected to the total molar flow on the reaction side.

may be attributed to the enhancement of the electronic transport in the BZCY72 electrolyte when a very high voltage is achieved, by imposing a current density. Therefore, the n-type electronic conductivity begins to prevail over the co-ionic transport, as reported by Babiniec et al. [10].

Regarding the voltage, during the time on stream in which the O.C.V. was measured, a stable voltage was recorded around -0.03 V, because of the H₂ concentration was higher in the sweep side (cathode). However, the voltage measured was greatly increased when the current density was applied, thus indicating the high magnitude of the area specific resistance (ASR) of the electrode (anode) and the consequent high overpotential. In particular, for the BZCY72 TM-1 the measured voltage was stabilized below 3 V.

FE-SEM backscattered (BSE) image of the BZCY72 TM-1 with the copper anode is shown in Figure 123. The bright phase present in both electrolyte and cathode corresponds to BZCY72, while the copper in the anode and the nickel in the cathode are visible as dark phases. Moreover, FE-SEM/EDS spectra of each component of the tubular membrane are exhibited in Figure 124 and enable to confirm the chemical composition of each layer. It should be noted that EDS analyses were recorded specifically on the points marked with the numbers, from 1 to 4 in Figure 123.

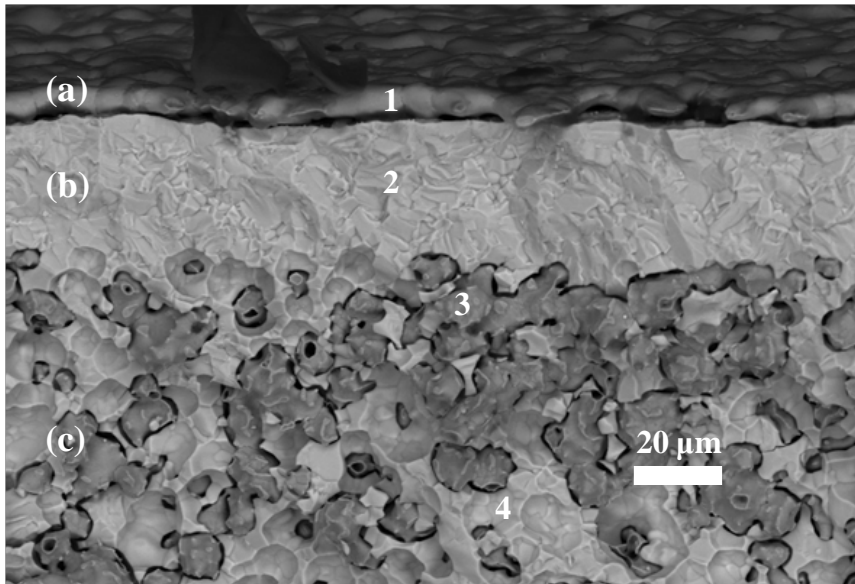


Figure 123. BSE FE-SEM image of the fractured cross-section of the BZCY72 TM-1, showing (a) copper anode, (b) BZCY72 electrolyte and (c) BZCY72-Ni cathode.

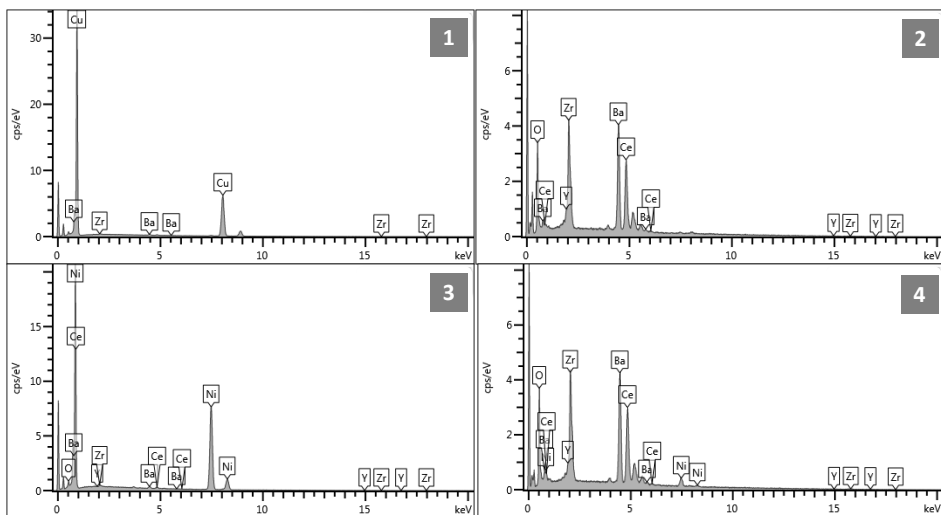


Figure 124. FE-SEM/EDS spectra recorded from the BZCY72 TM-1, corresponding to: 1. copper anode, 2. BZCY72 electrolyte, 3. Ni aggregates in the cathode and, 4. BZCY72 in the cathode.

Furthermore, Figure 125 shows the reduced BZCY72 TM-1 with the copper anode sintered. Moreover, the copper-thick-wire holder for the catalyst fixed bed is shown as well as the copper lead wire attached to the electrode.



Figure 125. Picture of the reduced BZCY72 TM-1 with the copper anode sintered (anode length ~ 4 cm).

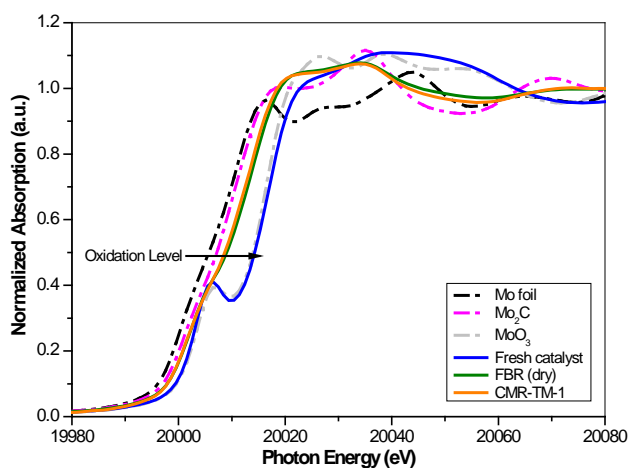


Figure 126. XANES spectra at Mo K-edge of Mo foil, Mo_2C , MoO_3 and 6%Mo/MCM-22 catalysts before and after MDA reaction (FBR and CMR).

The Mo K-edge XANES spectrum (Figure 126) of the 6%Mo/MCM-22 catalyst spent on the CMR-TM-1 experiment is almost alike that of the 6%Mo/MCM-22 catalyst spent on a FBR experiment carried out entirely in dry conditions. These results and those summarized in Table 72 suggest that different species of Mo may co-exist on the catalyst spent on the CMR-TM-1 experiment as Mo^{2+} , Mo^{4+} and Mo^{6+} , being mostly as Mo^{2+} and Mo^{4+} . Thus pointing out that the small amounts of H_2O formed in the reaction side, due to the concomitant H_2 extraction and O_2 injection, barely affect the oxidation state of Mo with respect to the experiment run in dry conditions (FBR) over time [8].

Table 72. Experimental XANES results of Mo foil, Mo₂C, MoO₃ and 6%Mo/MCM-22 catalysts before and after MDA reaction (FBR and CMR).

Sample	Mo K-edge energy (eV)	Formal oxidation state
Mo foil	20005	0
Mo ₂ C	20007	+2
MoO ₃	20014	+6
Fresh catalyst	20014	+6
FBR (dry)	20009	+2.8
CMR-TM-1	20008	+2.4

These XANES results were verified by those achieved by XPS [8] for the same catalysts, as can be observed in Figure 127 and Table 73. As abovementioned (section 7.1.3.2.), for the fresh catalyst the concentration of Mo⁶⁺ species is 100% on its surface. However, the spent catalysts present Mo⁶⁺, Mo⁵⁺/Mo⁴⁺ and Mo²⁺ species, being the concentration of each Mo species very similar for these catalysts.

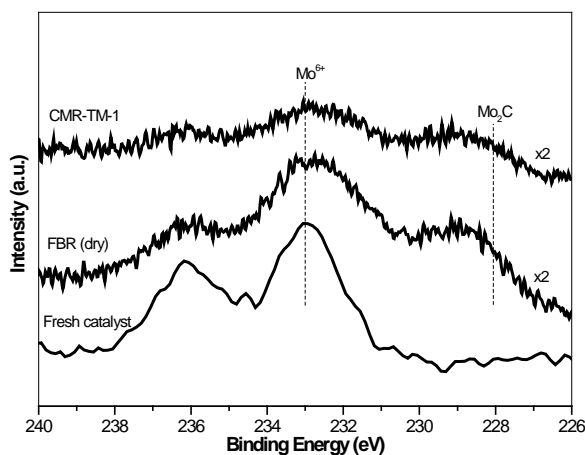


Figure 127. XPS Mo 3d_{5/2} and 3d_{3/2} spectra of 6%Mo/MCM-22 catalysts before and after MDA reaction (FBR and CMR).

Table 73. Surface oxidation state of Mo by XPS* on 6%Mo/MCM-22 catalysts before and after MDA reaction (FBR and CMR).

Sample	Mo ⁶⁺ (%)	Mo ⁵⁺ / Mo ⁴⁺ (%)	Mo ₂ C (%)
Fresh catalyst	100	0	0
FBR (dry)	39	17	44
CMR-TM-1	45	14	41

*Mo⁶⁺ (BE = 233.1 eV [11]), Mo⁵⁺ (BE = 234.4 eV [11]), Mo⁴⁺ (BE = 229.3 eV [12]) and Mo₂C (Mo²⁺) (BE = 227.9 eV [13]).

Table 74 details the TGA results obtained for the spent catalysts without and with H₂ extraction through BZCY72 TM-1. The average coke formation rate and the amount of coke are lower for the experiment carried out with H₂ removal (CMR-TM-1), despite its longer duration (~ 12 h). Thereby, it may be assumed that the controlled injection of oxide ions contributes to the reduction of the coke accumulation, since they probably react with H₂ to form H₂O which removes little amounts of coke. Moreover, for the CMR-TM-1 with H₂ extraction the amount of coke (g·g_{cat}⁻¹) per accumulated benzene mole is also lower, being almost half than for the experiment without the H₂ removal. This confirms the best MDA performance achieved by the CMR-TM-1 experiment.

Table 74. TGA results of spent 6%Mo/MCM-22 catalysts without and with H₂ removal through BZCY72 TM-1.

H ₂ removal from reaction side	TOS (h)	Average Coke Formation Rate (g·g _{cat} ⁻¹ ·h ⁻¹)	Amount of Coke (g·g _{cat} ⁻¹)	g·g _{cat} ⁻¹ ·mol _{benz.} ⁻¹
No (CMR-QT)	56.8	0.0055	0.314	7
Yes (CMR-TM-1)	69.3	0.0030	0.208	3

These TGA results are corroborated by those of elemental analysis, BET surface area and micropore volume of the spent catalysts, being the latter summarized in Table 75. By comparing with the fresh catalyst, both the BET

surface area and micropore volume are sharply reduced, being especially the most reduced those corresponding to the catalyst tested without H₂ removal (CMR-QT). Therefore, with respect to the fresh catalyst, the BET surface area is decreased around 77% and 64%, and the micropore volume roughly 88% and 73%, for the CMR-QT and the CMR-TM-1 experiments, respectively. In addition, for the catalyst tested without H₂ extraction (CMR-QT), the BET surface area and the micropore volume are reduced ~ 35% and 56%, with respect to the catalyst tested with H₂ removal (CMR-TM-1).

Table 75. BET surface area and micropore volume of spent 6%Mo/MCM-22 catalysts without and with H₂ removal through BZCY72 TM-1.

H₂ removal from reaction side	TOS (h)	S_{BET} (m²/g)	Micropore volume (cm³/g)
Fresh catalyst	0.00	398.94	0.151
No (CMR-QT)	56.8	92.11	0.018
Yes (CMR-TM-1)	69.3	142.34	0.041

Figure 128 displays the TPO profiles of carbon species of the 6%Mo/MCM-22 catalysts and Table 76 shows the TPO results. These results indicate that the controlled introduction of H₂O along the catalyst bed, by means of the O₂ injection through the BZCY72 TM-1, favors the reduction of both types of coke deposited on the catalyst, but mainly the aromatic type coke. Because of the coke associated with Mo species decreases roughly 28% and the coke related to Brønsted acid sites (aromatic-type carbon) is reduced ~ 51%, with respect to the catalyst tested without H₂ removal (CMR-QT). Therefore, the decrease observed for aromatic type coke may cause the high stability reached by injecting O₂ to the reaction side (CMR-TM-1), since this coke is considered the main responsible of the catalyst deactivation [14]. Moreover, these TPO results are in concordance with the TGA and the N₂ sorption (BET surface area and micropore volume) results shown previously.

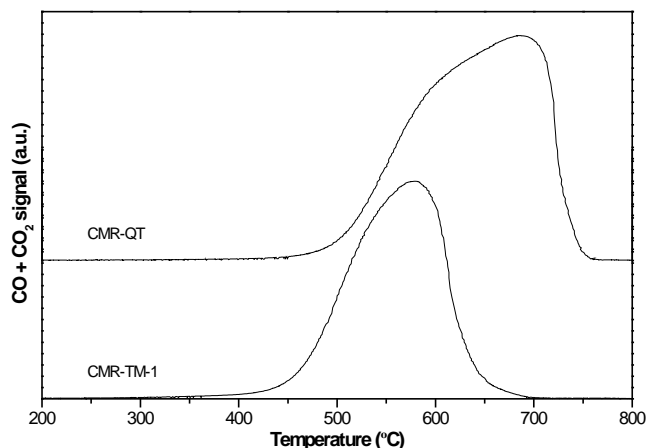


Figure 128. TPO profiles of carbon species over 6%Mo/MCM-22 catalysts after MDA reaction without (CMR-QT) and with H₂ removal (CMR-TM-1). Same scale of Y-axis.

By focusing on the temperature at maximum of both peaks (Table 76), it can be observed that for the catalyst tested without H₂ extraction (CMR-QT) this is rather high for both peaks. This points out that the coke characteristics (particle size, morphology, etc.) may be different between these catalysts [15].

Table 76. Results of the deconvoluted TPO profiles of carbon species over 6%Mo/MCM-22 catalysts tested without (CMR-QT) and with H₂ removal (CMR-TM-1).

H ₂ removal from reaction side	TOS (h)	Temperature at maximum (°C)		Percentage (%)		Amount of coke (g·g _{cat} ⁻¹)	
		Peak 1	Peak 2	Peak 1	Peak 2	Peak 1	Peak 2
No (CMR-QT)	56.8	620	695	75.24	24.76	0.2363	0.0778
Yes (CMR-TM-1)	69.3	551	594	81.75	18.25	0.1702	0.0380

In order to study the effect of the H₂ removal through BZCY72 TM-1 on the acidity of the 6%Mo/MCM-22 catalyst, NH₃ TPD experiments were also done. Figure 129 depicts the NH₃-TPD profiles of 6%Mo/MCM-22 catalysts before and after MDA reaction without (CMR-QT) and with H₂ extraction

(CMR-TM-1). The amount of acid sites at low and medium temperature was lower for both spent catalysts, especially for the catalyst tested without H₂ removal (CMR-QT). These acid sites correspond to the non-exchangeable cationic sites and the Brønsted acid sites, respectively.

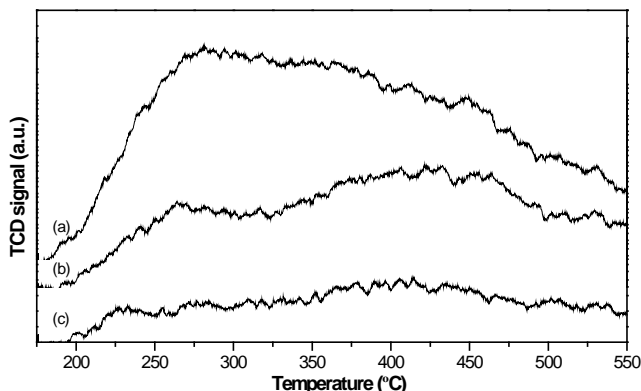


Figure 129. NH₃-TPD profiles of 6%Mo/MCM-22 catalysts (a) fresh, and tested with the (b) CMR-TM-1 and (c) CMR-QT. Same scale of Y-axis.

Table 77 details the NH₃ uptake at 175 °C and the maximum temperature (T_{\max}) for the 6%Mo/MCM-22 catalyst fresh and tested without and with H₂ removal. The highest acidity is exhibited by the fresh catalyst and, between both spent catalysts the acidity is higher for the catalyst tested by removing H₂ through TM-1. Thus, the reduction of coke accumulation, due to the simultaneous H₂ extraction and O₂ injection through TM-1, leads to higher catalyst acidity despite the longer duration of the CMR-TM-1 experiment (~ 12 h). Moreover, the acid strength distribution is different among the fresh and the spent catalysts since the maximum temperatures are rather different. While between the spent catalysts the acid strength distribution is very similar since the maximum temperatures are very alike.

Table 77. Acidity of 6%Mo/MCM-22 catalyst fresh and tested without (CMR-QT) and with H₂ removal (CMR-TM-1).

H ₂ removal from reaction side	TOS (h)	NH ₃ - uptake (μmol/g)	T _{max} (°C)
Fresh catalyst	0.0	526	281
No (CMR-QT)	56.8	123	415
Yes (CMR-TM-1)	69.3	264	422

10.2. Effect of the anode type on the BZCY72 tubular membrane on MDA reaction with H₂ removal

In this section, the most representative MDA results obtained using a cermet Mo₂C/Cu/BZCY72 anode are shown. This anode was used in several experiments previously to the copper anode implementation, and as discussed below, the MDA performance was improved using the latter. The results for the experiment done using the Tubular Membrane “2” (CMR-TM-2 with 4 cm of Mo₂C/Cu/BZCY72 anode) were compared with the results obtained using the CMR-TM-1 (section 10.1) and the CMR-QT-2 carried out at 700 °C (section 3.6.2.2.1.). The CMR-TM-2 experiment was also performed at 700 °C according to the procedure described in the sections 3.6.2.1.1. and 3.6.2.1.2.

The effect of the anode type on the BZCY72 TM on the methane conversion and the selectivity to main products after 9 h on stream is shown in Table 78. At this TOS, the current density imposed to the electrochemical cells was different, i. e. it was of 40 and 80 mA·cm⁻² for the CMR-TM-1 and CMR-TM-2, respectively. The lowest methane conversion is reached by the CMR-QT-2 without H₂ removal, and between the other experiments it is higher for the experiment in which a copper anode was employed (CMR-TM-1). Moreover, benzene and C₂ selectivities are very similar for the three experiments, being the former slightly higher for the CMR-QT-2 experiment. While a slight increase is

observed for toluene and naphthalene selectivities for the CMR-TM-2 experiment (cermet anode). However, the highest coke selectivity is obtained for the experiment without H₂ extraction (CMR-QT-2). The highest CO selectivity is achieved by the experiment in which a copper anode was used (CMR-TM-1).

Table 78. Effect of the anode type on BZCY72 TM on the methane conversion and the selectivity to main products after 9 h on stream of 6%Mo/MCM-22 catalyst.

H ₂ removal from reaction side	Anode	Methane Conversion (% C)	Selectivity (% C)					
			C ₆ H ₆	C ₂	C ₇ H ₈	C ₁₀ H ₈	Coke	CO
No (CMR-QT-2)	-	9.70	69.83	2.13	2.83	3.78	21.43	0.00
Yes (CMR-TM-1)	Copper	14.72	68.71	2.13	2.70	4.33	19.67	2.46
Yes (CMR-TM-2)	Mo ₂ C/Cu/BZCY72	10.96	69.47	2.42	3.29	5.50	18.30	1.02

Figure 130 displays the effect of the anode type on BZCY72 TM on the benzene yield. The current densities (shadowed areas) imposed to the cells were different and they are detailed in the section 3.6.2.1.2. The benzene yield obtained using the copper anode (CMR-TM-1) is the highest throughout the time on stream. However, for the Mo₂C/Cu/BZCY72 anode (CMR-TM-2), the benzene yield is also higher than without H₂ removal (CMR-QT-2). It should be noted that this behavior is mostly ascribed to the methane conversion increment, since the benzene selectivity is very similar for the three experiments. In particular, the methane conversion is increased due to the H₂ removal from the reaction side at both CMR-TM experiments, causing the shift of thermodynamic equilibrium. Specifically, the maximum benzene yield is reached at the same time for both CMR-TM experiments ~ 11 h, being 10.40% and 8.24% using the copper anode (TM-1) and the cermet anode (TM-2), respectively.

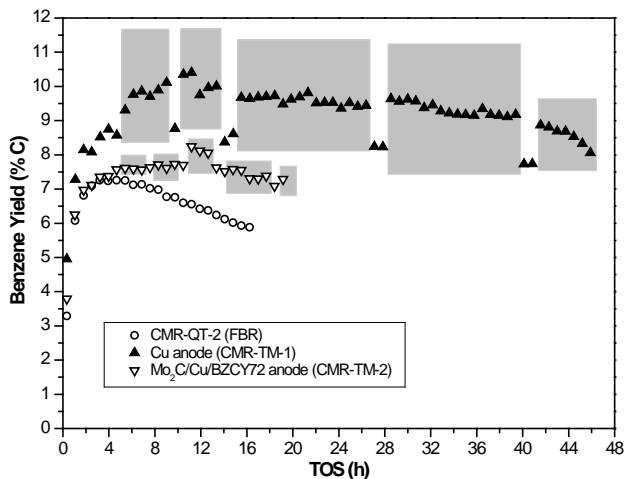


Figure 130. Effect of the anode type on BZCY72 TM-1 and TM-2 on the benzene yield versus the TOS of 6%Mo/MCM-22 catalyst. Shaded areas indicate when H_2 is extracted.

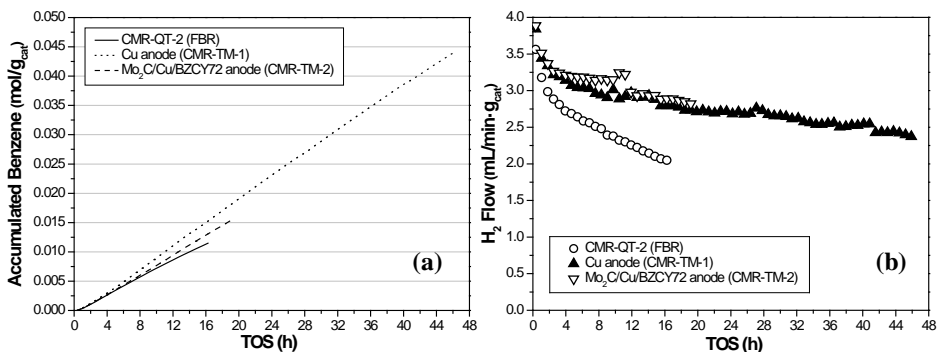


Figure 131. Effect of the anode type on BZCY72 TM-1 and TM-2 on the (a) accumulated benzene moles and (b) H_2 flow versus the TOS of 6%Mo/MCM-22 catalyst.

Regarding the accumulated benzene moles (Figure 131.a) these are higher for both experiments carried out by removing H_2 and injecting O_2 than for the CMR-QT-2. Moreover, between the experiments performed with H_2 extraction, the highest accumulated benzene moles over time are obtained for the CMR-TM-1, using the copper anode. Therefore, it can be concluded that

among these two anodes applied on the BZCY72 TM, the best MDA performance is achieved with the copper anode. In addition, the H₂ flow (Figure 131.b) is higher and very similar for both experiments run by extracting H₂, mainly due to the increase of the methane conversion.

After ~19 h on stream, the CH₄ leakage from the reaction side to the sweep side for the TM-2 was higher than 0.15%, hence the results were not quantitative.

Figure 132.a shows the total H₂ flux in the sweep side and the faradaic efficiency obtained for the CMR-TM-2 (Mo₂C/Cu/BZCY72 anode). When a current density of 40 mA·cm⁻² was applied, the H₂ flux increases up to 0.03 mL·min⁻¹·cm⁻² and remains stable. Thus, it is observed the same trend for the faradaic efficiency achieving ca. 11%. Nevertheless, the H₂ flux barely increases up to 0.035 mL·min⁻¹·cm⁻² when 80 mA·cm⁻² were imposed to the cell, while the faradaic efficiency sharply drops until roughly 6%. Lower values of both parameters are obtained for 119 mA·cm⁻². The H₂ flux obtained for BZCY72-TM-2 is much lower than the theoretical faradaic flux. This worse performance can be related to the increase of the electronic conduction in the BZCY72 electrolyte [10], which is ascribed to the higher overpotential related to the high ASR of this electrode (cermet anode). Furthermore, despite the reduction of the current density applied, the electrochemical performance is worsened. Both the H₂ flux measured in the sweep side and the faradaic efficiency suffer an increment from the 17th h on stream directly related to the increasing leakage abovementioned.

In this experiment (CMR-TM-2: Mo₂C/Cu/BZCY72 anode) due to experimental problems only few data from CO could be collected. Therefore, it was not possible to separate the H₂ pumped (removed) from the reaction side to the sweep side, from the H₂ produced by the water splitting reaction in sweep side. Anyway, the H₂ extracted from the reaction side is exhibited in Figure

132.b, reaching the maximum value (7.3%) by imposing 80 mA·cm⁻² for the first time. Thereby, comparing these results (CMR-TM-2: Mo₂C/Cu/BZCY72 anode) with those obtained using the copper anode (CMR-TM-1) depicted in Figure 122, it can be concluded that the best electrochemical performance (higher H₂ extracted and lower voltage) is obtained using the copper anode.

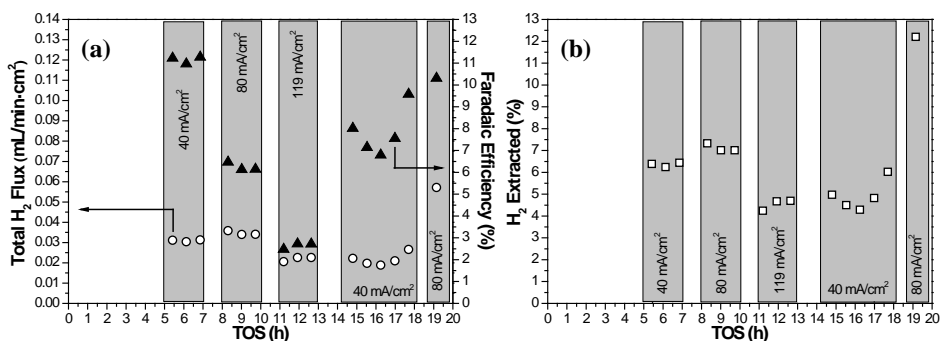


Figure 132. Electrochemical results of BZCY72 TM-2: (a) total H₂ flux in sweep side and faradaic efficiency and (b) H₂ extracted versus the TOS at 700 °C.

Shaded areas indicate when H₂ is extracted.

By focusing on the TGA results (Table 79), the CMR-TM-1 experiment carried out using the copper anode accumulates the highest amount of coke, which can be ascribed to the duration of this experiment. While for the shorter experiments, the amount of coke is slightly higher for the experiment run without H₂ extraction (CMR-QT-2) despite being 6 h shorter. Therefore, the oxide ions injection through the BZCY72 TM-2 favors the lower coke accumulation on the catalyst. However, the lowest amount of coke (g·g_{cat}⁻¹) per accumulated benzene mole is achieved by the CMR-TM-1 performed using the copper anode, followed closely by the CMR-TM-2 done using the cermet anode, despite the almost 23 h on stream in which the TM-1 shows a high leakage of CH₄ from the reaction side, reducing the benzene produced. These results reinforce that the best MDA performance is obtained using the copper anode.

Table 79. TGA results of spent 6%Mo/MCM-22 catalysts without and with H₂ removal through TM-1 (Cu anode) and TM-2 (Mo₂C/Cu/BZCY72 anode).

H ₂ removal from reaction side	TOS (h)	Average Coke Formation Rate (g·g _{cat} ⁻¹ ·h ⁻¹)	Amount of Coke (g·g _{cat} ⁻¹)	g·g _{cat} ⁻¹ ·mol _{benz.} ⁻¹
No (CMR-QT-2)	16.3	0.0072	0.117	6
Yes (CMR-TM-1)	69.3	0.0030	0.208	3
Yes (CMR-TM-2)	23.7	0.0046	0.108	4

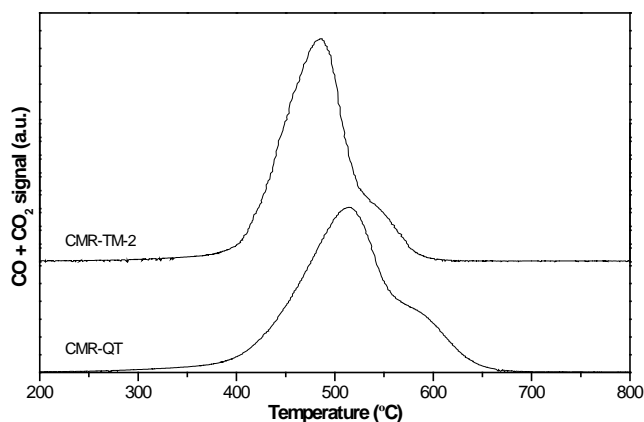


Figure 133. TPO profiles of carbon species over 6%Mo/MCM-22 catalysts after MDA reaction without (CMR-QT-2) and with H₂ removal (CMR-TM-2). Same scale of Y-axis.

The CO_x profiles obtained for the 6%Mo/MCM-22 catalysts by TPO technique are exhibited in Figure 133, except for the catalyst tested using the copper anode (CMR-TM-1) since its longer duration hinders the comparison with the other experiments. In addition, the TPO results are given in Table 80. For the catalyst tested by removing H₂ and injecting O₂ through TM-2 (cermet anode), both the coke related to Mo species and the coke associated with Brønsted acid sites (aromatic-type carbon) are reduced roughly 5 and 23%, respectively, with respect to the catalyst tested without H₂ extraction. Thus, confirming that the H₂O formed in the catalyst bed due to the O₂ injected

through the BZCY72 electrolyte, regardless of the anode employed, reacts preferentially with the aromatic type coke, the reduction of which causes the higher stability of this experiment with respect to the CMR-QT-2 experiment. Thereby, these results are in agreement with those of TGA. Regarding the coke characteristics, it can be said that these may be different [15] between both catalysts since the temperature at maximum of both peaks (Table 80) is slightly higher for the catalyst run without H₂ removal (CMR-QT-2).

Table 80. Results of the deconvoluted TPO profiles of carbon species over 6%Mo/MCM-22 catalysts tested without and with H₂ removal (CMR-TM-2).

H ₂ removal from reaction side	TOS (h)	Temperature at maximum (°C)		Percentage (%)		Amount of coke (g·g _{cat} ⁻¹)	
		Peak 1	Peak 2	Peak 1	Peak 2	Peak 1	Peak 2
No (CMR-QT-2)	16.3	508	601	86.10	13.90	0.1004	0.0162
Yes (CMR-TM-2)	23.7	479	555	88.42	11.58	0.0958	0.0125

10.3. Effect of the temperature on MDA reaction with H₂ removal

The temperature at which the experiments were carried out affects significantly the MDA performance [16]. Therefore, one experiment was done at 720 °C using the copper anode, 40 and 60 mA·cm⁻² and the Tubular Membrane “3” (CMR-TM-3), which results were compared with those obtained using the CMR-TM-1 and the CMR-QT (section 3.6.2.2.1.), both carried out at 710 °C. The CMR-TM-3 and CMR-TM-1 experiments were carried out according to the procedure described in the sections 3.6.2.1.1. and 3.6.2.1.2.

Figure 134 depicts the effect of the temperature by removing H₂ on the methane conversion and the H₂ flow normalized per gram of catalyst. The highest methane conversion (Figure 134.a) is reached for the experiment carried out at 720 °C during the first 19 h on stream, by applying 40 and

60 mA·cm⁻² to the TM-3, being especially higher until the 11th h on stream. This increment is thermodynamically expected [17] when a higher temperature is employed and, moreover, it is enhanced due to the equilibrium shift caused by the H₂ extraction from the reaction side through the BZCY72 TM-3. Concretely, for this experiment the catalyst begins to be deactivated after 40 h on stream, since the methane conversion and the benzene selectivity (not shown) decrease over time. Therefore, the TM-3 does not show a rising leakage of CH₄ from the reaction side to the sweep side. However, the methane conversion is slightly higher for the CMR-TM-1 experiment run at 710 °C after 27 h on stream. While, the methane conversion for the experiment done without H₂ extraction is lower than for the experiments performed with H₂ removal after 5 h on stream.

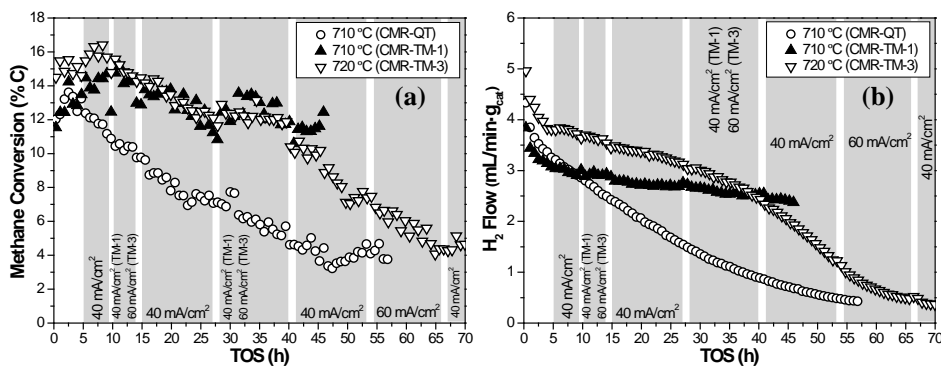


Figure 134. Effect of the temperature on the (a) methane conversion and (b) H₂ flow versus the TOS of 6%Mo/MCM-22 catalyst, without (CMR-QT) and with H₂ removal (CMR-TM-1 and TM-3). Shaded areas indicate when H₂ is extracted.

The highest H₂ flow (Figure 134.b) is obtained for the experiment carried out at 720 °C by removing H₂, this is mainly attributed to the higher methane conversion. Nevertheless, in this experiment the H₂ flow is not increased when the current density is not imposed to the TM-3, unlike for the TM-1 (710 °C).

The effect of the temperature by extracting H₂ on the selectivity to main products after 9 h on stream (by applying 40 mA·cm⁻²) is summarized in Table 81. By focusing on the experiments with H₂ extraction, CMR-TM-1 and CMR-TM-3, benzene, C₂ and coke selectivities are slightly higher for the latter experiment, which was run at 720 °C. Nonetheless, toluene, naphthalene and CO selectivities are slightly lower for this experiment (CMR-TM-3). Moreover, by comparing these results with those obtained without H₂ removal (CMR-QT), the trend observed is the same that in the section 10.1. (Table 71). Benzene, C₂ and toluene selectivities are lower for both experiments carried out by removing H₂, while the naphthalene and coke selectivities are slightly higher.

Table 81. Effect of the temperature on the selectivity to main products after 9 h on stream of 6%Mo/MCM-22 catalyst, without (CMR-QT) and with H₂ extraction through TM-1 and TM-3.

H ₂ removal from reaction side	Temperature (°C)	Selectivity (% C)					
		C ₆ H ₆	C ₂	C ₇ H ₈	C ₁₀ H ₈	Coke	CO
No (CMR-QT)	710	71.10	3.16	2.73	3.50	19.51	0.00
Yes (CMR-TM-1)	710	68.71	2.13	2.70	4.33	19.67	2.46
Yes (CMR-TM-3)	720	69.82	2.43	2.40	4.11	20.01	1.23

The effect of the temperature by removing H₂ on the benzene yield by imposing different current densities is displayed in Figure 135. The benzene yield achieved for the CMR-TM-3 at 720 °C is the highest until the 27th h on stream and then it becomes lower than that obtained for the CMR-TM-1 at 710 °C. This higher benzene yield is especially ascribed to the higher methane conversion and, in lesser extent to the slightly higher benzene selectivity obtained at 720 °C (also thermodynamically expected [17]) by removing H₂ (CMR-TM-3). In particular, the maximum benzene yield achieved for both experiments with H₂ removal carried out at 710 °C (CMR-TM-1) and 720 °C (CMR-TM-3) is 10.40% at ca. 11 h and 11.31% at ~ 7.60 h, respectively.

Furthermore, the benzene yield reached by extracting H_2 at 710 °C through TM-1 is more stable than at 720 °C through TM-3, since it shows a 2.5-fold decrease in the average deactivation rate.

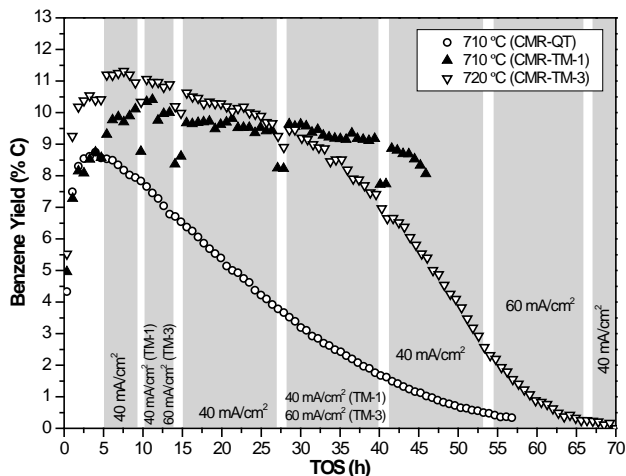


Figure 135. Effect of the temperature on the benzene yield versus the TOS of 6%Mo/MCM-22 catalyst, without (CMR-QT) and with H_2 removal (CMR-TM-1 and TM-3). Shaded areas indicate when H_2 is extracted.

As seen in Figure 136.a, the aromatics yield exhibits the same behavior than the benzene yield, reaching a maximum of 11.70% and 12.50% at around 11 h and 7.60 h for the CMR-TM-1 (710 °C) and the CMR-TM-3 (720 °C), respectively. Regarding the accumulated benzene moles (Figure 136.b), those obtained for the CMR-TM-3 experiment run at 720 °C by removing H_2 are the highest throughout the time on stream, achieving a plateau of $\sim 0.05 \text{ mol} \cdot \text{g}_{\text{cat}}^{-1}$ after 62 h. Nonetheless, the accumulated benzene moles for the experiment carried out at 710 °C with H_2 extraction (CMR-TM-1) increase almost linearly, overlapping its last values with those obtained for the CMR-TM-3 and appearing that will surpass them. However, the available data suggest that a slightly better MDA performance is obtained at 720 °C at least for 45 h on stream.

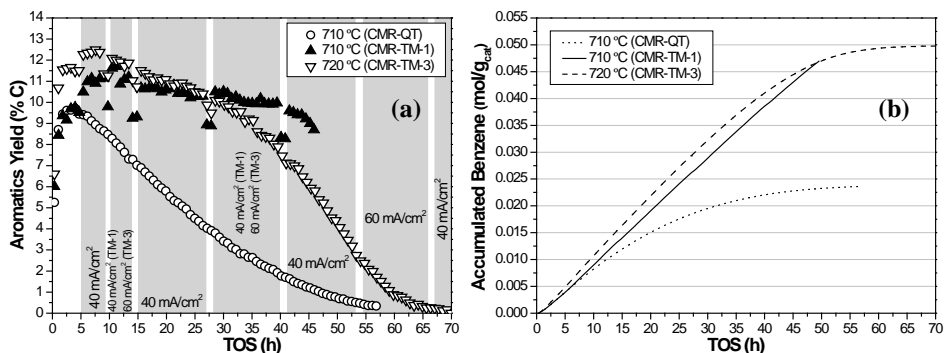


Figure 136. Effect of the temperature on the (a) aromatics yield and (b) accumulated benzene moles versus the TOS of 6%Mo/MCM-22 catalyst, without (CMR-QT) and with H_2 removal (CMR-TM-1 and TM-3). Shaded areas indicate when H_2 is extracted.

Figure 137.a shows that the total H_2 flux in the sweep side reached for the CMR-TM-3 rises when 40 mA·cm⁻² were imposed to the electrochemical cell, up to roughly 0.077 mL·min⁻¹·cm⁻², being this the maximum value obtained. However, when a current density of 60 mA·cm⁻² was applied, the total H_2 flux decreases, thereafter remaining in a range between 0.04 and 0.027 mL·min⁻¹·cm⁻². Moreover, in Figure 137.a the total H_2 flux is broken down into the H_2 fluxes that form it, the H_2 flux from protons and H_2 flux from oxide ions in the sweep side. In particular, the former and the latter contribute to the maximum total H_2 flux achieved by the TM-3 in 0.066 and 0.011 mL·min⁻¹·cm⁻², respectively. Both H_2 fluxes are scattered and the highest over time is the former (H_2 extracted), which participates in the total H_2 flux mainly over 70%.

In addition, the H_2 extracted and the O_2 injected for the CMR-TM-3 are depicted in Figure 137.b. A progressive increase over time is observed for the former after 27 h on stream, due to the gradual catalyst deactivation and, hence, the lower H_2 flow produced in the reaction side. Nevertheless, the O_2 injected

remains in the same range, lower than 0.2%, except for the first 3 h on stream by applying $40 \text{ mA} \cdot \text{cm}^{-2}$, in which it is a little bit higher.

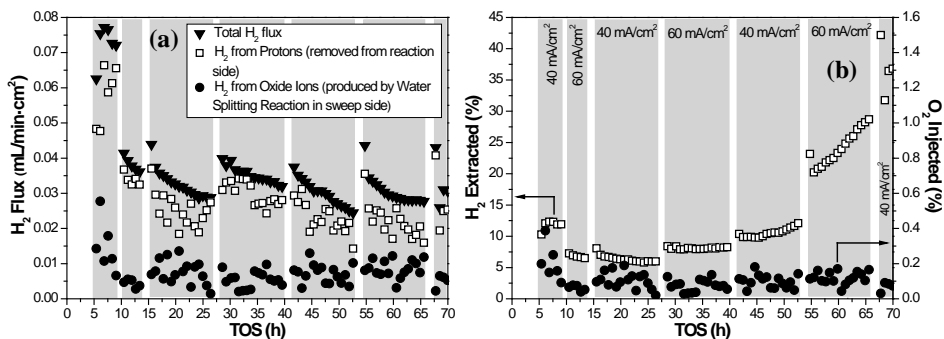


Figure 137. Electrochemical results of BZCY72 TM-3: (a) H_2 fluxes in sweep side and (b) H_2 extracted and O_2 injected versus the TOS at 720 °C. Shaded areas indicate when H_2 is extracted.

Regarding the TGA results shown in Table 82, it can be said that the amount of coke is reduced for both catalysts tested with H_2 extraction and O_2 injection, despite the longest duration of both experiments. Furthermore, between these catalysts used by extracting H_2 , the amount of coke is higher for the longest experiment (~ 28 h) and tested at 720 °C (CMR-TM-3). Nonetheless, for the catalyst tested at 720 °C, despite the effective coke suppression by means of the oxide ions injection through the BZCY72 TM-3, it is observed that the catalyst is progressively deactivated over time. Thus, suggesting that the O_2 injected through the TM-3 along the catalyst bed is insufficient to avoid the catalyst deactivation. Besides considering that the nature and/or the location of the coke within the zeolite pores may hamper its gasification. Additionally, the highest amount of coke ($\text{g} \cdot \text{g}_{\text{cat}}^{-1}$) per accumulated benzene mole is achieved without extracting H_2 , being almost the double than for the catalysts tested by removing H_2 . Nevertheless, in spite of the deactivation suffered by the spent catalyst in the experiment run at 720 °C (CMR-TM-3), the amount of coke per accumulated benzene mole obtained for

this experiment is the same than for the experiment performed at 710 °C (CMR-TM-1). This in part may be attributed to the increasing leakage of CH₄ present during the last 23 h of the CMR-TM-1 experiment, which causes increased coking and lower production of benzene.

Table 82. TGA results of spent 6%Mo/MCM-22 catalysts without and with H₂ removal through BZCY72 TM-1 and TM-3 at different temperatures.

Temperature (°C)	TOS (h)	Average Coke Formation Rate (g·g _{cat} ⁻¹ ·h ⁻¹)	Amount of Coke (g·g _{cat} ⁻¹)	g·g _{cat} ⁻¹ ·mol _{benz.} ⁻¹
710 (CMR-QT)	56.8	0.0055	0.314	7
710 (CMR-TM-1)	69.3	0.0030	0.208	3
720 (CMR-TM-3)	97.0	0.0031	0.296	3

The TPO profiles of carbon species of the 6%Mo/MCM-22 catalysts at different temperatures are illustrated in Figure 138 and the results are detailed in Table 81. By focusing on the TPO results for the catalysts tested by removing H₂, both types of coke are increased for the catalyst tested at 720 °C. Specifically, the coke related to Mo species and Brønsted acid sites (aromatic-type carbon) rises roughly 21 and 52%, respectively. Therefore, these results confirm those of TGA and indicate that the deactivation suffered by the catalyst at 720 °C may be related to the higher content of aromatic type coke (BAS) [14]. Moreover, by comparing the catalyst tested at 720 °C by extracting H₂ with that tested at 710 °C without H₂ removal (CMR-QT), it can be concluded that for the former the coke associated with Mo species is reduced ~ 8%, while the coke related to Brønsted acid sites is increased around 2%. Hence, this small difference between the amounts of coke related to Brønsted acid sites may be ascribed to the longer duration of the CMR-TM-3 experiment, since both catalysts are deactivated over time.

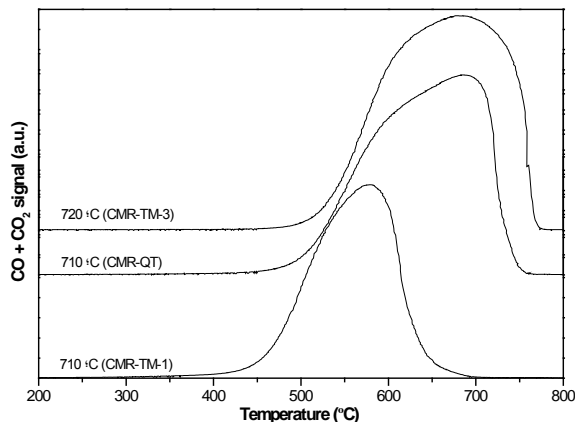


Figure 138. TPO profiles of carbon species over 6%Mo/MCM-22 catalysts after MDA reaction without (CMR-QT) and with H_2 removal (CMR-TM-1 and TM-3) at different temperatures. Same scale of Y-axis.

In addition, the temperature at maximum of both peaks (Table 83) is similar for the catalysts deactivated, that is, the catalyst tested at 710 °C without H_2 removal and the catalyst tested at 720 °C by removing H_2 . Thereby, it can be said that the coke characteristics (particle size, morphology, etc.) may be similar [15] between both deactivated catalysts. However, the temperature at maximum of both peaks for the catalyst tested at 710 °C with H_2 extraction is rather low than for the other two catalysts. Thus pointing out that its coke characteristics may be different among this catalyst and the other two.

Table 83. Results of the deconvoluted TPO profiles of carbon species over 6%Mo/MCM-22 catalysts tested without (CMR-QT) and with H_2 removal (CMR-TM-1 and TM-3) at different temperatures.

Temperature (°C)	TOS (h)	Temperature at maximum (°C)		Percentage (%)		Amount of coke ($g \cdot g_{cat}^{-1}$)	
		Peak 1	Peak 2	Peak 1	Peak 2	Peak 1	Peak 2
710 (CMR-QT)	56.8	620	695	75.24	24.76	0.2363	0.0778
710 (CMR-TM-1)	69.3	551	594	81.75	18.25	0.1702	0.0380
720 (CMR-TM-3)	97.0	644	719	73.08	26.92	0.2164	0.0797

10.4. Effect of co-feeding 10% of H₂ on MDA reaction with H₂ removal

H₂ has been added to the methane feed since it could be present in the feed gas of a possible industrial process in the future. Therefore, it may be interesting to study the MDA process by adding H₂ to the feed and removing H₂ from the reaction side through BZCY72 tubular membranes. Moreover, it is known (section 7.2.3. and [18-20]) that the co-feeding of H₂ improves the stability of the 6% Mo/MCM-22 catalyst in MDA reaction. Thereby, the combination of both mechanisms, that is to say, the addition of H₂ to the feed and the injection of O₂ from the sweep side may lead to a greater stability over time of the benzene yield.

This experiment, CMR-TM-4, was carried out by co-feeding a 10% of H₂ since the beginning of the MDA reaction according to the procedure described in the sections 3.6.2.1.1. and 3.6.2.1.2., by using the copper anode and the Tubular Membrane “4”. The highest methane conversion (Figure 139.a) is reached for the experiment performed without co-feeding 10% of H₂ and by removing H₂ (CMR-TM-1). Moreover, by focusing on the two experiments done by adding 10% of H₂, the methane conversion is higher for the experiment in which the H₂ is extracted and the O₂ is injected (CMR-TM-4). Thus, reducing greatly the negative effect provided by the addition of H₂ to the methane feed (sections 7.2.3.) on the MDA performance. It should be noted that the CMR-QT-3 experiment was carried out at 700 °C (section 3.6.2.2.1.). The CMR-TM-4 experiment was stopped after roughly 43 h on stream, being the CH₄ concentration measured in the sweep side (leakage) far below the limit concentration accepted to be used quantitatively. Therefore, neither the catalyst was deactivated nor the TM-4 was severely broken.

The same trend is observed for the H_2 flow normalized per gram of catalyst (Figure 139.b), achieving the highest H_2 flow for the experiment without co-feeding of H_2 (CMR-TM-1). The H_2 flow obtained for the CMR-TM-4 experiment decreases during the first 5 h on stream without extracting H_2 . While applying the different current densities to the cell, thereafter the H_2 flow remains almost constant over time, thus showing a higher stability than the H_2 flow for the CMR-TM-1 experiment. Further, the lower H_2 flow reached for the CMR-QT-3 experiment, during the time on stream in which H_2 was not co-fed, may be ascribed to the lower temperature at which this was run ($700\text{ }^\circ\text{C}$).

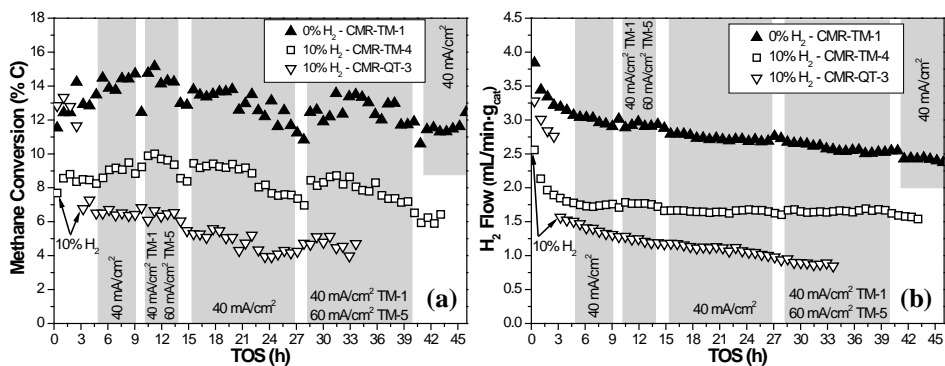


Figure 139. Effect of co-feeding 10% of H_2 by extracting H_2 on the (a) methane conversion and (b) H_2 flow versus the TOS of 6%Mo/MCM-22 catalyst.

Shadowed areas indicate when H_2 is extracted.

The selectivity to main products after 9 h on stream are detailed in Table 84, $40\text{ mA}\cdot\text{cm}^{-2}$ were applied at this TOS. C_2 and coke selectivities are higher for the experiments carried out by adding 10% of H_2 , especially for the experiment done without H_2 removal (CMR-QT-3). These results can be ascribed to a lower oligomerization of the C_2 species on the Brønsted acid sites of the zeolite, thus reducing markedly the aromatics formation. Hence, the aromatics selectivities, mainly for the benzene, are higher for the experiment performed without co-feeding H_2 (CMR-TM-1). While, between the experiments carried out by adding 10% of H_2 , the aromatics selectivities are

slightly higher by extracting H₂ through BZCY72 TM-4. These results reinforce the beneficial effect of the H₂ extraction and the O₂ injection on the MDA performance despite co-feeding 10% of H₂. Moreover, among the CMR-TM-1 and CMR-TM-4 experiments, the CO selectivity is higher for the CMR-TM-4 experiment by adding 10% of H₂.

Table 84. Effect of co-feeding 10% of H₂ without and with removing H₂ through TM-1 and TM-4 on the selectivity to main products after 9 h on stream of 6%Mo/MCM-22 catalyst.

H ₂ co-fed (%)	H ₂ extracted from reaction side	Selectivity (% C)					
		C ₆ H ₆	C ₂	C ₇ H ₈	C ₁₀ H ₈	Coke	CO
0	Yes (CMR-TM-1)	68.71	2.13	2.70	4.33	19.67	2.46
10	Yes (CMR-TM-4)	62.17	3.37	2.38	3.49	25.10	3.49
10	No (CMR-QT-3)	56.70	5.03	2.01	2.11	34.15	0.00

The same behavior observed for the methane conversion is illustrated for the benzene yield (Figure 140.a). The highest benzene yield is obtained for the CMR-TM-1 with H₂ removal and without co-feeding 10% of H₂ over time, reaching a maximum of 10.40% at ~ 11 h on stream. Nevertheless, lower benzene yield reached by adding H₂ to the feed (CMR-TM-4 and CMR-QT-3) is especially attributed to lower methane conversion obtained, since the benzene selectivity (not shown) for these experiments is slightly lower than for the CMR-TM-1 experiment. Moreover, the benzene yield reached by the CMR-TM-4 experiment is slightly more stable than for the CMR-TM-1, as it exhibits a 1.4-fold decrease in the average deactivation rate, thereby confirming the initial assumption. By focusing on the experiments done by adding 10% of H₂, the benzene yield for the CMR-TM-4 with H₂ removal is higher and more stable than that obtained without H₂ removal (CMR-QT-3). Concretely, for the former the benzene yield shows a 2.9-fold decrease in the average deactivation rate with respect to the latter. Furthermore, for these experiments the maximum

benzene yield reached is around 5.93% (at 10.50 h) and 4.34% (at 3.25 h), respectively.

In addition, by focusing on the accumulated benzene moles normalized per gram of catalyst (Figure 140.b), it is verified that the addition of 10% of H_2 to the feed worsens the MDA performance, since for both experiments the accumulated benzene moles are lower than for the experiment without co-feeding H_2 (CMR-TM-1). In particular, the maximum accumulated benzene moles for the catalyst tested by co-feeding 10% of H_2 and extracting H_2 from the reaction side (CMR-TM-4) are almost halved than without adding H_2 , $\sim 0.023 \text{ mol} \cdot \text{g}_{\text{cat}}^{-1}$ after ca. 43 h on stream.

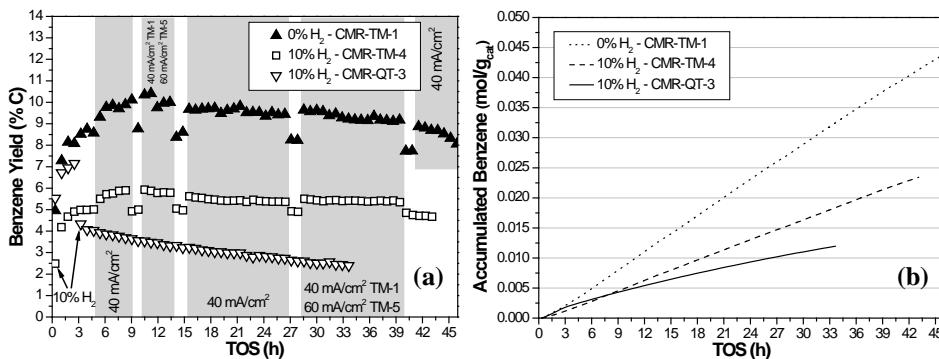


Figure 140. Effect of co-feeding 10% of H_2 without and with H_2 removal on the (a) benzene yield and (b) accumulated benzene moles versus the TOS of 6%Mo/MCM-22. Shaded areas indicate when H_2 is extracted.

Figure 141.a shows the H_2 flux measured in the sweep side for the CMR-TM-4. The first current density applied ($40 \text{ mA} \cdot \text{cm}^{-2}$) causes a gradual increase over time for the total H_2 flux. While the maximum total H_2 flux, around $0.115 \text{ mL} \cdot \text{min}^{-1} \cdot \text{cm}^{-2}$, is achieved by imposing $60 \text{ mA} \cdot \text{cm}^{-2}$. The H_2 flux obtained in sweep side thereafter remains in a range between 0.05 and $0.03 \text{ mL} \cdot \text{min}^{-1} \cdot \text{cm}^{-2}$. Moreover, Figure 141.a displays the H_2 fluxes the sum of which results in the total H_2 flux reached in the sweep side. The H_2 flux

extracted from the reaction side, also referred as H_2 from protons, contributes to the total H_2 flux mostly above 75%. In addition, Figure 141.b illustrates the H_2 extracted and the O_2 injected for the TM-4. In this case the maximum values of both parameters are achieved at the same TOS, 10.5 h, being 25.2 and 0.21%, respectively. As seen, for each current density imposed to the cell, except for the first time that $40 \text{ mA}\cdot\text{cm}^{-2}$ were applied, the H_2 extracted is gradually reduced over time. This behavior is directly related to the lower total H_2 flux obtained in the sweep side, as the H_2 flow reached in the reaction side (Figure 139.b) shows an exceptional stability.

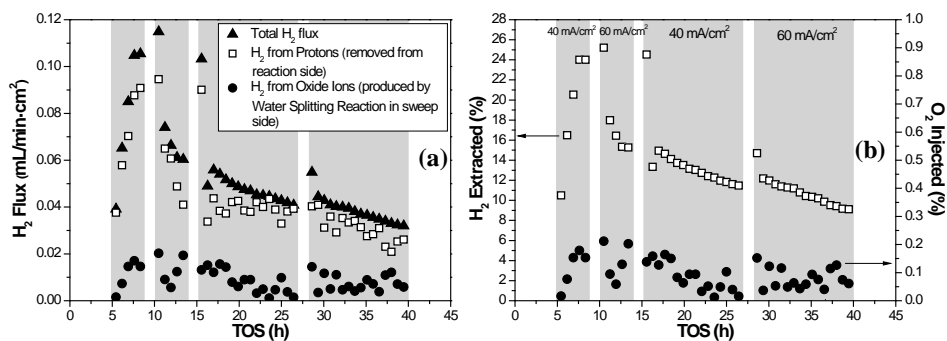


Figure 141. Electrochemical results of BZCY72 TM-4: (a) H_2 flux in sweep side and (b) H_2 extracted and O_2 injected versus the TOS by co-feeding 10% of H_2 .

Shaded areas indicate when H_2 is extracted.

Table 85 shows the TGA results obtained for the spent catalysts. By comparing the experiments done with H_2 removal, it can be observed that the amount of coke is higher for the experiment carried out without co-feeding 10% of H_2 (CMR-TM-1), what certainly is also influenced by its longer duration (~ 26 h). However, for the experiments done by co-feeding 10% of H_2 , the amount of coke is slightly higher for the experiment performed with H_2 removal (CMR-TM-4), this may be also related to its longer duration (~ 10 h). Nonetheless, the highest amount of coke per accumulated benzene mole is achieved by the CMR-QT-3 experiment with co-feeding of 10% of H_2 , being

more than the double reached by the CMR-TM-4 experiment. Therefore, the H₂ extraction and O₂ injection through TM-4 leads to a better MDA performance than for the CMR-QT-3.

Table 85. TGA results of spent 6%Mo/MCM-22 catalysts without and with H₂ removal through BZCY72 TM-1 and TM-4 by adding 0 and 10% of H₂.

H ₂ co-fed (%)	TOS (h)	Average Coke Formation Rate (g·g _{cat} ⁻¹ ·h ⁻¹)	Amount of Coke (g·g _{cat} ⁻¹)	g·g _{cat} ⁻¹ ·mol _{benz.} ⁻¹
0 (CMR-TM-1)	69.3	0.0030	0.208	3
10 (CMR-TM-4)	43.0	0.0026	0.112	2
10 (CMR-QT-3)	33.6	0.0030	0.0997	5

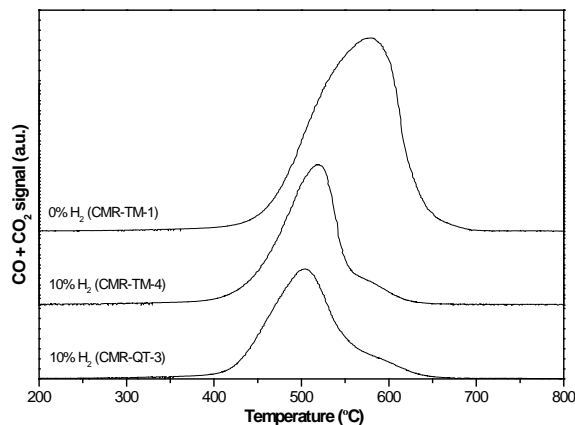


Figure 142. TPO profiles of carbon species over 6%Mo/MCM-22 catalysts after MDA reaction with and without H₂ removal by adding 0 and 10 % of H₂ to the methane feed. Same scale of Y-axis.

In Figure 142 the TPO profiles of carbon species of 6%Mo/MCM-22 catalyst are depicted and the results are given in Table 86. Moreover, as with the TPO results exhibited in the section 7.2., despite co-feeding 10% of H₂ the coke characteristics (particle size, morphology, etc.) for these three catalysts may be similar [15] since the temperature at maximum of both peaks (Table 86) is similar for them. In addition, the TPO results are in concordance with those of

TGA, briefly, the amount of both types of coke are lower for the catalysts tested by adding 10% of H₂ to the feed. However, the differences in the duration of these experiments may hinder the in-depth interpretation and discussion of TPO results.

Table 86. Results of the deconvoluted TPO profiles of carbon species over 6%Mo/MCM-22 catalysts tested without and with H₂ removal by adding 0 and 10% of H₂.

H ₂ co-fed (%)	TOS (h)	Temperature at maximum (°C)		Percentage (%)		Amount of coke (g·g _{cat} ⁻¹)	
		Peak 1	Peak 2	Peak 1	Peak 2	Peak 1	Peak 2
0 (CMR-TM-1)	69.3	551	594	81.75	18.25	0.1702	0.0380
10 (CMR-TM-4)	43.0	510	592	86.81	13.19	0.0975	0.0148
10 (CMR-QT-3)	33.6	500	593	86.43	13.57	0.0861	0.0135

10.5. Effect of the current density applied on the electrochemical cell on MDA reaction with H₂ removal

In this section the effect of the current density imposed and the way of applying it to the cell is studied aiming to improve both the MDA performance and the electrochemical performance. The CMR-TM-5 experiment was done using the Tubular Membrane “5” with 4 cm of copper anode, by applying 60 mA·cm⁻² with two different ascending current ramps as it is detailed in the sections 3.6.2.1.1. and 3.6.2.1.2.

The methane conversion (Figure 143.a) is very similar for the three experiments during the first 5 h on stream, despite applying the ascending current ramp for the CMR-TM-5. Nonetheless, when the different current densities were imposed to the TM, the methane conversion is higher for these two experiments, being particularly higher for the CMR-TM-5 experiment carried out by imposing 60 mA·cm⁻². Therefore, the use of both, the ascending

current ramp and $60 \text{ mA}\cdot\text{cm}^{-2}$, appears to be helpful for the MDA performance at least until roughly 8 h on stream. However, from this TOS the methane conversion is very similar and a little bit scattered for both CMR-TM experiments. The CMR-TM-5 experiment was stopped after ~ 71 h on stream, reaching a CH_4 concentration in the sweep side (leakage) rather low to the limit concentration to be quantitatively used.

Further, the H_2 flow normalized per gram of catalyst (Figure 143.b) is higher for the CMR-TM-5 from the 5th h on stream. This is closely related to both, the higher methane conversion and the higher aromatics selectivity (Figure 144.a) achieved by applying $60 \text{ mA}\cdot\text{cm}^{-2}$, during a certain period of time.

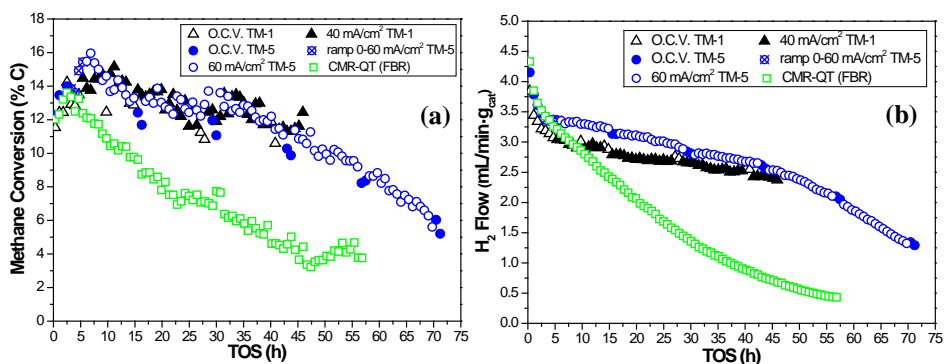


Figure 143. Effect of the current density imposed on BZCY72 TM-1 and TM-5 on the (a) methane conversion and (b) H_2 flow versus the TOS of 6%Mo/MCM-22 catalyst.

In the following table the selectivity to main products after 9 h on stream are shown. The lowest coke selectivity and the highest aromatics (benzene, toluene and naphthalene) and CO selectivities are achieved by the CMR-TM-5 experiment, using $60 \text{ mA}\cdot\text{cm}^{-2}$. These results suggest that the MDA performance is improved by using these new electrochemical conditions. Nevertheless, the C_2 selectivity obtained for this experiment is slightly higher

than for the CMR-TM-1 experiment and lower than for the CMR-QT experiment.

Table 87. Effect of the current density on the selectivity to main products after 9 h on stream of 6%Mo/MCM-22 catalyst by removing H_2 through TM-1 and TM-5.

H ₂ removal from reaction side	Current density (mA·cm ⁻²)	Selectivity (% C)					
		C ₆ H ₆	C ₂	C ₇ H ₈	C ₁₀ H ₈	Coke	CO
No (CMR-QT)	0	71.10	3.16	2.73	3.50	19.51	0.00
Yes (CMR-TM-1)	40	68.71	2.13	2.70	4.33	19.67	2.46
Yes (CMR-TM-5)	60	72.65	2.26	2.86	4.58	15.05	2.60

Concretely, the aromatics selectivity (Figure 144.a) for the CMR-TM-5 is the highest obtained during the first 25 h on stream. This points out that the equilibrium shift that takes place by imposing 60 mA·cm⁻² reaches a higher production of aromatics, mainly benzene, than by applying 40 mA·cm⁻². Despite the aromatics selectivity is decreased over time after 50 h on stream, the values reached are in a large extent higher than for the CMR-QT experiment (without H_2 removal).

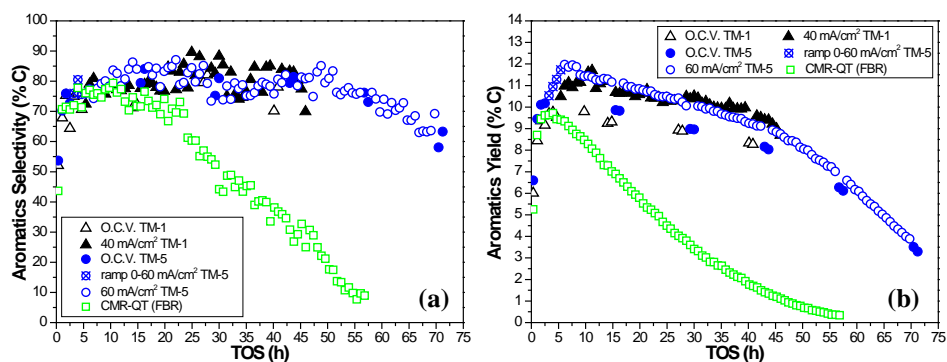


Figure 144. Effect of the current density imposed on BZCY72 TM-1 and TM-5 on the (a) aromatics selectivity and (b) aromatics yield versus the TOS of 6%Mo/MCM-22 catalyst.

Moreover, Figure 144.b shows that the highest aromatics yield is reached by imposing $60 \text{ mA}\cdot\text{cm}^{-2}$ (CMR-TM-5) during 27 h on stream, from which it is lower than by applying $40 \text{ mA}\cdot\text{cm}^{-2}$ (CMR-TM-1). This is due to both the higher methane conversion and the higher aromatics selectivity achieved during this period on stream for the CMR-TM-5 experiment. The maximum aromatics yield is roughly 9.70, 11.70 and 12% for the CMR-QT, CMR-TM-1 and CMR-TM-5 experiments, respectively.

In Figure 145.a it can be observed that the benzene yield shows the same trend than the aromatics yield (Figure 144.b) for these three experiments, obtaining a maximum of 8.74, 10.40 and 10.75% for the CMR-QT, CMR-TM-1 and CMR-TM-5 experiments, respectively. However, regarding the stability, the CMR-TM-1 ($40 \text{ mA}\cdot\text{cm}^{-2}$) experiment is slightly more stable than the CMR-TM-5 ($60 \text{ mA}\cdot\text{cm}^{-2}$), showing a 1.6-fold decrease in the average deactivation rate.

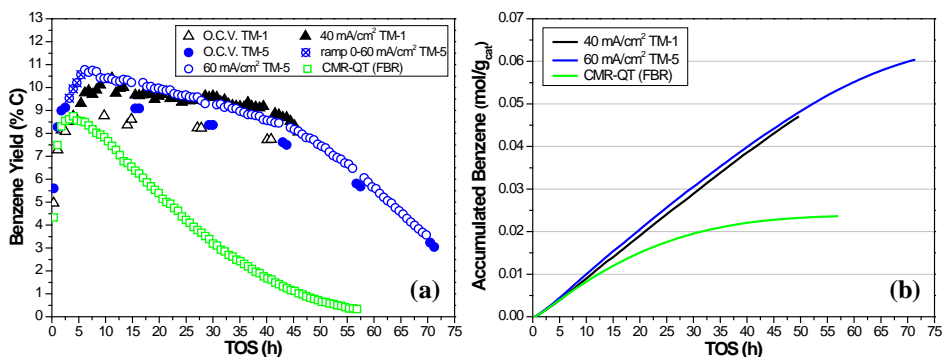


Figure 145. Effect of the current density imposed on BZCY72 TM-1 and TM-5 on the (a) benzene yield and (b) accumulated benzene moles versus the TOS of 6%Mo/MCM-22 catalyst.

In addition, the accumulated benzene moles normalized per gram of catalyst are illustrated in Figure 145.b. The highest accumulated benzene moles are reached by the experiment performed by imposing $60 \text{ mA}\cdot\text{cm}^{-2}$ (CMR-TM-5). It appears that after 63 h on stream the accumulated benzene moles are

slowed down noticeably, achieving $0.06 \text{ mol} \cdot \text{g}_{\text{cat}}^{-1}$ after 71.2 h on stream. Therefore, a slightly better MDA performance is obtained by applying $60 \text{ mA} \cdot \text{cm}^{-2}$ at least for 45 h on stream.

The total H_2 flux obtained in sweep side (Figure 146.a) increases after imposing $60 \text{ mA} \cdot \text{cm}^{-2}$ to the cell, being the maximum $\sim 0.154 \text{ mL} \cdot \text{min}^{-1} \cdot \text{cm}^{-2}$. However, a progressive reduction is observed over time, which may be attributed to the lower H_2 production (Figure 143.b) in the reaction side. In addition, the H_2 fluxes that contribute to the total H_2 flux obtained in the sweep side are shown in Figure 146.a. In particular, the highest H_2 flux is that removed from the reaction side (H_2 from protons) throughout the time on stream. Nevertheless, the H_2 flux from oxide ions (water splitting reaction) remains in a range between 0.011 and $0.020 \text{ mL} \cdot \text{min}^{-1} \cdot \text{cm}^{-2}$ after 7 h on stream. The H_2 flux from protons contributes to the total H_2 flux mainly above 77%.

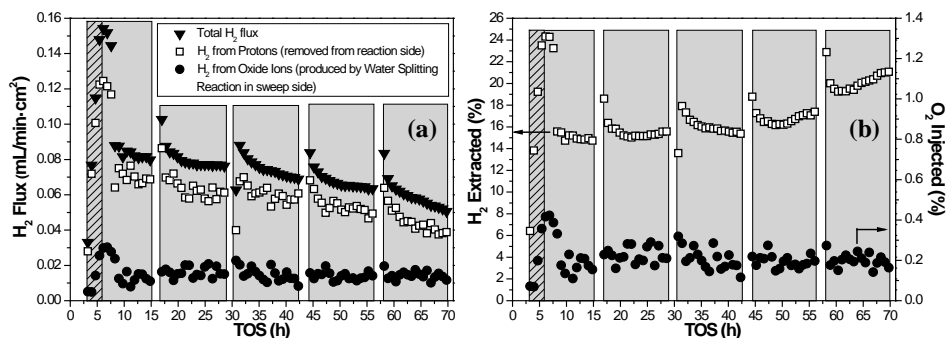


Figure 146. Electrochemical results of BZCY72 TM-5: (a) H_2 flux in sweep side and (b) H_2 extracted and O_2 injected versus the TOS by imposing $60 \text{ mA} \cdot \text{cm}^{-2}$.

Shaded areas indicate when H_2 is extracted.

Moreover, Figure 146.b displays the H_2 extracted and the O_2 injected for the TM-5. In this experiment, the H_2 extracted suffers an increment after 42 h on stream directly related to the abovementioned reduction of the H_2 flow in the reaction side (Figure 143.b). However, in the previous period of time, the maximum H_2 extracted was achieved by imposing for the first time

60 mA·cm⁻², being 24.3%. While the maximum O₂ injected was roughly 0.42%, being thereafter scattered and remaining in the range between 0.13 and 0.30%.

Table 88 details the TGA results obtained for the spent catalysts studied in this section. The highest amount of coke and the highest average coke formation rate are achieved by the catalyst tested without H₂ removal (CMR-QT), despite its shorter duration. Therefore, the H₂ extraction and the O₂ injection through the BZCY72 TM-5 reduce effectively the amount of coke accumulated on the catalyst. Nonetheless, despite the similar TOS of the CMR-TM experiments, the amount of coke for the catalyst tested by imposing 60 mA·cm⁻² (CMR-TM-5) is higher than for the catalyst tested by using 40 mA·cm⁻² (CMR-TM-1). Therefore, it is necessary to contemplate that the nature and/or the location of the coke may be decisive to allow its gasification/removal. In addition, by focusing on the amount of coke (g·g_{cat}⁻¹) per accumulated benzene mole, it can be concluded that the MDA performance is slightly improved for the CMR-TM-5 since it exhibits the lowest amount of coke per accumulated benzene mole. These TGA results were confirmed by those of elemental analysis.

Table 88. TGA results of spent 6%Mo/MCM-22 catalysts without and with H₂ removal through BZCY72 TM-1 and TM-5.

Current density (mA/cm ²)	TOS (h)	Average Coke Formation Rate (g·g _{cat} ⁻¹ ·h ⁻¹)	Amount of Coke (g·g _{cat} ⁻¹)	g·g _{cat} ⁻¹ ·mol _{benz.} ⁻¹
0 (CMR-QT)	56.8	0.0055	0.314	7
40 (CMR-TM-1)	69.3	0.0030	0.208	3
60 (CMR-TM-5)	71.2	0.0037	0.266	2

The TPO results are summarized in Table 89 and they are in agreement with those of TGA. Both types of coke accumulated on the 6%Mo/MCM-22 catalyst are reduced by extracting H₂ and injecting O₂ through BZCY72 TM-1 and TM-5. In particular, for the CMR-TM-5 the coke associated with Mo species and with Brønsted acid sites (aromatic-type carbon) decreases roughly

14 and 20%, respectively, with respect to the CMR-QT. While comparing both catalysts tested by removing H₂, for the CMR-TM-5 (60 mA·cm⁻²) the coke related to Mo species increases roughly 17% and the coke associated with Brønsted acid sites (aromatic-type carbon) rises ca. 39%, with respect to the CMR-TM-1 (40 mA·cm⁻²). Moreover, for the three spent catalysts the coke characteristics (particle size, morphology, etc.) may be different as the temperature at maximum of both peaks is rather different [15] among them, specially for the catalyst tested on the CMR-TM-1 experiment.

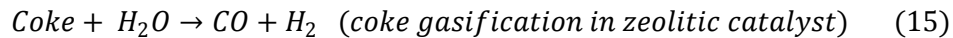
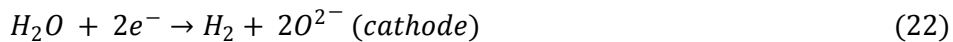
Table 89. Results of the deconvoluted TPO profiles of carbon species over 6%Mo/MCM-22 catalysts tested without (CMR-QT) and with H₂ removal (CMR-TM-1 and TM-5) by applying different current densities.

Current density (mA/cm ²)	TOS (h)	Temperature at maximum (°C)		Percentage (%)		Amount of coke (g·g _{cat} ⁻¹)	
		Peak 1	Peak 2	Peak 1	Peak 2	Peak 1	Peak 2
0 (CMR-QT)	56.8	620	695	75.24	24.76	0.2363	0.0778
40 (CMR-TM-1)	69.3	551	594	81.75	18.25	0.1702	0.0380
60 (CMR-TM-5)	71.2	654	731	76.63	23.37	0.2042	0.0623

10.6. Conclusions

The implementation of this novel catalytic membrane reactor (CMR) using the 6%Mo/MCM-22 catalyst and the co-ionic proton and oxide ion conducting BZCY72 tubular membrane, by imposing different current densities to the electrochemical cell, exceptionally improves the MDA performance and the catalyst stability for the five experiments carried out. This marked improvement observed lies in the concurrent and controlled H₂ extraction (Equations 20 and 21) and O₂ injection (Equations 22 and 23) along the catalyst bed in the CMR. On one hand, the H₂ extraction from the reaction side involves shifting the thermodynamic equilibrium of the MDA reaction, thus increasing

notably the methane conversion and slightly the aromatics selectivity, thereby reaching high aromatics yield. On the other hand, the O₂ injection to the reaction side causes the formation of small amounts of H₂O, which leads to the coke gasification (Equation 15) whereby an enhancement of the catalyst stability is achieved over time.



Firstly, by comparing the results achieved using the CMR-TM-1 with those obtained for the CMR-QT at 710 °C, it can be concluded that the best MDA performance is reached by extracting H₂ and injecting O₂ through the BZCY72 TM-1 when 40 mA·cm⁻² are imposed externally [8]. Because of the extraordinary increment of the methane conversion and, hence, the aromatics yield, besides the remarkably stability of the catalyst over time (~ 46 h) due to the coke gasification. The TGA, N₂ sorption and TPO results are in concordance, revealing that the amount of coke deposited on the catalyst tested for the CMR-TM-1 is considerably reduced with respect to that for the CMR-QT, despite its longer duration (~ 12 h). In particular, based on the TPO results it can be suggested that the great stability shown by the CMR-TM-1 may result from the major reduction of aromatic type coke [14]. Further, for the CMR-TM-1 the amount of coke per accumulated benzene mole is lower than for the CMR-QT, concretely less than halved. The XANES analyses at the Mo K-edge and the XPS Mo3d results of both catalysts disclose that the oxidation state of Mo species is very alike between them. In addition, regarding the acidity of the spent catalysts, that corresponding to the CMR-TM-1 is higher than for the

CMR-QT. However, the acid strength distribution is very similar for both catalysts.

Moreover, by focusing on the different anodes applied on the BZCY72 tubular membrane in this work, the copper (CMR-TM-1) and the Mo₂C/Cu/BZCY72 (CMR-TM-2) anodes, despite applying higher current densities for the CMR-TM-2, the best MDA and electrochemical performances were by far reached by using the copper anode. Nevertheless, the MDA performance exhibited by the CMR-TM-2 is better than by the CMR-QT-2. In this case, the TGA and TPO results are also in agreement, showing that the catalyst tested in the CMR-TM-2 accumulates less amount of coke than for the CMR-QT-2. These results highlight the challenging work that lies ahead in order to further research to improve the copper anode and even to test alternative electrode materials.

Besides the CMR-TM-1 experiment, another three experiments were carried out by using the copper anode but employing different experimental conditions and current densities. The best electrochemical performance obtained among these four experiments is for the CMR-TM-1 experiment carried out at 710 °C by imposing 40 mA·cm⁻² at different TOS. Furthermore, by comparing this experiment with the CMR-TM-4 in which a 10% of H₂ was co-fed, it can be said that the best MDA performance is achieved by the CMR-TM-1. Nonetheless, the MDA results obtained for the CMR-TM-4 are better than for the CMR-QT-3 experiment (without H₂ extraction and by co-feeding 10% of H₂). Hence, despite the detrimental effect of co-feeding 10% of H₂, the H₂ extraction and O₂ injection through the BZCY72 TM-4 enables to achieve these better results, since the former causes a higher methane conversion and the latter leads to a lower amount of coke per accumulated benzene mole.

However, the CMR-TM-3 (720 °C) and the CMR-TM-5 (60 mA·cm⁻² using different ascending current ramps) experiments reach a slightly better

MDA performance than the CMR-TM-1 at least during ~ 45 on stream, since the accumulated benzene moles normalized per gram of catalyst are slightly higher than for the CMR-TM-1 experiment. Further, especially the methane conversion and in lesser extent the benzene selectivity are higher for these two experiments (CMR-TM-3 and CMR-TM-5). Nevertheless, for the CMR-TM-3 and the CMR-TM-5 the benzene yield exhibits less stability over time than for the CMR-TM-1, starting to deactivate for both after roughly 40 h on stream. The catalysts tested on the CMR-TM-3 and the CMR-TM-5 experiments accumulate less amount of coke than the CMR-QT catalysts (without H₂ extraction), thus indicating the effectiveness of coke suppression by removing H₂ and injecting O₂ through the BZCY72 TM. Anyway, both catalysts are deactivated over time, thereby it can be suggested that the nature and/or the position of the coke in the zeolite channels prevents its gasification. Moreover, it can be supposed that an increment of the O₂ injected may prolong the catalyst lifetime, resulting likely in higher amounts of H₂O to remove the coke deposited, provided that a detrimental concentration of H₂O is not reached for the Mo species present on the catalyst.

10.7. References

- [1] D.J. Wang, J.H. Lunsford, M.P. Rosynek, *Topics in Catalysis*, 3 (1996) 289-297.
- [2] Y.D. Xu, X.H. Bao, L.W. Lin, *Journal of Catalysis*, 216 (2003) 386-395.
- [3] B.M. Weckhuysen, M.P. Rosynek, J.H. Lunsford, *Catalysis Letters*, 52 (1998) 31-36.
- [4] Z. Liu, L. Li, E. Iglesia, *Catalysis Letters*, 82 (2002) 175-180.
- [5] A.K. Kinage, R. Ohnishi, M. Ichikawa, *Catalysis Letters*, 88 (2003) 199-202.
- [6] J. Xue, Y. Chen, Y. Wei, A. Feldhoff, H. Wang, J. Caro, *ACS Catalysis*, 6 (2016) 2448-2451.

- [7] Z. Cao, H. Jiang, H. Luo, S. Baumann, W.A. Meulenberg, J. Assmann, L. Mleczko, Y. Liu, J. Caro, *Angewandte Chemie-International Edition*, 52 (2013) 13794-13797.
- [8] S.H. Morejudo, R. Zanon, S. Escolastico, I. Yuste-Tirados, H. Malerod-Fjeld, P.K. Vestre, W.G. Coors, A. Martinez, T. Norby, J.M. Serra, C. Kjolseth, *Science*, 353 (2016) 563-566.
- [9] H. Matsumoto, S. Hamajima, H. Iwahara, *Solid State Ionics*, 145 (2001) 25-29.
- [10] S.M. Babiniec, S. Ricote, N.P. Sullivan, *International Journal of Hydrogen Energy*, 40 (2015) 9278-9286.
- [11] C.D. Wagner, W.M. Riggs, L.E. Davis, J.F. Moulder, *Handbook of X-ray Photoelectron Spectroscopy*, First ed., Physical Electronics Division, Perkin-Elmer Corp., 1979.
- [12] K.S. Kim, W.E. Baitinger, J.W. Amy, N. Winograd, *Journal of Electron Spectroscopy and Related Phenomena*, 5 (1974) 351-367.
- [13] L. Ovari, J. Kiss, *Vacuum*, 80 (2005) 204-207.
- [14] D. Ma, D.Z. Wang, L.L. Su, Y.Y. Shu, Y. Xu, X.H. Bao, *Journal of Catalysis*, 208 (2002) 260-269.
- [15] C.A. Querini, S.C. Fung, *Appl. Catal. A-Gen.*, 117 (1994) 53-74.
- [16] K. Skutil, M. Taniewski, *Fuel Processing Technology*, 87 (2006) 511-521.
- [17] P.M. Bijani, M. Sohrabi, S. Sahebdelfar, *Chemical Engineering & Technology*, 35 (2012) 1825-1832.
- [18] Z. Liu, M.A. Nutt, E. Iglesia, *Catalysis Letters*, 81 (2002) 271-279.
- [19] H.T. Ma, R. Kojima, S. Kikuchi, M. Ichikawa, *Catalysis Letters*, 104 (2005) 63-66.
- [20] H.T. Ma, R. Ohnishi, M. Ichikawa, *Catalysis Letters*, 89 (2003) 143-146.

Chapter 11.

CONCLUSIONS

11. Conclusions

Methane dehydroaromatization reaction has been intensively studied in the present thesis, by focusing the investigation in three objectives for enhancing the activity and the stability on MDA reaction.

Study of different Mo/zeolite catalysts:

The zeolite and the Mo content employed to prepare the catalyst had a direct and a significant influence on the MDA performance. As revealed from the study of different 3%Mo/HZSM-5 catalysts, the Si/Al ratio and the crystal size of the zeolite were decisive. Concretely, the CBV3024E zeolite exhibited the highest and most stable benzene yield over time, possessing a Si/Al=15 and a crystal size of 0.1-0.25 μm . Moreover, the increase of the Mo content from 3 to 6% resulted in a better MDA performance for the CBV3024E zeolite.

In addition, the topology and the channel dimensions of the zeolite were greatly important. Among the eleven zeolites studied with 3% (wt.) of Mo, the HZSM-5, IM-5 and TNU-9 zeolites, which possess tridirectional channels and medium pore (10 MR), were the most favorable for MDA reaction, obtaining the best MDA results with the 3%Mo/HZSM-5 catalyst (CBV3024E). The small pore dimensions (Chabazite) blocked the benzene (kinetic diameter of 5 Å) diffusion. While, the zeolites with unidirectional or bidirectional channels also showed bad MDA results. However, by comparing this HZSM-5 zeolite with the MCM-22 (Si/Al=15) using 6% (wt.) of Mo, the latter exhibited better MDA performance than the former.

The manufacturing process used to produce the 6%Mo/HZSM-5 and 6%Mo/MCM-22 catalysts also affected the MDA performance. The new manufacturing process, by which the Extrudated I catalysts (6%Mo/HZSM-5 and 6%Mo/MCM-22) were obtained, led to a slightly worse MDA results than

using the Granulated catalysts. Nevertheless, the other new manufacturing process used to produce the 6%Mo/MCM-22 Extruded II catalyst caused a far worse MDA performance than the Granulated catalyst. This might be attributed to the internal diffusion effects as the particles size of the Extruded II catalyst was much greater than for the Granulated ones (almost two orders of magnitude).

Optimization of some process conditions:

Firstly, the catalyst activation played a significant role on the performance of the MDA reaction, being positive or negative. In particular, the pre-coking of the 6%Mo/HZSM-5 catalyst with TMB caused a negative effect on the MDA performance, since it caused higher formation of coke on the catalyst before the MDA reaction. However, the other two activations tested were positive for the MDA performance. Concretely, the 6%Mo/HZSM-5 catalyst activation with a gas mixture of CH₄:H₂, 1:4 (vol. ratio), during 1 h up to 700 °C and kept at this temperature for 2 h, led to the best MDA performance. Since the catalyst was pre-carburized and pre-reduced, forming the most stable and active Mo species for MDA reaction. Thereby, this activation (new activation) was also applied over the 6%Mo/MCM-22 catalyst, resulting in a better MDA performance than using the standard activation, but in lesser extent than for the 6%Mo/HZSM-5 catalyst.

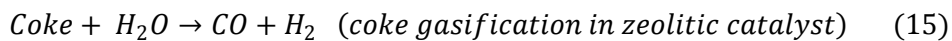
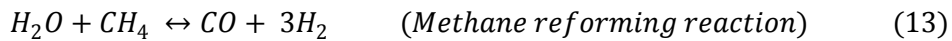
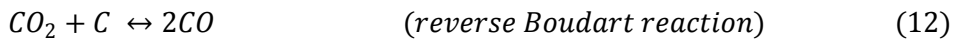
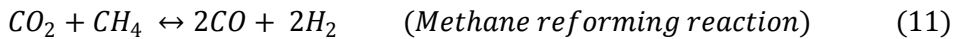
Moreover, by increasing the catalyst amount (0.6-1.8g) and the feed gas flow (15-45 mL·min⁻¹), in order to keep constant the space velocity at 1500 mL·h⁻¹·g_{cat}⁻¹ using the 6%Mo/HZSM-5 catalyst, the MDA results were slightly improved. Nevertheless, the space velocity strongly affected the MDA performance, as reflected in the results obtained with the 6%Mo/MCM-22 catalyst using the standard and the new activations. In particular, the best MDA performance was achieved at 1500 mL·h⁻¹·g_{cat}⁻¹, which might be related to the more efficient C₂ species oligomerization on the Brønsted acid sites. While

using higher space velocities ($3000 \text{ mL}\cdot\text{h}^{-1}\cdot\text{g}_{\text{cat}}^{-1}$), the interaction among the methane and the active sites of the catalysts was reduced. And for lower space velocities (835 and $750 \text{ mL}\cdot\text{h}^{-1}\cdot\text{g}_{\text{cat}}^{-1}$), the condensation of heavy aromatics was facilitated, resulting in higher coke deposition per accumulated benzene mole.

Furthermore, the co-feeding of H_2O , H_2 and CO_2 separately affected negatively the MDA performance, irrespective of the catalyst ($6\%\text{Mo}/\text{HZSM-5}$ or $6\%\text{Mo}/\text{MCM-22}$), at least for the concentrations employed on the present thesis. The addition of these three co-reactants was thermodynamically detrimental for the MDA performance since: (i) H_2 reduced the methane conversion owing to the equilibrium displacement, (ii) H_2O promoted the methane reforming reaction (Equation 13) and the coke gasification (Equation 15), and (iii) CO_2 favored the methane reforming reaction (Equation 11) and the reverse Boudart reaction (Equation 12). Besides these thermodynamic drawbacks, the addition of H_2O and CO_2 caused a partial re-oxidation of the Mo species on the catalyst, which was detrimental for the MDA performance. However, the H_2O vapor concentrations used in this work did not affect the framework aluminum. Despite the negative effects observed by co-feeding these three reactants, the stability of the catalyst was improved due to the successful suppression of coke. In particular, the co-feeding of 6% of H_2 achieved a greater reduction of the coke deposited on the $6\%\text{Mo}/\text{HZSM-5}$ and $6\%\text{Mo}/\text{MCM-22}$ catalysts, than by adding 1.08% of H_2O to the feed. Thus, revealing that the mechanism of the coke deposits removal was different for H_2O and H_2 .

The TOS at which H_2O was added to the methane feed was an important parameter, as it greatly influenced the MDA performance due to the need to carburize the Mo species in dry conditions, reaching the best results for the $6\%\text{Mo}/\text{MCM-22}$ catalyst by adding 1.08% of H_2O after 3 h in dry conditions. Moreover, by focusing on the co-feeding of 6% of H_2 over the $6\%\text{Mo}/\text{MCM-22}$ catalyst, there were several parameters that improved the

MDA performance, i.e.: the new activation of the catalyst, the use of higher feed flow and catalyst amount at $1500 \text{ mL}\cdot\text{h}^{-1}\cdot\text{g}_{\text{cat}}^{-1}$, and the addition of H_2 after 3 h on stream without addition of H_2 , which in turn reduced the amount of coke per accumulated benzene mole. Further, the addition of 0.288% of H_2O barely affected the MDA performance obtained by co-feeding different concentrations of H_2 (20, 15, 10 and 5%). It should be noted that for the addition of H_2O and H_2 , the best MDA results were obtained for the lowest concentrations co-fed.

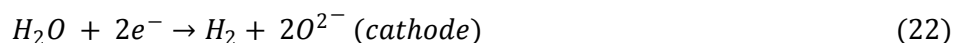


Finally, the catalyst regeneration with pure H_2 efficiently restored the catalytic activity for the 6%Mo/HZSM-5 and 6%Mo/MCM-22 catalysts in dry conditions, being slightly better for the former. Therefore, for the 6%Mo/MCM-22 catalyst the nature and location of the coke deposits somehow might hamper its elimination using H_2 . However, the catalyst regeneration for the 6%Mo/HZSM-5 catalyst tested in wet conditions was less effective than in dry conditions, which revealed the partial re-oxidation suffered by the Mo species on the catalyst.

Development and implementation of a CMR using the 6%Mo/MCM-22 catalyst and the BZCY72 tubular membrane:

This novel CMR enabled to achieve an exceptional MDA performance and catalyst stability due to the concomitant H_2 extraction (Equations 20 and 21) and O_2 injection (Equations 22 and 23), that took place along the catalyst bed by means of the BZCY72 tubular membrane, imposing a current to the

electrochemical cell. H₂ removal from the reaction side caused the thermodynamic equilibrium shift of the MDA reaction, increasing the methane conversion and thereby the aromatics yield. While, O₂ injection to the reaction side allowed the formation of H₂O in a controlled way, by which the coke accumulated was partially suppressed (coke gasification, Equation 15), thus resulting in higher catalyst stability. Moreover, the XANES analyses at the Mo K-edge and the XPS Mo3d results evidenced that these small amounts of H₂O introduced barely affected the oxidation state of the Mo species present on the 6%Mo/MCM-22 catalyst.



By comparing the MDA results obtained using two different anodes, the copper (CMR-TM-1) and the Mo₂C/Cu/BZCY72 (CMR-TM-2), the best MDA and electrochemical performances were achieved applying the copper anode. Although in both CMR-TM experiments the MDA results were better than in the CMR-QT experiment (without BZCY72 TM).

Furthermore, the copper anode was used in other three experiments by changing different reactions conditions. In one of them, 10% of H₂ was co-fed (CMR-TM-4), resulting in a better MDA performance than in the CMR-QT-3 experiment (without H₂ extraction and by co-feeding 10% of H₂). However, by comparing with the CMR-TM-1 experiment (without H₂ addition), the MDA and electrochemical performances were better for the latter. In the other two experiments, one was carried out at higher temperature, i.e., 720 °C (CMR-TM-3) and the other was done applying higher current density to the cell, i.e., 60 mA·cm⁻² and different ascending current ramps (CMR-TM-5). The best

electrochemical performance was reached for the CMR-TM-1 experiment. Nevertheless, despite the lower stability shown by the CMR-TM-3 and CMR-TM-5 experiments, a slightly better MDA performance was obtained than for the CMR-TM-1 at least for 45 h on stream. Since the accumulated benzene moles were slightly higher over time for these two experiments (CMR-TM-3 and CMR-TM-5) than for the CMR-TM-1.

LISTS

List I Figures

Figure 1. World primary energy consumption (Million tones oil equivalent: Mtoe) since 1988 until 2013 [5].....	25
Figure 2. World natural gas demand by sector in the New Policies Scenario (“bcm” stands billion cubic meters) [8].	28
Figure 3. Main methods used for methane processing [9].	29
Figure 4. Global benzene demand by segment in 2014 [15].	32
Figure 5. World consumption of benzene in 2014 [14].	34
Figure 6. Scheme of a H ₂ pump working principle.....	55
Figure 7. MDA with H ₂ removal through SrZr _{0.95} Yb _{0.05} O _{3-δ} membrane [111]. .	57
Figure 8. Methane dehydroaromatization in a Fixed-bed reactor and in a Membrane reactor with oxygen supply through BSCF membrane [110].	59
Figure 9. Projection of the rings of the ZSM-5 zeolite channels (a) 10 MR viewed along [100]; (b) 10 MR viewed along [010]; and projection of the structure (c) viewed along [100] [1].	69
Figure 10. Projection of the rings of the MCM-22 zeolite channels (a) 10 MR viewed normal to [001] between layers; (b) 10 MR viewed normal to [010] within layers; and projection of the structure (c) viewed along [100] [1].	71
Figure 11. Projection of the rings of the IM-5 zeolite channels: (a) 10 MR viewed along [100]; (b) 10 MR viewed along [010]; and projection of the structure (c) viewed along [100] [1].	73
Figure 12. Projection of the rings of the ITQ-13 zeolite channels: (a) 10 MR viewed along [001]; (b) 10 MR viewed along [010]; and projection of the structure (c) viewed along [010] [1].	74

- Figure 13. Projection of the rings of the TNU-9 zeolite channels: (a) 10 MR viewed along [010]; (b) 10 MR viewed along [10-1]; and projection of the structure (c) viewed along [010] [1].75
- Figure 14. Projection of the rings of the Chabazite zeolite channels: (a) 8 MR viewed normal to [001]; and projection of the structure (b) viewed along [010] [1].....76
- Figure 15. Projection of the rings of the ZSM-22 zeolite channels: (a) 10 MR viewed along [001]; and projection of the structure (b) viewed along [001] [1].77
- Figure 16. Projection of the rings of the NU-87 zeolite channels: (a) 10 MR viewed along [100]; and projection of the structure (b) viewed along [010] [1].78
- Figure 17. Projection of the rings of the Mazzite zeolite channels: (a) 12 MR viewed along [001]; (b) 8 MR viewed along [001]; and projection of the structure (c) viewed along [001] [1].79
- Figure 18. Projection of the rings of the Beta zeolite channels: (a) 12 MR viewed along [100]; (b) 12 MR viewed along [001]; and projection of the structure (c) viewed along [100] [1].80
- Figure 19. Projection of the rings of the Mordenite zeolite channels: (a) 12 MR viewed along [001]; (b) 8 MR viewed along [001]; and projection of the structure (c) viewed along [001] [1].81
- Figure 20. Picture of the reduced tubular membrane (length ~ 25 cm).84
- Figure 21. Photoelectric effect: an X-ray is absorbed and a core level electron is ejected from the atom [16].91
- Figure 22. Simplified scheme of the “Reactor PH4”, the reaction system used to perform the catalytic experiments using the Fixed Bed Reactor.96

Figure 23. Scheme of the Fixed Bed Reactor (FBR).	97
Figure 24. Chromatogram of MDA products over 3% (wt.) Mo/CBV3020 after 1 h of reaction (detail of heavy products).	100
Figure 25. Chromatogram of MDA products over 3% (wt.) Mo/CBV3020 after 10 h of reaction (detail of heavy products).	101
Figure 26. Simplified scheme of the new “Reactor PH4”, reaction system used to perform the catalytic-electrochemical experiments using the Catalytic Membrane Reactor.	117
Figure 27. CMR reaction zone enlargement.	118
Figure 28. Scheme of the Catalytic Membrane Reactor (CMR).	119
Figure 29. Scheme of the CM Reactor with Quartz Tube (CMR-QT).	129
Figure 30. XRD patterns of 3%Mo/HZSM-5 catalysts before the MDA reaction.	138
Figure 31. Effect of the HZSM-5 zeolite on the (a) methane conversion and (b) H ₂ flow of 3%Mo/HZSM-5 catalysts versus the TOS at 700 °C.	139
Figure 32. Effect of the HZSM-5 zeolite on the (a) benzene yield versus the TOS and (b) benzene yield versus the methane conversion of 3%Mo/HZSM-5 catalysts at 700°C.	141
Figure 33. Effect of the Si/Al ratio of 3%Mo/HZSM-5 catalyst on the selectivity to main products and the methane conversion after 9 h on stream.	143
Figure 34. Effect of the crystal size of 3%Mo/HZSM-5 catalyst on the selectivity to main products and the methane conversion after 9 h on stream.	144
Figure 35. Effect of the Mo content of the Mo/HZSM-5 catalysts on the methane conversion versus the TOS at 700 °C.	145

Figure 36. Effect of the Mo content of the Mo/HZSM-5 catalysts on the (a) benzene yield versus the TOS and (b) benzene yield versus the methane conversion.....	146
Figure 37. Effect of the Mo content on the catalytic performance after 2.33 h of MDA reaction.	147
Figure 38. XRD patterns of 3% and 6% (wt.) Mo/HZSM-5 catalysts before and after MDA reaction.	148
Figure 39. Effect of the zeolite of the 3%Mo/zeolite catalysts on the (a) benzene yield versus the TOS and (b) benzene yield versus the methane conversion. .	151
Figure 40. Effect of the zeolite of the 3%Mo/zeolite catalysts on the H ₂ flow versus the TOS at 700 °C.	151
Figure 41. Effect of the zeolite of 6%Mo/zeolite catalysts on the (a) benzene yield versus the TOS and (b) benzene yield versus methane conversion.	155
Figure 42. Effect of the zeolite of 6%Mo/zeolite catalysts on the H ₂ flow versus the TOS at 700 °C.	155
Figure 43. FE-SEM image of the MCM-22 zeolite (Si/Al ~ 15) synthesized without seeding.	156
Figure 44. FE-SEM images of the MCM-22 zeolite (Si/Al ~ 15) synthesized using seeding.....	157
Figure 45. Enlarged FE-SEM images of the MCM-22 zeolite (Si/Al ~ 15) synthesized using seeding.....	157
Figure 46. FE-SEM images of the 6% Mo/MCM-22 catalyst (powder).....	158
Figure 47. Enlarged FE-SEM images of the 6% Mo/MCM-22 catalyst (powder).	158

- Figure 48. TPO profiles of carbon species over spent 6%Mo/HZSM-5 and 6%Mo/MCM-22 catalysts (Si/Al=15). Same scale of Y-axis..... 160
- Figure 49. XRD patterns of 6% (wt.) Mo/MCM-22 catalyst before and after MDA reaction. 162
- Figure 50. Effect of the 6%Mo/HZSM-5 catalyst activation on the benzene yield versus the TOS at 700 °C and 1.2 bar. 171
- Figure 51. Effect of the 6%Mo/HZSM-5 catalyst activation on the (a) accumulated benzene moles and (b) H₂ flow versus the TOS at 700 °C..... 172
- Figure 52. Effect of the 6%Mo/MCM-22 catalyst activation on the (a) benzene yield and (b) accumulated benzene moles versus the TOS at 700 °C. 174
- Figure 53. Effect of the 6%Mo/MCM-22 catalyst activation on the H₂ flow versus the TOS at 700 °C and 1.2 bar. 175
- Figure 54. TPO profiles of carbon species over 6%Mo/MCM-22 catalysts activated with different procedures. Same scale of Y-axis..... 176
- Figure 55. Effect of the 6%Mo/HZSM-5 catalyst amount and the feed gas flow on the (a) methane conversion and (b) aromatics yield versus the TOS..... 184
- Figure 56. Effect of the 6%Mo/HZSM-5 catalyst amount and the feed gas flow on the (a) benzene yield versus the TOS, (b) benzene yield versus the methane conversion, (c) toluene and (d) naphthalene yields versus the TOS at 700 °C. 185
- Figure 57. Effect of the space velocity on the benzene yield versus the TOS of the 6%Mo/MCM-22 catalyst at 700 °C and 1.2 bar (standard activation)..... 187
- Figure 58. Effect of the space velocity on the (a) accumulated benzene moles and (b) H₂ flow versus the TOS of the 6%Mo/MCM-22 catalyst at 700 °C (standard activation)..... 188

- Figure 59. Effect of the space velocity on the (a) methane conversion and (b) H₂ flow versus the TOS of the 6%Mo/MCM-22 catalyst (new activation) at 700 °C. 190
- Figure 60. Effect of the space velocity on the (a) benzene yield and (b) accumulated benzene moles versus the TOS of the 6%Mo/MCM-22 catalyst (new activation) at 700 °C..... 191
- Figure 61. Effect of the space velocity on the catalytic performance after 2.50 h of MDA reaction. 192
- Figure 62. TPO profiles of carbon species over 6%Mo/MCM-22 catalysts tested using different space velocities (new activation). Same scale of Y-axis. 194
- Figure 63. Effect of the H₂O vapor concentration in the methane feed on the equilibrium methane conversion at 700 °C and 1 bar. 200
- Figure 64. Effect of the H₂O vapor concentration in the methane feed on the equilibrium selectivities to aromatics, C₂, CO and CO₂ at 700 °C and 1 bar. Inset figure shows an enlarged version of the C₂, toluene and CO₂ selectivities. 201
- Figure 65. Effect of the H₂O addition to the methane feed on the (a) benzene yield and (b) accumulated benzene moles versus the TOS of 6%Mo/HZSM-5 catalyst at 700 °C. 204
- Figure 66. Effect of co-feeding H₂O on the H₂ flow versus the TOS of 6%Mo/HZSM-5 catalyst at 700 °C..... 205
- Figure 67. Effect of the addition of 1.08% of H₂O to the methane feed after different periods of time in dry conditions on the benzene yield versus the TOS of 6%Mo/MCM-22 catalyst at 700 °C. 208
- Figure 68. Effect of co-feeding 1.08% of H₂O after different periods of time in dry conditions on the accumulated benzene moles versus the TOS of 6%Mo/MCM-22 catalyst at 700 °C. Inset figure shows an enlarged version. . 209

- Figure 69. Effect of co-feeding 1.08% of H₂O after different periods of time in dry conditions on the H₂ flow versus the TOS of 6%Mo/MCM-22 catalyst...210
- Figure 70. Effect of co-feeding H₂O on the (a) benzene yield and (b) accumulated benzene moles versus the TOS of 6%Mo/MCM-22 catalyst.....214
- Figure 71. Effect of the H₂O addition to the methane feed on the H₂ flow versus the time on stream of 6%Mo/MCM-22 catalyst at 700 °C and 1.2 bar.....215
- Figure 72. XANES spectra at Mo K-edge of Mo foil, Mo₂C, MoO₃ and 6%Mo/MCM-22 catalysts before and after MDA in dry and wet conditions..216
- Figure 73. XPS Mo 3d_{5/2} and 3d_{3/2} spectra of 6%Mo/MCM-22 catalysts before and after MDA reaction in dry and wet conditions.....217
- Figure 74. TPO profiles of carbon species over 6%Mo/MCM-22 catalysts after MDA reaction by co-feeding 0, 0.86 and 1.08% of H₂O. Same scale of Y-axis.220
- Figure 75. NH₃-TPD profiles of 6%Mo/MCM-22 catalysts after MDA reaction by co-feeding (a) 0.86%, (b) 1.08% and (c) 0% of H₂O, and (d) before MDA reaction. Same scale of Y-axis.....222
- Figure 76. ²⁷Al MAS NMR spectra of fresh and spent 6%Mo/MCM-22 catalyst by co-feeding 0, 0.86 and 1.08% of H₂O. Same scale of Y-axis.223
- Figure 77. Effect of the H₂ concentration in the methane feed on the equilibrium methane conversion at 700 °C and 1 bar.....226
- Figure 78. Effect of the H₂ concentration in the methane feed on the equilibrium selectivities to aromatics and C₂ hydrocarbons at 700 °C and 1 bar.227
- Figure 79. Effect of co-feeding H₂ and H₂O on the equilibrium methane conversion at 700 °C and 1 bar.228
- Figure 80. Effect of co-feeding H₂ and H₂O on the equilibrium selectivities to (a) benzene, (b) naphthalene and (c) toluene at 700 °C and 1 bar.....229

- Figure 81. Effect of co-feeding H_2 and H_2O on the equilibrium selectivities to (a) ethylene, (b) ethane, (c) CO and (d) CO_2 at 700 °C and 1 bar..... 230
- Figure 82. Effect of co-feeding 6% of H_2 on the benzene yield versus the TOS of 6%Mo/HZSM-5 and 6%Mo/MCM-22 catalysts at 700 °C. 232
- Figure 83. Effect of co-feeding 6% of H_2 on the (a) benzene accumulated and (b) H_2 flow versus the TOS of 6%Mo/HZSM-5 and 6%Mo/MCM-22 catalysts. 233
- Figure 84. TPO profiles of carbon species over 6%Mo/MCM-22 catalysts without and with co-feeding 6% of H_2 . Same scale of Y-axis..... 234
- Figure 85. Effect of co-feeding H_2 on the (a) benzene yield and (b) accumulated benzene versus the TOS of 6%Mo/MCM-22 catalysts at 700 °C..... 237
- Figure 86. Effect of co-feeding H_2 on the H_2 flow versus the time on stream of 6%Mo/MCM-22 catalysts at 700 °C..... 238
- Figure 87. TPO profiles of carbon species over 6%Mo/MCM-22 catalysts after MDA reaction by co-feeding 0, 6 and 10% of H_2 . Same scale of Y-axis..... 239
- Figure 88. Effect of co-feeding different concentrations of H_2 without and with H_2O addition on the (a) methane conversion and (b) C_2 yield versus the time on stream of 6%Mo/MCM-22 catalyst at 700 °C..... 241
- Figure 89. Effect of co-feeding different concentrations of H_2 without and with H_2O addition on the benzene yield versus the TOS of 6%Mo/MCM-22 catalyst. 242
- Figure 90. Effect of co-feeding different concentrations of H_2 without and with H_2O addition on the H_2 flow versus the TOS of 6%Mo/MCM-22 catalyst..... 243
- Figure 91. Effect of co-feeding different concentrations of H_2 without and with H_2O addition on the (a) coke yield and (b) CO yield versus the TOS of 6%Mo/MCM-22 catalyst at 700 °C. 244

- Figure 92. TPO profiles of carbon species over 6%Mo/MCM-22 catalysts after MDA reaction by co-feeding H₂ and without and with co-feeding 0.288% of H₂O. Same scale of Y-axis.....245
- Figure 93. Effect of CO₂ concentration in the methane feed on the equilibrium methane conversion at 700 °C and 1 bar.....247
- Figure 94. Effect of the CO₂ concentration in the feed on the equilibrium selectivities to aromatics, C₂ hydrocarbons and CO at 700 °C and 1 bar. Inset figure shows an enlarged version of the C₂ and toluene selectivities.248
- Figure 95. Effect of co-feeding 2% of CO₂ on the benzene yield versus the TOS of 6%Mo/HZSM-5 and 6%Mo/MCM-22 catalysts at 700 °C.251
- Figure 96. Effect of co-feeding 2% of CO₂ on the (a) accumulated benzene and (b) H₂ flow versus the TOS of 6%Mo/HZSM-5 and 6%Mo/MCM-22 catalysts.252
- Figure 97. TPO profiles of carbon species over (a) 6%Mo/HZSM-5 and (b) 6%Mo/MCM-22 catalysts after MDA reaction without and with co-feeding 2% of CO₂. Same scale of Y-axis in each graph.....254
- Figure 98. Effect of the 6%Mo/HZSM-5 catalyst regeneration with H₂ in dry conditions on the (a) methane conversion and (b) H₂ flow versus the TOS....264
- Figure 99. Effect of the 6%Mo/HZSM-5 catalyst regeneration with H₂ in dry conditions on the (a) benzene, (b) toluene and (c) naphthalene yields versus the TOS at 700 °C.....264
- Figure 100. Effect of the 6%Mo/HZSM-5 catalyst regeneration with H₂ in dry conditions on the (a) C₂ and (b) coke yields versus the TOS at 700 °C.....265
- Figure 101. Effect of the 6%Mo/HZSM-5 catalyst regeneration with H₂ in wet conditions on the (a) methane conversion and (b) H₂ flow versus the TOS....266

- Figure 102. Effect of the 6%Mo/HZSM-5 catalyst regeneration with H₂ in wet conditions on the (a) benzene, (b) toluene and (c) naphthalene yields versus the TOS at 700 °C.267
- Figure 103. Effect of the 6%Mo/HZSM-5 catalyst regeneration with H₂ in wet conditions on the (a) C₂ and (b) coke yields versus the TOS at 700 °C.....268
- Figure 104. Effect of the 6%Mo/MCM-22 catalyst regeneration with H₂ in dry conditions on the (a) methane conversion and (b) H₂ flow versus the TOS....269
- Figure 105. Effect of the 6%Mo/MCM-22 catalyst regeneration with H₂ in dry conditions on the (a) benzene, (b) toluene and (c) naphthalene yields versus the TOS at 700 °C.270
- Figure 106. Effect of the 6%Mo/MCM-22 catalyst regeneration with H₂ in dry conditions on the (a) C₂ and (b) coke yields versus the TOS at 700 °C.....271
- Figure 107. Effect of the catalyst manufacturing process on the benzene yield versus the TOS of 6%Mo/HZSM-5 and 6%Mo/MCM-22 catalysts at 700 °C.277
- Figure 108. Effect of the catalyst manufacturing process on the (a) accumulated benzene moles and (b) H₂ flow versus the TOS of 6%Mo/HZSM-5 and 6%Mo/MCM-22 catalysts at 700 °C.....278
- Figure 109. TPO profiles of carbon species over (a) 6%Mo/HZSM-5 and (b) 6%Mo/MCM-22 catalysts after MDA, produced using the standard (Granulated) and the new (Extrudated I) procedure. Same scale of Y-axis.....279
- Figure 110. NH₃-TPD profiles of (1) 6%Mo/HZSM-5 and (2) 6%Mo/MCM-22 catalysts: Granulated (a) after and (c) before MDA reaction; and Extrudated I (b) after and (d) before MDA reaction. Same scale of Y-axis.281

- Figure 111. Effect of the new catalyst manufacturing process on the (a) methane conversion and (b) benzene yield versus the TOS of 6%Mo/MCM-22 catalyst at 700 °C.....284
- Figure 112. FE-SEM image of the “Extrudated II” 6% Mo/MCM-22 catalyst, showing axial cross-section view.....285
- Figure 113. FE-SEM image of the “Extrudated II” 6% Mo/MCM-22 catalyst, showing radial cross-section view.286
- Figure 114. Picture of the “Extrudated II” 6% Mo/MCM-22 catalyst.....286
- Figure 115. TPO profiles of carbon species over 6%Mo/MCM-22 catalysts after 16.3 h of MDA reaction, produced using the standard (Granulated) and the new (Extrudated II) procedure. Same scale of Y-axis.....288
- Figure 116. NH₃-TPD profiles of 6%Mo/MCM-22 catalysts produced using the new procedure (Extrudated II) (a) after and (c) before MDA reaction; and the standard procedure (Granulated) (b) after and (d) before MDA reaction. Same scale of Y-axis.289
- Figure 117. Effect of the H₂ removal through BZCY72 TM-1 on the (a) methane conversion and (b) H₂ flow versus the TOS of 6%Mo/MCM-22 catalyst at 710 °C. Shaded areas indicate when H₂ is extracted.297
- Figure 118. Scheme of electrochemical and side reactions at the CMR using a BZCY72 tubular membrane.....298
- Figure 119. Effect of the H₂ removal through BZCY72 TM-1 on the benzene yield versus the TOS of 6%Mo/MCM-22 catalyst at 710 °C. Shaded areas indicate when H₂ is extracted (Current ON).299
- Figure 120. Effect of the H₂ removal through BZCY72 TM-1 on the (a) aromatics yield and (b) accumulated benzene moles versus the TOS of 6%Mo/MCM-22 catalyst. Shaded areas indicate when H₂ is extracted.....300

- Figure 121. Electrochemical results of BZCY72 TM-1: total H₂ flux in sweep side and faradaic efficiency versus the TOS at 710 °C. Shadowed areas indicate when H₂ is extracted.301
- Figure 122. Electrochemical results of BZCY72 TM-1: (a) H₂ fluxes and (b) H₂ extracted and O₂ injected versus the TOS at 710 °C. Shadowed areas indicate when H₂ is extracted.302
- Figure 123. BSE FE-SEM image of the fractured cross-section of the BZCY72 TM-1, showing (a) copper anode, (b) BZCY72 electrolyte and (c) BZCY72-Ni cathode.304
- Figure 124. FE-SEM/EDS spectra recorded from the BZCY72 TM-1, corresponding to: 1. copper anode, 2. BZCY72 electrolyte, 3. Ni aggregates in the cathode and, 4. BZCY72 in the cathode.304
- Figure 125. Picture of the reduced BZCY72 TM-1 with the copper anode sintered (anode length ~ 4 cm).....305
- Figure 126. XANES spectra at Mo K-edge of Mo foil, Mo₂C, MoO₃ and 6%Mo/MCM-22 catalysts before and after MDA reaction (FBR and CMR)..305
- Figure 127. XPS Mo 3d_{5/2} and 3d_{3/2} spectra of 6%Mo/MCM-22 catalysts before and after MDA reaction (FBR and CMR).306
- Figure 128. TPO profiles of carbon species over 6%Mo/MCM-22 catalysts after MDA reaction without (CMR-QT) and with H₂ removal (CMR-TM-1). Same scale of Y-axis.309
- Figure 129. NH₃-TPD profiles of 6%Mo/MCM-22 catalysts (a) fresh, and tested with the (b) CMR-TM-1 and (c) CMR-QT. Same scale of Y-axis.....310
- Figure 130. Effect of the anode type on BZCY72 TM-1 and TM-2 on the benzene yield versus the TOS of 6%Mo/MCM-22 catalyst. Shadowed areas indicate when H₂ is extracted.....313

- Figure 131. Effect of the anode type on BZCY72 TM-1 and TM-2 on the (a) accumulated benzene moles and (b) H₂ flow versus the TOS of 6%Mo/MCM-22 catalyst. 313
- Figure 132. Electrochemical results of BZCY72 TM-2: (a) total H₂ flux in sweep side and faradaic efficiency and (b) H₂ extracted versus the TOS at 700 °C. Shadowed areas indicate when H₂ is extracted. 315
- Figure 133. TPO profiles of carbon species over 6%Mo/MCM-22 catalysts after MDA reaction without (CMR-QT-2) and with H₂ removal (CMR-TM-2). Same scale of Y-axis. 316
- Figure 134. Effect of the temperature on the (a) methane conversion and (b) H₂ flow versus the TOS of 6%Mo/MCM-22 catalyst, without (CMR-QT) and with H₂ removal (CMR-TM-1 and TM-3). Shadowed areas indicate when H₂ is extracted. 318
- Figure 135. Effect of the temperature on the benzene yield versus the TOS of 6%Mo/MCM-22 catalyst, without (CMR-QT) and with H₂ removal (CMR-TM-1 and TM-3). Shadowed areas indicate when H₂ is extracted. 320
- Figure 136. Effect of the temperature on the (a) aromatics yield and (b) accumulated benzene moles versus the TOS of 6%Mo/MCM-22 catalyst, without (CMR-QT) and with H₂ removal (CMR-TM-1 and TM-3). Shadowed areas indicate when H₂ is extracted. 321
- Figure 137. Electrochemical results of BZCY72 TM-3: (a) H₂ fluxes in sweep side and (b) H₂ extracted and O₂ injected versus the TOS at 720 °C. Shadowed areas indicate when H₂ is extracted. 322
- Figure 138. TPO profiles of carbon species over 6%Mo/MCM-22 catalysts after MDA reaction without (CMR-QT) and with H₂ removal (CMR-TM-1 and TM-3) at different temperatures. Same scale of Y-axis. 324

- Figure 139. Effect of co-feeding 10% of H₂ by extracting H₂ on the (a) methane conversion and (b) H₂ flow versus the TOS of 6%Mo/MCM-22 catalyst. Shaded areas indicate when H₂ is extracted. 326
- Figure 140. Effect of co-feeding 10% of H₂ without and with H₂ removal on the (a) benzene yield and (b) accumulated benzene moles versus the TOS of 6%Mo/MCM-22. Shaded areas indicate when H₂ is extracted. 328
- Figure 141. Electrochemical results of BZCY72 TM-4: (a) H₂ flux in sweep side and (b) H₂ extracted and O₂ injected versus the TOS by co-feeding 10% of H₂. Shaded areas indicate when H₂ is extracted. 329
- Figure 142. TPO profiles of carbon species over 6%Mo/MCM-22 catalysts after MDA reaction with and without H₂ removal by adding 0 and 10 % of H₂ to the methane feed. Same scale of Y-axis. 330
- Figure 143. Effect of the current density imposed on BZCY72 TM-1 and TM-5 on the (a) methane conversion and (b) H₂ flow versus the TOS of 6%Mo/MCM-22 catalyst. 332
- Figure 144. Effect of the current density imposed on BZCY72 TM-1 and TM-5 on the (a) aromatics selectivity and (b) aromatics yield versus the TOS of 6%Mo/MCM-22 catalyst. 333
- Figure 145. Effect of the current density imposed on BZCY72 TM-1 and TM-5 on the (a) benzene yield and (b) accumulated benzene moles versus the TOS of 6%Mo/MCM-22 catalyst. 334
- Figure 146. Electrochemical results of BZCY72 TM-5: (a) H₂ flux in sweep side and (b) H₂ extracted and O₂ injected versus the TOS by imposing 60 mA·cm⁻². Shaded areas indicate when H₂ is extracted. 335

List II Tables

Table 1. Main uses of aromatic products in 2011 [16].	33
Table 2. ZSM-5 zeolites used in the preparation of the catalysts.	70
Table 3. BET surface area, micropore volume and acidity of the synthesized MCM-22 (Si/Al ~ 15).	72
Table 4. Products obtained in the chromatograms showed in Figure 24 and Figure 25.	102
Table 5. H ₂ O vapor concentration used in the experiments performed with H ₂ removal through BZCY72 tubular membranes.	122
Table 6. Current densities used with TM-1 at different TOS.	125
Table 7. Current densities used with TM-2 at different TOS.	126
Table 8. Current densities used with TM-3 at different TOS.	126
Table 9. Current densities used with TM-4 at different TOS	127
Table 10. Current densities used with TM-5 at different TOS.	128
Table 11. Crystal sizes and Si/Al ratios of the different HZSM-5.	137
Table 12. Effect of the HZSM-5 zeolite on the selectivity to main products after 9 h on stream of 3%Mo/HZSM-5 catalysts.	139
Table 13. TGA results of spent 3% (wt.) Mo/HZSM-5 catalysts.	142
Table 14. Effect of the Mo content of the Mo/HZSM-5 catalysts on the selectivity to main products and the H ₂ flow after 9 h on stream.	145
Table 15. TGA results of spent 3% and 6% (wt.) Mo/HZSM-5 catalysts.	147
Table 16. Different zeolites used to prepare the catalysts with 3% (wt.) Mo. .	149

Table 17. Effect of zeolite on the methane conversion and selectivity to main products after 9 h on stream of the catalysts with 3% (wt.) of Mo.	150
Table 18. TGA results of spent 3% (wt.) Mo/zeolite catalysts.	152
Table 19. Topology and channel dimensions of the HZSM-5 and MCM-22 zeolites used to prepare the catalysts with 6% of Mo.	153
Table 20. Effect of the zeolite on the selectivity to main products and methane conversion after 9 h on stream of 6%Mo/zeolite catalysts.	154
Table 21. TGA results of spent 6% (wt.) Mo/zeolite catalysts.	159
Table 22. BET surface area and micropore volume for the 6% (wt.) Mo/zeolite catalysts (Si/Al=15) before and after MDA reaction.	160
Table 23. Results of the deconvoluted TPO profiles of carbon species over 6%Mo/HZSM-5 and 6%Mo/MCM-22 catalysts (Si/Al=15).	161
Table 24. Acidity of the synthesized MCM-22 and 6%Mo/MCM-22 catalyst.	162
Table 25. Type of catalyst activation and code used in MDA reaction.	169
Table 26. Effect of the 6%Mo/HZSM-5 catalyst activation on the methane conversion and the selectivity to main products after 9 h on stream.	170
Table 27. TGA results of spent 6%Mo/HZSM-5 catalysts activated with different procedures.	173
Table 28. Effect of the 6%Mo/MCM-22 catalyst activation on the methane conversion and the selectivity to main products after 9 h on stream.	173
Table 29. TGA results of spent 6%Mo/MCM-22 catalysts activated with different procedures.	175
Table 30. Results of the deconvoluted TPO profiles of carbon species over 6%Mo/MCM-22 catalysts activated with different procedures.	177

Table 31. Effect of the 6%Mo/HZSM-5 catalyst amount and the feed gas flow on the selectivity to main products after 9 h on stream at $1500 \text{ mL} \cdot \text{h}^{-1} \cdot \text{g}_{\text{cat}}^{-1}$. . .	183
Table 32. TGA results of spent 6%Mo/HZSM-5 catalysts.	186
Table 33. Effect of the space velocity on the methane conversion and the selectivity to main products after 9 h on stream of 6%Mo/HZSM-5 catalyst.	187
Table 34. TGA results of spent 6%Mo/MCM-22 catalysts (standard activation) using different space velocities.	189
Table 35. Effect of the space velocity on the selectivity to main products after 9 h on stream of 6%Mo/MCM-22 catalyst.	190
Table 36. TGA results of spent 6%Mo/MCM-22 catalysts (new activation) using different space velocities.	193
Table 37. Results of the deconvoluted TPO profiles of carbon species over 6%Mo/MCM-22 catalysts tested at different space velocities (new activation).	194
Table 38. Effect of co-feeding H_2O on the methane conversion and the selectivity to main products after 9 h on stream of 6%Mo/HZSM-5 catalyst.	203
Table 39. TGA results of spent 6%Mo/HZSM-5 catalysts with and without addition of H_2O	206
Table 40. Effect of co-feeding 1.08% of H_2O after different TOS in dry conditions on the methane conversion and the selectivity to main products after 9 h on stream of 6%Mo/MCM-22 catalyst.	207
Table 41. TGA results of spent 6%Mo/MCM-22 catalysts with and without addition of 1.08% of H_2O after different periods of time in dry conditions.	211
Table 42. Effect of co-feeding H_2O on the methane conversion and the selectivity to main products after 9 h on stream of 6%Mo/MCM-22 catalyst.	212

Table 43. Experimental XANES results of Mo foil, Mo ₂ C, MoO ₃ and 6%Mo/MCM-22 catalysts before and after MDA in dry and wet conditions..	216
Table 44. Surface oxidation state of Mo by XPS* on 6%Mo/MCM-22 catalysts before and after MDA reaction in dry and wet conditions.....	218
Table 45. TGA results of spent 6%Mo/MCM-22 catalysts with and without addition of H ₂ O.....	218
Table 46. BET surface area and micropore volume for the spent 6%Mo/MCM-22 catalysts with and without addition of H ₂ O.	219
Table 47. Results of the deconvoluted TPO profiles of carbon species over 6%Mo/MCM-22 catalysts with and without addition of H ₂ O.	221
Table 48. Acidity of 6%Mo/MCM-22 catalysts before and after MDA reaction with and without addition of H ₂ O determined by NH ₃ -TPD.	222
Table 49. Effect of co-feeding 6% of H ₂ on the methane conversion and the selectivity to main products after 9 h on stream of 6%Mo/HZSM-5 and 6%Mo/MCM-22 catalysts.....	231
Table 50. TGA results of spent 6%Mo/HZSM-5 and 6%Mo/MCM-22 catalysts with and without addition of 6% of H ₂ to the methane feed.....	233
Table 51. Results of the deconvoluted TPO profiles of carbon species over 6%Mo/MCM-22 catalysts without and with co-feeding 6% of H ₂	235
Table 52. Effect of co-feeding H ₂ on the methane conversion and the selectivity to main products after 9 h on stream of 6%Mo/MCM-22 catalyst.	236
Table 53. TGA results of spent 6%Mo/MCM-22 catalysts with and without addition of H ₂ to the methane feed.....	239
Table 54. Results of the deconvoluted TPO profiles of carbon species over 6%Mo/MCM-22 catalysts with co-feeding 0, 6 and 10% of H ₂	240

Table 55. TGA results of spent 6%Mo/MCM-22 catalysts with co-feeding H ₂ and without and with the addition of 0.288% of H ₂ O.....	245
Table 56. Results of the deconvoluted TPO profiles of carbon species over 6%Mo/MCM-22 catalysts with co-feeding H ₂ and without and with the addition of 0.288% of H ₂ O.	246
Table 57. Effect of co-feeding 2% of CO ₂ on the methane conversion and the selectivity to main products after 9 h on stream of 6%Mo/HZSM-5 and 6%Mo/MCM-22 catalysts.....	250
Table 58. TGA results of spent 6%Mo/HZSM-5 and 6%Mo/MCM-22 catalysts without and with co-feeding 2% of CO ₂	253
Table 59. Results of the deconvoluted TPO profiles of carbon species over 6%Mo/HZSM-5 catalysts with and without addition of 2% of CO ₂	255
Table 60. TGA results of spent 6%Mo/HZSM-5 catalyst subjected to a regeneration with pure H ₂ after 19.70 h on stream in dry conditions.	266
Table 61. TGA results of spent 6%Mo/HZSM-5 catalyst subjected to a regeneration with pure H ₂ after 38.7 h on stream in wet conditions.....	268
Table 62. TGA results of spent 6%Mo/MCM-22 catalyst after two regenerations with pure H ₂ after 24.3 and 46.3 h on stream in dry conditions.	271
Table 63. Effect of the catalyst manufacturing process on the methane conversion and the selectivity to main products after 9 h on stream of 6%Mo/HZSM-5 and 6%Mo/MCM-22 catalysts.....	276
Table 64. TGA results of spent 6%Mo/HZSM-5 and 6%Mo/MCM-22 catalysts produced using the standard (Granulated) and the new (Extrudated I) procedure.	278

Table 65. Results of the deconvoluted TPO profiles of carbon species over 6%Mo/HZSM-5 and 6%Mo/MCM-22 catalysts produced using the standard (Granulated) and the new (Extrudated I) procedure.	280
Table 66. Acidity of 6%Mo/HZSM-5 and 6%Mo/MCM-22 catalysts before (fresh) and after (spent) MDA reaction using the standard (Granulated) and the new (Extrudated I) procedure determined by NH ₃ -TPD.....	282
Table 67. Effect of the new catalyst manufacturing process on the selectivity to main products after 9 h on stream of 6%Mo/MCM-22 catalysts.....	283
Table 68. TGA results of spent 6%Mo/MCM-22 catalysts produced using the standard (Granulated) and the new (Extrudated II) procedure.....	287
Table 69. Results of the deconvoluted TPO profiles of carbon species over 6%Mo/MCM-22 catalysts produced using the standard (Granulated) and the new (Extrudated II) procedure.	288
Table 70. Acidity of fresh and spent 6%Mo/MCM-22 catalysts prepared by the standard (Granulated) and the new (Extrudated II) procedure determined by NH ₃ -TPD.....	289
Table 71. Effect of the H ₂ removal through BZCY72 TM-1 on the selectivity to main products after 9 h on stream of 6%Mo/MCM-22 catalyst.	297
Table 72. Experimental XANES results of Mo foil, Mo ₂ C, MoO ₃ and 6%Mo/MCM-22 catalysts before and after MDA reaction (FBR and CMR)..	306
Table 73. Surface oxidation state of Mo by XPS* on 6%Mo/MCM-22 catalysts before and after MDA reaction (FBR and CMR).	307
Table 74. TGA results of spent 6%Mo/MCM-22 catalysts without and with H ₂ removal through BZCY72 TM-1.	307
Table 75. BET surface area and micropore volume of spent 6%Mo/MCM-22 catalysts without and with H ₂ removal through BZCY72 TM-1.	308

Table 76. Results of the deconvoluted TPO profiles of carbon species over 6%Mo/MCM-22 catalysts tested without (CMR-QT) and with H ₂ removal (CMR-TM-1).	309
Table 77. Acidity of 6%Mo/MCM-22 catalyst fresh and tested without (CMR-QT) and with H ₂ removal (CMR-TM-1).....	311
Table 78. Effect of the anode type on BZCY72 TM on the methane conversion and the selectivity to main products after 9 h on stream of 6%Mo/MCM-22 catalyst.	312
Table 79. TGA results of spent 6%Mo/MCM-22 catalysts without and with H ₂ removal through TM-1 (Cu anode) and TM-2 (Mo ₂ C/Cu/BZCY72 anode)....	316
Table 80. Results of the deconvoluted TPO profiles of carbon species over 6%Mo/MCM-22 catalysts tested without and with H ₂ removal (CMR-TM-2).	317
Table 81. Effect of the temperature on the selectivity to main products after 9 h on stream of 6%Mo/MCM-22 catalyst, without (CMR-QT) and with H ₂ extraction through TM-1 and TM-3.....	319
Table 82. TGA results of spent 6%Mo/MCM-22 catalysts without and with H ₂ removal through BZCY72 TM-1 and TM-3 at different temperatures.....	323
Table 83. Results of the deconvoluted TPO profiles of carbon species over 6%Mo/MCM-22 catalysts tested without (CMR-QT) and with H ₂ removal (CMR-TM-1 and TM-3) at different temperatures.	324
Table 84. Effect of co-feeding 10% of H ₂ without and with removing H ₂ through TM-1 and TM-4 on the selectivity to main products after 9 h on stream of 6%Mo/MCM-22 catalyst.	327
Table 85. TGA results of spent 6%Mo/MCM-22 catalysts without and with H ₂ removal through BZCY72 TM-1 and TM-4 by adding 0 and 10% of H ₂	330

Table 86. Results of the deconvoluted TPO profiles of carbon species over 6%Mo/MCM-22 catalysts tested without and with H ₂ removal by adding 0 and 10% of H ₂	331
Table 87. Effect of the current density on the selectivity to main products after 9 h on stream of 6%Mo/MCM-22 catalyst by removing H ₂ through TM-1 and TM-5.	333
Table 88. TGA results of spent 6%Mo/MCM-22 catalysts without and with H ₂ removal through BZCY72 TM-1 and TM-5.....	336
Table 89. Results of the deconvoluted TPO profiles of carbon species over 6%Mo/MCM-22 catalysts tested without (CMR-QT) and with H ₂ removal (CMR-TM-1 and TM-5) by applying different current densities.	337

List III Abbreviations

AES: Auger electrons.

AHM: Ammonium Heptamolybdate.

BAS: Brønsted Acid Sites.

BCZY: $\text{BaCe}_{0.9-x}\text{Zr}_x\text{Y}_{0.1}\text{O}_{3-\delta}$; δ is the oxygen deficiency per unit formula.

BE: Binding Energy.

BSCF: $\text{Ba}_{0.5}\text{Sr}_{0.5}\text{Co}_{0.8}\text{Fe}_{0.2}\text{O}_{3-\delta}$; δ is the oxygen deficiency per unit formula.

BSE: Backscattered Electrons.

BTXs: Benzene, Toluene and Xylenes hydrocarbons.

BZCY72: $\text{BaZr}_{0.7}\text{Ce}_{0.2}\text{Y}_{0.1}\text{O}_{3-\delta}$; δ is the oxygen deficiency per unit formula.

CCGTs: Combined-Cycle Gas Turbines.

cermet: composite material composed of ceramic (cer) and metallic (met) materials.

CHP: Combined Heat and Power.

CMR: Catalytic Membrane Reactor.

CMR-QT: Catalytic Membrane Reactor with Quartz Tube.

CMR-TM: Catalytic Membrane Reactor with Tubular Membrane.

CNG: Compressed Natural Gas.

CP-MAS NMR: Cross Polarization Magic-Angle Spinning Nuclear Magnetic Resonance.

DME: Dimethyl Ether.

EDS: Energy Dispersive X-ray Spectroscopy.

EPR: Electron Paramagnetic Resonance.

EXAFS: Extended X-ray Absorption Fine-Structure.

FBR: Fixed Bed Reactor.

FCC: Fluid Catalytic Cracking.

fcc: face centered cubic structure.

FE-SEM: Field Emission Scanning Electron Microscopy.

FID: Flame Ionization Detector.

FTIR: Fourier Transform Infrared.

GC: Gas Chromatograph.

GC-MS: Gas Chromatography and Mass Spectrometry.

GHG: Greenhouse Gases.

hcp: hexagonally close packed structure.

ICP-OES: Inductively Coupled Plasma Optical Emission Spectroscopy.

IR: Infrared.

LNG: Liquefied Natural Gas.

LPG: Liquefied Petroleum Gas.

LWM0.4: $\text{La}_{5.5}\text{W}_{0.6}\text{Mo}_{0.4}\text{O}_{11.25-\delta}$; δ is the oxygen deficiency per unit formula.

MAS NMR: Magic-Angle Spinning Nuclear Magnetic Resonance.

MDA: Methane Dehydroaromatization.

MR: Member Ring.

NH_3 -TPD: Ammonia Temperature Programmed Desorption.

NMR: Nuclear Magnetic Resonance.

OECD: Organization for Economic Cooperation and Development.

PET: Polyethylene Terephthalate.

PID: *Proportional Integral Derivative*.

RT: Room temperature.

S_{BET} : BET Surface Area.

SCY: $\text{SrCe}_{0.95}\text{Yb}_{0.05}\text{O}_{3-\delta}$; δ is the oxygen deficiency per unit formula.

SEM: Scanning Electron Microscopy.

Syngas: Synthesis Gas.

TCD: Thermal Conductivity Detector.

TGA/DTA: Thermogravimetric and Derivative Thermogravimetric Analyses.

TM: Tubular Membrane.

TMB: 1,2,4-trimethylbenzene.

TMI: Transition Metal Ion.

TOS: Time on Stream.

TPH: Temperature Programmed Hydrogenation.

TPO: Temperature Programmed Oxidation.

TPR: Temperature Programmed Reduction.

TPSR: Temperature Programmed Surface Reaction.

VN: four-way pneumatic valve.

vol. ratio: volumetric ratio.

WHSV: Weight Hourly Space Velocity.

XAFS: X-ray Absorption Fine Structure.

XANES: X-Ray Absorption Near Edge Structure.

XPS: X-Ray Photoelectron Spectroscopy.

XRD: X-Ray Diffraction.

% (wt.): weight percent.

Resumen/Resum/Summary

Resumen

La presente tesis se ha centrado en el estudio intensivo del proceso de deshidroaromatización de metano en condiciones no oxidativas para producir benceno e hidrógeno de forma directa. Sin embargo, el proceso de MDA está limitado termodinámicamente y, además, el catalizador acumula rápidamente grandes cantidades de depósitos carbonosos, lo que dificulta su comercialización. Por tanto, esta tesis tiene como objetivos fundamentales la mejora de la actividad catalítica y la estabilidad del catalizador en la reacción MDA.

Los catalizadores Mo/zeolita son ampliamente utilizados en la reacción MDA, los cuales son bifuncionales, es decir, los sitios de Mo están involucrados en la deshidrogenación del metano y la formación de las especies CH_x , las cuales se dimerizan a especies C_2H_y , y los sitios ácidos de Brønsted de la zeolita oligomerizan éstas especies C_2H_y , formando principalmente benceno y naftaleno. Por lo que, diferentes catalizadores Mo/zeolita se prepararon utilizando zeolitas tanto comerciales como sintetizadas en el laboratorio. Observando así que la zeolita y el contenido de Mo utilizados en el catalizador afectan significativamente el rendimiento de la reacción MDA. Tanto la topología y las dimensiones de los canales de la zeolita como su relación Si/Al y su tamaño de cristal son también importantes en los resultados obtenidos de la reacción MDA. Concretamente, el mejor rendimiento de MDA fue obtenido por el catalizador 6%Mo/MCM-22.

Se probaron diferentes procedimientos de activación del catalizador, obteniendo el mejor rendimiento de la reacción MDA y estabilidad del catalizador usando una mezcla gaseosa de $\text{CH}_4:\text{H}_2$, 1:4 (relación en volumen) durante 1 h hasta 700 °C y manteniendo esta temperatura durante 2 h. Esta

activación del catalizador provoca la pre-carburización y pre-reducción de las especies de Mo, obteniendo las más activas y estables en la reacción de MDA. Además, en la presente tesis se estudió el efecto de la velocidad espacial. Los mejores resultados de MDA se obtuvieron con $1500 \text{ mL}\cdot\text{h}^{-1}\cdot\text{g}_{\text{cat}}^{-1}$, ya que con mayores velocidades espaciales el metano apenas puede interaccionar con los sitios catalíticos. Mientras que con menores velocidades espaciales la condensación de los hidrocarburos aromáticos pesados se ve favorecida, provocando una mayor acumulación de coque en el catalizador. Por otra parte, co-alimentando H_2O , H_2 y CO_2 por separado se obtuvo una mayor estabilidad tanto del catalizador 6%Mo/HZSM-5 como del 6%Mo/MCM-22, debido a la supresión parcial del coque depositado. Sin embargo, la actividad catalítica empeoró al añadir estos co-reativos ya que, por un lado, la adición de H_2O , H_2 y CO_2 a la alimentación de metano es perjudicial termodinámicamente y, por otro lado, el H_2O y el CO_2 re-oxidan parcialmente las especies Mo del catalizador. Termodinámicamente, el H_2 provoca un cambio en el equilibrio y, por tanto, una disminución de la conversión de metano; el H_2O favorece la reacción de reformado de metano y la gasificación de coque; y el CO_2 promueve la reacción de reformado de metano y la reacción inversa de Boudart.

En la presente tesis se ha llevado a cabo el desarrollo y la implementación de un reactor catalítico de membrana (CMR) que integra el catalizador 6%Mo/MCM-22 y la membrana tubular BZCY72. El rendimiento de la reacción MDA y la estabilidad del catalizador fueron excepcionalmente mejorados usando este CMR imponiendo una corriente a la celda electroquímica, cambiando o no las condiciones de operación estándar. Estos buenos resultados fueron obtenidos debido a la simultánea extracción de H_2 del lado de reacción y la inyección de O_2 a este lado mediante la membrana tubular BZCY72. Así, la extracción de H_2 se traduce en un desplazamiento del equilibrio termodinámico de la reacción MDA, lo que causa el aumento de la conversión de metano y a su vez del rendimiento de aromáticos. Además, la

inyección de O₂ implica la formación de agua en baja concentración, la que reacciona con el coque acumulado (gasificación de coque), aumentando la estabilidad del catalizador.

Resum

La present tesi s'ha centrat en l'estudi intensiu del procés de deshidroaromatització de metà en condicions no oxidatives per produir benzé i hidrogen de forma directa. No obstant això, el procés de MDA està limitat termodinàmicament i, a més, el catalitzador acumula ràpidament grans quantitats de dipòsits carbonosos, el que dificulta la seva comercialització. Per tant, aquesta tesi té com a objectius fonamentals la millora de l'activitat catalítica i l'estabilitat del catalitzador en la reacció MDA.

Els catalitzadors Mo/zeolita són àmpliament utilitzats en la reacció MDA, els quals són bifuncionals, és a dir, els llocs de Mo estan involucrats en la deshidrogenació del metà i la formació de les espècies CH_x , les quals es dimeritzen a espècies C_2H_y , i els llocs àcids de Brønsted de la zeolita oligomeritzen aquestes espècies C_2H_y , formant principalment benzè i naftalè. Per tant, diferents catalitzadors Mo/zeolita es van preparar utilitzant zeolites tant comercials com sintetitzades al laboratori. Observant així que la zeolita i el contingut de Mo utilitzats en el catalitzador afecten significativament el rendiment de la reacció MDA. Tant la topologia i les dimensions dels canals de la zeolita com la seva relació Si/Al i el seu tamany de cristall són també importants en els resultats obtinguts de la reacció MDA. Concretament, el millor rendiment de MDA va ser obtingut pel catalitzador 6%Mo/MCM-22.

Es van provar diferents procediments d'activació del catalitzador, obtenint el millor rendiment de la reacció MDA i estabilitat del catalitzador usant una mescla de gasos de CH_4 : H_2 , 1: 4 (relació en volum) durant 1 h fins a 700 °C i mantenint aquesta temperatura durant 2 h. Aquesta activació del catalitzador provoca la pre-carburització i pre-reducció de les espècies de Mo, obtenint les més actives i estables en la reacció de MDA. A més, en la present tesi es va estudiar l'efecte de la velocitat espacial. Els millors resultats de MDA es van obtenir amb $1500 \text{ mL} \cdot \text{h}^{-1} \cdot \text{g}_{\text{cat}}^{-1}$, ja que amb majors velocitats espacials el

metà gairebé no pot interaccionar amb els llocs catalítics. Mentre que amb menors velocitats espacials la condensació dels hidrocarburs aromàtics pesants es veu afavorida, provocant una major acumulació de coc en el catalitzador. D'altra banda, co-alimentant H_2O , H_2 i CO_2 per separat es va obtenir una major estabilitat tant del catalitzador 6%Mo/HZSM-5 com del 6%Mo/MCM-22, a causa de la supressió parcial del coc dipositat. No obstant això, l'activitat catalítica empitjorà en afegir aquests co-reactius ja que, d'una banda, l'addició d' H_2O , H_2 i CO_2 a l'alimentació de metà és perjudicial termodinàmicament i, d'altra banda, el H_2O i el CO_2 re-oxiden parcialment les espècies Mo del catalitzador. Termodinàmicament, el H_2 provoca un canvi en l'equilibri i, per tant, una disminució de la conversió de metà; l' H_2O afavoreix la reacció de reformat de metà i la gasificació de coc; i el CO_2 promou la reacció de reformat de metà i la reacció inversa de Boudart.

En la present tesi s'ha dut a terme el desenvolupament i la implementació d'un reactor catalític de membrana (CMR) que integra el catalitzador 6%Mo/MCM-22 i la membrana tubular BZCY72. El rendiment de la reacció MDA i l'estabilitat del catalitzador van ser excepcionalment millorats usant aquest CMR imposant un corrent a la cel·la electroquímica, canviant o no les condicions d'operació estàndard. Aquests bons resultats van ser obtinguts a causa de la simultània extracció d' H_2 del costat de reacció i la injecció d' O_2 a aquest costat per mitjà de la membrana tubular BZCY72. Així, l'extracció d' H_2 es tradueix en un desplaçament de l'equilibri termodinàmic de la reacció MDA, el que causa l'augment de la conversió de metà i alhora del rendiment d'aromàtics. A més, la injecció d' O_2 implica la formació d'aigua en baixa concentració, la qual reacciona amb el coc acumulat (gasificació de coc), augmentant l'estabilitat del catalitzador.

Summary

The present thesis has focused on the intensive study of the methane dehydroaromatization process under non-oxidative conditions for producing benzene and H_2 in a direct way. Nevertheless, MDA process is thermodynamically limited and, moreover, the catalyst quickly accumulates large amounts of carbonaceous deposits, which hinders its commercialization. Therefore, this thesis has as fundamental purposes the improvement of the catalytic activity and the stability of the catalyst on MDA reaction.

The catalysts widely used on MDA reaction are Mo/zeolite, which are bifunctional, i.e., Mo sites are involved in the methane dehydrogenation and formation of CH_x species, which are dimerized to C_2H_y species, and Brønsted acid sites of the zeolite oligomerize these C_2H_y species, forming mostly benzene and naphthalene. Thereby, different Mo/zeolite catalysts were prepared using commercial zeolites as well as zeolites synthesized on the laboratory. Thus, observing that the zeolite and the Mo content employed on the catalyst affected significantly the MDA performance. The topology and the channel dimensions of the zeolite as well as its Si/Al ratio and crystal size were also important on the MDA results obtained. Concretely, the best MDA performance was achieved by the 6%Mo/MCM-22 catalyst.

Different catalyst activation procedures were tested, achieving the best MDA performance and catalyst stability using a gas mixture of $CH_4:H_2$, 1:4 (vol. ratio) during 1 h up to 700 °C and maintaining this temperature for 2 h. This catalyst activation leads to the pre-carburization and pre-reduction of the Mo species, obtaining the most active and stable on MDA reaction. Moreover, the effect of the space velocity was studied in the present thesis. The best MDA results were reached at $1500 \text{ mL}\cdot\text{h}^{-1}\cdot\text{g}_{\text{cat}}^{-1}$, as at higher space velocities methane barely can interact with the catalytic sites. While at lower space velocities the condensation of the heavy aromatic hydrocarbons is facilitated, causing higher

coke accumulation on the catalyst. Furthermore, higher catalyst stability was obtained by co-feeding H₂O, H₂ and CO₂ separately using the 6%Mo/HZSM-5 catalyst as well as the 6%Mo/MCM-22, due to the partial suppression of coke deposited. However, the catalytic activity was worsen by adding these co-reactants because of, on one hand, thermodynamically the addition of H₂O, H₂ or CO₂ to the methane feed is detrimental and, on the other hand, H₂O and CO₂ partially re-oxidize the Mo species of the catalyst. Thermodynamically, H₂ causes an equilibrium shift and, therefore, a decrease on the methane conversion; H₂O favors the methane reforming reaction and coke gasification; and CO₂ promotes the methane reforming reaction and the reverse Boudart reaction.

The development and implementation of a catalytic membrane reactor (CMR) that integrates the 6%Mo/MCM-22 catalyst and the BZCY72 tubular membrane has been carried out on the present thesis. The MDA performance and the stability of the catalyst were exceptionally improved using this CMR by imposing a current to the electrochemical cell, changing or not the standard operating conditions. These good results were obtained due to the simultaneous H₂ removal from MDA reaction side and O₂ injection to this side through the BZCY72 tubular membrane. Thus, the H₂ extraction results in the thermodynamic equilibrium displacement of MDA reaction, which causes the increase of the methane conversion and in turn of the aromatics yield. Moreover, the O₂ injection involves the formation of H₂O in low concentration, which reacts with coke accumulated (coke gasification), rising the stability of the catalyst.

Scientific Contribution

Publications

- S. H. Morejudo, **R. Zanón**, S. Escolástico, I. Yuste-Tirados, H. Malerød-Fjeld, P. K. Vestre, W. G. Coors, A. Martínez, T. Norby, J. M. Serra, C. Kjølseth. Direct conversion of methane to aromatics in a catalytic co-ionic membrane reactor. *Science*, 353 (2016) 563-566.

Congress participation

Oral presentations

- C. Kjølseth, H. Malerød-Fjeld, S. H. Morejudo, **R. Zanón**, J. M. Serra, D. Beeaff, C. Vigen, I. Yuste-Tirados, P. K. Vestre. Intensified conversion of natural gas using proton conducting ceramics. *18th International Conference on Solid State Protonic Conductors*. Oslo (Norway), 2016.
- S. H. Morejudo, **R. Zanón**, S. Escolástico, I. Yuste-Tirados, H. Malerød-Fjeld, P. K. Vestre, W. G. Coors, A. Martínez, T. Norby, J. M. Serra, C. Kjølseth. Direct conversion of methane to aromatics in a catalytic co-ionic membrane reactor. *11th Natural Gas Conversion Symposium*. Tromsø (Norway), 2016.
- S. Escolástico, C. Solís, **R. Zanón**, J. M. Serra. Outstanding hydrogen permeation through composite mixed conducting composites. *14th International Conference European Ceramic Society*. Toledo (Spain), 2015.
- S. Escolástico, C. Solís, **R. Zanón**, J. M. Serra. Hydrogen permeation through $\text{La}_{5.5}\text{WO}_{11.25-8}\text{-La}_{0.87}\text{Sr}_{0.13}\text{CrO}_3$ composites. *IX Ibero-American Congress on Membrane Science and Technology*. Santander (Spain), 2014.
- S. Escolástico, **R. Zanón**, C. Solís, J. M. Serra. Optimization of biomass-fueled IGCC plants by the integration of protonic membranes. *4th International Workshop of UBIOCHEM (CM0903) COST Action*, Valencia (Spain), 2013.

Poster presentations

- **R. Zanón**, S. H. Morejudo, C. Kjølsest, J. M. Serra. Effect of hydrogen removal through BZCY72 tubular membranes in methane dehydroaromatization reaction. *Ionic and protonic ceramic membranes for green energy applications*. Valencia (Spain), 2015.
- S. H. Morejudo, **R. Zanón**, J. M. Serra, C. Kjølsest, S. Svelle. Effect of zeolite support and Mo content in dehydroaromatization of methane over Mo/zeolite catalysts. *16th Symposium on Catalysis*. Oslo (Norway), 2014.
- C. Solís, S. Escolástico, **R. Zanón**, J.M. Serra. Conductivity relaxation study of $\text{La}_6\text{WO}_{12}$. *Inorganic membranes for Green Chemical Production and Clean Power Generation-Summer school*. Valencia (Spain), 2013.
- S. Escolástico, **R. Zanón**, C. Solís, J. Seeger, M. Ivanova, W. Meulenberg, J. M. Serra. Hydrogen separation through doped $\text{La}_{5.5}\text{WO}_{11.25-8}$ based membranes. *Inorganic membranes for Green Chemical Production and Clean Power Generation-Summer school*. Valencia (Spain), 2013.

Agradecimientos / Acknowledgements

Quiero expresar mi agradecimiento a todas aquellas personas que me han apoyado y ayudado durante todo este tiempo, casi seis años, en la realización de esta tesis doctoral.

En primer lugar, agradecerle a José Manuel Serra la oportunidad que me brindó para trabajar en el Instituto de Tecnología Química y realizar la tesis doctoral, así como por transmitirme sus conocimientos y confiar en mí, sin duda alguna he aprendido mucho. Señalar que el apoyo financiero a través del CSIC se lo debo a Protia, AS, hoy en día Coorstek Membrane Sciences, parte fundamental para la realización de esta tesis.

También agradecer a mis compañeros del laboratorio de energías renovables (pilas) los buenos momentos que hemos pasado, sois unas personas excepcionales y sin vosotros no habría sido lo mismo, ha sido un placer trabajar a vuestro lado. En especial, agradecer a María Fabuel y Sonia toda la ayuda que me han prestado, sin la cual este trabajo hubiese sido mucho más complicado. A Julio alias “el malig”, por estar siempre dispuesto a darme un susto y hacerme reír, ahora a tope con las “zzzz”. A Laura, una sarrionera muy capaz, por no dudar en echarme un cable si lo he necesitado. A María Balaguer y Fidel, mis compis gatunos, con los que es muy fácil compartir historias felinas y risas. A David por estar siempre dispuesto a ayudar y resolver cualquier duda. También a Nuria, la cabecita loca del lab, con sus idas y venidas al cubo. A Sara siempre amable y dispuesta a echar una mano si es necesario, con su Juan que no deja de llamarla. A Mateusz un currante de pies a cabeza que, junto con David, casi siempre cierra el laboratorio. A los últimos en incorporarse a este equipo: Juan E., Álvaro, Juan B. (con ese huerto a tope) y Sebastián. Y entre los que ya no están, a Vicente, Cecilia y Cyril, se os extraña.

Además, agradecer a todos los miembros de taller, caracterización y administración del ITQ su ayuda en el desempeño de este trabajo.

Y por último agradecer a mi familia, en especial a mi madre y a David, toda su ayuda, comprensión y apoyo incondicional. Por estar siempre ahí, a las buenas y a las malas, dándolo todo sin esperar nada a cambio. Hacéis que la vida sea más fácil.